INVESTIGATION OF CYTOTOXICITY AND ION FLUX INDUCED BY VARIOUS AGGREGATION STATES OF AMYLOID-BETA PEPTIDES

by

Panchika Prangkio

A dissertation submitted in partial fulfillment
of the requirements for the degree of
Doctor of Philosophy
(Biomedical Engineering)
in The University of Michigan
2011

Doctoral Committee:

Associate Professor Michael Mayer, Chair
Associate Professor David Samuel Sept
Assistant Professor Mohamed E.H. El-Sayed
Assistant Professor Sarah Veatch

ฝูงชนกำเนิดคล้าย คลึงกัน

ใหญ่ย่อมเพศผิวพรรณ แผกบ้าง

ความรู้อาจเรียนกันทัน กันหมด

เว้นแต่ชั่วดีกระด้าง ห่อนแก้ ฤาไหว

- King Rama V

Born men are we all and one,

Brown black by the sun cultured.

Knowledge can be won alike,

Only the heart differs from man to man.

-Translated by M.R. Seni Pramoj

DEDICATION

To my parents for your love, great support, and encouragement

ACKNOWLEDGEMENTS

I would like to thank my advisor, Dr. Michael Mayer, for providing me an opportunity to work with such an important research topic. I have learned a great deal of knowledge while being in his laboratory. I really appreciate his patience, guidance for my research, and his advices for my future career.

I also would like to show my gratitude to the rest of my dissertation committees:

Dr. David Sept, for his time and valuable suggestions on statistical analyses.

Dr. Mohamed El-Sayed, for providing access to equipments in his laboratory, as well as great suggestions on my works.

Dr. Sarah Veatch, for her insights and suggestions on my works.

The work of this thesis would not have been possible without helps and supports from my colleagues, family and friends. I would like to thank these people whom I will address in the following:

Dr. Ricardo Capone, for his mentoring at the beginning of my works, and providing a lot of great advices.

Dr. Jerry Yang, for providing a number of molecules for the studies and also his valuable suggestions on my research.

Dr. Raymond Scott Turner, and Dr. Indu Saluja, for their suggestions regarding clinical perspectives

Dr. Divya Rao, for her guidance and valuable discussions in biochemistry perspectives

Erik Yusko, for his helps with TEM imaging, and his suggestions on my thesis

Brandon Bruhn, for his feedbacks on my thesis.

Felipe Garcia Quiroz, Anna Sauer, Kevin Lance, Axel Fanget, for their contributions in data collection and helpful discussions on my research.

The other current and former lab members, Kim Horger, Dr. Haiyan Liu, Yazan Billeh, Marian Adamson, Dr. Sheereen Majd, Dr. Jeff Uram, Dr. Daniel Estes. I really appreciate their helpful suggestions, especially feedbacks during group seminars, and their friendship over the years. I am really grateful to know all of you.

My parents and family, for your unconditional love, supports, encouragement, and for shaping me the way I am today.

Nirand Pisutha-arnond, for being supportive, encouraging, and also being a great help with programming.

My friends, especially Niravun Pavenayotin, Thitiporn Sukaew, Phapanin Charoenpol, Rhatarporn Kessom, Sirarat Sarntivijai, and Tul Suriyaluck, for their friendship, supports and sharing wonderful moments in Michigan

Lastly, I would like to thank the Thai government for a prestigious scholarship, which allows me to study abroad and experience the world.

TABLE OF CONTENTS

LIST OF FIGURES

Figure

LIST OF TABLES

Table

LIST OF ABBREVIATIONS

Aβ	amyloid-β
AD	Alzheimer's disease
APP	amyloid precursor protein
BLM	Black lipid membranes
BTA	benzothiazole
BTA-EG_4	benzothiazole tetra-ethylene glycol
BTA-EG_6	benzothiazole hexa-ethylene glycol
CD	circular dichroism
DOPS	1,2-dioleoyl-*sn*-glycero-3-phospho-L-serine
DOTAP	1,2-dioleoyl-3-trimethylammonium - propane
DiphyPC	1,2-diphytanoyl-*sn*-glycero-3-phosphatidylcholine
DiphyPG	1,2-diphytanoyl-*sn*-glycero-3 phosphatidylglycerol
DPPE	1,2-Dipalmitoyl-*sn*-Glycero-3-[phospho*rac*-(1-glycerol)]

gA	gramicidin A
HEPES	4-(2-hydroxyethyl) piperazine-1-ethanesulfonic acid
HFIP	hexafluoroisopropanol
LUV	large unilamellar vesicles
MLR	multiple linear regression
OEG	oligo(ethylene glycol)
PBS	phosphate-buffered saline
PEG	poly(ethylene glycol)
PLB	planar lipid bilayers
POPC	1-palmitoyl-2-oleoyl- *sn* -glycero-3-phosphocholine
POPE	1-palmitoyl-2-oleoyl-*sn*- glycero-3-phosphoethanolamine
POPG	1-palmitoyl-2-oleoyl-*sn*-glycero-3-phospho-(1'-*sn*-glycerol)
SDS-PAGE	sodium dodecyl sulfat polyacrylamide gel electrophoresis
TBS	tris-buffered saline
TEM	transmission electron microscope
ThT	thioflavin T
Tris	tris (hydroxymethyl) amino methane

ABSTRACT

INVESTIGATION OF CYTOTOXICITY AND ION FLUX INDUCED BY VARIOUS AGGREGATION STATES OF AMYLOID-BETA PEPTIDES

by

Panchika Prangkio

Chair: Michael Mayer

The pathological feature of Alzheimer's disease (AD) involves accumulation of amyloid-beta (Aβ) peptides into plaques in brain tissues. Two species of Aβ peptides, $A\beta_{1-40}$ and $A\beta_{1-42}$, have been identified as the major components of the amyloid plaques. Most studies have reported that the intermediate oligomeric forms of Aβ are responsible for neurodegeneration; the exact mechanisms of neurotoxicity, however, are still unclear. An increasing number of evidence indicates that Aβ peptides can form pores in neuronal membranes and cause uncontrolled ion flux through cellular membranes, leading to a disruption of the ion homeostasis.

In this thesis, with regard to a controversy on the mechanism of Aβ-induced ion flux: ion channel formation *versus* thinning membrane hypotheses, we provided an

evidence that Aβ can form pores which permit ion flux through the artificial lipid and neuronal membranes, while the proposed membrane thinning effect was due to the residual amounts of the solvent hexafluoroisopropanol, which was used in the preparation procedure. In addition, we used planar lipid bilayer recordings to study the formation of ion channel, and cytotoxicity assays to determine the toxicity of Aβ from various preparation methods of Aβ. We characterized the aggregation states of Aβ using biochemical and biophysical techniques to correlate the relative abundance of aggregated Aβ species with pore formation and cytotoxicity. Our statistical analyses revealed that pore formation was correlated most strongly with tetramers to hexamers, while cytotoxicity correlated with tetramers to 18 mers. The partial overlap of Aβ oligomers that induced the highest probability of pore formation with those that were most toxic suggests that pore formation is likely a contributing mechanism to the toxicity of Aβ.

In the second part of this research, we characterized two synthetic molecules containing oligo(ethylene glycol), which self-assemble to form ion channels across lipid membranes. We found that these molecules also exhibited antibacterial activity against gram-positive bacteria, which might be appealing as a starting material for the development of antibiotics.

Chapter 1

Introduction to Alzheimer's Disease and Amyloid beta (Aβ) Peptides

1.1 General overview of Alzheimer's disease (AD)

Alzheimer's disease (AD) is the most common neurodegenerative disorder which is associated with loss of memory and cognitive abilities. It was discovered in 1906 by Dr. Alois Alzheimer, a German psychiatrist, who examined the post-mortem of the brain tissues of a 51-year-old woman who died after suffering from memory impairment and abnormal behaviors (*1*). After a few years of investigation, he revealed that the brain tissues of his patient contained abnormal fibrillar structures, and numerous deposits (lesions) within the cerebral cortex. Since then, these two abnormal structures, known as neurofibrillary tangles (NFT) and amyloid plaques, have been considered as the hallmarks of AD. The major components of amyloid plaques are amyloid-β (Aβ) peptides, while the NFT are mainly composed of hyperphosphorylated tau proteins, which are crucial for microtubule assembly and axonal transport (*2, 3*). The progression of AD results from an injury and loss of nerve cells in the brain, especially in the cerebral cortex which is associated with learning, memory, and behaviors.

Currently, AD affects more than 35 million people worldwide and 5.5 million in the United States, mostly above the age of 65 (*2*). As of 2011, AD is the 6th leading cause of death in the U.S with an estimated cost of 183 billion dollars per year (*4*). The occurrence of AD doubles every 5 years and the number of AD patients is expected to

approach 13.2 to 16 million cases in the U.S. by 2050 (*2*). Despite the extensive studies on AD in the past century, the exact mechanisms of AD pathogenesis are still unclear. Increasing evidence supports a causative role for amyloid beta peptides (Aβ) in AD pathogenesis as Aβ triggers neurotoxicity in brain cells via several mechanisms.

The work presented here focuses on the so-called "ion channel formation" mechanism, which states that Aβ induces the neurotoxicity by forming pores in cellular membranes, which disrupts ion homeostasis (*5-8*). We examined the relationship between aggregated species, pore formation, and cytotoxicity and determined the aggregation conditions of Aβ that are most likely to form pores through the lipid membranes as well as induce cytotoxicity.

1.2 Amyloid-β peptides and their roles in AD pathology

1.2.1 Amyloid cascade hypothesis

With regard to pathology of AD, two major hypotheses have been postulated to explain the molecular mechanisms of AD: the cholinergic hypothesis and amyloid cascade hypothesis (*9*). As demonstrated in *Fig.* 1-1, the cholinergic hypothesis, which preceded the amyloid cascade hypothesis, suggests that a decline of choline acetyltransferase (ChAT) and acetyl cholinesterase (AchE), which leads to a deficit of acetylcholine neurotransmitter, causes an impairment of cognitive and memory functions (*10*). The amyloid cascade hypothesis, which has received considerable support from a number of research groups (*11-16*), states that the neurodegenerative process is initiated by the overproduction of Aβ, leading to aggregation and accumulation of Aβ plaques. Along the cascade, there are multiple neurotoxic pathways that may contribute

to the pathogenesis of AD, including disruption of Ca^{2+} homeostasis, free radical production, excitotoxicity, inflammation of neurons, progressive synaptic activity, and hyperphosphorelation of tau (*12, 17*).

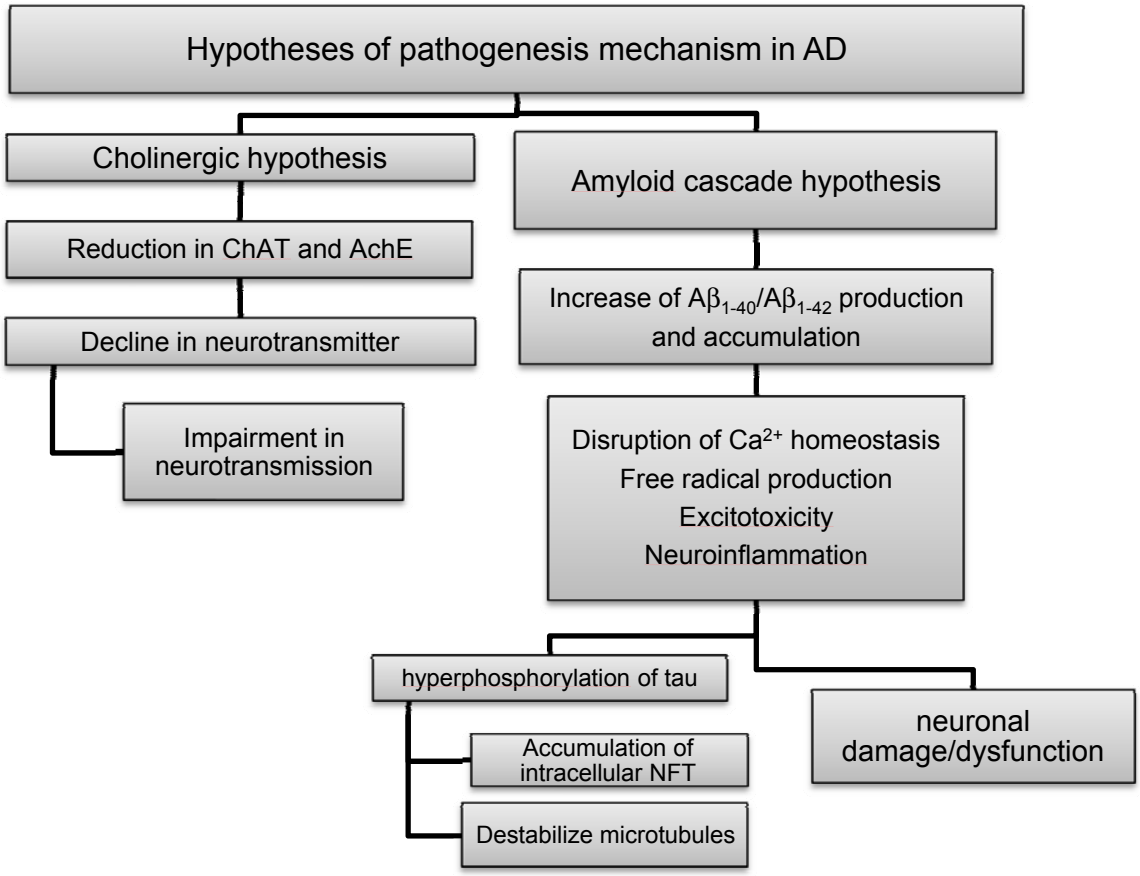

Figure 1-1. Major hypotheses of AD pathogenesis. The cholinergic hypothesis states a reduction of neurotransmitters causes a dysfunctional cholinergic system, which leads to a memory loss. In the amyloid cascade hypothesis, AD pathogenesis is initiated by an overproduction of Aβ, which accumulates and forms amyloid plaques, resulting in a series of subsequent events that leads to cell death (*9*).

Currently, there is no treatment for AD that can stop the deterioration of brain cells and prevent dementia; however, treatments that can alleviate the symptoms of AD

have become available, including acetylcholine esterase inhibitors, antioxidant agents, nonsteroidal anti-inflammatory drugs (NSAIDs), amyloid-β-peptide vaccination, secretase inhibitors, Aβ aggregation antagonist, Cu^{+} and Fe^{2+} chelators, neurotrophic factors, lipid-modulating agents, antidepressants, and cholesterol-lowering drugs (*2, 9, 18-20*).

Nevertheless, these treatments cannot rescue patients from loss of cognitive abilities and memory in the long run, because these treatments cannot modify the pathogenesis of disease, and some treatments have negative side effects (*9*). Hence, it is critically important to increase our understanding of pathways and the mechanisms of AD and to seek new strategies for treatment of this fatal neurodegenerative disease. An understanding of AD pathogenesis may shed light on the development of therapeutic treatments for other protein-misfolding diseases, such as Parkinson's disease (PD), type II diabetes, Huntington's disease, rheumatoid arthritis, and spongiform encephalopathies (or "mad cow" disease). These diseases are characterized by the aggregation of proteins that share common biophysical characteristics or similar biochemical properties with Aβ, including α-synuclein, islet amyloid polypeptide (IAPP or amylin), polyglutamine, serum amyloid A (SAA), and prion peptide 106-126 (*21, 22*).

1.2.2 Molecular properties of amyloid β

Amyloid β peptides (Aβ), which consists of 39-43 amino acids, are natural products of metabolism typically produced in nerve cells by cleavage of a transmembrane protein called amyloid precursor protein (APP). Studies have shown that APP is expressed in various neuronal and non-neuronal cells but the function of

APP is not fully understood (*23*). APP can undergo proteolytic processing via two pathways: the non-amyloidogenic and amyloidogenic pathways. The more common pathway, non-amyloidogenic pathway is mediated by α-secretase and γ-secretase and yields two non-pathogenic peptide fragments called sAPPα and C83. The cleavage of APP by α-secretase occurs within the domain of Aβ, thereby precluding the production of Aβ (see Figure 1-2). Some studies have demonstrated that sAPPα has neurotrophic functions (*24*). The generation of Aβ is a result of the amyloidogenic pathway that involves cleavage of APP by β-secretase and γ-secretase. Although Aβ is a normal product of APP proteolysis and is found in plasma and cerebral spinal fluid (CSF), an imbalance between production and clearance of Aβ leads to Aβ accumulation and formation of insoluble deposits called “senile plaques” or “amyloid plaques,” which are hallmarks for AD (*25, 26*). On the other hand, the density of amyloid plaques in the cerebral cortex showed a weak correlation with severity of dementia in Alzheimer’s patients (*20, 27*).

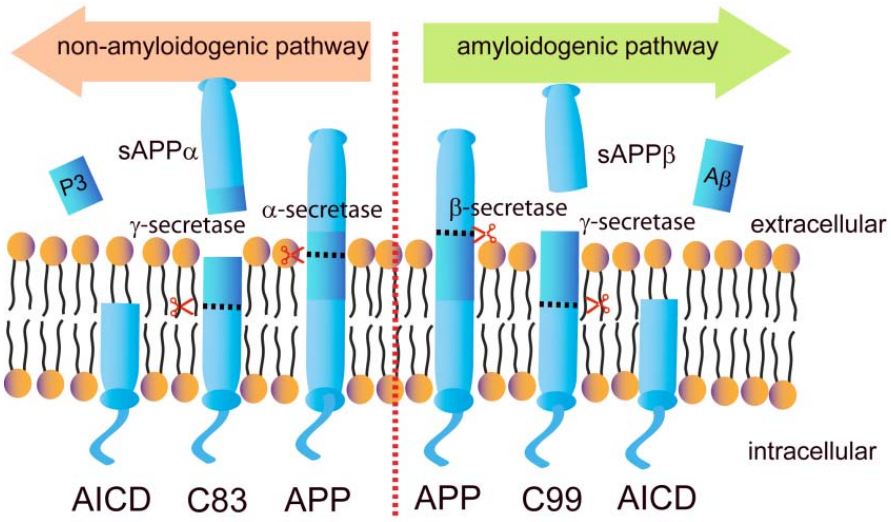

Figure 1-2. Amyloid β (Aβ) peptide is produced via proteolysis of a transmembrane protein called APP, which consists of 696-770 amino acids. APP undergoes two enzymatic pathways: the non-amyloidogenic pathway and amyloidogenic pathways. In the amyloidogenic pathway, APP is cleaved by β-secretase and γ-secretase and released Aβ into extracellular matrix. In healthy people, most APP proteolysis is processed via the non-amyloidogenic pathway, which precludes the generation of Aβ. Figure adapted from reference (*23*).

The major components of amyloid plaques are $A\beta_{1\text{-}40}$ and $A\beta_{1\text{-}42}$. Both species of Aβ exist in plasma and CSF at nanomolar concentrations (*28, 29*). Despite a small difference in the number of amino acids (*i.e.*, Ile^{41} and Ala^{42}), $A\beta_{1\text{-}40}$ and $A\beta_{1\text{-}42}$ exhibit different neurotoxicity and biophysical behavior. $A\beta_{1\text{-}42}$ is more hydrophobic and prone to aggregation than $A\beta_{1\text{-}40}$. Toxicity studies revealed that $A\beta_{1\text{-}42}$ is more toxic than $A\beta_{1\text{-}40}$. In addition, some research groups have revealed that $A\beta_{1\text{-}42}$ is more physiologically relevant than $A\beta_{1\text{-}40}$, while $A\beta_{1\text{-}40}$ is the predominant Aβ species found in vivo (*30*).

In general, Aβ peptides exhibit stochastic mechanisms of aggregation as demonstrated by several biophysical and biological studies, especially with the less soluble and more pathogenic $A\beta_{1-42}$ (*31*). Aβ peptides are initially secreted as soluble monomers and readily assemble into dimer, trimer, and multimeric complexes in a nucleation-dependent process which further aggregate into protofibrils, and eventually insoluble amyloid fibrils (*32, 33*). The aggregation of Aβ varies considerably even between samples in the same preparation as it is influenced by a number of parameters (*34*), including the species of peptides, solvent hydrophobicity, ionic strength, pH, temperature, solvent history, peptide concentration, initial aggregation state, buffer type, peptide counter ions, and the presence of partially oxidized or pre-aggregated forms (seeds) of the peptide. The major difficulty for conclusive studies relates to the tendency of Aβ to aggregate in aqueous solution, forming heterogeneous Aβ assemblies, that makes it difficult to obtain reproducible results of functional experiments (*34, 35*). It is; therefore, important to obtain a well-defined initial aggregation state and to characterize the aggregation states of Aβ in the molecular studies.

To date, monomeric Aβ and fibrils appear to have a minor contribution to neurotoxicity, whereas increasing evidence implicates the prefibrillar intermediate species that contain 2 to 50 Aβ subunits collectively referred to as “small oligomers” or “low-molecular-weight oligomers” (*16*), are responsible for the neurotoxicity and memory impairment in rat and mouse models (*16, 22, 36-38*).

Table 1-1 summarizes the findings of defined size of Aβ species and their relevance in memory loss and neurotoxicity in several research groups (*14, 36, 37*).

.

Table 1-1. Specific assemblies of Aβ and their relevance in neurotoxicity

Aβ assembly	Characteristics	Neurotoxicity	Ref.
Monomer	small globule that is ~ 1.3 nm in height as revealed by AFM	neuroprotective under trophic deprivation; fails to evoke Ca^{2+} influx across cell membrane	(*39, 40*)
Dimer	stabilized by SDS; found in both human AD patients and rat Cerebral Spinal fluid (CSF)	activates glial cells; leads to nerve cell death; abolishes long-term potentiation (LTP) completely	(*38, 41-44*)
Trimer	extracted from Chinese hamster oocytes (CHO) that expressed human APP	fully inhibits hippocampal LTP in vitro and in vivo; transiently impairs the recall of complex learned behavior in rats	(*45*)
Tetramer	separated by size-exclusion chromatography from synthetic $A\beta_{1-42}$ and characterized by western blotting	yields the highest toxicity in neuroblastoma cells and primary hippocampal neurons, but does not necessarily inhibit LTP	(*46, 47*)
Pentamer/ Hexamer	early observable assembly of $A\beta_{1-42}$, that self-associates into larger oligomers	considered stable oligomeric species that are neurotoxic	(*48*)

Prefibrillar oligomer (PFO)	spherical particle of 3-10 nm; appears at early incubation time; considered as precursor of annular protofibrils (APFs)	showed higher toxicity and membrane-permeabilizing activity than APFs	(*49*)
Aβ-Derived Diffusible Ligands (ADDLs)	synthetic Aβ oligomers with a smaller molecular weight than an annulus; between 17-42 kDa (corresponding to tetramers to 12 mers)	affects neural signal transduction pathways	(*50, 51*)
Aβ globulomer	pure, highly water-soluble globular 60-kDa oligomeric form of $A\beta_{1-42}$; persistent structural entity formed independently of fibrillar aggregation pathway (corresponding to 13 mer)	binds specifically to dendritic processes of neurons in hippocampal cell cultures; completely blocks LTP in rat hippocampal slices	(*52, 53*)
Aβ*56	$A\beta_{1-42}$ with molecular weight of 56 kDa; detected in the endogenous brains of an APP transgenic mouse line (corresponding to 13 mer)	correlates with memory loss of transgenic mice	(*54*)
Protofibril (PF)	intermediate of synthetic Aβ fibrillization with diameter of ~ 6-8 nm and length up to 200 nm from AFM; apparent mass > 100 kDa	alters hippocampal synapse physiology and learning behavior of rats	(*33, 55, 56*)

Insoluble amyloid fibrils	highly aggregated forms of Aβ	impairs the late phase of LTP; toxic in rat hippocampal culture; promotes toxicity in primary cortical neurons via interaction with APP	(*24, 57, 58*)
Lipid induced oligomers	obtained from co-incubation of mature Aβ fibrils with membrane particles, resulting in reversion to an oligomer	causes cytotoxicity in hippocampal primary neurons; causes significant cognitive decline in mice	(*59*)

The inconsistent results of neurotoxic forms of Aβ across the different laboratories could arise from different preparation methods of Aβ that affect the aggregation state of the protein (*14, 34*).

1.3 Studies of ion channel hypothesis

1.3.1 Ion channel hypothesis

Since the amyloid cascade hypothesis have proposed that multiple neurotoxic pathways may lead to cell death (*12, 17*), a number of subsequent studies have emerged. One aspect this thesis focuses on is the Aβ-induced-ion channel hypothesis which states that non-fibrillar Aβ interacts with cell membranes and induces aberrant ion channel formation in neuronal membranes, leading to excessive Ca^{2+} influx and disruption of Ca^{2+} homeostasis (*5-8*).

In 1993, Arispe et al. discovered that Aβ can form cation-selective channels when incorporated into planar lipid bilayers in electrophysiological studies (*60*). The characteristics of these ion channels including ion conductance, kinetic behavior, ion selectivity, and pharmacological properties suggest diverse types of Aβ ion channels (*21, 61*). On the other hand, some research groups reported difficulty in observing channel activity of $Aβ_{1-40}$ or $Aβ_{1-42}$ in electrophysiological studies (*62*). Most research groups have observed discrepancies in the toxicity of Aβ, likely due to the variability in initial aggregation state of peptides from different suppliers or the same supplier with different batches (*63, 64*). Aβ-induced ion flux was also observed in various biological membranes, including lipid membranes, and cellular membranes —in both neuronal and

non-neuronal cells (*21*). Some studies have revealed that Aβ channel activity could be blocked by various agents such as Congo red (*65*), Zn^{2+}, Al^{3+}, Tris (*66, 67*), and the other synthesized molecules, such as the short peptide, NA7 which contains 7 amino acids that are complementary to the sequence of Aβ peptides (*68*), and two small molecules, MRS2481 and MRS2485 (*69*).

The ability of Aβ to form pores in biological membranes and discovery of specific blockers provide strong evidence supporting the ion channel hypothesis. In addition, evidence of pore-like structure of Aβ oligomers has been revealed by atomic force microscopy (AFM), and electron microscopy (EM). AFM images demonstrated that tetrameric to hexameric Aβ oligomers reconstituted in DOPC lipid bilayers can form annular pores with inner diameter of roughly 2.0 nm diameter and outer diameter of 8-12 nm (*28, 70*). EM revealed that the outer diameter of the annular pores was in the range of 7 to10 nm and inner diameter was between 1.5 to 2 nm (*36, 71, 72*). These pore structures were also observed in neuronal cell membranes and mitochondria-like organelles from brain tissue of AD patients, but the size of pores was larger than those observed in vitro, with outer and inner diameters of 16 nm and 10 nm, respectively (*73*). Recently, Schauerte *et al*. reported by single-molecule spectroscopy that the smallest oligomer that can permeabilize lipid membranes is a hexamer, while 12-14 mers yield the highest conductivity (*74*).

Using molecular dynamics (MD) simulations, Jang et al. demonstrated the possible arrangement of Aβ oligomeric pores in lipid bilayers, which is in agreement with experimental data (*75, 76*). The studies revealed that the “preferred” size of ion channel ranged from 16 to 24 mers. Other research groups independently reported by MD that

the plausible structure of Aβ pores may consist of the tetramer (*77*) and hexamer (*77, 78*)

Despite strong supports for the ion channel formation hypothesis, other mechanisms by which Aβ alters cellular Ca^{2+} homeostasis have been proposed. Glabe and co-workers demonstrated that soluble oligomers of Aβ disrupt lipid membrane integrity by thinning the membrane and causing non-specific leakiness without the formation of the defined pore structures (*79-81*). Other research groups proposed that Aβ directly and indirectly modulates the existing ion channel proteins, receptors (*82-88*), transporter and pumps (*89, 90*). Figure 1-3 illustrates the proposed mechanisms in which Aβ oligomers triggers neurotoxicity by inducing Ca^{2+} influx.

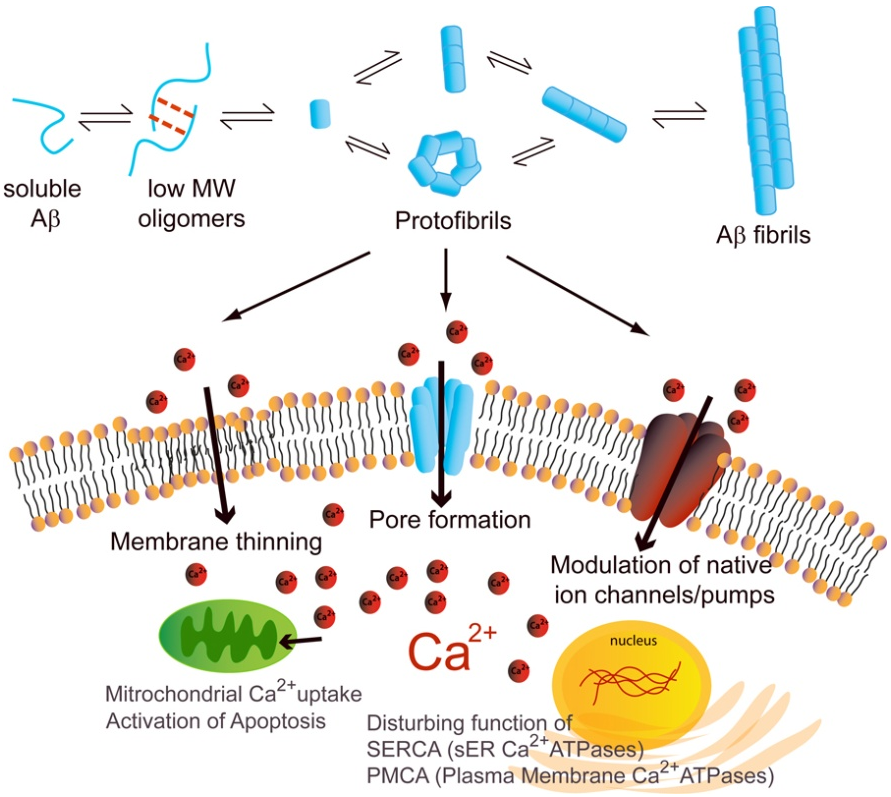

Figure 1-3. Schematic illustration of Aβ aggregation and the proposed mechanisms for Aβ-induced disruption of Ca^{2+} homeostasis. Aβ monomers aggregate into β-sheet oligomers, and eventually fibrils, which compose amyloid plaques. The intermediate Aβ oligomers are considered to be the toxic species that associate with cellular membranes and evoke the unregulated influx of Ca^{2+} through plasma membranes via several possible mechanisms, including pore formation, membrane thinning, and modulation of native Ca^{2+} channels. An increase in intracellular concentration of Ca^{2+} can lead to other neurotoxic pathways such as apoptosis and alteration of ATPase functions. Figure adapted from references (*5, 7, 16*).

It is widely accepted that Aβ causes the dysregulation of intracellular Ca^{2+}, yet the exact mechanism of Aβ toxicity is still not fully understood. The controversy regarding how Aβ interacts with the lipid membrane and the disrupts Ca^{2+} homeostasis

has been going on for decades, which has slowed the progress toward understanding the mechanism of neurotoxicity induced by Aβ. In chapter 2 of this thesis, we address this controversy and provide evidence that Aβ is able to induce a stepwise ion flux across planar lipid bilayers as opposed to thinning of membrane. We show that the previously reported gradual increase in transmembrane current arises from the residues of the solvent, hexafluoroisopropanol (HFIP) used in the preparation.

1.3.2 Membrane model systems and techniques to study the Aβ-lipid membrane interaction

1.3.2.1 Membrane models

Natural cell membranes, widely referred to as plasma membranes, are composed of a lipid bilayer embedded with transmembrane proteins, ion channels, receptors, and glycoproteins (*36*). The structural complexity of biological membranes reflects their diverse functions, including selective transport of molecules between the intra-and extracellular compartments.

With regard to the complexity of biological membranes, researchers have created simplified membrane models for in vitro studies of the physiological behavior of cell membranes. The development of membrane models made it possible to investigate electrical properties of lipid membranes, transport phenomena, protein-membrane interactions, and other membrane characteristics in a systematically controlled environment (*91*).

In this thesis, two major membrane models that we employed are 1) planar lipid bilayers (PLBs), also referred to as black lipid membranes or bilayer membranes (BLMs), which are lipid films separating two aqueous solutions, and 2) liposomes or vesicles, which are enclosed spherical bilayer lipid membranes. These model membranes provide a simplified system for examining the ability of molecules (*e.g*. Aβ peptides in different aggregation states) to form pores on lipid membranes. PLBs are among the oldest membrane models and are the standard for ion channel recording experiments (*36, 92*). Liposomes or vesicles are spherical lipid bilayers of various sizes internally filled with water or aqueous solution. There are three major classes of vesicles: 1) small unilamellar vesicles (SUVs), with diameters in the range of 20-50 nm, 2) large unilamellar vesicles (LUVs), with diameters of approximately 100 nm, and 3) giant unilamellar vesicles (GUVs), with diameters in the range of 1-10 μm (*36*). Due to the similarity in shape and size of cells, liposomes are considered to be most biologically relevant mimic of natural cell membranes, and have been used in a number of applications, including dye-leakage assays, vehicles for drug delivery, and gene therapy (*36*).

1.3.2.2 Electrophysiological technique for studying ion channel

A cell derives its electrical properties mostly from its membrane, which is composed of lipids and proteins, such as ion channels and transporters (*93*). An electrical potential difference (ΔV) exists between the intracellular and extracellular compartments of the lipid membrane. Conductance (G) is a measure of the ability of

ions or charged particles to move between two compartments with an electrical potential difference. Conductance is also written as the reciprocal of resistance (*R*) (*94*). When ion channels are formed in the membrane, the flux of ions between the intra-and extracellular compartments, typically known as current (*I*) can be measured which is described by Ohm's law, Eq. (1-1):

$$I = \frac{\Delta V}{R} = G\Delta V \qquad (1\text{-}1)$$

Typically, the electrophysiology experiments can be performed on cellular and artificial membranes, which behave similarly to an insulator or capacitor. Capacitance (*C*) is a measure of how much charge (*Q*) can be stored on the membrane for a given potential difference across it, as defined by Eq. (1-2):

$$C = \frac{Q}{\Delta V} \qquad (1\text{-}2)$$

The capacitance depends on the dielectric constant and surface area of the membrane, as shown in the following relationship in Eq. (1-3):

$$C = \frac{\varepsilon \varepsilon_0 A}{d} \qquad (1\text{-}3)$$

where ε is the dielectric constant of the membrane

ε_0 is the dielectric constant of free space (8.8542×10^{-12} C V^{-1} m^{-1})

A is the surface area of the membrane, and

d is the thickness of the membranes

In our studies, we will sometimes refer to the conductance term as the measurement of ion flux through the membrane, since voltage was held constant throughout the electrophysiological recordings. Capacitance is an important quantity used to determine the existence and the stability of the lipid bilayer in the electrophysiological studies, as the values of capacitance depend on the surface area and the thickness of the membrane.

Single-channel recordings technique with planar lipid bilayer (PLB) has been extensively used to measure biophysical properties of molecules that conduct ions across the membrane. There are two primary techniques for PLB formation that have been used, the “painted” (*95*), and the “folded” (*96*) techniques, but the fundamental characteristics of the bilayers in both methods are the same (*91*). Figure 1-4 illustrates a conventional experimental setup for bilayer recording, consisting of two compartments which are separated by a lipid bilayer located across an aperture in a hydrophobic film or material, such as Teflon. Each compartment is filled with an electrolyte containing the ions of interest and is connected to the amplifier by electrodes. An ion channel or pore-forming agent is typically inserted into the membrane by addition to the chamber, followed by vigorous mixing. The current due to the conductivity of ion channels is measured as a function of time.

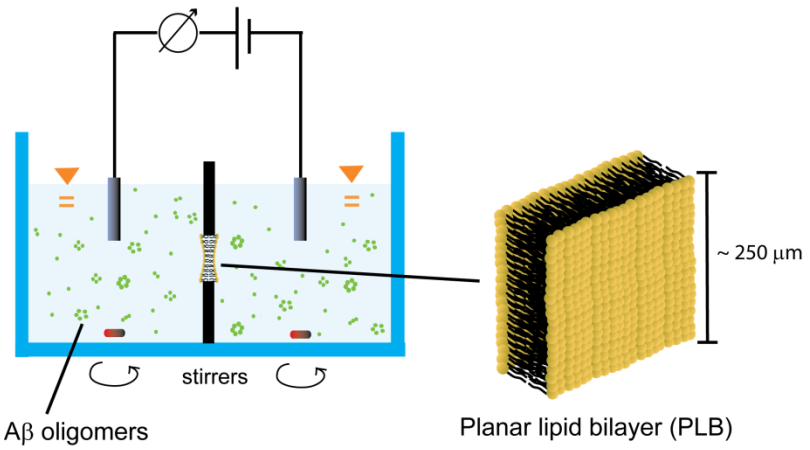

Figure 1-4. A conventional PLB setup consists of a chamber with two compartments, electrodes, and a membrane support. A lipid membrane is formed on an aperture of ~50-250 μm size between the *cis* and *trans* compartments of the chamber by various techniques, such as "painting" or "folding" techniques. Magnetic stirrers are generally required for mixing of added compounds.

The advantages of the PLB technique are high sensitivity in measuring ionic current flowing through a single ion channel, and the possibility to modify the environment of ion channel (*e.g*. ionic composition, pH, lipid composition). However, the limitations of this technique include the instability of the PLB in response to vibrations and hydrostatic pressure gradients, as well as the noise during recording.

Another powerful electrophysiological technique is patch-clamping, which was a breakthrough in 1970s and has been adopted by a number of laboratories in various applications (*93*). This technique provides a sensitive measurement of the current flowing through a single ion channel within the membrane of a living cell. One application of patch-clamping is to examine the ability of Aβ peptides to form ion channels in the cell membrane. It has been shown that Aβ peptides can induce current

flux in living cells such as rat cortical neurons (*97*), hNT cells (*6*), and gonadotropin releasing hormone (GnRH) secreting neurons (*98*). Yet, in practice, there are several limitations of this technique such as difficulties in controlling the intracellular environment, manual manipulation of an individual cell, selection of the cells, and specialized equipment and expertise are necessary (*93*).

In part of this thesis, we adopted a semi-automated patch-clamp device that is commercially available, the so-called "Port-a-Patch" (Nanion Technologies, Munich, Germany), to study Aβ-induced ion channels on cell membranes. We examined the ability of Aβ to form pores in membranes of neuroblastoma cell line (SH-SY5Y), and in primary cortical neurons from transgenic mice that express human amyloid precursor protein (hAPP) and human presenilin 1 (hPS-1).

1.4 Summary of thesis

The main work of this thesis focuses on the ion channel hypothesis with regard to the question of which aggregation states of Aβ are likely to form pore across the lipid membrane and yields the highest toxicity in mammalian cells. In the initial phase of the research, we explored several preparation methods of Aβ and optimized for ion channel recordings in PLBs and cytotoxicity assays in a human neuroblastoma cells. Along the process of the developing the ion flux and cytotoxicity assays, we discovered that one of the common preparation methods of Aβ oligomers, which requires HFIP to break up the large Aβ aggregates, yielded a gradual increase in transmembrane current independently from the presence of Aβ. We proved that the "thinning membrane" mechanism as previously reported was due to the residues of HFIP from the

preparation. In chapter 2, we show that Aβ induces ion flux through membranes of artificial lipid and neuronal cells by pore formation rather than non-specific membrane thinning. This finding strengthens the ion channel hypothesis.

In chapter 3, we compare several preparation methods of Aβ as reported in the literatures with regards to the likelihood of pore formation in the PLBs. We characterized the aggregation states of both $A\beta_{1-40}$ and $A\beta_{1-42}$ from different preparations by using biochemical and biophysical techniques in order to correlate the aggregation states of Aβ with pore formation and cytotoxicity.

We further investigated the effect of Aβ at various aggregation states on the membrane permeabilization in the liposomes by using proton leakage and dye leakage assays. We found the effect of aggregation states on leakage of protons or dyes was different from the results obtained via electrophysiological studies. We discuss the results with regard to liposome influx assays in chapter 4.

In searching for inhibitors of Aβ-induced ion flux and neurotoxicity, we examined the inhibitory effect of a number of small molecules that have high binding affinities to Aβ. These small molecules were designed and studied by our collaborators in Professor Yang's laboratory. We did not find molecules which could reduce Aβ-induced ion flux completely. Unexpectedly, we discovered that two synthesized molecules, which are derivatives of benzothiazole (BTA) attached to oligo(ethylene glycol), which we called BTA-EG_4 and BTA-EG_6, could form well-defined channels independent from the presence of Aβ. In chapter 5, we investigated the characteristics of these self-assembled ion channels. We found that these molecules also exhibited the anti

bacterial activity against gram-positive bacteria, *Bacillus subtilis*, which might be appealing for development of antibiotics.

References

1. Hardy, J. (2006) A hundred years of Alzheimer's disease research, Neuron 52, 3-13.
2. Querfurth, H. W., and LaFerla, F. M. (2010) Mechanisms of disease Alzheimer's disease, *New Engl. J. Med*. 362, 329-344.
3. Terwel, D., Dewachter, I., and Van Leuven, F. (2002) Axonal transport, tau protein, and neurodegeneration in Alzheimer's disease, *Neuromolecular Med*. 2, 151-165.
4. Association, A. s. (2011) 2011 Alzheimer's Disease: Facts and Figures, Alzheimer's & Dementia 7.
5. Arispe, N., Diaz, J. C., and Simakova, O. (2007) A beta ion channels. Prospects for treating Alzheimer's disease with A beta channel blockers, *BBA-Biomembranes* 1768, 1952-1965.
6. Arispe, N., Pollard, H. B., and Rojas, E. (1994) Beta-Amyloid Ca2+-Channel Hypothesis for Neuronal Death in Alzheimer-Disease, *Mol. Cell. Biochem*. 140, 119-125.
7. Shirwany, N. A., Payette, D., Xie, J., and Guo, Q. (2007) The amyloid beta ion channel hypothesis of Alzheimer's disease, *Neuropsychiatr Dis Treat* 3, 597-612.
8. Haass, C., and Selkoe, D. J. (2007) Soluble protein oligomers in neurodegeneration: lessons from the Alzheimer's amyloid beta-peptide, *Nat. Rev. Mol. Cell Biol*. 8, 101-112.
9. Parihar, M. S., and Hemnani, T. (2004) Alzheimer's disease pathogenesis and therapeutic interventions, *J. Clin. Neurosci.* 11, 456-467.
10. Francis, P. T., Palmer, A. M., Snape, M., and Wilcock, G. K. (1999) The cholinergic hypothesis of Alzheimer's disease: a review of progress - Reply, *J. Neurol. Neurosurg. Ps.* 67, 558-558.
11. Selkoe, D. J. (1991) The Molecular Pathology of Alzheimers-Disease, *Neuron* 6, 487-498.
12. Hardy, J. A., and Higgins, G. A. (1992) Alzheimers-Disease - the Amyloid Cascade Hypothesis, *Science* 256, 184-185.
13. Bhatia, R., Lin, H., and Lal, R. (2000) Fresh and globular amyloid b protein (1-42) induces rapid cellular degeneration: evidence for AβP channel-mediated cellular toxicity, *FASEB J.* 14, 1233-1243.
14. Broersen, K., Rousseau, F., and Schymkowitz, J. (2010) The culprit behind amyloid beta peptide related neurotoxicity in Alzheimer's disease: oligomer size or conformation?, *Alzheimers Res Ther* 2, 12.
15. Kourie, J. I. (2001) Mechanisms of amyloid beta protein-induced modification in ion transport systems: Implications for neurodegenerative diseases, *Cell. Mol. Neurobiol*. 21, 173-213.
16. Demuro, A., Parker, I., and Stutzmann, G. E. (2010) Calcium Signaling and Amyloid Toxicity in Alzheimer Disease, *J. Biol. Chem*. 285, 12463-12468.
17. Hardy, J., and Selkoe, D. J. (2002) The Amyloid Hypothesis of Alzheimer's Disease: Progress and Problems on the Road to Therapeutics, *Science* 297, 353-356.
18. Mattson, M. P. (2004) Pathways towards and away from Alzheimer's disease, *Nature* 430, 631-639.

19. Scarpini, E., Schelterns, P., and Feldman, H. (2003) Treatment of Alzheimer's disease; current status and new perspectives, *The Lancet Neurology* 2, 539-547.
20. Walsh, D. M., and Selkoe, D. J. (2007) Aβ Oligomers - a decade of discovery, *J. Neurochem*. 101, 1172-1184.
21. Kagan, B. L., Azimov, R., and Azimova, R. (2004) Amyloid peptide channels, *J. Membr. Biol*. 202, 1-10.
22. Kagan, B. L., and Thundimadathil, J. (2010) Amyloid Peptide Pores and the Beta Sheet Conformation, Proteins: Membrane Binding and Pore Formation 677, 150-167.
23. LaFerla, F. M., Green, K. N., and Oddo, S. (2007) Intracellular amyloid-beta in Alzheimer's disease, *Nat. Rev. Neurosci.* 8, 499-509.
24. Lorenzo, A., Yuan, M. L., Zhang, Z. H., Paganetti, P. A., Sturchler-Pierrat, C., Staufenbiel, M., Mautino, J., Sol Vigo, F., Sommer, B., and Yankner, B. A. (2000) Amyloid beta interacts with the amyloid precursor protein: a potential toxic mechanism in Alzheimer's disease, *Nat. Neurosci.* 3, 460-464.
25. Masters, C. L., Simms, G., Weinman, N. A., Multhaup, G., McDonald, B. L., and Beyreuther, K. (1985) Amyloid Plaque Core Protein in Alzheimer's Disease and Down Syndrome, *Proc. Nat. Acad. Sci (USA)* 82, 4245-4249.
26. Wong, C. W., Quaranta, V., and Glenner, G. G. (1985) Neuritic Plaques and Cerebrovascular Amyloid in Alzheimer-Disease Are Antigenically Related, *Proc. Nat. Acad. Sci (USA)* 82, 8729-8732.
27. Katzman, R. (1986) Alzheimer's Disease, *New Engl. J. Med.* 314, 964-973.
28. Lin, H. A. I., Bhatia, R., and Lal, R. (2001) Amyloid {beta} protein forms ion channels: implications for Alzheimer's disease pathophysiology, *FASEB J*. 15, 2433-2444.
29. Selkoe, D. J. (1994) Normal and Abnormal Biology of the beta-Amyloid Precursor Protein, *Annu. Rev. Neurosci*. 17, 489-517.
30. Shao, H. Y., Jao, S. C., Ma, K., and Zagorski, M. G. (1999) Solution structures of micelle-bound amyloid beta-(1-40) and beta-(1-42) peptides of Alzheimer's disease, *J. Mol. Biol.* 285, 755-773.
31. Hortschansky, P., Schroeckh, V., Christopeit, T., Zandomeneghi, G., and Fandrich, M. (2005) The aggregation kinetics of Alzheimer's beta-amyloid peptide is controlled by stochastic nucleation, *Protein Sci.* 14, 1753-1759.
32. Bitan, G., Lomakin, A., and Teplow, D. B. (2001) Amyloid beta-protein oligomerization - Prenucleation interactions revealed by photo-induced cross-linking of unmodified proteins, *J. Biol. Chem*. 276, 35176-35184.
33. Walsh, D. M., Lomakin, A., Benedek, G. B., Condron, M. M., and Teplow, D. B. (1997) Amyloid beta-protein fibrillogenesis - Detection of a protofibrillar intermediate, *J. Biol. Chem*. 272, 22364-22372.
34. Zagorski, M. G., Yang, J., Shao, H. Y., Ma, K., Zeng, H., and Hong, A. (1999) Methodological and chemical factors affecting amyloid beta peptide amyloidogenicity, Amyloid, Prions, and Other Protein Aggregates 309, 189-204.
35. Jan, A., Hartley, D. M., and Lashuel, H. A. (2010) Preparation and characterization of toxic A beta aggregates for structural and functional studies in Alzheimer's disease research, *Nat. Protoc*. 5, 1186-1209.
36. Butterfield, S. M., and Lashuel, H. A. (2010) Amyloidogenic Protein Membrane Interactions: Mechanistic Insight from Model Systems, *Angew. Chem. Int. Ed. Engl*. 49, 5628-5654.
37. Pountney, D. L., Voelcker, N. H., and Gai, W. P. (2005) Annular alpha-synuclein oligomers are potentially toxic agents in alpha-synucleinopathy. Hypothesis, *Neurotox. Res*. 7, 59-67.
38. Shankar, G. M., Li, S. M., Mehta, T. H., Garcia-Munoz, A., Shepardson, N. E., Smith, I., Brett, F. M., Farrell, M. A., Rowan, M. J., Lemere, C. A., Regan, C. M., Walsh, D. M.,

Sabatini, B. L., and Selkoe, D. J. (2008) Amyloid-beta protein dimers isolated directly from Alzheimer's brains impair synaptic plasticity and memory, *Nat. Med*. 14, 837-842.
39. Demuro, A., Mina, E., Kayed, R., Milton, S. C., Parker, I., and Glabe, C. G. (2005) Calcium Dysregulation and Membrane Disruption as a Ubiquitous Neurotoxic Mechanism of Soluble Amyloid Oligomers, *J. Biol. Chem*. 280, 17294-17300.
40. Giuffrida, M. L., Caraci, F., Pignataro, B., Cataldo, S., De Bona, P., Bruno, V., Molinaro, G., Pappalardo, G., Messina, A., Palmigiano, A., Garozzo, D., Nicoletti, F., Rizzarelli, E., and Copani, A. (2009) beta-Amyloid Monomers Are Neuroprotective, *J. Neurosci*. 29, 10582-10587.
41. Podlisny, M. B., Ostaszewski, B. L., Squazzo, S. L., Koo, E. H., Rydell, R. E., Teplow, D. B., and Selkoe, D. J. (1995) Aggregation of Secreted Amyloid beta-Protein into Sodium Dodecyl Sulfate-Stable Oligomers in Cell Culture, *J. Biol. Chem*. 270, 9564-9570.
42. Walsh, D. M., Tseng, B. P., Rydel, R. E., Podlisny, M. B., and Selkoe, D. J. (2000) The oligomerization of amyloid beta-protein begins intracellularly in cells derived from human brain, *Biochemistry* 39, 10831-10839.
43. Klyubin, I., Betts, V., Welzel, A. T., Blennow, K., Zetterberg, H., Wallin, A., Lemere, C. A., Cullen, W. K., Peng, Y., Wisniewski, T., Selkoe, D. J., Anwyl, R., Walsh, D. M., and Rowan, M. J. (2008) Amyloid beta protein dimer-containing human CSF disrupts synaptic plasticity: Prevention by systemic passive immunization, *J. Neurosci.* 28, 4231-4237.
44. Shankar, G. M., Leissring, M. A., Adame, A., Sun, X., Spooner, E., Masliah, E., Selkoe, D. J., Lemere, C. A., and Walsh, D. M. (2009) Biochemical and immunohistochemical analysis of an Alzheimer's disease mouse model reveals the presence of multiple cerebral A beta assembly forms throughout life, *Neurobiol. Dis*. 36, 293-302.
45. Townsend, M., Shankar, G. M., Mehta, T., Walsh, D. M., and Selkoe, D. J. (2006) Effects of secreted oligomers of amyloid beta-protein on hippocampal synaptic plasticity: a potent role for trimers, *J. Physiol.-London* 572, 477-492.
46. Harmeier, A., Wozny, C., Rost, B. R., Munter, L. M., Hua, H. Q., Georgiev, O., Beyermann, M., Hildebrand, P. W., Weise, C., Schaffner, W., Schmitz, D., and Multhaup, G. (2009) Role of Amyloid-beta Glycine 33 in Oligomerization, Toxicity, and Neuronal Plasticity, *J. Neurosci*. 29, 7582-7590.
47. Ono, K., Condron, M. M., and Teplow, D. B. (2009) Structure-neurotoxicity relationships of amyloid beta-protein oligomers, *Proc. Nat. Acad. Sci (USA)* 106, 14745-14750.
48. Bitan, G., Kirkitadze, M. D., Lomakin, A., Vollers, S. S., Benedek, G. B., and Teplow, D. B. (2003) Amyloid beta-protein (A beta) assembly: A beta 40 and A beta 42 oligomerize through distinct pathways, *Proc. Nat. Acad. Sci (USA)* 100, 330-335.
49. Kayed, R., Pensalfini, A., Margol, L., Sokolov, Y., Sarsoza, F., Head, E., Hall, J., and Glabe, C. (2009) Annular Protofibrils Are a Structurally and Functionally Distinct Type of Amyloid Oligomer, *J. Biol. Chem*. 284, 4230-4237.
50. Gong, Y. S., Chang, L., Viola, K. L., Lacor, P. N., Lambert, M. P., Finch, C. E., Krafft, G. A., and Klein, W. L. (2003) Alzheimer's disease-affected brain: Presence of oligomeric A beta ligands (ADDLs) suggests a molecular basis for reversible memory loss, *Proc. Nat. Acad. Sci (USA)* 100, 10417-10422.
51. Lambert, M. P., Velasco, P. T., Chang, L., Viola, K. L., Fernandez, S., Lacor, P. N., Khuon, D., Gong, Y. S., Bigio, E. H., Shaw, P., De Felice, F. G., Krafft, G. A., and Klein, W. L. (2007) Monoclonal antibodies that target pathological assemblies of A beta, *J. Neurochem.* 100, 23-35.
52. Barghorn, S., Nimmrich, V., Striebinger, A., Krantz, C., Keller, P., Janson, B., Bahr, M., Schmidt, M., Bitner, R. S., Harlan, J., Barlow, E., Ebert, U., and Hillen, H. (2005) Globular amyloid b-peptide$_{1-42}$ oligomer - a homogenous and stable neuropathological protein in Alzheimer's disease, *J. Neurochem.* 95, 834-847.

53. Gellermann, G. P., Byrnes, H., Striebinger, A., Ullrich, K., Mueller, R., Hillen, H., and Barghorn, S. (2008) A beta-globulomers are formed independently of the fibril pathway, *Neurobiol. Dis.* 30, 212-220.
54. Lesne, S., Koh, M. T., Kotilinek, L., Kayed, R., Glabe, C. G., Yang, A., Gallagher, M., and Ashe, K. H. (2006) A specific amyloid-beta protein assembly in the brain impairs memory, *Nature* 440, 352-357.
55. Harper, J. D., Wong, S. S., Lieber, C. M., and Lansbury, P. T. (1997) Observation of metastable A beta amyloid protofibrils by atomic force microscopy, *Chem. Biol*. 4, 119-125.
56. Hartley, D. M., Walsh, D. M., Ye, C. P. P., Diehl, T., Vasquez, S., Vassilev, P. M., Teplow, D. B., and Selkoe, D. J. (1999) Protofibrillar intermediates of amyloid beta-protein induce acute electrophysiological changes and progressive neurotoxicity in cortical neurons, *J. Neurosci*. 19, 8876-8884.
57. Bucciantini, M., Giannoni, E., Chiti, F., Baroni, F., Formigli, L., Zurdo, J. S., Taddei, N., Ramponi, G., Dobson, C. M., and Stefani, M. (2002) Inherent toxicity of aggregates implies a common mechanism for protein misfolding diseases, *Nature* 416, 507-511.
58. Puzzo, D., and Arancio, O. (2006) Fibrillar beta-amyloid impairs the late phase of long term potentiation, *Curr. Alzheimer Res*. 3, 179-183.
59. Martins, I. C., Kuperstein, I., Wilkinson, H., Maes, E., Vanbrabant, M., Jonckheere, W., Van Gelder, P., Hartmann, D., D'Hooge, R., De Strooper, B., Schymkowitz, J., and Rousseau, F. (2008) Lipids revert inert A beta amyloid fibrils to neurotoxic protofibrils that affect learning in mice, *EMBO J*. 27, 224-233.
60. Arispe, N., Pollard, H. B., and Rojas, E. (1993) Giant Multilevel Cation Channels Formed by Alzheimer-Disease Amyloid Beta-Protein [a-Beta-P-(1-40)] in Bilayer-Membranes, *Proc. Nat. Acad. Sci (USA)* 90, 10573-10577.
61. Kourie, J., Henry, C., and Farrelly, P. (2001) Diversity of Amyloid β Protein Fragment [1–40]-Formed Channels, *Cell. Mol. Neurobiol*. 21, 255-284.
62. Mirzabekov, T. A., Silberstein, A. Y., and Kagan, B. L. (1999) Use of planar lipid bilayer membranes for rapid screening of membrane active compounds, *Methods Enzymo*l 294, 661-674.
63. May, P. C., Gitter, B. D., Waters, D. C., Simmons, L. K., Becker, G. W., Small, J. S., and Robison, P. M. (1992) Beta-Amyloid Peptide Invitro Toxicity - Lot-to-Lot Variability, *Neurobiol. Aging* 13, 605-607.
64. Brining, S. K. (1997) Predicting the in vitro toxicity of synthetic beta-amyloid (1-40), *Neurobiol. Aging* 18, 581-589.
65. Hirakura, Y., Lin, M. C., and Kagan, B. L. (1999) Alzheimer amyloid a beta 1-42 channels: Effects of solvent, pH, and Congo Red. (vol 57, pg 458, 1999), *J. Neurosci. Res*. 58, 726-726.
66. Arispe, N., Pollard, H. B., and Rojas, E. (1996) Zn2+ interaction with Alzheimer amyloid beta protein calcium channels, *Proc. Nat. Acad. Sci (USA)* 93, 1710-1715.
67. Arispe, N., Rojas, E., and Pollard, H. B. (1993) Alzheimer-Disease Amyloid Beta-Protein Forms Calcium Channels in Bilayer-Membranes - Blockade by Tromethamine and Aluminum, *Proc. Nat. Acad. Sci (USA)* 90, 567-571.
68. Diaz, J. C., Linnehan, J., Pollard, H., and Arispe, N. (2006) Histidines 13 and 14 in the A beta sequence are targets for inhibition of Alzheimer's disease A beta ion channel and cytotoxicity, *Biol. Res.* 39, 447-460.
69. Diaz, J. C., Simakova, O., Jacobson, K. A., Arispe, N., and Pollard, H. B. (2009) Small molecule blockers of the Alzheimer A beta calcium channel potently protect neurons from A beta cytotoxicity, *Proc. Nat. Acad. Sci (USA)* 106, 3348-3353.
70. Quist, A., Doudevski, I., Lin, H., Azimova, R., Ng, D., Frangione, B., Kagan, B., Ghiso, J., and Lal, R. (2005) Amyloid ion channels: A common structural link for protein-misfolding disease, *Proc. Nat. Acad. Sci (USA)* 102, 10427-10432.

71. Lashuel, H. A., Hartley, D., Petre, B. M., Walz, T., and Lansbury, P. T. (2002) Neurodegenerative disease - Amyloid pores from pathogenic mutations, *Nature* 418, 291-291.
72. Lashuel, H. A., Hartley, D. M., Petre, B. M., Wall, J. S., Simon, M. N., Walz, T., and Lansbury, P. T. (2003) Mixtures of wild-type and a pathogenic (E22G) form of A beta 40 in vitro accumulate protofibrils, including amyloid pores, *J. Mol. Biol.* 332, 795-808.
73. Inoue, S. (2008) In situ A beta pores in AD brain are cylindrical assembly of A beta protofilaments, *Amyloid-Journal of Protein Folding Disorders* 15, 223-233.
74. Schauerte, J. A., Wong, P. T., Wisser, K. C., Ding, H., Steel, D. G., and Gafni, A. (2010) Simultaneous Single-Molecule Fluorescence and Conductivity Studies Reveal Distinct Classes of A beta Species on Lipid Bilayers, *Biochemistry* 49, 3031-3039.
75. Jang, H., Arce, F. T., Capone, R., Ramachandran, S., Lal, R., and Nussinov, R. (2009) Misfolded Amyloid Ion Channels Present Mobile beta-Sheet Subunits in Contrast to Conventional Ion Channels, *Biophys. J*. 97, 3029-3037.
76. Jang, H., Zheng, J., and Nussinov, R. (2007) Models of beta-amyloid ion channels in the membrane suggest that channel formation in the bilayer is a dynamic process, *Biophys. J*. 93, 1938-1949.
77. Strodel, B., Lee, J. W. L., Whittleston, C. S., and Wales, D. J. (2010) Transmembrane Structures for Alzheimer's A beta(1-42) Oligomers, *J. Am. Chem. Soc*. 132, 13300-13312.
78. Shafrir, Y., Durell, S. R., Anishkin, A., and Guy, H. R. (2010) Beta-barrel models of soluble amyloid beta oligomers and annular protofibrils, *Proteins-Structure Function and Bioinformatics* 78, 3458-3472.
79. Kayed, R., Head, E., Thompson, J. L., McIntire, T. M., Milton, S. C., Cotman, C. W., and Glabe, C. G. (2003) Common structure of soluble amyloid oligomers implies common mechanism of pathogenesis, *Science* 300, 486-489.
80. Sokolov, Y., Kozak, J. A., Kayed, R., Chanturiya, A., Glabe, C., and Hall, J. E. (2006) Soluble Amyloid Oligomers Increase Bilayer Conductance by Altering Dielectric Structure, *J. Gen. Physiol*. 128, 637-647.
81. Sokolov, Y. V., Kayed, R., Kozak, A., Edmonds, B., McIntire, T. M., Milton, S., Cahalan, M., Glabe, C. G., and Hall, J. E. (2004) Soluble amyloid oligomers increase lipid bilayer conductance by increasing the dielectric constant of the hydrocarbon core, *Biophys. J.* 86, 382A-382A.
82. Joslin, G., Krause, J., Hershey, A., Adams, S., Fallon, R., and Perlmutter, D. (1991) Amyloid-b peptide, substance P, and bombesin bind to the serpin- enzyme complex receptor, *J. Biol. Chem*. 266, 21897-21902.
83. Querfurth, H. W., Jiang, J., Geiger, J. D., and Selkoe, D. J. (1997) Caffeine Stimulates Amyloid β-Peptide Release from b-Amyloid Precursor Protein-Transfected HEK293 Cells, *J. Neurochem*. 69, 1580-1591.
84. Stutzmann, G. E. (2007) The Pathogenesis of Alzheimers Disease Is It a Lifelong "Calciumopathy"?, *Neuroscientist* 13, 546-559.
85. Ueda, K., Shinohara, S., Yagami, T., and Asakura, K. (1997) Amyloid b Protein Potentiates Ca^{2+} Influx Through L-Type Voltage-Sensitive Ca^{2+} Channels: A Possible Involvement of Free Radicals, *J. Neurochem*. 68, 265-271.
86. Yankner, A. L. a. B. A. (1994) b-Amyloid neurotoxicity requires fibril formation and is inhibited by Congo red, *Proc. Natl. Acad. Sci. (USA)* 91, 12243-12247.
87. Mark, R., Hensley, K., Butterfield, D., and Mattson, M. (1995) Amyloid b-peptide impairs ion-motive ATPase activities: evidence for a role in loss of neuronal Ca2+ homeostasis and cell death, *J. Neurosci.* 15, 6239-6249.
88. Ye, C., Ho-Pao, C. L., Kanazirska, M., Quinn, S., Rogers, K., Seidman, C. E., Seidman, J. G., Brown, E. M., and Vassilev, P. M. (1997) Amyloid-β; proteins activate Ca^{2+}-permeable channels through calcium-sensing receptors, *J. Neurosci. Res*. 47, 547-554.

89. Green, K. N., Demuro, A., Akbari, Y., Hitt, B. D., Smith, I. F., Parker, I., and LaFerla, F. M. (2008) SERCA pump activity is physiologically regulated by presenilin and regulates amyloid b production, *J. Cell Biol*. 181, 1107-1116.
90. Lam, F. C., Liu, R., Lu, P., Shapiro, A. B., Renoir, J.-M., Sharom, F. J., and Reiner, P. B. (2001) b-Amyloid efflux mediated by p-glycoprotein, *J. Neurochem*. 76, 1121-1128.
91. Tien, H. T. O.-L., Angelica (2000) Membrane biophysics as viewed from experimental bilayer lipid membranes, 1st ed., Elsevier, Amsterdam, Netherland.
92. Van Gelder, P., Dumas, F., and Winterhalter, M. (2000) Understanding the function of bacterial outer membrane channels by reconstitution into black lipid membranes, *Biophys. Chem.* 85, 153-167.
93. Sakmann, B. N., Erwin (2009) Single-Channel Recording, 2nd ed., Springer New York.
94. Hille, B. (2001) Ion Channels of Excitable Membranes, 3rd ed., Sinauer Associates, Inc., Sunderland.
95. Mueller, P., Wescott, W. C., Rudin, D. O., and Tien, H. T. (1963) Methods for Formation of Single Bimolecular Lipid Membranes in Aqueous Solution, *J. Phys. Chem.* 67, 534-&.
96. Montal, M., and Mueller, P. (1972) Formation of bimolecular membranes from lipid monolayers and a study of their electrical properties, *Proc. Nat. Acad. Sci (USA)* 69, 3561 - 3566.
97. Furukawa, K., Abe, Y., and Akaike, N. (1994) Amyloid-Beta Protein-Induced Irreversible Current in Rat Cortical-Neurons, *Neuroreport* 5, 2016-2018.
98. Kawahara, M., and Kuroda, Y. (1997) Alzheimer's amyloid beta-protein forms Ca^{2+}-permeable channels in neuronal cells and its aggregation is stimulated by aluminum, *J. Neurochem*. 69, S46-S46.

Chapter 2

Amyloid-beta (Aβ) Ion Channels in Artificial Lipid Bilayers and Neuronal Cells[1]

Understanding the pathogenicity of amyloid-beta (Aβ) peptides constitutes a major goal in research on Alzheimer's disease (AD). One hypothesis entails that Aβ peptides induce uncontrolled, neurotoxic ion flux through cellular membranes. The exact biophysical mechanism of this ion flux is, however, a subject of an ongoing controversy which has attenuated progress towards understanding the importance of Aβ-induced ion flux in AD. The work presented here addresses two prevalent controversies regarding the nature of transmembrane ion flux induced by Aβ peptides. First, the results clarify that Aβ can induce stepwise ion flux across planar lipid bilayers as opposed to a gradual increase in transmembrane current; they show that the previously reported gradual thinning of membranes with concomitant increase in transmembrane current arises from residues of the solvent hexafluoroisopropanol, which is commonly used for the preparation of amyloid samples. Second, the results provide additional evidence suggesting that Aβ peptides can form ion channels in cellular membranes that are

[1] This chapter contains a content of publication, Capone, R., Quiroz, F. G., **Prangkio, P**., Saluja, I., Sauer, A. M., Bautista, M. R., Turner, R. S., Yang, J., and Mayer, M. (2009) Amyloid-beta-Induced Ion Flux in Artificial Lipid Bilayers and Neuronal Cells: Resolving a Controversy, *Neurotox. Res. 16*, 1-13. My contributions in this study include performing a portion of bilayer recordings, characterizing the cytotoxicity of HFIP on neuroblastoma cells.

independent from the postulated ability of Aβ to modulate intrinsic cellular ion channels or transporter proteins.

2.1 Introduction

One of the current hypotheses for the pathology of Alzheimer's disease (AD) proposes that amyloid-beta (Aβ) peptides induce aberrant, neurotoxic ion flux across cellular membranes (*1-20*). The resulting difficulty of neurons to regulate their intracellular concentration of ions, in particular calcium ions, has been associated with cell death (*9, 21*) and may thus contribute to cognitive impairment typical for AD. Understanding the underlying mechanisms that cause Aβ-induced ion flux may hence be crucial for developing new strategies to reduce the toxicity of Aβ in AD.

Increasing evidence shows that exposure of cells to Aβ leads to elevated concentrations of intracellular calcium ions (*1, 9, 15, 21-29*); the predominant cellular mechanism for this disruption of Ca^{2+} homeostasis remains, however, a focus of intense studies. The four mechanisms that have been proposed are: 1) Aβ assembles into oligomers to form Aβ ion channels in cell membranes (*1-20, 22, 30-35*), 2) Aβ interacts with membranes in such a way that it generally lowers the dielectric barrier for ions to cross the membrane (e.g. by thinning the membrane) (*23, 36-39*), 3) Aβ modulates, directly or indirectly, the activity of existing ion channel proteins or receptors (*14, 25, 27, 40-57*), or 4) Aβ modulates, directly or indirectly, the activity of cellular ion transporters and pumps (*58, 59*). Experimental evidence for each of these mechanisms has been provided and it is possible that several mechanisms act together to disrupt Ca^{2+} homeostasis.

The work presented here examined the first three mechanisms. It employed electrophysiological techniques to measure ion flux by current recordings across bilayer lipid membranes (using BLM recordings) or across cellular plasma membranes (using whole-cell patch clamp recordings). This approach excluded the study of ion flux by transporter proteins or ion pumps because the ion flux generated by these proteins is too slow to be detectable by current recordings (*60*). Instead, we asked if Aβ can form ion pores in artificial lipid bilayers, in membranes of a human neuronal cell line (SH-SY5Y), and in primary neurons from transgenic mice that express human amyloid precursor protein (hAPP) and human presenilin 1 (hPS-1).

2.2 Results and discussion

Recently, three articles highlighted an ongoing controversy with regard to the exact biophysical characteristics of Aβ-induced transmembrane ion flux across artificial lipid membranes (*61-63*). These articles debate two mechanistic hypotheses. On the one hand, the "Aβ ion channel hypothesis" suggests that Aβ assembles into pore-like structures in lipid membranes, leading to stepwise (or spike-like) fluctuations of transmembrane current that is typical for ion channels (*1-20, 22, 30-35*). On the other hand, the "Aβ membrane thinning hypothesis" postulates a generalized and gradually increasing ion flux as a result of Aβ-induced reduction of the dielectric barrier of membranes, for instance, by thinning of membranes (*37-39*).

Here, we examined, in detail, the two pivotal protocols for measuring Aβ induced conductance through artificial lipid bilayers to resolve this controversy. The protocol that leads to ion flux by gradual membrane thinning involves solubilizing $A\beta_{1-40}$ or $A\beta_{1-42}$ in the

solvent hexafluoroisopropanol (HFIP), followed by dilution in water, and purging of HFIP by a stream of nitrogen gas (*23, 36-39, 64*). Figure 2-1A shows the gradual increase in ion flux through a planar lipid bilayer upon exposure of membranes to these Aβ samples. Figure 2-1A is consistent with previous reports that used the same HFIP-based experimental procedure (*37-39*). Figure 2-1B, however, shows a similar gradual increase in conductance following the exact same protocol but in the *absence* of Aβ. This control experiment thus shows that Aβ was not required for the observed gradual increase in transmembrane conductance but that residues of HFIP alone could be responsible for the observed ion flux.[2]

[2]One of the previously reported results that supported the hypothesis of Aβ-induced gradual thinning of membranes was the observation that an anti-Aβ antibody could reduce the observed transmembrane ion flux caused by these Aβ preparations. These experiments were carried out with Aβ samples that were also prepared with an HFIP purging protocol (*23, 37-39*). We repeated this experiment with the modification that we added bovine serum albumin (BSA) instead of adding an anti-Aβ antibody. In approximately half of these trials, we found a reduction in transmembrane ion flux by adding BSA to the bilayer chamber. The results were thus similar to the effect attributed previously to the anti-Aβ antibody. Furthermore, when we induced transmembrane ion flux by adding HFIP only, we observed again a reduction in conductance by addition of BSA to bilayer chambers that did not contain Aβ. These results suggest that a specific anti-Aβ antibody was not required to reduce gradually increasing ion flux that was induced by samples containing HFIP.

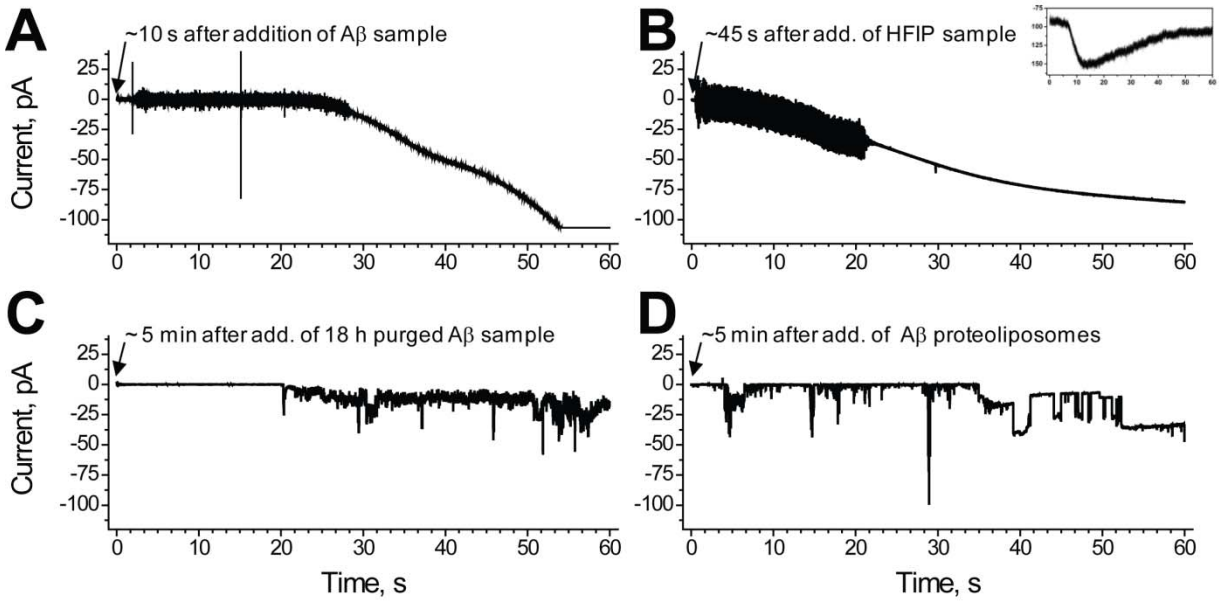

Figure 2-1. Ion flux across lipid bilayers upon exposure to samples with 1 μM amyloid-β peptides (Aβ), which were prepared by two different protocols. **A)** Gradual increase in transmembrane ion flux upon addition of an Aβ sample that was prepared by purging the solvent hexafluoroisopropanol (HFIP) for 10 min (*37, 39*). The "noisy" part of the current trace is a result of mixing. **B)** Gradual increase in transmembrane ion flux following the exact same protocol as in (A) but in the absence of Aβ. Inset, gradual increase in ion flux across the membranes of SH-SY5Y cells upon addition of HFIP (final concentration ~6 mM). **C)** Transmembrane ion flux upon addition of an Aβ sample prepared according to previous reports (*37, 39*) but with 18 h instead of 10 min of purging to remove HFIP. **D)** Stepwise fluctuations in transmembrane ion flux after incorporating a proteoliposome preparation of Aβ that was prepared without using HFIP (*1*). The applied voltage was -150 mV in all recordings. Membranes were prepared from DOPC:DOPE lipids at a 1:1 (w/w) ratio by the "folding method" over a pore (diameter 150 μm) in a Teflon film that was pretreated with 5% squalene in pentane.

To investigate whether this gradual increase in conductance could be reproduced by exposure of membranes to defined concentrations of HFIP (in the absence of Aβ), we examined the effect of HFIP on cell membranes (*Fig.* 2-1B inset) and on planar lipid bilayers of various lipid compositions (*Fig.* 2-2A and 2-2B). We found that, in all of these membranes, solutions containing 1-6 mM (corresponding to 0.01-0.06% v/v) concentrations of HFIP induced a gradual increase in ion flux similar to the results shown in *Fig.* 2-1B and similar to results described previously (*37-39*).[3]

[3] These results together with previous work (*65)* show that even low concentrations of HFIP can adversely affect membranes and alter their permeability for ions. Unlike other short chain alcohols, HFIP affects membranes similarly as long chain alcohols (*66-68*).

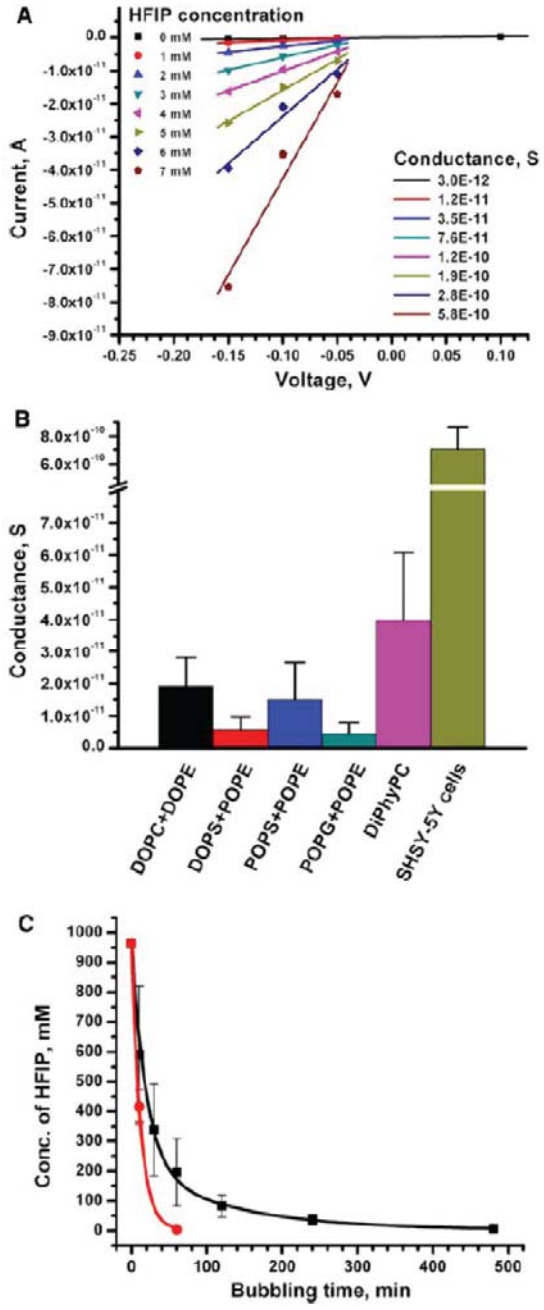

Figure 2-2. Transmembrane ion flux induced by samples containing well-defined concentrations of HFIP as well as removal of HFIP from Aβ samples as a function of the time of purging with nitrogen gas. **A)** Current versus voltage curves of transmembrane

conductance as a function of HFIP concentration (Aβ was not present in these experiments). The slopes of the linear best fits represent the conductance (in Siemens, $S = \Omega^{-1}$) of ions across a planar lipid bilayer made from a 1:1 (w/w) mixture of DOPS and POPE. The absolute magnitudes of these conductance values varied between repeated experiments and between different membrane compositions; however, the relative dose-response effect of increasing concentration of HFIP on the conductance remained the same. **B)** Transmembrane conductance induced by 1 mM HFIP (equivalent to 0.01% v/v) in planar lipid bilayers of various lipid compositions and by ~6 mM HFIP in cell membranes. All indicated lipid mixtures were prepared in a 1:1 (w/w) ratio. All experiments were repeated at least three times, the error bars represent the standard deviation from the mean conductance. **C)** Removal of HFIP from samples containing 100 μL of HFIP and 900 μL of water (concentration of HFIP ~1 M) as a function of purging time with nitrogen gas. The data indicated by red circles correspond to a flow rate of N_2 gas of ~30 mL min^{-1}. The data indicated by black squares correspond to a flow rate of 2-3 mL min^{-1}. All points represent average values (± standard deviation) from 2-6 repeated experiments. Note, for purging times longer than 10 min with a flow rate of ~30 mL min^{-1}, we observed that significant amounts of the foam that formed during purging escaped the microtube, thus rendering this flow rate impractical for purging times longer than 10 min.

Since HFIP induced a significant, gradual increase in transmembrane ion flux in all tested membranes, we investigated its toxicity on SH-SY5Y cells using the MTT viability assay. We found that HFIP was toxic to SH-SY5Y cells in a dose-dependent manner: a concentration of HFIP of ~30 mM (~0.3% v/v) reduced the viability of SH-SY5Y cells to 50% (*Fig.* 2-3). At HFIP concentrations above ~60 mM (~0.6% v/v), we

observed a 90% reduction in viability of these cells.[4] Based on these results, we emphasize that it is critically important to remove HFIP completely before attempting to investigate the effect of Aβ or other samples prepared with HFIP, on cytotoxicity or on bilayer membranes.

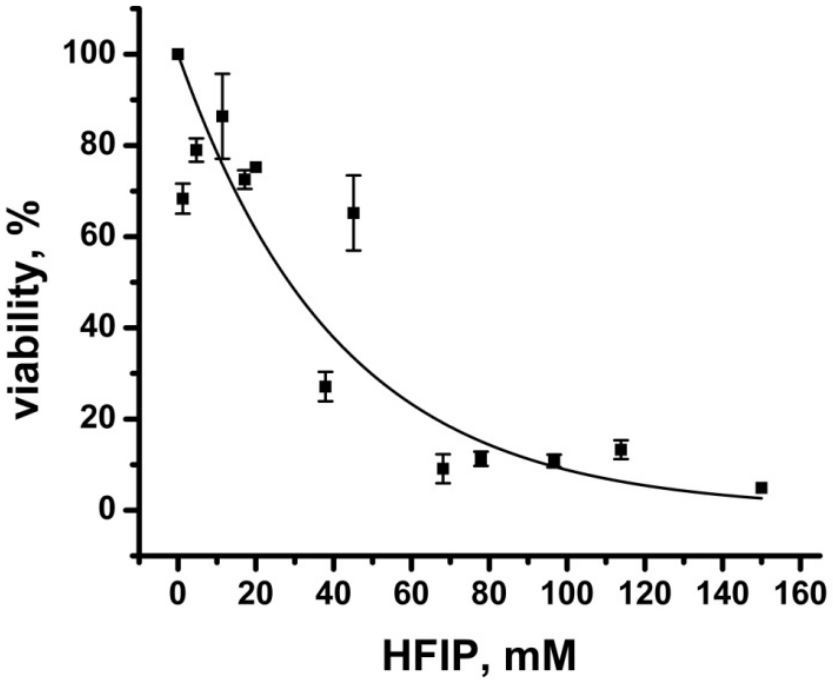

Figure 2-3. Viability of human SH-SY5Y neuroblastoma cells as a function of overnight exposure to increasing concentrations of HFIP. Data are represented relative to control cells that were treated the same way but without HFIP (corresponding to 100% viability). The solid line represents a best fit to a first order exponential decay function of the form:

Viability (%) = 100% × $e^{-([HFIP] \text{ in mM } / (41.2 \pm 1.2) \text{ mM})}$, N = 13, R^2 = 0.91.

[4] For comparison, the ethanol concentration necessary to achieve similar cell toxicity is higher than 200 mM (*69*)

In order to examine the contribution of HFIP to the reported transmembrane ion flux across lipid bilayers in detail, we determined the residual concentration of HFIP after purging Aβ samples (*Fig*. 2-2C). In the previously described protocol of preparing Aβ samples by purging of HFIP (*23, 36-39, 64*), the Aβ samples were subjected to a gentle stream of N_2 gas for 5-10 min. We found by gas chromatography and mass spectrometry (GC-MS) analysis of Aβ samples prepared in the same fashion that the residual concentrations of HFIP exceeded 200 mM in the Aβ samples (*Fig.* 2-2C) even after purging for 30 min at a flow rate of 2-3 mL min^{-1} or after purging for 10 min at a fast flow rate of ~30 mL min^{-1} (purging times longer than 10 min at this fast flow rate were not practical since they led to loss of Aβ by excessive foam formation). Addition of these Aβ samples to planar lipid bilayers or to cell membranes led to a gradual increase in transmembrane ion flux that was similar to the one shown in *Fig.* 2-1B (the final concentration of HFIP in the bilayer chamber ranged from 5 to 20 mM). These results suggest that the reported gradual increase in conductance (*37-39*) was due to incomplete removal of residual HFIP in these Aβ samples. In contrast, when we purged HFIP from Aβ samples for 18 h, we found that 1) the residual concentration of HFIP in the Aβ samples was consistently below 10 mM and 2) that addition of these Aβ samples to membranes (which resulted in a final concentration of HFIP below 0.2 mM) did not result in a gradual increase in ion flux. Instead, we observed in ~75% of these experiments a stepwise ion flux as reported previously by several research groups (*Fig*.

2-1C) (*1-20, 22, 30-35*).[5] These ion channel-like current fluctuations were reminiscent of the originally reported Aβ-induced transmembrane ion flux that led to the Aβ ion channel hypothesis in AD (*1, 22*). For comparison, *Fig.* 2-1D shows such stepwise current fluctuations through planar lipid bilayers using the original protocol for preparation of Aβ samples (*1*) that did not employ HFIP (or using a protocol for preparation of Aβ samples that removed HFIP completely by lyophilization for two days prior to dissolving Aβ in aqueous solution).

The results presented here, along with evidence from other groups (*1-20, 30-34, 70-72*), clearly demonstrate that Aβ peptides are indeed capable of forming ion pores in artificial membranes. They also show that stepwise ion flux is the predominant mode of ion flux across artificial bilayers provided that the samples of Aβ are free of organic solvent. If gradual thinning would be the predominant mechanism of Aβ-induced ion flux, then we would have expected to detect a gradual shift of the recorded current baseline under the same conditions where we observe measurable stepwise ion flux. Since all solvent-free Aβ preparations that we tested did not lead to gradual shifts in current baseline, we conclude that the postulated effect of Aβ to lower the dielectric barrier by gradual thinning of membranes – if existent – is small compared to the ion flux induced by Aβ pores. We also note that, to the best of our knowledge, all reports that observed gradual membrane thinning employed Aβ samples that were prepared with HFIP in combination with relatively short durations of purging (< 30 min) by a gentle gas

[5] In the remaining ~25% of the trials, we observed a flat baseline without any detectable transmembrane current.

stream (*37*-*39*). We, therefore, attribute the reported gradual increase in ion flux to residual HFIP in Aβ samples. This conclusion resolves the controversy with regard to Aβ-induced ion flux across artificial lipid bilayers; the results presented here confirm that Aβ can form ion pores in bilayer membranes.

After establishing the stepwise nature of Aβ-induced ion flux through planar lipid bilayers, two questions remain: 1) can Aβ form ion pores in *cellular* membranes and 2) what is the predominant mechanism of Aβ-induced ion flux across these cellular membranes? These questions are difficult to answer definitively because of the many direct and indirect pathways that can lead to ion flux in living cells. Here, we provide additional evidence in support of the hypothesis that Aβ is capable of forming independent pores in cellular membranes (*8*).

In order to compare ion flux induced by Aβ in artificial lipid bilayers with Aβ-induced ion flux across cellular membranes, we performed whole-cell patch clamp recordings on a human neuroblastoma cell line (SH-SY5Y cells) that we exposed to an exogenously introduced Aβ preparation (prepared after completely removing HFIP by lyophilization for two days). In addition, we carried out whole-cell recordings from transgenic, primary neurons that produced Aβ endogenously. In both cell types, we performed all recordings close to the resting membrane potential of the cells (*i.e.*, at a constant applied voltage of -80 mV) in order to minimize the activity of voltage-gated ion channel proteins that are naturally (endogenously) expressed in cells.

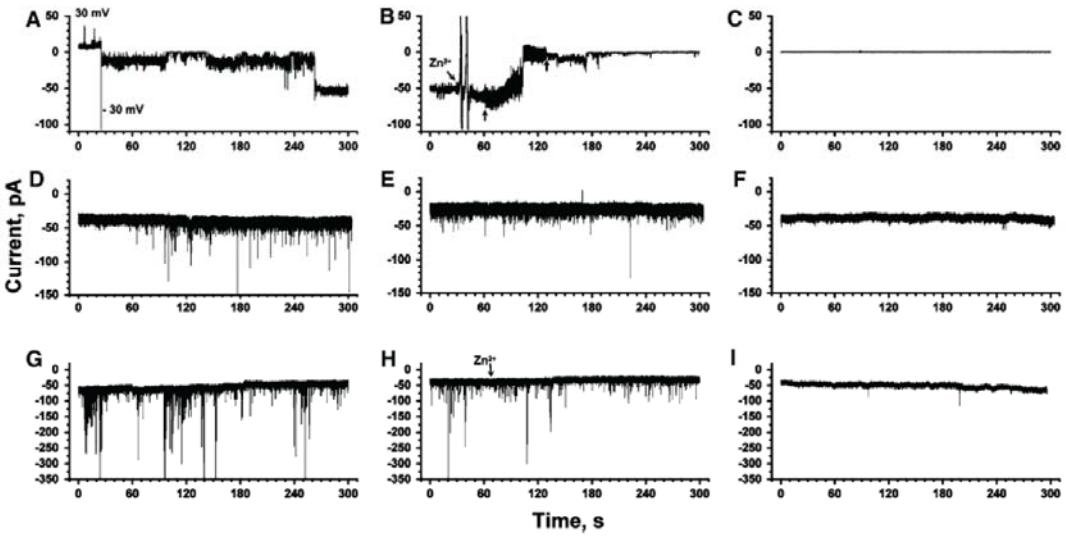

Figure 2-4. Comparison of Aβ-induced transmembrane ion flux across planar lipid bilayers, across plasma membranes of a neuroblastoma cell line, and across plasma membranes of primary cortical neurons from mouse embryos. **A)** Aβ-induced ion flux across a planar lipid bilayer (1:1 w/w POPC:POPE). Aβ was introduced by proteoliposome fusion (final concentration of Aβ = 1-2 μM). The applied potential was +30 mV or –30 mV as indicated. **B)** Effect of the addition (arrow) of Zn^{2+} on the same membrane as in (A). The small vertical arrows indicate the beginning and end of mixing. **C)** Control experiment with a membrane of the same composition as in (A) and (B) that did not contain Aβ. **D)** Whole-cell planar patch clamp recording of Aβ-induced transmembrane currents across the plasma membrane of human neuroblastoma cells (SH-SY5Y). Aβ was added to a final concentration of ~10 μM to the extracellular solution. The applied potential was –80 mV. **E)** Recording from the same cell and under the same conditions as in (D) but after addition of ~2 mM Zn^{2+} to the extracellular solution. **F)** Control experiment of a whole-cell recording from a SH-SY5Y cell in the absence of Aβ in the extracellular solution. **G)** Whole-cell planar patch clamp recording from a primary cortical neuron of a transgenic mouse embryo that expressed human Aβ endogenously. The applied potential was -80 mV. **H)** Effect of the addition of Zn^{2+} on a recording from the same cell as in (G). **I)** Control experiment with a wild-type cortical neuron that did not express Aβ.

Figure 2-4 shows stepwise (or spike-like) Aβ-induced transmembrane ion flux in both cell types, regardless of whether Aβ was added exogenously (*Fig.* 2-4D) or produced endogenously by transgenic primary neurons (*Fig.* 2-4G). It also demonstrates that both cell types showed no (or very rare) current fluctuations in the absence of Aβ (*Fig*. 2-4F, I). We performed sixteen recordings of Aβ ion channel activity on SY-SH5Y cells and observed Aβ-induced ion flux in twelve experiments (~75%), while addition of Aβ induced no changes in ion flux in the remaining four experiments. Typically Aβ-induced current spikes occurred 5-15 min after addition of Aβ, but in at least one recording the activity started within less than 30 s suggesting that Aβ can induce a measurable current flux quite rapidly.

In the case of the primary transgenic neurons, we recorded from eight cells that were extracted from three different transgenic embryos; seven of these recordings (~88%) showed a significant increase in the frequency of current spikes (*Fig*. 2-4G) compared to control recordings from wild-type neurons (*Fig*. 2-4I). Only one of eleven control recordings from primary, wild-type neurons showed a frequency in current fluctuations similar to transgenic neurons; the other ten control cells displayed a significantly lower frequency of current spikes than transgenic neurons.

Since Zn^{2+} ions have previously been reported to block Aβ-induced stepwise ion flux (*7, 8, 12, 18, 35, 73, 74*), we added Zn^{2+} to determine its effect on the observed current fluctuations. In both, the SH-SY5Y and the transgenic cells, addition of Zn^{2+} reduced Aβ-induced ion flux significantly (*Figs*. 2-4E and 2-4H). The inhibitory effect of Zn^{2+} in these two cell types was similar to the Zn^{2+}-induced inhibition of Aβ ion channels

in artificial lipid bilayers (*Fig.* 2-4B).

As mentioned above, control experiments, in which Aβ was neither introduced exogenously nor produced endogenously, did not result in significant stepwise or spike-like ion flux under the same experimental conditions (*Figs*. 2-4F and 2-4I), indicating that Aβ was required to induce measurable ion flux across cellular membranes. These results hence pose the question: did this measurable ion flux result from activation of endogenous, cellular ion channel proteins or was it a consequence of self-assembly of Aβ to pores in cellular membranes?

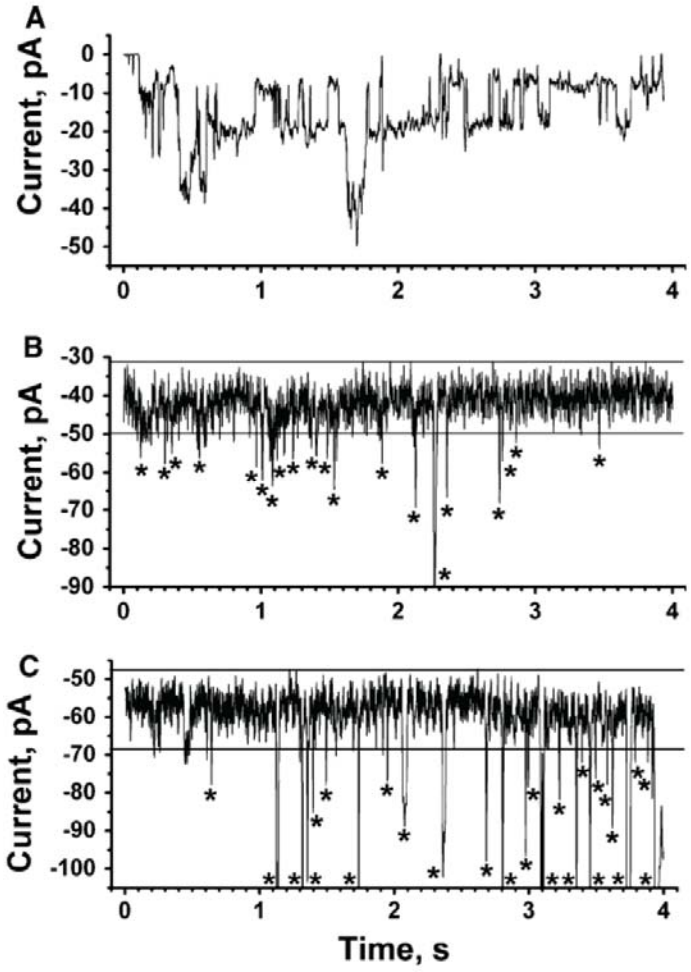

Figure 2-5. Comparison of short recordings with expanded time axis of Aβ-induced ion flux across planar lipid bilayers, across plasma membranes of SH-SY5Y cells, and across plasma membranes of transgenic cortical neurons. **A)** Aβ-induced ion flux through a planar lipid bilayer. The final concentration of Aβ was 10 μM (applied potential -30 mV). **B)** Aβ-induced ion flux through membranes of SH-SY5Y cells. The final concentration of Aβ was ~10 μM in the extracellular solution (applied potential -80 mV). Current fluctuations significantly above baseline current noise are indicated with an asterisk. **C)** Aβ-induced ion flux through the plasma membranes of a cortical neuron that expressed Aβ (applied potential -80 mV). Current fluctuations significantly above baseline current noise are indicated with an asterisk.

A comparison of Aβ-induced ion flux (*Fig.* 2-5) revealed that the average duration of stepwise (spike-like) current fluctuations was significantly longer in bilayer experiments than in cellular recordings (although bilayer experiments also revealed short-lived events). In contrast, the duration of Aβ-induced current events was similar in SH-SY5Y cells compared to transgenic primary neurons. The frequency of large-amplitude current events (*i.e.*, events that were larger than four times the standard deviation of the current noise) ranged from ~3 Hz in SH-SY5Y cells to ~10 Hz in bilayer experiments and was, thus, similar in magnitude. The single channel conductance of events ranged between 0.2-1.7 nS in planar lipid bilayers and between 0.2-0.6 nS in both SH-SY5Y cells and transgenic neurons. Although these conductance values are not directly comparable (since the ion concentrations and lipid compositions in the bilayer and cellular experiments could not be matched precisely), this comparison suggests that the conductance of Aβ-induced stepwise ion flux in bilayers and live cells was on the same order of magnitude.

In order to minimize the possibility that endogenous, cellular ion channels would be activated by Aβ, we performed all recordings close to the resting membrane potential (-80 mV) and we added a mixture of ion channel blockers to the extracellular solution; this mixture included (final concentration in the extracellular solution): 20 mM tetraethylammonium (TEA) ions to block potassium channels (*75-78*), 1 μM tetrodotoxin to block sodium channels (*77-79*), 2 μM nifedipine to block L-type calcium channels, and 2 μM ω-conotoxin to block N-type calcium channels (*80-85*). *Fig*. 2-6A shows that Aβ-induced ion flux persisted in the presence of these blockers. Only the addition of Zn^{2+} caused a significant reduction in Aβ-induced, large-amplitude current fluctuations in

these cells. Since Aβ ion channels in artificial bilayers are blocked effectively by Zn^{2+} (*Fig*. 2-4B), the Zn^{2+}-dependent blockage of Aβ-induced ion flux shown in *Fig.* 2-6A suggests that Aβ is also capable of forming ion channels in live cells. These results do not exclude the possibility that Aβ may activate endogenous cellular channels; these channels would, however, have to fulfill at least three characteristics: 1) they would have to be activated at -80 mV, 2) they would have to be insensitive to the cocktail of blockers, and 3) they would have to be sensitive to Zn^{2+} ions.

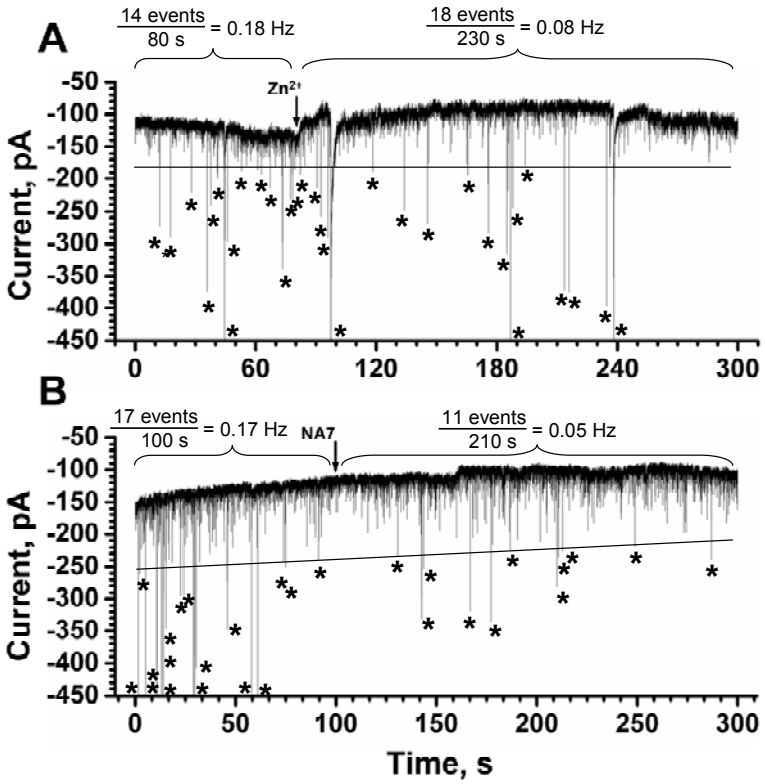

Figure 2-6. Reduction of Aβ-induced ion flux across the plasma membrane of SH-SY5Y cells by Zn^{2+} ions or NA7 peptides. **A)** Effect of Zn^{2+} (final concentration ~2 mM) on Aβ-induced ion flux. Note, these recordings were carried out in the presence of a mixture of

ion channel blockers containing 20 mM TEA, 1 μM tetrodotoxin, 2 μM nifedipine, and 2 μM ω-conotoxin; these ion channel blockers did not affect Aβ-induced ion flux but reduced the probability that intrinsic ion channels may be responsible for the observed current spikes. Large-amplitude current spikes, *i.e.* spikes with amplitudes above the threshold (black solid line), are indicated with an asterisk. **B)** Effect of NA7 peptide (final concentration ~100 μM) on Aβ-induced transmembrane ion flux. Large-amplitude current spikes, *i.e.* spikes with amplitudes above the threshold (black solid line), are indicated with an asterisk. Both recordings were carried out with an applied potential of –80 mV.

Since it is, in principle, possible that Zn^{2+} ions blocked endogenous, cellular ion channels, we also tested the effect of a specific blocker of Aβ-induced transmembrane ion flux in these cell experiments. Arispe and coworkers reported that a peptide called NA7 (corresponding to the amino acid sequence EVHHQKL of residues 11 to 17 of Aβ, is an effective and specific blocker of Aβ ion channels (*19, 86*). When we tested this peptide in SH-SY5Y cells, we found, in three of four recorded cells, up to a 3-fold reduction in the frequency of large-amplitude channel events induced by Aβ (*Fig*. 2-6B). This result further supports the hypothesis that Aβ can form independent ion channels in cellular membranes by self-assembly.

2.3 Conclusion

In conclusion, the work presented here demonstrates that Aβ can form stepwise transmembrane ion flux in artificial membranes. The previously postulated membrane thinning that was reported to lead to gradual increase in transmembrane ion flux is likely not attributable to Aβ, but instead is due to residues of the solvent HFIP used to prepare samples of Aβ. We found that HFIP is membrane-active and cytotoxic in the low

millimolar range. Therefore, it is critical to remove HFIP in any amyloid samples before they are used in membrane or cellular studies. In addition, we present evidence that Aβ is capable of inducing stepwise transmembrane ion fluctuations in living cells. Although we cannot rule out the possibility that Aβ activates intrinsic ion channels or ion pumps in cells, the results presented here suggest that Aβ is capable of self-assembling into independent ion channels. This conclusion is based on the following four observations: 1) Since Aβ clearly forms stepwise ion fluctuations in planar lipid bilayers, it is plausible that it can form similar transmembrane ion fluctuations in cellular membranes. 2) Aβ-induced stepwise ion fluctuations in cellular membranes occur at the resting potential of cells (where the activity of intrinsic ion channels is minimal) and persist in the presence of molecules that block the most common ion channel proteins. 3) In contrast, these Aβ-induced stepwise ion fluctuations in cellular membranes are blocked by Zn^{2+} ions and a heptapeptide derived from the sequence of Aβ (both Zn^{2+} ions and this heptapeptide are known to block Aβ ion channels in artificial bilayers (*86*)). 4) Finally, Aβ-induced stepwise ion fluctuations in cellular membranes resemble Aβ-induced stepwise ion fluctuations in artificial membranes with regards to their frequency and amplitude of current events. Based on these observations, we conclude that the formation of ion channels from Aβ could contribute to disruption of Ca^{2+} homeostasis that is commonly associated with Alzheimer's disease.

2.4 Materials and methods

2.4.1 Chemicals

We purchased $A\beta_{1-40}$ and $A\beta_{1-42}$ from Biopeptides Inc. and from Bachem Inc., hexafluoroisopropanol (HFIP) (GC grade) from Fluka, and the following seven lipids from Avanti Polar Lipids: 1-Palmitoyl-2-Oleoyl-*sn*-Glycero-3-Phosphoethanolamine (POPE), 1-Palmitoyl-2-Oleoyl-*sn*-Glycero-3-[Phospho-L-Serine] (POPS), 1,2-Dioleoyl-*sn*-Glycero-3-Phosphocholine (DOPC), 1,2-Dioleoyl-*sn*-Glycero-3-Phosphoethanolamine (DOPE), 1,2-Dioleoyl-*sn*-Glycero-3-Phosphoserine (DOPS), 1,2-Diphytanoyl-*sn*-Glycero-3-Phosphocholine (DiPhyPC), 1-Palmitoyl-2-Oleoyl-*sn*-Glycero-3-[Phospho-*rac*-(1-glycerol)] (POPG). All other chemicals were purchased from Sigma Aldrich; SH-SY5Y cells were obtained from ATCC.

2.4.2 Preparation of solutions of Aβ by purging HFIP with nitrogen gas

We prepared samples of Aβ by following exactly a previously reported protocol (*23, 36-39*). Briefly, we dissolved 1 mg of Aβ peptide in 400 μL of HFIP and incubated this solution for 15 min. We mixed 100 μL of the resulting, clear Aβ solution in HFIP with 900 μL of deionized water in a siliconized 1.5 mL microtube. After incubation at room temperature for 15 min, we centrifuged the samples for 15 min at 14,000 $\times$ *g* and transferred the supernatant fraction (900 - 950 μL) to a new siliconized tube. To purge HFIP from these samples, we bubbled nitrogen gas for 10 min through these samples, while adjusting the gas flow to ~30 mL min^{-1}, which was the maximum flow rate that did not result in excessive foaming and splashing of the sample. For purging times longer than 10 min, we had to reduce the flow rate of the N_2 gas to 2-3 mL min^{-1} in order to

avoid significant loss of material due to slow but steady accumulation and expulsion of foam from the sample. We analyzed aliquots of these samples for residual HFIP concentration by gas chromatography-mass spectrometry (GC-MS) and tested their ability to induce transmembrane ion flux in planar lipid bilayers and cell membranes.

2.4.3 Quantification of HFIP concentrations by GC-MS analysis

This analysis was carried out by injecting a sample volume of 2 µL into a: Finnigan Trace GC-MS with the following settings: run in electron impact ionization mode using a 30 m long, 0.25 mm ID Supelco SLB-5 column, with a film thickness of 0.25 µm. Helium was used as carrier gas at a constant flow rate of 1.0 mL min^{-1}; the injector temperature was 200° C; the run was performed in split mode with a ratio of 1:100; the interface temperature was 250° C, and the ion source block temperature was 220° C. The temperature of the GC oven was held at 40° C for 2 min and then increased to 150° C at a rate of 40 C min^{-1}. The MS ion source filament was set to an emission current of 150 µA at 70 eV. HFIP standards and calibration curves were generated each day. Samples with unknown HFIP concentrations were measured using an external calibration curve; no internal standards were used. The quantification was based on the area under the GC peak in the chromatogram. Data was acquired and processed using Excalibur software, version 1.1.

2.4.4 Formation of planar lipid bilayers

The two reported original procedures that are at the basis of the controversy regarding the nature of Aβ-induced ion flux across artificial lipid membranes (*1, 36*) employed different methods to generate planar lipid bilayers. We, therefore, prepared

planar lipid bilayers (also called black lipid membranes or bilayer lipid membranes, BLMs) either by the so-called “folding technique” (*87-90*), which employs apposition of lipid monolayers over a pore with a diameter of ~150 μm in a Teflon film or by the so-called “painting technique” (*88, 91*), which applies a solution of lipids in decane or heptane over a pore with a diameter of ~250 μm in a Delrin septum.

For the folded bilayers (*Fig.* 2-1, *Fig.* 2-2B columns DOPC+DOPE and DiPhyPC), we pretreated the Teflon film with 2 μL of 5% (v/v) squalene in pentane and then formed the bilayers using 5 μL of either DiPhyPC or a 1:1 (w/w) mixture of a lipid solution in pentane that contained DOPC and DOPE. The total lipid concentration of these solutions in pentane was 20 - 25 mg mL^{-1} (*88, 92*). The electrolyte contained 70 mM KCl buffered with 10 mM HEPES, pH 7.4.

For the painted bilayers, we used a bilayer cup (Warner Instruments, Delrin perfusion cup, volume 1 mL) and the following four lipid mixtures at a 1:1 (w/w) ratio: POPG : POPE, DOPS : POPE, or DOPC : DOPE in heptane, or POPE : POPS in decane. The total lipid concentration of these solutions in heptane or decane was 10 - 20 mg mL^{-1}. In order to promote fusion of Aβ proteoliposomes into bilayers, we used an ionic gradient formed by filling the cis side (the side of proteoliposome addition) with 370 mM KCl and the trans side of the bilayer setup with 70 mM KCl. For these experiments, we prepared bilayers using a 1:1 (w/w) mixture of DOPC and DOPE (*Fig.* 2-1D) or POPC and POPE (*Fig.* 2-4 panels A, B, and C); the proteoliposomes containing Aβ were prepared as described previously (*1*).

2.4.5 Incorporation of Aβ into lipid membranes

In order to repeat the procedure for preparing Aβ samples that was previously

described to lead to membrane thinning of planar lipid bilayers (*23, 36-39*), we prepared Aβ samples by using the solvent HFIP exactly as described and added the resulting solutions to both compartments of the bilayer chamber. We diluted these samples more than 50-fold such that the final concentration of Aβ was 0.5-2.0 μM in each chamber of the bilayer setup.

In order to repeat the alternative Aβ procedure, which was previously described to lead to stepwise ion flux across planar lipid bilayers (*1*), we added 10-20 μL of the Aβ proteoliposome solution (this solution contained Aβ at a concentration of 0.4 - 0.8 mg mL^{-1}) to the cis compartment (volume 1 mL) and stirred for 5-10 min. All planar lipid bilayers experiments with each lipid composition were performed at least 3 times, more typically 5-7 times.

2.4.6 Current recordings

Before carrying out bilayer recordings, we verified that both, the painted and the folded bilayers were stable for several minutes (while applying a voltage of at least ± 100 mV) and that the membrane capacitances were above 90 pF. When both criteria were fulfilled, we added Aβ (0.5-4.0 μM final concentration of Aβ) or HFIP (0.5-7.0 mM final concentration of HFIP without any Aβ present) to both chambers of the bilayer setup.

We performed all recordings in “voltage clamp mode” using Ag/AgCl electrodes. We used a filter-cutoff frequency of 2 kHz, and a sampling frequency of 15 kHz for all bilayer recordings. For representation in figures, we filtered the current traces with a digital Gaussian low-pass filter with a cutoff frequency of 100 Hz.

For whole-cell patch clamp recordings, we used the following three solutions: 1)

intracellular solution containing 75 mM KCl, 10 mM NaCl, 70 mM KF, 2 mM $MgCl_2$, 10 mM EGTA, and 10 mM HEPES buffer (pH 7.2), 2) extracellular solution containing 160 mM NaCl, 4.5 mM KCl, 1 mM $MgCl_2$, 2 mM $CaCl_2$, 5 mM D-glucose, and 10 mM HEPES buffer (pH 7.4), and 3) a "seal enhancer" solution containing 80 mM NaCl, 3 mM KCl, 10 mM $MgCl_2$, 35 mM $CaCl_2$ and 10 mM HEPES/NaOH (pH 7.4), which was added to the extracellular compartment to promote the formation of seals between the cells and the glass chip with electrical resistances higher than 1 GΩ.

In order to introduce Aβ into membranes of SH-SY5Y cells, we first established whole-cell recording conditions followed by adding ~5 μL of extracellular solution containing Aβ to a volume of ~20 μL of extracellular solution (this Aβ solution was prepared without the use of HFIP by stirring for ~14 h at room temperature prior to use). The final concentration of Aβ in the extracellular solution during the recording was ~10 μM.

In order to measure the effect of Aβ and HFIP samples on SH-SY5Y cells, we used a semi-automated, chip-based electrophysiology instrument (Port-a-patch, Nanion Inc.) that allowed for recordings with seal resistances of 1-6 GΩ. We held the voltage at -80 mV in the intracellular compartment versus ground in the extracellular compartment to measure Aβ-induced ion channel activity. At this potential, SH-SY5Y cells did not show significant intrinsic ion channel activity. Samples containing Aβ or HFIP were only added after confirming the stability of the recording (*i.e.*, after observing a quiescent baseline for 3-5 min). For all whole-cell recordings, we used a filter cutoff frequency of 1 kHz.

In order to determine the effect of Zn^{2+} ions or the peptide NA7 on Aβ-induced transmembrane ion flux, we added 1-10 mM (final concentration) of $ZnCl_2$ or $Zn(NO_3)_2$ or 100 – 140 μM (final concentration) of the NA7 peptide to the bilayer chambers or to the extracellular solutions.

2.4.7 Preparation of primary neurons

Wild type female mice (C57BL/6J) were crossed with double transgenic hAPPswe/hPS-1ΔE9 male mice, obtained from Jackson Laboratory (Bar Harbor, Maine) to generate wild-type, and hAPPswe/hPS-1 transgenic embryos. Primary cortical neuron cultures were prepared from the brains of E16 embryos. Briefly, the cerebral cortices were dissected in calcium-free and magnesium-free Hank's balanced salt solution and incubated with a 0.125% trypsin solution for 10 min at 37°C. The trypsin was inactivated with Dulbecco's modified Eagle's medium containing 10% fetal bovine serum, and the cortical tissue was further dissociated by serial trituration using a Pasteur pipette. The resulting cell suspensions were diluted in neurobasal medium supplemented with B27 supplements (Gibco BRL, Grand Island, New York, USA), and plated onto poly-D-lysine-coated Petri dishes. Neurons were maintained at 37°C in a 5% CO_2 atmosphere for 4-7 days, before the experiments (*93*). We carried out the planar patch-clamp experiments between day 4 and day 7 of culture. The neurons were detached using a protocol previously described and validated by Lecoeur *et al.* with minor modifications (*94*). These modifications entailed: 1) reducing the incubation time with trypsin-EDTA from 15 to 14 min at 37° C and 2) dissociating cell aggregates by increasing the number of successively aspirating and dispensing the cell suspension to 7 times with a 1 mL pipette tip and to 15 times with a 200 μL pipette tip.

2.4.8 Cytotoxicity assay of HFIP with SH-SY5Y cells

We cultured SH-SY5Y human neuroblastoma cells in DMEM/F-12 (1:1) medium with 10% fetal bovine serum, 4 mM glutamax, penicillin (100 units mL^{-1}) and streptomycin (100 µg mL^{-1}) in 5% CO_2 at 37° C. We plated cells in 96-well plates overnight starting with 50,000 cells $well^{-1}$. After overnight incubation at 37 °C, we exchanged the media with Opti-MEM, and treated cells for 24 h. We determined the cell viability using an MTT toxicology kit (Tox-1, from Sigma) according to the instructions from the supplier.

Acknowledgements

This work was supported by the Wallace H. Coulter Foundation and a NSF Career Award 02-111 (M.M.). M.R.B and J.Y. acknowledge support from the Alzheimer's Disease Research Center (3P50 AG005131) and a grant from the Alzheimer's Association (NIRG-08-91651). P.P. acknowledges a fellowship from the government of Thailand. A.M.S. acknowledges a scholarship from Solvay Inc. We thank James Windak from the University of Michigan, Instrument Services, for measurements of HFIP concentrations by GC-MS.

References

1. Arispe, N., Rojas, E., and Pollard, H. B. (1993) Alzheimer-Disease Amyloid b-Protein Forms Calcium Channels in Bilayer-Membranes - Blockade by Tromethamine and Aluminum, *Proc. Nat. Acad. Sci (USA)* 90, 567-571.
2. Arispe, N., Pollard, H. B., and Rojas, E. (1993) Giant Multilevel Cation Channels Formed by Alzheimer-Disease Amyloid Beta-Protein Ab-P-(1-40) in Bilayer-Membranes, *Proc. Nat. Acad. Sci (USA)* 90, 10573-10577.
3. Baglioni, S., Casamenti, F., Bucciantini, M., Luheshi, L. M., Taddei, N., Chiti, F., Dobson, C. M., and Stefani, M. (2006) Prefibrillar Amyloid Aggregates Could Be Generic Toxins in Higher Organisms, *J. Neurosci*. 26, 8160-8167.
4. Bahadi, R., Farrelly, P. V., Kenna, B. L., Curtain, C. C., Masters, C. L., Cappai, R., Barnham, K. J., and Kourie, J. I. (2003) Cu^{2+}-induced modification of the kinetics of Ab(1-42) channels, Am *J Physiol Cell Physiol* 285, C873-880.
5. Bhatia, R., Lin, H., and Lal, R. (2000) Fresh and globular amyloid b protein (1-42) induces rapid cellular degeneration: evidence for AbP channel-mediated cellular toxicity, *FASEB J.* 14, 1233-1243.
6. Devi, L., Prabhu, B. M., Galati, D. F., Avadhani, N. G., and Anandatheerthavarada, H. K. (2006) Accumulation of Amyloid Precursor Protein in the Mitochondrial Import Channels of Human Alzheimer's Disease Brain Is Associated with Mitochondrial Dysfunction, *J. Neurosci.* 26, 9057-9068.
7. Kagan, B. L., Azimov, R., and Azimova, R. (2004) Amyloid Peptide Channels, *J. Membrane Biol*. 202, 1-10.
8. Kawahara, M., Arispe, N., Kuroda, Y., and Rojas, E. (1997) Alzheimer's disease amyloid b-protein forms Zn^{2+}-sensitive, cation-selective channels across excised membrane patches from hypothalamic neurons, *Biophys. J*. 73, 67-75.
9. Khachaturian, Z. S. (1987) Hypothesis on the Regulation of Cytosol Calcium Concentration and the Aging Brain, *Neurobiol Aging* 8, 345-346.
10. Koh, J.-y., Yang, L. L., and Cotman, C. W. (1990) b-Amyloid protein increases the vulnerability of cultured cortical neurons to excitotoxic damage, Brain Res. 533, 315-320.
11. Lal, R., Lin, H., and Quist, A. P. (2007) Amyloid β ion channel: 3D structure and relevance to amyloid channel paradigm, *BBA- Biomembranes* 1768, 1966-1975.
12. Lin, H., Zhu, Y. J., and Lal, R. (1999) Amyloid b Protein (1-40) Forms Calcium-Permeable, Zn2+-Sensitive Channel in Reconstituted Lipid Vesicles, *Biochemistry* 38, 11189-11196.
13. Lin, H., Bhatia, R., and Lal, R. (2001) Amyloid b protein forms ion channels: implications for Alzheimer's disease pathophysiology, *FASEB J* 15, 2433-2444.
14. Mark, R., Hensley, K., Butterfield, D., and Mattson, M. (1995) Amyloid β-peptide impairs ion-motive ATPase activities: evidence for a role in loss of neuronal Ca^{2+} homeostasis and cell death, *J. Neurosci*. 15, 6239-6249.
15. Mattson, M. P., and Chan, S. L. (2003) Calcium orchestrates apoptosis, *Nat Cell Biol* 5, 1041-1043.
16. Palop, J. J., Chin, J., Roberson, E. D., Wang, J., Thwin, M. T., Bien-Ly, N., Yoo, J., Ho, K. O., Yu, G.-Q., Kreitzer, A., Finkbeiner, S., Noebels, J. L., and Mucke, L. (2007) Aberrant Excitatory Neuronal Activity and Compensatory Remodeling of Inhibitory Hippocampal Circuits in Mouse Models of Alzheimer's Disease, *Neuron* 55, 697-711.
17. Quist, A., Doudevski, I., Lin, H., Azimova, R., Ng, D., Frangione, B., Kagan, B., Ghiso, J., and Lal, R. (2005) Amyloid ion channels: A common structural link for protein-misfolding disease, *Proc. Nat. Acad. Sci (USA)* 102, 10427-10432.
18. Rhee, S. K., Quist, A. P., and Lal, R. (1998) Amyloid b Protein-(1-42) Forms Calcium-permeable, Zn2+-sensitive Channel, *J. Biol. Chem.* 273, 13379-13382.

19. Simakova, O., and Arispe, N. J. (2006) Early and Late Cytotoxic Effects of External Application of the Alzheimer's Aβ *Biochemistry* 45, 5907-5915.
20. Simakova, O., and Arispe, N. J. (2007) The Cell-Selective Neurotoxicity of the Alzheimer's Aβ Peptide Is Determined by Surface Phosphatidylserine and Cytosolic ATP Levels. Membrane Binding Is Required for Aβ Toxicity, *J. Neurosci*. 27, 13719-13729.
21. Mattson, M., Cheng, B., Davis, D., Bryant, K., Lieberburg, I., and Rydel, R. (1992) b - Amyloid peptides destabilize calcium homeostasis and render human cortical neurons vulnerable to excitotoxicity, *J. Neurosci.* 12, 376-389.
22. Pollard, H. B., Rojas, E., and Arispe, N. (1993) A New Hypothesis for the Mechanism of Amyloid Toxicity, Based on the Calcium-Channel Activity of Amyloid-Beta Protein (Aβ -P) in Phospholipid-Bilayer Membranes, In Alzheimers Disease: Amyloid Precusor Proteins, Signal Transduction, and Neuronal Transplantation, pp 165-168.
23. Demuro, A., Mina, E., Kayed, R., Milton, S. C., Parker, I., and Glabe, C. G. (2005) Calcium Dysregulation and Membrane Disruption as a Ubiquitous Neurotoxic Mechanism of Soluble Amyloid Oligomers, *J. Biol. Chem*. 280, 17294-17300.
24. Stutzmann, G. E. (2007) The Pathogenesis of Alzheimers Disease Is It a Lifelong "Calciumopathy"?, *Neuroscientist* 13, 546-559.
25. Cheung, K.-H., Shineman, D., Müller, M., Cárdenas, C., Mei, L., Yang, J., Tomita, T., Iwatsubo, T., Lee, V. M. Y., and Foskett, J. K. (2008) Mechanism of Ca2+ Disruption in Alzheimer's Disease by Presenilin Regulation of InsP3 Receptor Channel Gating, *Neuron* 58, 871-883.
26. Kawahara, M., Kuroda, Y., Arispe, N., and Rojas, E. (2000) Alzheimer's b-Amyloid, Human Islet Amylin, and Prion Protein Fragment Evoke Intracellular Free Calcium Elevations by a Common Mechanism in a Hypothalamic GnRH Neuronal Cell Line, *J. Biol. Chem.* 275, 14077-14083.
27. Nimmrich, V., Grimm, C., Draguhn, A., Barghorn, S., Lehmann, A., Schoemaker, H., Hillen, H., Gross, G., Ebert, U., and Bruehl, C. (2008) Amyloid β Oligomers (A b1-42 Globulomer) Suppress Spontaneous Synaptic Activity by Inhibition of P/Q-Type Calcium Currents, *J. Neurosci*. 28, 788-797.
28. Khachaturian, Z. S. (1989) Introduction and Overview on Calcium, Membranes, Aging, and Alzheimer's Disease, *Ann. NY. Acad. Sci*. 568, 1-4.
29. Tu, H., Nelson, O., Bezprozvanny, A., Wang, Z., Lee, S.-F., Hao, Y.-H., Serneels, L., De Strooper, B., Yu, G., and Bezprozvanny, I. (2006) Presenilins Form ER Ca2+ Leak Channels, a Function Disrupted by Familial Alzheimer's Disease-Linked Mutations, *Cell* 126, 981-993.
30. Jang, H., Zheng, J., Lal, R., and Nussinov, R. (2008) New structures help the modeling of toxic amyloidß ion channels, *Trends in Biochem. Sci*. 33, 91-100.
31. Hirakura, Y., Lin, M.-C., and Kagan, B. L. (1999) Alzheimer amyloid b;1-42 channels: Effects of solvent, pH, and congo red, *J. Neurosci*. Res. 57, 458-466.
32. Micelli, S., Meleleo, D., Picciarelli, V., and Gallucci, E. (2004) Effect of Sterols on b-Amyloid Peptide (AbP 1-40) Channel Formation and their Properties in Planar Lipid Membranes, *Biophys. J*. 86, 2231-2237.
33. Kagan, B. L., Hirakura, Y., Azimov, R., Azimova, R., and Lin, M.-C. (2002) The channel hypothesis of Alzheimer's disease: current status, *Peptides* 23, 1311-1315.
34. Zhu, Y. J., Lin, H., and Lal, R. (2000) Fresh and nonfibrillar amyloid b protein(1-40) induces rapid cellular degeneration in aged human fibroblasts: evidence for AbP-channel-mediated cellular toxicity, *FASEB J*. 14, 1244-1254.
35. Kourie, J., Henry, C., and Farrelly, P. (2001) Diversity of Amyloid β Protein Fragment [1–40]-Formed Channels, *Cell. Mol. Neurobiol*. 21, 255-284.
36. Kayed, R., Head, E., Thompson, J. L., McIntire, T. M., Milton, S. C., Cotman, C. W., and Glabe, C. G. (2003) Common structure of soluble amyloid oligomers implies common mechanism of pathogenesis, *Science* 300, 486-489.

37. Kayed, R., Sokolov, Y., Edmonds, B., McIntire, T. M., Milton, S. C., Hall, J. E., and Glabe, C. G. (2004) Permeabilization of lipid bilayers is a common conformation-dependent activity of soluble amyloid oligomers in protein misfolding diseases, *J. Biol. Chem*. 279, 46363-46366.
38. Sokolov, Y., Kozak, J. A., Kayed, R., Chanturiya, A., Glabe, C., and Hall, J. E. (2006) Soluble Amyloid Oligomers Increase Bilayer Conductance by Altering Dielectric Structure, *J. Gen. Physiol*. 128, 637-647.
39. Sokolov, Y. V., Kayed, R., Kozak, A., Edmonds, B., McIntire, T. M., Milton, S., Cahalan, M., Glabe, C. G., and Hall, J. E. (2004) Soluble amyloid oligomers increase lipid bilayer conductance by increasing the dielectric constant of the hydrocarbon core, *Biophys. J*. 86, 382A-382A.
40. Deshpande, A., Mina, E., Glabe, C., and Busciglio, J. (2006) Different Conformations of Amyloid β Induce Neurotoxicity by Distinct Mechanisms in Human Cortical Neurons, *J. Neurosci*. 26, 6011-6018.
41. Dreses-Werringloer, U., Lambert, J.-C., Vingtdeux, V., Zhao, H., Vais, H., Siebert, A., Jain, A., Koppel, J., Rovelet-Lecrux, A., Hannequin, D., Pasquier, F., Galimberti, D., Scarpini, E., Mann, D., Lendon, C., Campion, D., Amouyel, P., Davies, P., Foskett, J. K., Campagne, F., and Marambaud, P. (2008) A Polymorphism in CALHM1 Influences Ca2+ Homeostasis, Aβ Levels, and Alzheimer's Disease Risk, *Cell* 133, 1149-1161.
42. Stutzmann, G. E., Smith, I., Caccamo, A., Oddo, S., LaFerla, F. M., and Parker, I. (2006) Enhanced Ryanodine Receptor Recruitment Contributes to Ca2+ Disruptions in Young, Adult, and Aged Alzheimer's Disease Mice, *J. Neurosci.* 26, 5180-5189.
43. Stutzmann, G. E., Smith, I., Caccamo, A., Oddo, S., Parker, I., and Laferla, F. (2007) Enhanced Ryanodine-Mediated Calcium Release in Mutant PS1-Expressing Alzheimer's Mouse Models, *Ann. NY.Acad. Sci*. 1097, 265-277.
44. Morimoto, T., Ohsawa, I., Takamura, C., Ishiguro, M., Nakamura, Y., and Kohsaka, S. (1998) Novel Domain-Specific Actions of Amyloid Precursor Protein on Developing Synapses, *J. Neurosci*. 18, 9386-9393.
45. Ye, C., Ho-Pao, C. L., Kanazirska, M., Quinn, S., Rogers, K., Seidman, C. E., Seidman, J. G., Brown, E. M., and Vassilev, P. M. (1997) Amyloid-b; proteins activate Ca2+-permeable channels through calcium-sensing receptors, *J. Neurosci. Res*. 47, 547-554.
46. Dougherty, J. J., Wu, J., and Nichols, R. A. (2003) β-Amyloid Regulation of Presynaptic Nicotinic Receptors in Rat Hippocampus and Neocortex, *J. Neurosci.* 23, 6740-6747.
47. Novarino, G., Fabrizi, C., Tonini, R., Denti, M. A., Malchiodi-Albedi, F., Lauro, G. M., Sacchetti, B., Paradisi, S., Ferroni, A., Curmi, P. M., Breit, S. N., and Mazzanti, M. (2004) Involvement of the Intracellular Ion Channel CLIC1 in Microglia-Mediated β-Amyloid-Induced Neurotoxicity, *J. Neurosci*. 24, 5322-5330.
48. Ueda, K., Shinohara, S., Yagami, T., and Asakura, K. (1997) Amyloid β Protein Potentiates Ca2+ Influx Through L-Type Voltage-Sensitive Ca^{2+} Channels: A Possible Involvement of Free Radicals, *J. Neurochem*. 68, 265-271.
49. Verdier, Y., Zarándi, M., and Penke, B. (2004) Amyloid b-peptide interactions with neuronal and glial cell plasma membrane: binding sites and implications for Alzheimer's disease, *J.Pept. Sci*. 10, 229-248.
50. Wang, H.-Y., Lee, D. H. S., Davis, C. B., and Shank, R. P. (2000) Amyloid Peptide Aβ1-42 Binds Selectively and with Picomolar Affinity to a7 Nicotinic Acetylcholine Receptors, *J. Neurochem*. 75, 1155-1161.
51. Yankner, B. A., Duffy, L. K., and Kirschner, D. A. (1990) Neurotrophic and Neurotoxic Effects of Amyloid b Protein: Reversal by Tachykinin Neuropeptides, *Science* 250, 279-282.
52. Yankner, B. A., Caceres, A., and Duffy, L. K. (1990) Nerve growth factor potentiates the neurotoxicity of b amyloid, *Proc. Nat. Acad. Sci (USA)* 87, 9020-9023.

53. Joslin, G., Krause, J., Hershey, A., Adams, S., Fallon, R., and Perlmutter, D. (1991) Amyloid-b peptide, substance P, and bombesin bind to the serpin- enzyme complex receptor, *J. Biol. Chem*. 266, 21897-21902.
54. Rovira, C., Arbez, N., and Mariani, J. (2002) Aβ(25-35) and Aβ(1-40) act on different calcium channels in CA1 hippocampal neurons, *Biochem. Biophys. Res. Commun*. 296, 1317-1321.
55. Lopez, J. R., Lyckman, A., Oddo, S., LaFerla, F. M., Querfurth, H. W., and Shtifman, A. (2008) Increased intraneuronal resting [Ca^{2+}] in adult Alzheimer's disease mice, *J. Neurochem*. 105, 262-271.
56. Fedrizzi, L., Lim, D., Carafoli, E., and Brini, M. (2008) Interplay of the Ca2+-binding protein DREAM with presenilin in neuronal Ca2+ signaling, *J. Biol. Chem.*, M804152200.
57. Querfurth, H. W., Jiang, J., Geiger, J. D., and Selkoe, D. J. (1997) Caffeine Stimulates Amyloid β-Peptide Release from b-Amyloid Precursor Protein-Transfected HEK293 Cells, *J. Neurochem*. 69, 1580-1591.
58. Green, K. N., Demuro, A., Akbari, Y., Hitt, B. D., Smith, I. F., Parker, I., and LaFerla, F. M. (2008) SERCA pump activity is physiologically regulated by presenilin and regulates amyloid b production, *J. Cell Biol*. 181, 1107-1116.
59. Lam, F. C., Liu, R., Lu, P., Shapiro, A. B., Renoir, J.-M., Sharom, F. J., and Reiner, P. B. (2001) β-Amyloid efflux mediated by p-glycoprotein, *J. Neurochem*. 76, 1121-1128.
60. Gennis, R. B. (1989) Biomembranes, 1 ed., Springer-Verlag, New York.
61. Eliezer, D. (2006) Amyloid Ion Channels: A Porous Argument or a Thin Excuse?, *J. Gen. Physiol.* 128, 631-633.
62. Marx, J. (2007) Alzheimer's disease - Fresh evidence points to an old suspect: Calcium, *Science* 318, 384-385.
63. Fagan T, K. B., Corbin D, Hwang W, Glabe C, Nault L, Lal R, Teplow D, Albensi B, Sokolov Y. (2006) Alzheimer Research Forum Live Discussion: Now you see them, now you don't: The amyloid channel hypothesis, *J. Alzheimers Dis*. 9, 219-224.
64. Valincius, G., Heinrich, F., Budvytyte, R., Vanderah, D. J., McGillivray, D. J., Sokolov, Y., Hall, J. E., and Losche, M. (2008) Soluble amyloid β oligomers affect dielectric membrane properties by bilayer insertion and domain formation: Implications for cell toxicity, *Biophys. J*. 95, 4845-4861
65. Ennaceur, S. M., and Sanderson, J. M. (2005) Micellar aggregates formed following the addition of hexafluoroisopropanol to phospholipid membranes, Langmuir 21, 552-561.
66. Ebihara, L., Hall, J. E., MacDonald, R. C., McIntosh, T. J., and Simon, S. A. (1979) Effect of benzyl alcohol on lipid bilayers. A comparison of bilayer systems, *Biophys. J.* 28, 185-196.
67. Gutknecht, J., and Tosteson, D. C. (1970) Ionic Permeability of Thin Lipid Membranes: Effects of n-alkyl alcohols, polyvalent cations, and a secondary amine, *J. Gen. Phys.* 55, 359-374.
68. Ueda, I., and Yoshida, T. (1999) Hydration of lipid membranes and the action mechanisms of anesthetics and alcohols, *Chem. Phys. Lipids* 101, 65-79.
69. Luo, J., and Miller, M. W. (1998) Growth factor-mediated neural proliferation: target of ethanol toxicity, *Brain Res. Rev*. 27, 157-167.
70. Mirzabekov, T., Lin, M. C., Yuan, W. L., Marshall, P. J., Carman, M., Tomaselli, K., Lieberburg, I., and Kagan, B. L. (1994) Channel Formation in Planar Lipid Bilayers by a Neurotoxic Fragment of the β-Amyloid Peptide, *Biochem. Biophys. Res. Commun*. 202, 1142-1148.
71. Hirakura, Y., Lin, M.-C., and Kagan, B. (1999) Erratum: Hirakura Y, Lin M-C, Kagan BL. 1999. Alzheimer amyloid b;1-42 channels: Effects of solvent, pH, and Congo Red. J Neurosci Res 57:458-466, J. Neurosci. Res. 58, 726.

72. Arispe, N. J., Diaz, J. C., and Flora, M. (2008) Efficiency of histidine-associating compounds for blocking the Alzheimer's Aβ channel activity and cytotoxicity, *Biophys. J* 95, 4879-4889.
73. Arispe, N., Pollard, H. B., and Rojas, E. (1996) Zn2+ interaction with Alzheimer amyloid b protein calcium channels, *Proc. Nat. Acad. Sci (USA)* 93, 1710-1715.
74. Lin, M.-c. A., and Kagan, B. L. (2002) Electrophysiologic properties of channels induced by Aβ25-35 in planar lipid bilayers, *Peptides* 23, 1215-1228.
75. Mathie, A., Wooltorton, J. R. A., and Watkins, C. S. (1998) Voltage-activated potassium channels in mammalian neurons and their block by novel pharmacological agents, *Gen. Pharmacol.* 30, 13-24.
76. Tosetti, P., Taglietti, V., and Toselli, M. (1998) Functional Changes in Potassium Conductances of the Human Neuroblastoma Cell Line SH-SY5Y During In Vitro Differentiation, *J. of Neurophys*. 79, 648-658.
77. Guyon, A., Rovère, C., Cervantes, A., Allaeys, I., and Nahon, J. L. (2005) Stromal cell-derived factor-1a; directly modulates voltage-dependent currents of the action potential in mammalian neuronal cells, *J. Neurochem*. 93, 963-973.
78. Forsythe, I. D., Lambert, D. G., Nahorski, S. R., and Linsdell, P. (1992) Elevation of Cytosolic Calcium by Cholinoceptor Agonists in SH-SY5Y Human Neuroblastoma-Cells - Estimation of the Contribution of Voltage-Dependent Currents, *Brit. J. Pharmacol*. 107, 207-214.
79. Toselli, M., Tosetti, P., and Taglietti, V. (1996) Functional changes in sodium conductances in the human neuroblastoma cell line SH-SY5Y during in vitro differentiation, *J. of Neurophys* 76, 3920-3927.
80. McDonald, R. L., Vaughan, P. F. T., and Peers, C. (1994) Muscarinic (M(1)) Receptor-Mediated Inhibition of K+-Evoked [H-3] Noradrenaline Release from Human Neuroblastoma (SH-SY5Y) Cells Via Inhibition of L-Type and N-Type Ca2+ Channels, *Brit. J. Pharmacol.* 113, 621-627.
81. Reeve, H. L., Vaughan, P. F. T., and Peers, C. (1994) Calcium-Channel Currents in Undifferentiated Human Neuroblastoma (SH-SY5Y) Cells - Actions and Possible Interactions of Dihydropyridines and Omega-Conotoxin, *Eur. J. Neurosci*. 6, 943-952.
82. Reeve, H. l., Vaughan, P. F. T., and Peers, C. (1995) Inhibition of N-type Ca2+ channel currents in human neuroblastoma (SH-SY5Y) cells by muscarine via stimulation of M3 receptors, *Neuropharmacology* 34, 319-326.
83. McDonald, R. L., Vaughan, P. F. T., Beck-Sickinger, A. G., and Peers, C. (1995) Inhibition of Ca2+channel currents in human neuroblastoma (SH-SY5Y) cells by neuropeptide Y and a novel cyclic neuropeptide Y analogue, *Neuropharmacology* 34, 1507-1514.
84. Furukawa, K., Wang, Y., Yao, P. J., Fu, W., Mattson, M. P., Itoyama, Y., Onodera, H., D'Souza, I., Poorkaj, P. H., Bird, T. D., and Schellenberg, G. D. (2003) Alteration in calcium channel properties is responsible for the neurotoxic action of a familial frontotemporal dementia tau mutation, *J. Neurochem*. 87, 427-436.
85. Billups, D., Billups, B., Challiss, R. A. J., and Nahorski, S. R. (2006) Modulation of Gq-Protein-Coupled Inositol Trisphosphate and Ca^{2+} Signaling by the Membrane Potential, *J. Neurosci.* 26, 9983-9995.
86. Arispe, N., Diaz, J. C., and Simakova, O. (2007) Aβ ion channels. Prospects for treating Alzheimer's disease with Aβ channel blockers, *BBA-Biomembranes* 1768, 1952-1965.
87. Montal, M., and Mueller, P. (1972) Formation of bimolecular membranes from lipid monolayers and a study of their electrical properties, *Proc. Nat. Acad. Sci (USA)* 69, 3561-3566.
88. Capone, R., Blake, S., RinconRestrepo, M., Yang, J., and Mayer, M. (2007) Designing Nanosensors Based on Charged Derivatives of Gramicidin A, *J. Am. Chem. Soc*. 129, 9737-9745.

89. Blake, S., Capone, R., Mayer, M., and Yang, J. (2008) Chemically Reactive Derivatives of Gramicidin A for Developing Ion Channel-Based Nanoprobes, *Bioconjugate Chem*. 19, 1614-1624.
90. Mayer, M., Kriebel, J. K., Tosteson, M. T., and Whitesides, G. M. (2003) Microfabricated Teflon Membranes for Low-Noise Recordings of Ion Channels in Planar Lipid Bilayers, *Biophys. J*. 85, 2684-2695.
91. Mueller, P., Rudin, D. O., Tien, H. T., and Wescott, W. C. (1962) Reconstitution of Cell Membrane Structure in Vitro and Its Transformation into an Excitable System, *Nature* 194, 979-980.
92. Mayer, M., Semetey, V., Gitlin, I., Yang, J., and Whitesides, G. M. (2008) Using Ion Channel-Forming Peptides to Quantify Protein-Ligand Interactions, *J. Am. Chem. Soc.* 130, 1453-1465.
93. Saluja I., Saunders T. L., and Turner R. S. (2006) Modulation of neuronal APP metabolism by X11a/mint-1/APBA1. In, In Alzheimer's Disease: New Advances. Medimond International Proceedings.
94. Lecoeur, H., Chauvier, D., Langonne, A., Rebouillat, D., Brugg, B., Mariani, J., Edelman, L., and Jacotot, E. (2004) Dynamic analysis of apoptosis in primary cortical neurons by fixed- and real-time cytofluorometry, *Apoptosis* 9, 157-169.

Chapter 3

The Abundance of Aβ Oligomer (tetramer-18mers) Correlates with Pore Formation and Cytotoxicity

In this chapter, we examined whether preparations of amyloid-beta (Aβ) that are most likely to form detectable ion pores in planar lipid bilayers were also the most cytotoxic preparations to a human neuroblastoma cell line (SH-SY5Y cells). To this end, we determined which aggregation protocol of Aβ samples led to maximal pore formation and characterized these samples with regard to β-sheet content, thioflavin T fluorescence, and relative abundance of oligomers of different size in the mixture. Planar lipid bilayer experiments revealed that the probability of pore formation was highest with Aβ samples that had aggregated at 22 °C in deionized water for 2-3 days in the case of $A\beta_{1\text{-}40}$ or for 2 days in the case of $A\beta_{1\text{-}42}$. Cytotoxicity studies demonstrated that the most cytotoxic Aβ samples were those that had aggregated for 10 d in the case of $A\beta_{1\text{-}40}$, and 3 d or $A\beta_{1\text{-}42}$. Finally, multiple linear regression and Pearson's correlation analyses revealed that pore formation was correlated most strongly with the relative abundance of tetramers to hexamers, while cytotoxicity correlated with the relative abundance of tetramers to 18 mers. The partial overlap of Aβ oligomers that induced the highest probability of pore formation with those that were most toxic suggests that pore formation may be a contributing mechanism to the toxicity of Aβ in vitro. The

observation that this overlap is not complete, however, suggests that the cytotoxic effects of Aβ are not solely due to pore formation.

3.1 Introduction

Alzheimer's disease (AD) is characterized by the accumulation of amyloid-β peptide (Aβ) aggregates in the brain. These aggregates form insoluble amyloid plaques that are the hallmarks of the AD (*1-3*). The major components of these amyloid plaques are Aβ peptides with 40 ($Aβ_{1-40}$) and 42 amino acids ($Aβ_{1-42}$), which are thought to play an important role in AD pathogenesis (*4-9*). The pathogenic mechanism leading to AD is, however, not fully understood and several hypotheses are being actively investigated (*10*).

These different hypotheses are based on evidence that Aβ peptides can cause neurotoxicity by triggering inflammatory responses, oxidative damage, dysregulation of ion homeostasis including Ca^{2+} ions, and altered kinase and phosphatase activities that can lead to neurofibrillary tangles.

With regard to the question, which size of Aβ oligomers is the most important for the pathogenesis of AD, several in vitro neurotoxicity and in vivo studies in mouse models of AD (*11*) implicated the following oligomers as the main triggers of AD: dimers (*12-16*), trimers (*17*), tetramers to 9 mers (also called Aβ-derived diffusible ligands, ADDLs, with an estimated mass of 17-42 kDa) (*18-20*), 13 mers (also called Aβ *56) (*21, 22*), and protofibrils containing aggregates larger than 100 kDa, which correspond to

22 mers and bigger aggregates (*23-25*). In addition to these oligomeric species, some studies have revealed that insoluble Aβ fibrils induce neurotoxicity and impair synaptic transmission (*26-28*).

In the work presented here, we investigated the hypothesis that Aβ peptides disrupt the ion homeostasis in neurons, the so-called Aβ ion channel hypothesis. Pore formation by Aβ is one plausible mechanism for neurotoxicity, since such pores could mediate the flux of Ca^{2+} ions and thereby lead to cell death (*6, 29-33*).

Various biochemical and biophysical techniques have indicated a range of aggregated Aβ species that could potentially form ion channel-like structures in artificial lipid bilayers and in neuronal membranes (*34-36*). Jang *et al*. proposed based on molecular dynamics (MD) simulations that 16 to 24 mers of Aβ arranged to four to six subunits (*37*), which are compatible with the dimension and shape of putative Aβ pore structures obtained from atomic force microscopy (AFM) (*38, 39*). In separate MD studies, Strodel *et al*. identified tetramers or hexamers as the most stable structures that could form Aβ pores (*40*), while Shifrir *et al*. suggested that Aβ channels contain assemblies of six hexamers (*41*). Recently, Schauerte *et al.* combined single molecule fluorescence spectroscopy with conductivity measurement and reported that hexamers were the smallest Aβ oligomeric structure which could permeabilize lipid membranes, while 12 to 14 mers resulted in pores with the largest conductivity for ions (*42*).

Here we used planar lipid bilayer (PLB) recordings to study the formation of ion pores by various Aβ preparations (*33, 38, 43-49*). One of the challenges that we encountered with this functional and sensitive assay is that various Aβ preparations did

not always lead to repeatable ion channel formation in PLBs (*31*). The reasons for this poor reproducibility are that aggregation of Aβ samples is a complex, stochastic process (*50*), that depends on factors, such as ionic strength, pH, concentration of Aβ peptides, solvent history, and chemical nature of impurities in the Aβ samples (*33, 48, 50-61*). Moreover, the initial aggregation state of Aβ samples varies considerably between different commercial suppliers (*54*) (see *Appendix*, *Fig.* A3-1), and even between batches from the same supplier (*62, 63*), making it difficult to reproduce functional experiments such as ion channel recordings on planar lipid bilayer, and neurotoxicity assays that depend on the aggregation state of Aβ (*54, 64*).

Previous work typically addressed this challenge by preparing Aβ stock solutions either in strongly basic solutions (*65*) or in organic solvents, such as hexafluoroisopropanol (HFIP) (*9, 66, 67*), trifluroacetic acid (TFA) (*68*), or dimethylsulfoxide (DMSO)(*48, 69*), in which Aβ aggregates either dissociate or at least aggregate more slowly than in water. The intention of these approaches was that starting conditions for the aggregation of Aβ would be somewhat reproducible (*54*). However, these organic solvents can produce artifacts in functional experiments with Aβ samples, if they are not removed effectively. For example, residues of HFIP can cause significant ion flux through cellular membranes, and PLBs by thinning lipid membranes (*33, 70*).

In order to provide defined starting conditions for Aβ aggregation while minimizing solvent artifacts, we pre-treated Aβ samples with HFIP, which dissociates most of the large aggregates, followed by lyophilization for two days to remove the

solvent below its detection limit by fluorine NMR (*33*). We used these pre-treated Aβ samples as the starting material to compare five different preparation methods for the formation of aggregated Aβ species and for the capability of these preparations to form ion pores in PLBs.

We then used the most appropriate Aβ preparation method to address the question which size of Aβ aggregates induces maximal pore formation in lipid membranes and which one causes maximal cytotoxicity—and, ultimately, is there a relationship between these two? To this end, we correlated the relative abundance of Aβ oligomers with specific sizes in a mixture of aggregated Aβ species with pore formation and cell death. We used Pearson correlation analysis and multiple linear regression (MLR) models to describe a linear relationship between pore formation or cytotoxicity and a set of independent variables, which were the relative abundance of Aβ oligomers of different size as obtained from SDS-PAGE. Based on this approach, we selected three fitting parameters for the MLR models, which represent three different size ranges of Aβ aggregates. Based on coefficients that resulted from fitting the data to these models, we revealed which aggregated Aβ species were most important for pore formation or cytotoxicity. We found that pore formation in PLB was most correlated with relative abundance of tetramers to hexamers of Aβ, while cytotoxicity was most correlated with relative abundance of tetramers to 18 mers. A similar approach might be useful for other amyloid peptides which share the capability to form ion pores in lipid membranes.

3.2 Results and Discussion

3.2.1 Pretreatment of Aβ with HFIP combined with HFIP removal is critical for the reproducibility of experiments

Initial aggregation states of Aβ samples often vary between different suppliers and sometimes between batches from the same suppliers, (see *Appendix*, *Fig.*A3-1), resulting in irreproducibility of experiments that test the function of various Aβ species such as ion channel formation. In order to examine Aβ samples with reproducible initial aggregation states, we dissolved Aβ in hexafluoroisopropanol (HFIP) to break up fibrils and large aggregates (*9, 66, 67*). These samples were then lyophilized for two days to remove HFIP below the detection limit by fluorine NMR (see *Appendix, Fig.*A3-2). In the case of $A\beta_{1-40}$ samples, this HFIP-treatment dissociated all Aβ oligomers larger than tetramers as confirmed by Western blot analysis and improved the solubility of Aβ in water (see *Appendix*, *Fig.*A3-1). In the case of $A\beta_{1-42}$, this procedure was not as effective, but it was able to dissolve the largest aggregates (> 225 kDa) (see *Appendix*, *Fig.*A3-1). Based on the importance of the initial aggregation state for the kinetics of aggregation of Aβ samples (*51, 56, 64, 71*), we carried out all experiments with HFIP-treated Aβ samples, unless otherwise indicated.

3.2.2 Pore formation is maximal after incubating Aβ samples for 2-3 days

Figure 3-1 illustrates that both $A\beta_{1-40}$ and $A\beta_{1-42}$ caused channel-like ion flux across planar lipid bilayers that could be inhibited by Zn^{2+} ions, as reported previously by

several research groups (*29, 31, 33, 38, 39, 45, 48, 72-77*). The conductance values of these ion channel events were not well-defined and ranged from 100 pS to 10 nS and the open pore lifetimes from milliseconds to several minutes.

As reported previously, not every experiment with these five different aggregation methods that we tested (Table 3-1, A-E) led to pore formation. This variability was possibly due to the stochastic nature of both the aggregation process (*31, 50, 54, 74*), and the interaction of these aggregates with lipid membranes (*78, 79*). When comparing the ion channel activity from aggregated Aβ samples that were produced with different aggregation methods (Table 3-1), we did not observe significant differences in conductance or lifetime (or overall "appearance" of the current traces).

In order to correlate the probability of pore formation by Aβ samples with the abundance of various Aβ aggregates and with cytotoxicity, we first determined which of the five pre-incubation methods of Aβ samples led to the highest probability of pore formation in planar lipid bilayers. For this comparison, we defined measured current fluctuations as pore formation if the following five criteria were met: *i)* ion flux had to have an amplitude significantly different from the baseline current (*i.e*., at least ten times the standard deviation of the current noise) *ii)* ion flux had to occur toward the expected polarity of the applied electric field, *iii)* ion flux had to occur within 30 min after the addition of Aβ to minimize the effect of artifacts by Aβ-independent membrane destabilization over time, *iv)* ion flux had to last for at least 5 min, and *v)* ion flux had to be reduced significantly after the addition of Zn^{2+} ions.

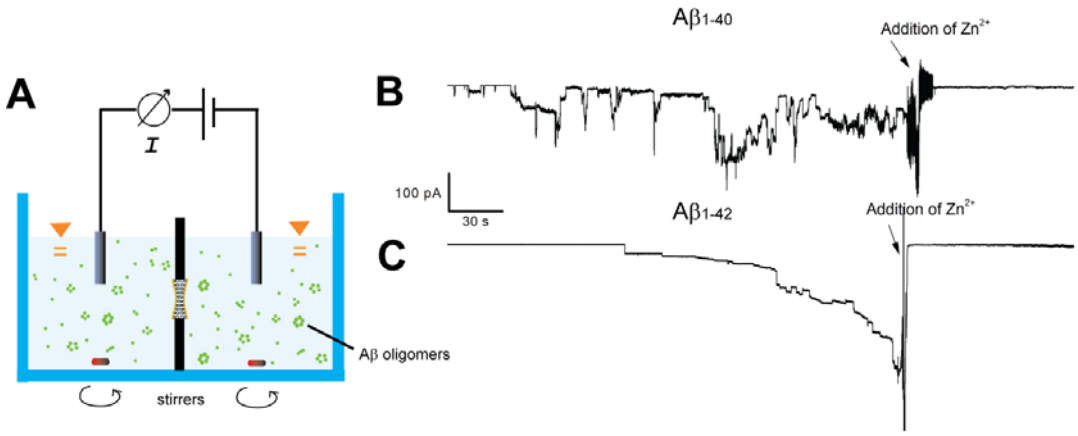

Figure 3-1. Electrophysiological recordings for studying pore formation in planar lipid bilayers induced by $A\beta_{1\text{-}40}$ and $A\beta_{1\text{-}42}$. **A)** Cartoon illustrating the experimental setup. Lipid bilayers were created by the so-called "painting technique" over a 250-μm aperture between two electrolyte compartments. **B)** Example of a current recording of transmembrane ion flux induced by 15 μM $A\beta_{1\text{-}40}$ prepared by incubation in deionized water for 1 d using method A in Table 3-1. **C)** Example of transmembrane current induced by 15 μM $A\beta_{1\text{-}42}$ prepared by method A for 3 d. Addition of Zn^{2+} to a final concentration of 10 mM (indicated by the vertical arrows) inhibited Aβ-induced ion flux. The planar lipid bilayer was formed from a 1:1 (w/w) mixture of DOPS: POPE lipids in *n*-heptane; the recording electrolyte was composed of 70 mM KCl with 10 mM HEPES at a pH of 7.4. The applied voltage was at -50 mV.

Table 3-1 shows the results from this comparison. We observed the highest probability of ion channel formation with method D and E, which were both based on fusing Aβ-containing proteoliposomes into preformed PLB. Unfortunately, these methods also destabilized bilayers in the absence of Aβ in the liposomes, leading to false positives in one third of control experiments. Other disadvantages of these two methods were that Ca^{2+}-induced fusion of Aβ proteoliposomes with live cells was not

practical and therefore this method did not allow comparison of pore formation by Aβ in PLBs with toxicity assays on live cells, which was one of the goals of this study. Moreover, fusion of positively charged Aβ proteoliposomes led to strong cytotoxicity by the control liposomes without Aβ.

Finally, since the modified Kayed protocol (method C) and experiments with non-HFIP treated Aβ (method B) led to relatively low probabilities of ion channel formation, we chose simple incubation of HFIP-treated Aβ in water for various times (method A) for all further experiments. This method was, within statistical error, one of the most efficient ones and had the advantage that we could monitor aggregation over time (from 1-4 h to 20 d) while making it possible to characterize based on circular dichroism and ThT fluorescence as well as the relative abundance of monomers, dimers, trimers, etc., to protofibrils (> 49 mers).

Using pre-incubation of Aβ in water (method A), *Fig*. 3-2A shows that the probability of pore formation was highest when Aβ samples were pre-incubated for 2-3 d in the case of $A\beta_{1\text{-}40}$ or for 2 d in the case of $A\beta_{1\text{-}42}$. In contrast, pore formation was least likely when Aβ samples were pre-incubated for 0 d or 20 d. Control experiments, in which we added only diH_2O without Aβ, revealed ion flux in 1 of 11 experiments; this activity was likely due to a sporadic instability of bilayers within the 30-min recording period that is typical for bilayer recordings (*80*). To test statistical significance of the difference in success rate of pore formation by various preparation methods of Aβ samples, compared to the respective control experiments, we used Barnard's exact test to calculate *p*-values for the success rates based on the binary response (*81, 82*) that

was either pore formation was observed or pore formation was not observed within 30 minutes after adding the various sample to trans compartment of the bilayer chamber.

Table 3-1. **Comparison of different Aβ aggregation procedures with regard to their ability to form detectable ion channels in planar lipid bilayer recordings**

Preparation Method	Short description of preparation method	Final [Aβ], μM	Statistics of ion flux observation, % [a, b]		
			Control (no Aβ)	$Aβ_{1-40}$	$Aβ_{1-42}$
A	$diH_2O_{0\,d}$	15-25	10 ± 10	20 ± 10	15 ± 10
A	$diH_2O_{1\,d}$	15-25	10 ± 10	35 ± 15	30 ± 15
A	$diH_2O_{2\,d}$	15-25	10 ± 10	55 ± 15 (**)	40 ± 15 (*)
A	$diH_2O_{3\,d}$	15-25	10 ± 10	50 ± 15 (**)	25 ± 10
A	$diH_2O_{10\,d}$	15-25	10 ± 10	30 ± 15	10 ± 10
A	$diH_2O_{20\,d}$	15-25	10 ± 10	20 ± 10	0
B	(non-lyophilized Aβ),$diH_2O_{0\,d}$	15-25	10 ± 10	20 ± 15	40 ± 15
C	HFIP/ $diH_2O_{2\,d}$	10-25	10 ± 10	30 ± 15	15 ± 10
D	proteoliposomes (DOPS)	1-5	30 ± 15	65 ± 15 (**)	80 ± 10 (**)
E	proteoliposomes (positively charged)	1-5	35 ± 10	75 ± 10 (**)	70 ± 15 (*)

[a] Aβ ion channel activity was defined as a stepwise or spike-like current fluctuation from baseline within 30 min after addition of Aβ. The planer lipid bilayer was composed of DOPS:POPE (1:1) lipids dissolved in *n*-heptane at a concentration of 20 mg mL^{-1}.

[b] The errors are standard errors of proportion of success rate in pore formation calculated by S.E. = $\sqrt{p(100-p)/n}$, when *p* the fraction of observed pore formation (in %) and *n* is the number of PLB experiments. The statistical significance of Aβ ion channel activity compared to the respective control sample is determined by Barnard's exact test (* $p < 0.1$, and ** $p < 0.05$)

3.2.3 Cytotoxicity is maximal after pre-incubating Aβ_{1-40} for ten days and Aβ_{1-42} for one to ten days

In order to compare the cytotoxicity of the five different Aβ preparation procedures (method A-E) used here, we performed cell viability assays with a human neuroblastoma cell line. We observed maximal cytotoxicity with method A after pre-incubation for ten days, while the toxicity of $A\beta_{1-42}$ was highest between one and ten days of pre-incubation (*Fig.*3-2B). In addition to yielding maximal toxicity, method A made it possible to compare the results from cytotoxicity assays with those from the probability of pore formation, since both assays were done with the same samples.

As mentioned before, the two proteoliposome-based methods (method D and E) were not suitable for toxicity assays, either because of inefficient Ca^{2+}-induced fusion with live cells or because of strong toxicity of fusing positively-charged proteoliposomes. Table 3-2 also illustrates that a functional assay such as testing an Aβ preparation for cytotoxicity depended on the initial aggregation state of Aβ or on the formulation of Aβ. For instance, Aβ samples that were not dissociated in HFIP, but were instead used directly as received from different suppliers (method B), caused varying degrees of cell death. Similar results have been reported by other groups (*55, 62, 63*).

Table 3-2. Cell death induced by different preparations of Aβ

Preparation Method	Short description of preparation method	Final [Aβ], μM	Cell death, % [a]	
			$Aβ_{1-40}$	$Aβ_{1-42}$
A	$diH_2O_{0\ d}$	20	15 ± 2 (***)	13 ± 2 (***)
A	$diH_2O_{1\ d}$	20	26 ± 2 (***)	39 ± 2 (***)
A	$diH_2O_{2\ d}$	20	35 ± 2 (***)	43 ± 2 (***)
A	$diH_2O_{3\ d}$	20	38 ± 2 (***)	44 ± 2 (***)
A	$diH_2O_{10\ d}$	20	45 ± 3 (***)	43 ± 3 (***)
A	$diH_2O_{20\ d}$	20	28 ± 3 (***)	36 ± 4 (***)
$B^{b}_{GL\ Bioscience}$	(non-lyophilized Aβ),$diH_2O_{0\ d}$	20	22 ± 4 (***)	40 ± 7 (***)
$B^{b}_{Biopeptide}$	(non-lyophilized Aβ),$diH_2O_{0\ d}$	20	5 ± 2 (*)	46 ± 6 (***)
C	HFIP/ $diH_2O_{2\ d}$	20	31 ± 4 (***)	40 ± 4 (***)
D	proteoliposomes (DOPS)	1-10	not possible	not possible
E	proteoliposomes (positively charged)	1-10	not possible	not possible

[a] Cell death was defined as 100%- viability in %, The errors are standard errors of the mean.

[b] Biopeptide and GL Bioscience indicate two different suppliers of Aβ

The statistical significance of Aβ ion channel activity compared to the respective control sample is determined by Students' *t* test (* $p < 0.1$, and *** $p < 0.01$)

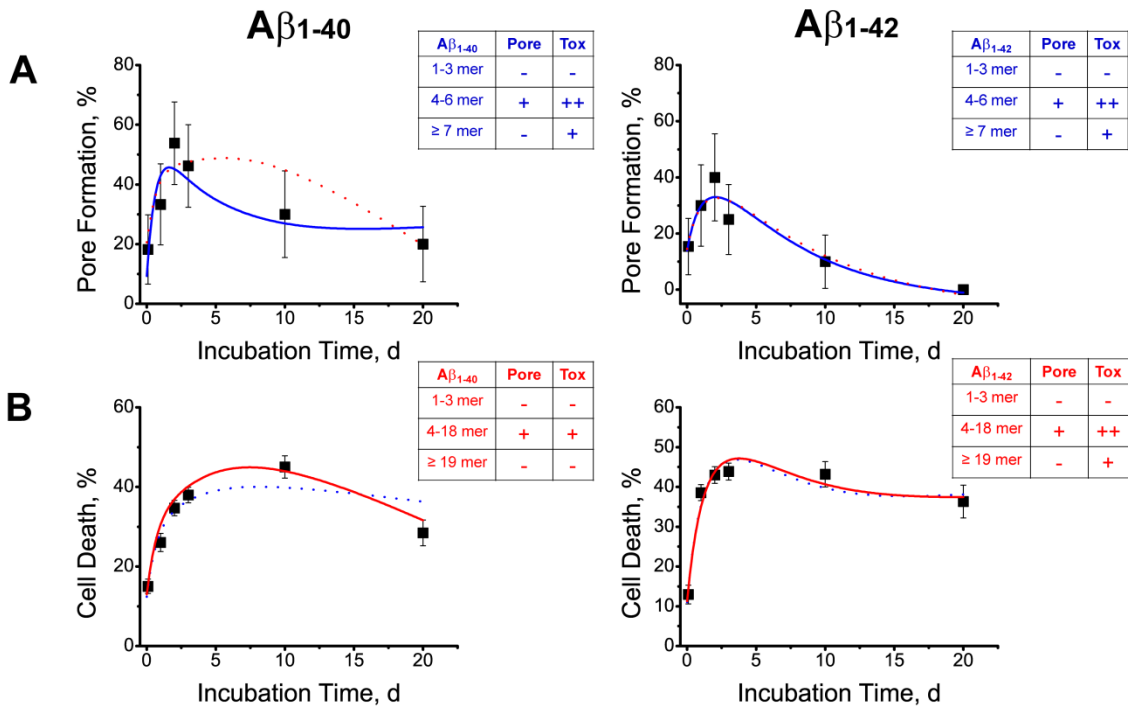

Figure 3-2. Comparison of pore formation, and cytotoxicity as a function of aggregation time of Aβ samples prepared by method A. **A)** Percentage of experiments that showed pore formation in planar lipid bilayers. Each point represents 10-15 experiments; error bars represent the error of proportion. The solid blue curve is a plot of probability of pore formation (*P*) obtained from multiple linear regression model as a function of relative abundance of oligomers (*X*) from different size ranges, $\boldsymbol{P} = 8.67 - 1.03*\boldsymbol{X_{1\text{-}3mer}} + 4.96*\boldsymbol{X_{4\text{-}6mer}} - 0.80*\boldsymbol{X_{\geq 7mer}}$ for $A\beta_{1\text{-}40}$, and $\boldsymbol{P} = 9.05 - 0.43*\boldsymbol{X_{1\text{-}3mer}} + 3.86*\boldsymbol{X_{4\text{-}6\ mer}} - 1.00*\boldsymbol{X_{\geq 7mer}}$ for $A\beta_{1\text{-}42}$. The sign of coefficients for all parameters is summarized in the table adjacent to the graph, suggesting correlation (+) or anti-correlation (-) of the parameter for prediction of pore formation. **B)** Cell death of human neuroblastoma SH-SY5Y cells 24 h after exposure to serum-free media containing 20 μM Aβ prepared by method A. Percentage cell death was defined as 100% - cell viability (in %) as determined by MTT assay from 5-15 independent experiments. The solid red curve is a plot obtained from multiple linear regression function which describes the percentage of cell death or cytotoxicity (*T*) as a function of relative abundance of oligomers (*X*) from different size ranges, $\boldsymbol{T} = - 0.34 -$

$0.26*\boldsymbol{X}_{1\text{-}3mer} + 1.87*\boldsymbol{X}_{4\text{-}18\ mer} - 0.42*\boldsymbol{X}_{\geq 19mer}$ for $A\beta_{1\text{-}40}$, and $\boldsymbol{T} = 0.05 - 0.58*\boldsymbol{X}_{1\text{-}3mer} + 2.95*\boldsymbol{X}_{4\text{-}18\ mer} + 0.04*\boldsymbol{X}_{\geq 19mer}$ for $A\beta_{1\text{-}42}$.

3.2.4. During aggregation, the relative abundance of small Aβ oligomers decreases, of intermediate sizes undergoes a maximum, and of large sizes increases.

In order to correlate both pore formation and cytotoxicity with the aggregation state of Aβ samples, we used SDS-PAGE combined with Western blot analysis to estimate the relative abundance of monomeric and oligomeric species of Aβ as a function of pre-incubation time in diH_2O. In order to prevent dissociation of Aβ oligomers during SDS-PAGE, we crosslinked the samples for 20 minutes with 12 mM glutaraldehyde before heating and running the gels (*83*).

We used image analysis of grey levels in scanned images from Western blots after SDS-PAGE (*e.g. Fig.* 3-3) to determine relative abundance of different-sized Aβ species with the following resolution: monomer, dimer, trimer, tetramer, pentamer, and hexamer. For larger oligomers, individual species were difficult to distinguish on the gel; therefore we determined the relative abundance of oligomers larger than hexamers based on the molecular weight markers. This approach resulted in the following resolution of ranges in molecular weight: 34-55 kDa, 55-78 kDa, and 78-210 kDa, which correspond approximately to 8-13 mers, 14-18 mers, and 19-49 mers, respectively. *Fig.* 3-3 shows bands from aggregated forms of Aβ that did not leave the sample wells of the electrophoresis gels. We labeled these (proto)fibrillar species as > 49 mers.

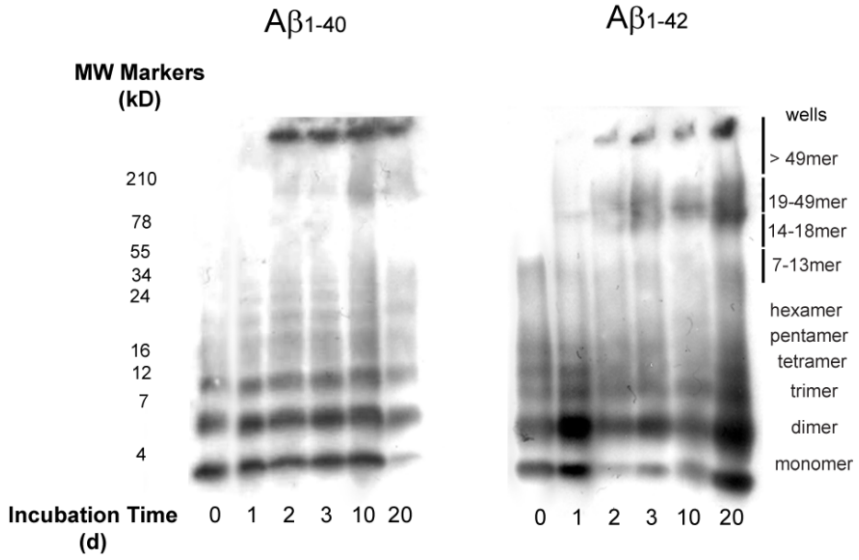

Figure 3-3. Separation of Aβ samples prepared by method A by SDS-PAGE followed by Western blot analysis. $A\beta_{1\text{-}40}$ *(left)* and $A\beta_{1\text{-}42}$ *(right)* were incubated in diH_2O for 0, 1, 2, 3, 10, and 20 days. All samples were crosslinked with 12 mM glutaraldehyde before electrophoresis was carried out using a 16.5% Tris-Tricine gel. The position of molecular-weight markers are indicated on the left.

Figure 3-4 shows that the relative abundance of low molecular weight aggregates (*i.e.,* monomers to trimers) decreased as a function of aggregation time, while the relative abundance of intermediate-sized oligomers (tetramer to 13 mers in the case of $A\beta_{1\text{-}40}$ and tetramer to hexamers in the case of $A\beta_{1\text{-}42}$) underwent a maximum and the relative abundance of high molecular weight species (> 18 mers) increased.

In order to fit the kinetic data in *Fig.* 3-4, we used one of the simplest models to describe the formation of Aβ oligomers (O) and (proto-) fibrils (F) from monomers (M) by

a system of two consecutive, first-order, reversible reactions, without considering stoichiometric coefficients or mechanistic details:

$$M \underset{k_2}{\overset{k_1}{\rightleftharpoons}} O \underset{k_4}{\overset{k_3}{\rightleftharpoons}} F$$

As discussed by G.N. Vriens, this approach can be used to model data empirically and makes it possible to describe the time-dependent mole fraction of the reactant and product by an equation of the form (*84*).

$$y = y_0 + A_1 \cdot e^{B_1 \cdot t} + A_2 \cdot e^{B_2 \cdot t} \qquad (3\text{-}1)$$

Here we used equation (3-1) to carry out empirical fits to the relative abundance of each species as a function of time in *Fig.* 3-4. The red curves in *Fig.* 3-4 illustrate that this simple model was indeed able to fit the time-dependent changes of the mole fraction of each oligomer species well. Therefore, on a very basic level, the kinetics of oligomerization and fibrillization of Aβ that we found in *Fig.* 3-4 could be described by a series of consecutive reversible reactions, as might have been predicted by G.N. Vriens. Regardless of their possible mechanistic relevance, these empirical fits were useful for the work presented here, because they describe, quantitatively, the trends of the relative abundance of each Aβ species during the course of the aggregation. These trends are also useful for correlating the relative abundance of various species with the probability of pore formation and with cytotoxicity, because they result from curve fits to all six points in each graph and therefore represent the trend of an entire data set in each graph rather than a single point within each graph.

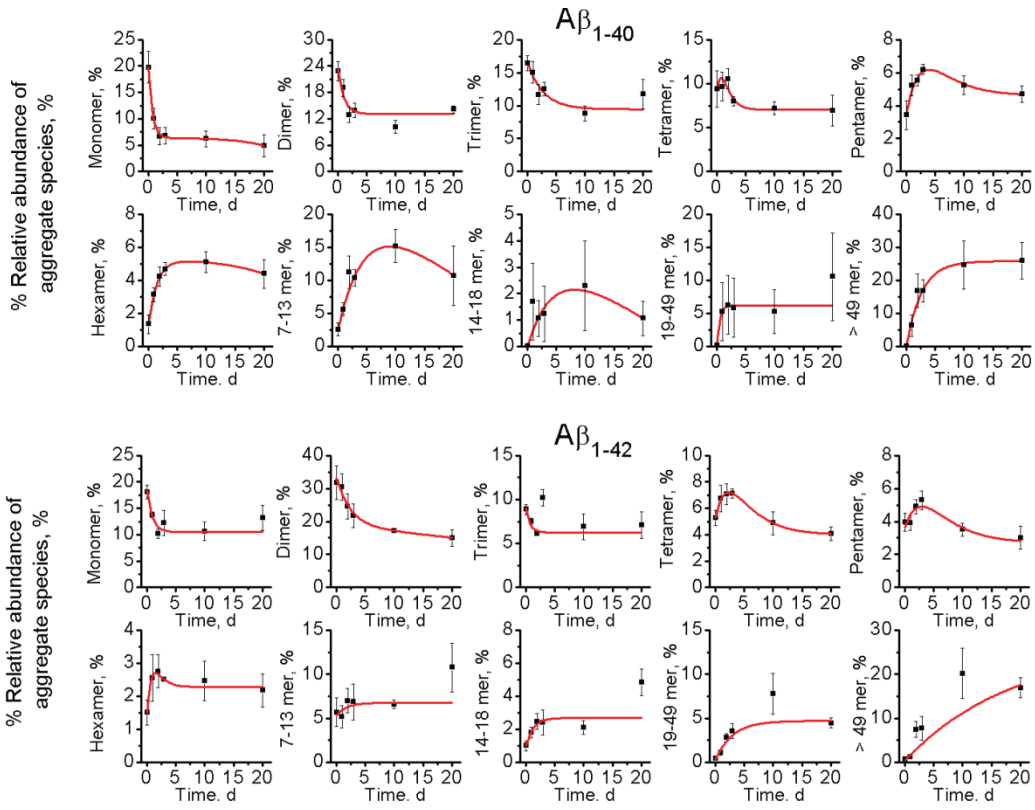

Figure 3-4. Relative abundance of aggregated Aβ species of different size as a function of pre-incubation time as determined by quantitative image analysis from Western blot analysis after SDS-PAGE. Each point represents the mean value of the relative abundance of each species from 4-6 gels; error bars represent the standard error of the mean. The red curves are best curve fits of equation *(1)* to the data.

We also quantified the relative abundance of each Aβ species from the other Aβ preparations (Method B-E). SDS-PAGE/Western blotting experiments showed that the presence of lipid membranes in the proteoliposome formulations accelerated the aggregation of both $A\beta_{1\text{-}40}$ and $A\beta_{1\text{-}42}$ compared to Method A (see *Appendix, Fig.* A3-3).

For comparison with Western blot analysis, we used silver staining for protein detection since the immunoreactivity of oligomers can be conformation dependent (*85*). Results with $A\beta_{1\text{-}40}$ showed that the silver stain detection; however, had low sensitivity for the aggregated species larger than hexamers (see *Appendix, Fig.* A3-4, and *Fig.* A3-5). The bands from aggregated Aβ species with intermediate and high molecular weight were not as clearly visible on silver stained gels than on gels developed by Western blotting (as reported previously by other research groups) (*85, 86*). Both detection techniques revealed similar trends for the change of relative abundance of small oligomer sizes, but accurate quantification for the aggregated species greater than hexamers, was difficult with silver staining. Therefore, we performed Western blot analysis for most of the gels used in this work.

3.2.5 Pore formation and cytotoxicity correlate with the relative abundance of oligomers of intermediate size.

In order to determine the correlation between the aggregated Aβ species of different size and pore formation or cytotoxicity, we used Pearson's correlation analysis. We used the experimental data for pore formation or cytotoxicity at various aggregation time points, while we used calculated relative abundance values of Aβ aggregates as obtained from the fit to equation *(1)* at each respective time point for each species (as shown in *Fig*. 3-4).

Figure 3-5 demonstrates Pearson's correlation coefficients, *r*, between the relative abundance of different-sized Aβ aggregates and pore formation or cytotoxicity (see Eq.*A3-1*, *Appendix*). Among all of the aggregated Aβ species, we found the strongest correlation with pore formation or cytotoxicity for the intermediate aggregated Aβ species. The probability of pore formation correlated the most with pentamers (r = 0.808, p = 0.028) of $A\beta_{1\text{-}40}$ and tetramers (r = 0.688, p = 0.087) of $A\beta_{1\text{-}42}$. In contrast, we found a strong correlation between cell death and hexamers (r = 0.971, p < 0.001) of $A\beta_{1\text{-}40}$, and for 14-18 mers (r = 0.952, p = 0.001) of $A\beta_{1\text{-}42}$.

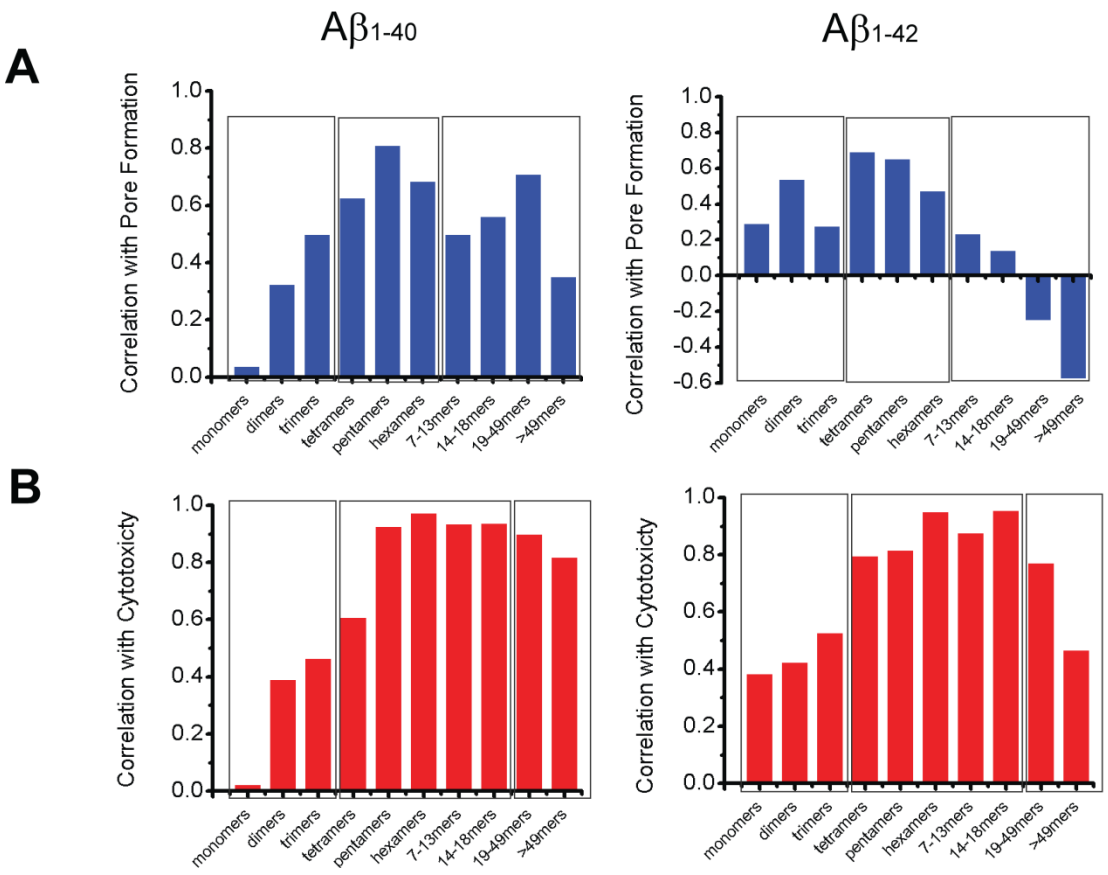

Figure 3-5. Summary of Pearson's correlation coefficients between the relative abundance of different-sized aggregate species of $A\beta_{1\text{-}40}$ and $A\beta_{1\text{-}42}$ with **A)** pore

formation or **B)** cytotoxicity. Aβ aggregates with similar correlation with pore formation or cytotoxicity for both $A\beta_{1-40}$ and $A\beta_{1-42}$ were arranged in the same group as indicated by the boxed areas.

Overall, Pearson's correlation analyses suggested that Aβ oligomers ranging from tetramers through hexamers were the dominant aggregated species which most correlated with pore formation, and tetramers through 18-mers for cytotoxicity as indicated in *Fig.* 3-5. These findings represent a similar range of Aβ oligomer sizes as reported previously to correlate with pore formation based on various techniques: this range includes tetramer through 14-mer for $A\beta_{1-40}$, and tetramer through 24-mer for $A\beta_{1-42}$ (*30, 36-38, 40-42*). In previously reported cytotoxicity studies, the most toxic aggregated species were found within the range of dimers to the insoluble fibrils (*12, 13, 15, 16, 20, 23, 24, 26, 28, 87-91*).

3.2.6 Multiple linear regression models describe the relationship between multiple Aβ oligomer species and pore formation or cell death

One of the main goals of this work was to test, which size range of Aβ aggregates led to maximal probability of pore formation in PLBs and which one caused maximal cytotoxicity. In order to answer this question, we employed a multiple linear regression (MLR), which is a method widely used to describe a linear relationship between a dependent variable and a set of independent variables (*92*). For the approach taken here, the independent variables (X_i) were relative abundance of all

aggregated species (in %) as obtained from quantification analyses of SDS-PAGE combined with Western blot. While the dependent or response variable (*y*) of interest was either the probability of pore formation (in %) or cell death (in %) as described in equation *(A3-2)* (see *Appendix*). MLR can be used to describe pore formation or cytotoxicity as a function of the relative abundance of Aβ aggregates of all sizes starting from monomers to large aggregates (> 49 mers). The abundance of Aβ species in each combination was expressed with its own X_i value, which changed during the course of the aggregation.

We determined the relative importance of each aggregated Aβ species by comparing coefficients of all variables by assuming that relatively high values of coefficients suggested relatively important variables for the response. We selected three parameters for "simplicity of description" for a model in order to use as few meaningful variables as possible to make it easier to understand the process (*92*). Based on the Pearson's correlation coefficients given in *Fig*. 3-5, we selected the appropriate predicting variables for MLR models to describe pore formation and cytotoxicity, where these variables represent three different size ranges of aggregates, including 1) small Aβ aggregates (< tetramers), 2) intermediate Aβ oligomers (tetramers through hexamers or tetramers through 18-mers), and 3) (proto) fibrils (> hexamers or > 18-mers). We used the data of relative abundance of Aβ aggregated species, pore formation and cytotoxicity to fit with MLR models and obtained coefficients for the models as summarized in Table 3-3. Based on adjusted R^2 values, *p*-values and residual mean squares (RMS) values obtained for each model, we found that the MLR model of the same sets of predicting parameters (either model I or model II) could not fit equally well for both pore formation

and cytotoxicity, in the case of $A\beta_{1\text{-}40}$; however the dominant Aβ aggregates for both cases appear to be the intermediate oligomers as determined by the values of coefficients. In the case of $A\beta_{1\text{-}42}$, both models could describe pore formation and cytotoxicity reasonably well.

Table 3-3. Summary of multiple linear regression models, which best described the probability of pore formation (*P*) and percentage of cell death (*T*) by various aggregate species of Aβ[†]

Model	$A\beta_{1\text{-}40}$	Adjusted R^2	*p*-values[†]	RMS[‡]
I	$P = -1.03*X_{1\text{-}3\ mer} + 4.96*X_{4\text{-}6\ mer} - 0.80*X_{\geq 7\ mer} - 8.67$	0.683	p_1=0.108, p_2=0.049, p_3 =0.154, p_4=0.403	80.07
II	$P = -0.81*X_{1\text{-}3\ mer} + 3.75*X_{4\text{-}18\ mer} - 2.28*X_{\geq 19\ mer} + 10.09$	0.616	p_1=0.164, p_2=0.065, p_3=0.113, p_4=0.380,	97.17
I	$T = -0.08*X_{1\text{-}3\ mer} + 1.33*X_{4\text{-}6\ mer} + 0.40*X_{\geq 7\ mer} - 0.55$	0.859	p_1=0.809, p_2=0.272, p_3=0.231, p_4=0.930	32.50
II	$T = -0.26*X_{1\text{-}3\ mer} + 1.87*X_{4\text{-}18\ mer} - 0.42*X_{\geq 19\ mer} - 0.336$	0.971	p_1=0.115, p_2=0.012, p_3=0.218, p_4=0.905	6.76
Model	**$A\beta_{1\text{-}42}$**	**Adjusted R^2**	***p*-values[†]**	**RMS[‡]**
I	$P = -0.43*X_{1\text{-}3\ mer} + 3.86*X_{4\text{-}6\ mer} - 1.00*X_{\geq 7\ mer} + 9.05$	0.831	p_1=0.140, p_2=0.021, p_3=0.049, p_4 =0.210	32.34
II	$P = -0.51*X_{1\text{-}3\ mer} + 2.35*X_{4\text{-}18\ mer} - 1.73*X_{\geq 19\ mer} + 9.02$	0.809	p_1=0.131, p_2=0.030, p_3=0.020, p_4=0.236	36.60
I	$T = -0.52*X_{1\text{-}3\ mer} + 3.98*X_{4\text{-}6\ mer} + 0.57*X_{\geq 7\ mer} + 0.09$	0.966	p_1=0.021, p_2=0.003, p_3=0.849, p_4=0.988	31.00
II	$T = -0.58*X_{1\text{-}3\ mer} + 2.95*X_{4\text{-}18\ mer} + 0.04*X_{\geq 19\ mer} + 0.05$	0.961	p_1=0.029, p_2=0.005, p_3=0.031, p_4=0.982	35.54

[†] *p*-values correspond to statistical significance for coefficients of fitting parameters and a constant for each MLR model starting from the left of the equation

[‡] RMS: residual mean squares is a measure of closeness of the observed (y_i) and predicted values from the model ($\hat{y}_i$), which are calculated from $\sum \frac{(y_i-\hat{y}_i)^2}{n-p-1}$, when *n* is a number of observation, and *p* is a number of fitting parameters in the model

The results from these MLR models suggest that aggregated Aβ species of intermediate size were the most important for pore formation (tetramers through hexamers), while smaller or larger aggregates than this size range were less important. For cytotoxicity, the dominant Aβ aggregates were tetramers through 18-mers for both $A\beta_{1\text{-}40}$ and $A\beta_{1\text{-}42}$. In the case of $A\beta_{1\text{-}42}$, the oligomers larger than 18-mers partially contributed to the cytotoxicity, suggesting that cytotoxic forms of $A\beta_{1\text{-}42}$ were found in a broader size range than $A\beta_{1\text{-}40}$.

In addition, we extrapolated the predicted probability of pore formation and cytotoxicity using these selected MLR models on the plots of experimental data in *Fig*. 3-2A and 3-2B, where the solid curve represented the appropriate model for each case (model I for pore formation, and model II for cytotoxicity), while the dotted curve corresponded to the model, which yielded a less satisfactory fit. Although both model I and II for each case of pore formation or cytotoxicity presented in Table 3-3 and *Fig.* 3-2A and 3-2B varied slightly in their prediction of the dominant Aβ species between the models, the coefficients with the largest values in these models converged to the similar range of most important Aβ oligomer sizes. Figure 3-6 illustrates the final results obtained from the models suggesting that the important Aβ oligomers for pore formation ranged from tetramers through hexamers, while tetramers through 18-mers were most cytotoxic.

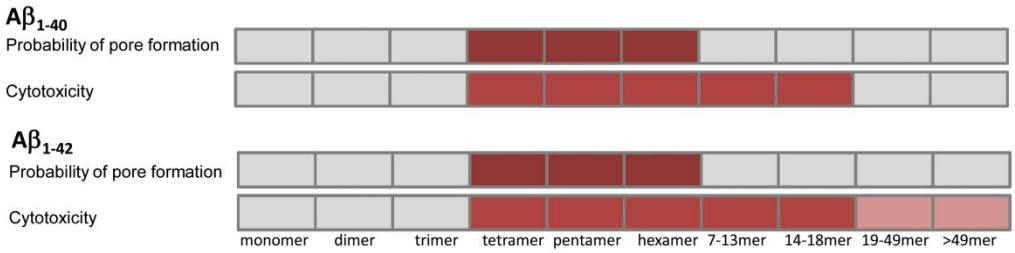

Figure 3-6. Comparison of the size of Aβ aggregates that led to maximal pore formation with those that cause maximal cytotoxicity determined from multiple linear regression models. The dark shade of color indicated relatively strong correlation with the parameter of interest (pore formation or cytotoxicity) compared to all size range of Aβ aggregates based on the values of coefficients. The presence of tetramers through hexamers suggested the strongest contribution to probability of pore formation, while tetramers through 18-mers most correlated with cytotoxicity.

3.2.7 Characterization of aggregation of Aβ by Thioflavin T binding assay, circular dichroism, and transmission electron microscopy

We used thioflavin T (ThT) fluorescence to monitor the formation of Aβ fibrils and measured the circular dichroism (CD) spectra from 190 to 260 nm to examine the extent of secondary structure in the samples of $A\beta_{1-40}$ and $A\beta_{1-42}$ in diH_2O after pre-incubation times of 0, 1, 2, 3, 10, and 20 d. Figure 3-7 shows that the ThT signal in the $A\beta_{1-40}$ samples reached approximately 80% of the maximum intensity within 2 days. After this time point, further increases in ThT fluorescence were much slower. Samples of $A\beta_{1-42}$ aggregated faster than $A\beta_{1-40}$; we observed approximately 60% of the maximum intensity after 1 day of incubation and approximately 80% after 2 days.

With regard to secondary structure, CD data revealed that the relative amount of β-sheet followed a similar trend as the ThT signal, *i.e*., a rapid increasing during the first 1-2 days, followed by a slower increase as aggregation continued (see *Fig*. 3-8 and Table 3A-1). Interestingly, the time point where the rate of ThT and CD signal slowed corresponded to the maximal probability of pore formation and cytotoxicity.

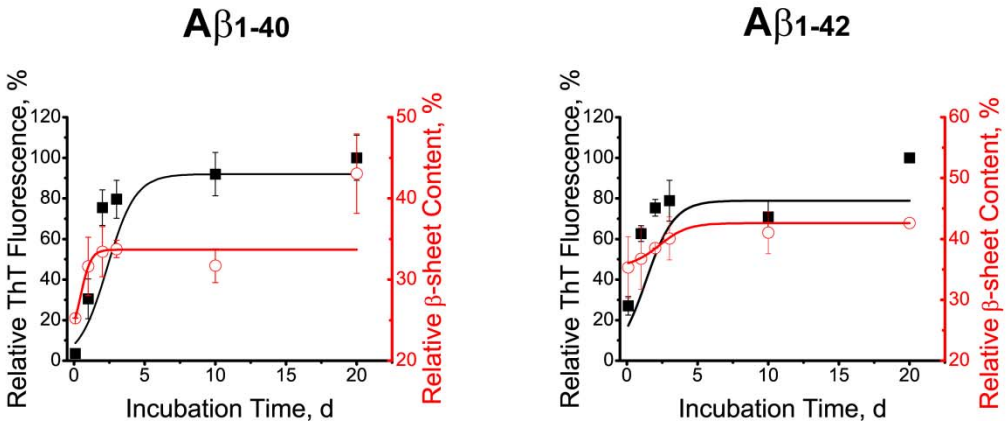

Figure 3-7 Fibril formation of Aβ over time determined by relative intensity of ThT fluorescence *(black)*, and the relative β-sheet content (in %) as determined from CD spectra *(red)*. The solid curves are fits of ThT fluorescence intensity or β-sheet content (y) as a function of time (t) to a sigmoidal function, $y = A_1 - \frac{A_2}{1+\exp\left(\frac{t-t_0}{t_1}\right)}$, where A_1, A_2, t_0, t_1 are constants. Each point represents an average value from 5-20 experiments for ThT binding assays, and from 3-5 experiments for CD experiments.

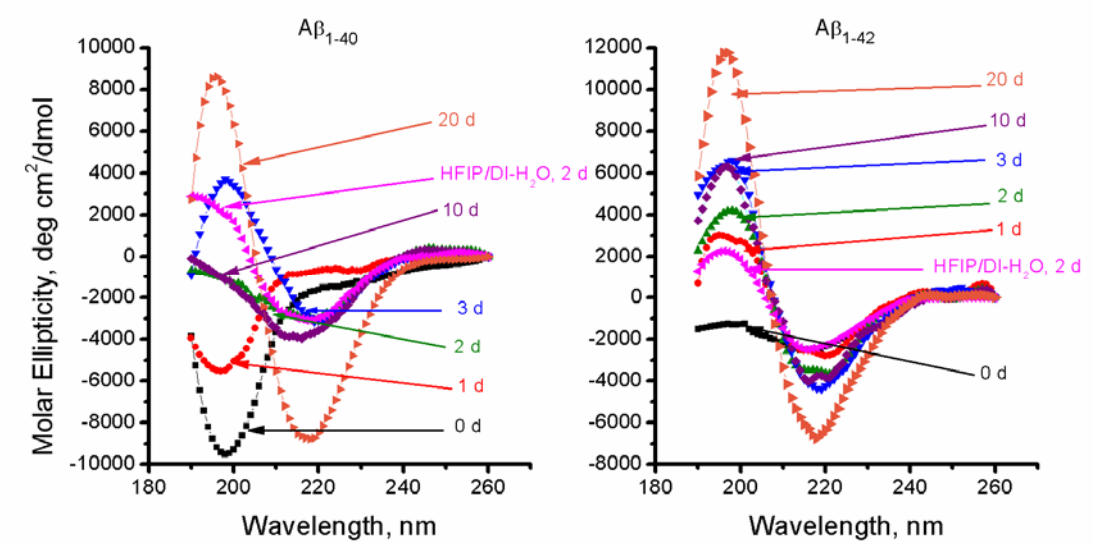

Figure 3-8. Circular dichroism spectra of $A\beta_{1-40}$ (left panel) and $A\beta_{1-42}$ (right panel) samples prepared by method A. using increasing incubation times. Aβ samples were diluted in 10 mM sodium phosphate buffer to a final concentration of 20 μM. With increasing incubation time, the β-sheet content in Aβ samples increased, while the random coil content decreased.

We also confirmed by Transmission electron microscope imaging that aggregates of $A\beta_{1-40}$ and fibrils evolved over the aggregation time. Figure 3-9 revealed that Aβ samples at 0-d incubation contain mostly the small amorphous aggregates, developed into protofibrils, and eventually long fibrillar structures as the incubation time progressed. We began to observe Aβ fibrils after 2 days of incubation and these structures were predominant after 3 d of incubation.

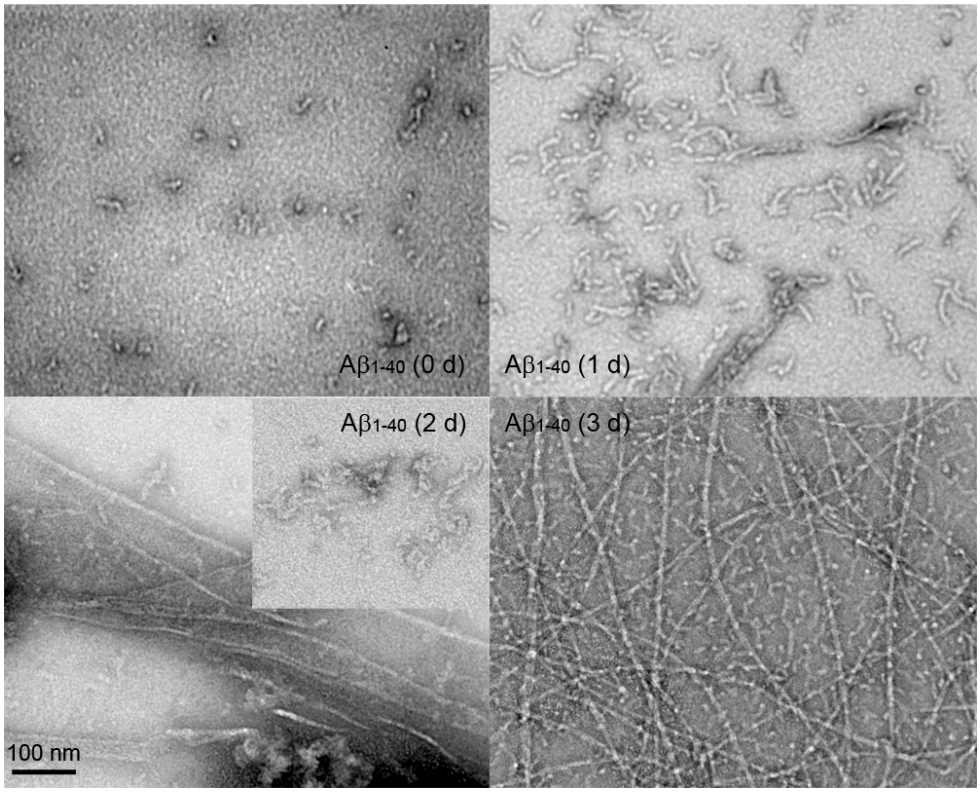

Figure 3-9. Transmission electron micrographs of $A\beta_{1\text{-}40}$ at various aggregation states. $A\beta_{1\text{-}40}$ sample was prepared in diH_2O at a final concentration of 1 mg mL^{-1}, and was incubated under a controlled temperature at 22 °C while shaking at 750 RPM.

3.3 Conclusion

One of the proposed mechanisms of Aβ-induced neurotoxicity is pore formation. At least six studies based on various techniques (*22, 49-53*) have identified that aggregated forms of Aβ with a broad range of sizes can form pore-like structures in lipid membranes. We used MLR models and Pearson's correlation analyses to determine the relationship between the relative abundance of various aggregated species of Aβ

and probability of pore formation in PLB as well as cytotoxicity in human neuroblastoma cells. These MLR models suggested that the probability of pore formation by $A\beta_{1-40}$ or $A\beta_{1-42}$ correlated with the relative abundance of tetramers through hexamers, while cytotoxicity was correlated with the relative abundance of tetramers through 18-mers. We concluded that the overlap between the most important Aβ oligomer species for pore formation and cytotoxicity for $A\beta_{1-40}$, and $A\beta_{1-42}$ suggests that pore formation may indeed be an important contributor to Aβ-induced cytotoxicity. Altogether, the results presented here identify Aβ oligomers with four to 18 monomers as the most relevant for both pore formation and cytotoxicity.

3.4 Materials and Methods

3.4.1. Chemicals

We purchased all of the lipids from Avanti Polar Lipids Inc. (Birmingham, AL), while we obtained Aβ peptides, both $A\beta_{1-40}$ and $A\beta_{1-42}$, from Biopeptide Inc. (San Diego, CA), GL Biochem Ltd. (Shanghai), and Bachem Inc. (Torrance, CA). We obtained 1,1,1,3,3,3 hexafluoro-2-propanol (HFIP) (GC grade, > 95% purity) from Fluka; potassium chloride (KCl), HEPES, and hexane from Fisher Scientific. All other chemicals and reagents were obtained from Sigma-Aldrich (St. Louis, MO).

3.4.2. Lipid preparation

The lipid compositions used for forming planar lipid bilayers were DOPS:POPE (1:1, w/w) at a concentration of 20 mg mL^{-1} in *n*-heptane. After drying 200-300 μL of the lipid solution in chloroform in a glass vial with a rotary evaporator under vacuum for 1 h, we resuspended the resulting lipid film in *n*-heptane or *n*-hexane.

3.4.3. Formation of planar lipid bilayers

We used a lipid mixture of DOPS:POPE(1:1) in *n*-heptane for the formation of all bilayers in bilayer recording experiments. We prepared planar lipid bilayers using the "painting method" (*93, 94*) by applying a solution of 20 mg mL^{-1} DOPS:POPE in *n*-heptane over an aperture with a diameter of ~250 μm in a Delrin cup (Warner Instruments). Before bilayer formation, we pretreated these apertures with a droplet of a solution of 20 mg mL^{-1} DOPS:POPE in *n*-hexane. Both compartments of the bilayer chamber (cis and trans) were filled symmetrically with electrolytes containing 70 mM KCl with 10 mM HEPES buffer adjusted to pH 7.4 with HCl unless indicated otherwise. For each experiment, we confirmed the stability of the lipid membrane by applying a voltage of ± 100 mV for 10 min before addition of Aβ or control samples to both compartments followed by stirring for 5 min using a magnetic stir bar and stir plate for planar bilayer recordings (SPIN-2, Warner Instruments). We monitored the capacitance of the bilayers throughout the recordings using the built-in capacitance compensation of the amplifiers (see below) and continued the current recording up to 1 hour after addition of Aβ samples to monitor the ion channel activity with an applied voltage of – 50 mV. In most

experiments, we also tested the inhibition of Aβ ion channel activity by addition of $Zn(NO_3)_2$ to a final concentration of 10 mM.

3.4.4. Current recordings across planar lipid bilayers

For current recordings, we used amplifiers in voltage clamp mode (Geneclamp-500 amplifier from Axon Instruments, or a BC-535 amplifier from Warner Instruments). The compartment of the bilayer chamber that was connected to the amplifier head stage by a Ag/AgCl electrode is referred to as cis compartment, the other one as trans compartment. We monitored the ionic current across the planar bilayers with a filter cutoff frequency of 2 kHz of the built-in 4-Pole Bessel filter of the amplifiers and recorded currents using an A/D converter card from National Instruments (PCI-6221) with a sampling frequency of 15 kHz and LabVIEW 7.1 software. For analysis, data were filtered with a Gaussian filter at 100 Hz and analyzed by using the software Clampfit 9.2 software (Axon Instruments).

3.4.5. Preparation of Aβ samples

To break up large aggregates of Aβ, we dissolved all Aβ powders that we obtained from different suppliers in HFIP at a concentration of 1 mM and incubated these solutions for 24 hours at room temperature in a glass vial. We then diluted these samples in cold (4 °C) deionized water at a 2:1 (v/v) ratio (H_2O:HFIP). After aliquoting the resulting Aβ solution into glass vials, we immediately froze these aliquots in liquid

nitrogen followed by lyophilization for two days to remove HFIP below the detection limit by fluorine NMR (see *Fig.* A3-2, *Appendix*). Unless noted otherwise, we used the Aβ powder from these HFIP-treated lyophilisates for all experiments.

Method A: Aggregation of Aβ in deionized H_2O

Before starting the aggregation process, we dissolved the Aβ powder in diH_2O at a concentration of 1 mg mL^{-1} in siliconized microvials (Fisher Scientific, Pittsburg, PA), shock-froze 50-300 μL of these solutions in liquid nitrogen and stored them at -80 °C. To start the aggregation of Aβ samples, we thawed these Aβ samples and incubated them while shaking at 750 RPM at a temperature of 22 °C in a thermomixer (Eppendorf, Hauppauge, NY) for 1, 2, 3, 10 and 20 d (with an error of ± 4 h for each day). The 0-d sample was typically used within 0-2 h after thawing the samples.

Method B: Aggregation of non-HFIP treated Aβ in deionized H_2O

This method was exactly the same as method A, with the exception that we used Aβ powder as obtained from the suppliers without HFIP treatment.

Method C : Aggregation of Aβ in HFIP/ diH_2O for 2 d

This method is a modified version of a preparation method of amyloid oligomers reported by Kayed *et al*. (*43, 44, 95*). We made modifications to minimize the artifacts by remaining HFIP solvent in the Aβ samples (*33*). Briefly, we resuspended 1.0 mg of lyophilized Aβ powder in 400 μL HFIP for 15 min at room temperature. We then diluted 100 μL of this Aβ solution with 900 μL deionized H_2O in a siliconized microvial, and

incubated this solution for 15 min at room temperature, followed by centrifugation at 14,000 x g for 15 min at 22 °C. We transferred 950 μL of the supernatant to a new siliconized microvial and exposed it to shaking at 750 RPM for 2 d (48 ± 4 h) at a temperature of 22 °C. During this incubation, we kept the lid of the microvial open, in order to remove HFIP by evaporation. We have shown previously that this method removed HFIP sufficiently to carry out planar bilayer recording without detectable artifacts (*33*). We calculated the final concentration of Aβ from the remaining volume of Aβ solution after this two-day incubation.

Method D and E: Aggregation of Aβ in proteoliposomes

To prepare proteoliposomes with Aβ, we followed the original method described by Arispe *et al* (*29*) (method D). We evaporated 20 μL DOPS lipids in chloroform (20 mg mL^{-1}) in a glass vial with a rotary evaporator under vacuum for 1 h and formed liposomes using the gentle rehydration method in 30 μL of a 1 M potassium aspartate solution with a pH of 7.2, followed by bath sonication for 10-15 min. We mixed the liposome suspension with 1 mg mL^{-1} Aβ solution in water to reach a final concentration of 0.4-0.5 mg mL^{-1} of Aβ. This mixture was then sonicated for 10-15 min to produce Aβ proteoliposomes.

In order to initiate fusion of Aβ proteoliposomes into a preformed PLB, we added 10-30 μL of the Aβ proteoliposome solution to the *cis* compartment to reach a final concentration of ~ 1-5 μM of Aβ. In order to promote fusion, we established an ionic gradient of 370 mM KCl with 1 mM $CaCl_2$ on the *cis* side and 70 mM KCl on the *trans* side of the bilayer setup.

In an alternative approach, (method E) with the intent to remove the requirement of Ca^{2+}-mediated fusion, we adapted this method by forming liposomes containing positively charged lipids, 1,2-dioleoyl-3-trimethylammonium-propane (DOTAP) before incorporating Aβ. Instead of using 100% DOPS lipids, we used a mixture of DOTAP:DOPS:POPE:POPC (3:1:4:2, by weight). Fusion of these positively charged proteoliposomes did not require an ionic gradient for planar lipid bilayer recordings as they fused spontaneously to the PLB.

3.4.6 Cytotoxicity assay

SH-SY5Y human neuroblastoma cells obtained from ATCC were maintained in 5% CO_2 at 37 °C in Dulbecco's Modified Eagle's medium (DMEM)/F-12 (1:1) containing 10% (v/v) fetal bovine serum, 4 mM glutamax, 100 U mL^{-1} penicillin and 100 μg mL^{-1} streptomycin. All cell culture reagents were purchased from Invitrogen (Carlsbad, CA). We seeded cells in 96-well plate (50,000 cells $well^{-1}$) 24 h before performing cell viability assays. We diluted Aβ samples as described previously with serum-free Opti-MEM medium (*33*). We exchanged the culture medium with the fresh Aβ-containing Opti-MEM medium such that the final concentration of Aβ was 20 μM. After 24 h of incubation, we determined cell viability using an MTT cell proliferation assay (ATCC), according to the instructions from the supplier.

3.4.7 SDS-PAGE/Western blotting

In order to maintain the aggregation state of Aβ samples during SDS-PAGE, we crosslinked the Aβ peptides with 12 mM glutaraldehyde for 20 min, followed by addition of 1 M Tris buffer to stop the reactions (*38, 83*)}. We then diluted these Aβ samples in Tricine sample buffer (Bio-rad), containing 200 mM Tris-HCl at pH 6.8, 40% glycerol, 2% w/v SDS, 0.04% w/v Coomassie Blue G-250, and 2% β-mercaptoethanol, and heated them at 95˚C for 5 min. We separated these samples by SDS-PAGE using 50 ng of Aβ for each sample using a 1-mm-thick, 16.5% Tris-Tricine SDS gel (Bio-rad) in 100 mM Tris-HCl, 100 mM tricine, and 0.1 % SDS (unless indicated otherwise), operating at 100 V. We then transferred the samples from the gel to a polyvinylidene fluoride (PVDF) membrane (PerkinElmer Life Science). After incubation in a blocking solution containing 5% w/v nonfat dry milk in Tris-buffered saline (TBS) with 0.0625% w/v Tween 20 for 1 h at room temperature with a gentle agitation, we washed the membrane three times for 5 minutes with 50 mM Tris, 150 mM NaCl, and 0.05% Tween20 (TBS-T), and then incubated the membrane with a primary antibody 6E10 (monoclonal antibody against Aβ) diluted in 5% nonfat dry milk in TBS-T (1:4000 dilution, v/v) for 1.5 hour, followed by washing three times with TBS-T for 5 minutes each time. We then incubated the gels with an anti-mouse IgG-horseradish peroxidase conjugated secondary antibody (Southern Biotech, Birmingham, AL) diluted in 5% nonfat dry milk in TBS-T (1:8000 dilution, v/v) for 1 hour under a gentle agitation.

We detected the Aβ aggregated species on the PVDF membrane by using an enhanced chemiluminescence detection kit (ECL, PerkinElmer Life Sciences) according to a protocol from supplier. We developed images of gels using Hope Micro-MAX film

processor Model 319 (Hope X-ray Products Inc., Warminster, PA). We estimated the molecular mass of the Aβ aggregates based on rainbow molecular weight markers (Amersham Biosciences, Pittsburg, PA) and SeeBlue Plus2 pre-stained standard markers (Invitrogen, Carlsbad, CA)

3.4.8 SDS-PAGE/silver staining

For silver staining detection, we used the same type of gel as used in Western blotting. We loaded each well in the gels with 2 μg of the different Aβ samples. After gel electrophoresis, we fixed the polyacrylamide gels by incubating them for 90 minutes in an aqueous solution containing 10% (v/v) acetic acid, and 45% (v/v) ethanol under a gentle agitation, followed by washing the gels with diH_2O for 30 minutes. After incubating the gel in 32.5 μM dithiothreitol (DTT) for 30 minutes, we stained the proteins with 0.1% (w/v) silver nitrate for 30 minutes, followed by rinsing the gels in diH_2O. In the developing step, we soaked the gels in the developing solution (an aqueous solution containing 0.0365% (v/v) formaldehyde and 3%(w/v) Na_2CO_3) until the bands on the gel were visible. We then rinsed the gel with diH_2O, incubated the gels with 5% acetic acid for 1 minute to stop the destaining process, and imaged the gels with a dual light transluminator (Fotodyne Inc. Hartland, WI).

3.4.9 Quantification of the relative abundance of Aβ species

After obtaining the scanned images of gels from Western blotting or silver staining in TIFF format, we converted the images into 256 grayscale mode, and adjusted the levels of brightness and contrast of the scanned image by using Adobe Photoshop CS3 software to maximize the dynamic range of the resulting image histograms which represent a distribution of intensity of all image pixels. We then imported each image into Matlab 7.9 software and determined the intensity values of all image pixels by using the Image Processing Toolbox of the program. For each lane of the gel, we obtained a matrix which contained intensity values ranging from 0 to 255, corresponding to the image pixels, where 0 corresponds to the darkest pixel, and 255 correspond to the lightest pixel on the image. We scaled the intensity of the darkest pixel on the band to 1 and the lightest pixel located in the area outside the band to 0, and combined these values in each row of the matrix to obtain an intensity profile for each Aβ sample. To determine the relative abundance of each aggregated Aβ species (*i.e.*, monomer, dimer, trimer, etc.), we integrated the area under the respective peak on the intensity profile and divided it by the sum of the intensity values from all pixels in the same lane. For the aggregated species which were larger than hexamers, individual species were not distinguishable on the gel; therefore we estimated the relative abundance of oligomers based on the positions of molecular weight markers on the same gel and combined the intensity of the pixels with the following ranges: 34-55 kDa, 55-78 kDa, and 78-210 kDa, which correspond to approximately 8-13 mers, 14-18 mers, and 19-49 mers, respectively.

3.4.10 ThT binding to aggregates of Aβ peptides

To monitor the fibril formation of Aβ as a function of the incubation time, we measured the fluorescence intensity of ThT after different incubation times. For each incubation time point, we diluted 30 μL of each Aβ sample to a final concentration of 10 μM Aβ with an aqueous buffer containing 10 mM of NaH_2PO_4/Na_2HPO_4 pH 7.0, 150 mM NaCl, and 15 μM of ThT (*96*). After mixing, we transferred 30 μL of the resulting Aβ sample into a disposable cuvette (Precision Cells, Inc., Farmingdale, NY), and incubated the sample for 5 minutes at room temperature. We measured the intensity of ThT fluorescence at an emission wavelength of 485 nm using an excitation wavelength of 440 nm, with a Fluorolog-3 spectrofluorometer (Horiba Jobin Yvon, Edison, NJ). We calculated the relative ThT fluorescence intensity with respect to the maximum fluorescence when Aβ was incubated for 20 d.

3.4.11 Circular Dichroism Spectrometry

We measured the CD spectra of 20 μM Aβ samples in 10 mM NaH_2PO_4/Na_2HPO_4 pH 7.4 at a temperature of 25 °C using a wavelength range of 190-260 nm in a quartz cuvette with a path length of 0.1 cm (Starna), and an Aviv model 202 circular dichroism spectrometer (Aviv Biomedical Inc., Lakewood, NJ). Each CD spectrum was averaged from 5 consecutive scans and followed by a subtraction of its buffer control spectrum which was averaged from 3 consecutive scans. The secondary structures of Aβ were analyzed using the CONTINLL algorithm, which is available through the CDPro software with reference basis set of SDP42 (*97*).

3.4.12 Transmission Electron Microscopy

We prepared the samples for TEM analysis by using negative staining method. We applied 5 μL of each Aβ sample which was pre-incubated at various aggregation times to glow-discharged Formvar/carbon coated on 200 mesh copper grids (Fisher scientific). After adsorption for 2 min, we washed the grids with 5 μL deionized water, and applied a 5-μL drop of 2% uranyl acetate for 1 min. We blotted off the excess fluid on the grids with filter paper and allowed the grids to dry. We examined the images of negatively stained Aβ structures, using JEOL 3011 High resolution electron microscope (Jeol Ltd., Tokyo, Japan).

3.4.13 Statistical analysis

To determine statistical significance of differences between Aβ samples from different pre-incubation times, we determined all *p*-values using a two-sample Student's *t*-test from the Origin 8.0 software package (Northampton, MA). Since the results from the pore formation experiments were binary responses, we used Barnard's exact test, which is a statistical test to determine the exact *p*-values between binary responses (see *Appendix*). We obtained a Matlab algorithm for calculating Barnard's exact test from the Matlab Central site (*98*).

Chapter 3 Appendix

A3-1. Comparison of aggregation states of Aβ samples from different suppliers with and without HFIP-treatment and lyophilization for 2 d

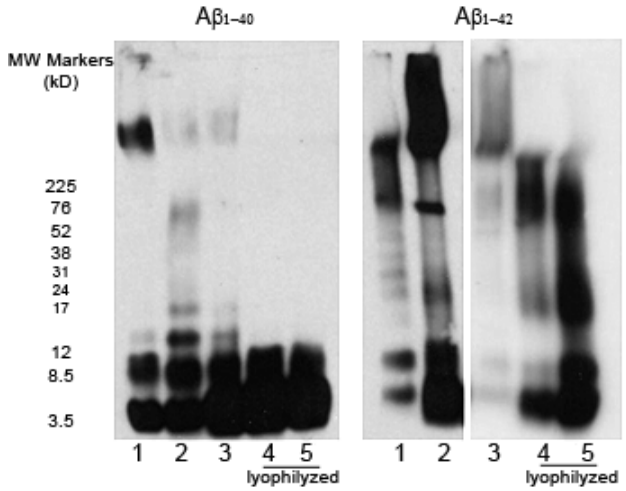

Figure A3-1. SDS-PAGE/Western Blot of Aβ samples from different suppliers with or without treatment with HFIP followed by lyophilization. All Aβ samples were prepared freshly in deionized H_2O at a concentration of 1 mg mL^{-1}. Each well in the 18%Tris-HCl gel (Bio-rad) was loaded with 0.2 μg of Aβ. Lane 1 = Bachem (non-lyophilized); 2 = GL Biochem, Ltd (Shanghai) (non-lyophilized); 3 = Biopeptide Inc. (non- lyophilized); 4 = GL Biochem, Ltd (Shanghai) (lyophilized); and 5 = Biopeptide Inc. (lyophilized). Aggregation of Aβ varies in commercial sources. HFIP treatment followed by lyophilyzation removed all aggregates of Aβ larger than ~ 12 kDa in the case of $Aβ_{1-40}$ and it removed large Aβ aggregates (>225 kDa) in the case of $Aβ_{1-42}$.

A3-2. Detection of HFIP by ^{19}F-NMR in Aβ samples after lyophilization for 2 d

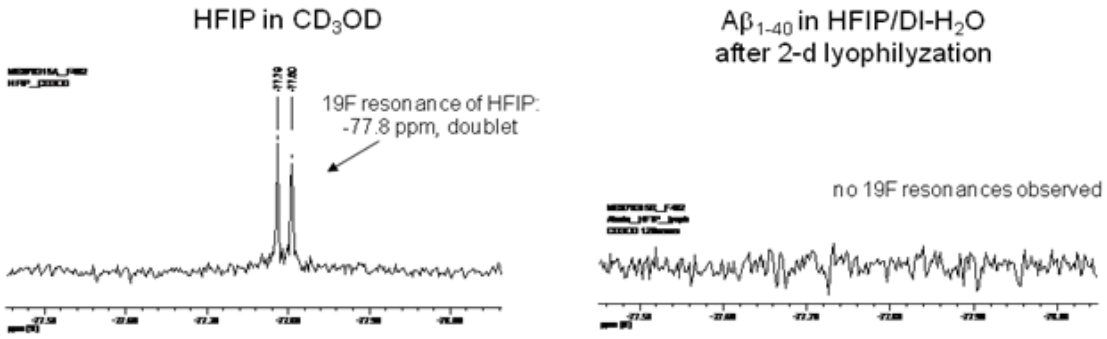

Figure A3-2. ^{19}F-NMR spectroscopy of HFIP in CD_3OD *(left)* and $A\beta_{1-40}$ sample that was incubated with HFIP and then lyophilized for two days as described in the Materials and Methods section *(right).* ^{19}F resonance of HFIP gave a doublet at -77.8 ppm, while the peak was absent after Aβ was lyophilized in HFIP for 48 h.

A3-3. Comparison of aggregation states of Aβ from various preparation methods

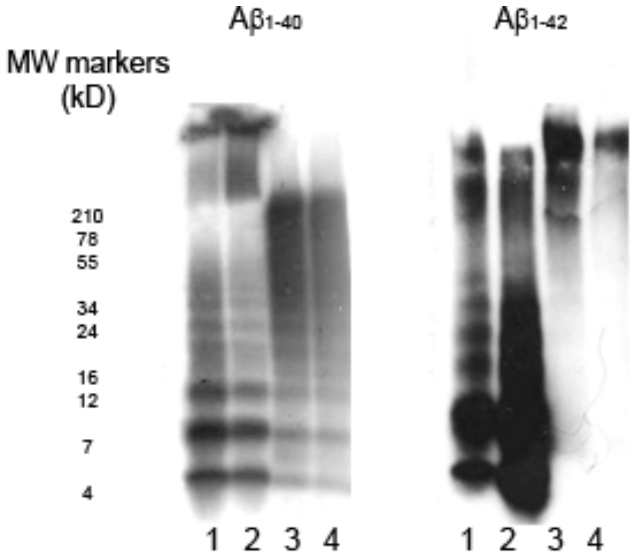

Figure A3-3. SDS-PAGE/Western blotting of $A\beta_{1-40}$ and $A\beta_{1-42}$ samples from various preparation methods. **1)** Method B: non-HFIP treated Aβ in di-H_2O with 0-d incubation; **2)** Method C: Modified Kayed preparation (HFIP/di-H_2O that entailed evaporation of HFIP during 2-d incubation); **3)** Method D: Aβ proteoliposomes containing DOPS; and **4)** Method E: Aβ proteoliposomes containing 30% of positively charged lipids, DOTAP. The high molecular weight oligomers from these four samples indicate that these preparations accelerated the aggregation of Aβ compared to preparations in diH_2O (*e.g.* lanes 4 and 5 in Figure 3-1) (*78, 79*).

A3-4. Determination of aggregation states of Aβ by SDS-PAGE/silver staining

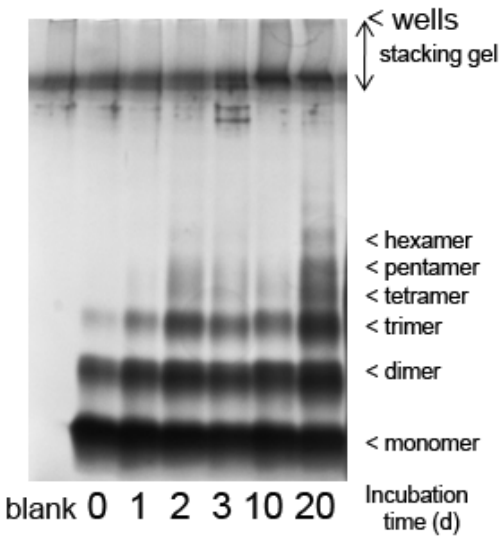

Figure A3-4. Silver staining after SDS-PAGE of $A\beta_{1\text{-}40}$ samples prepared by method A for 0 - 20 d. Two micrograms of sample was loaded into each well. The relative amount of intermediate (dimers to hexamers) or large aggregates of Aβ (the species in lane 10 and 20 in the stacking gel) increased with incubation time. The stacking portion of the silver stained gel appeared with a dark background even in the absence of protein (blank) as shown in the first lane on the left of the gel, making quantitative analysis of large aggregates difficult.

A3-5. Quantification of relative abundance of aggregate species with silver staining detection technique

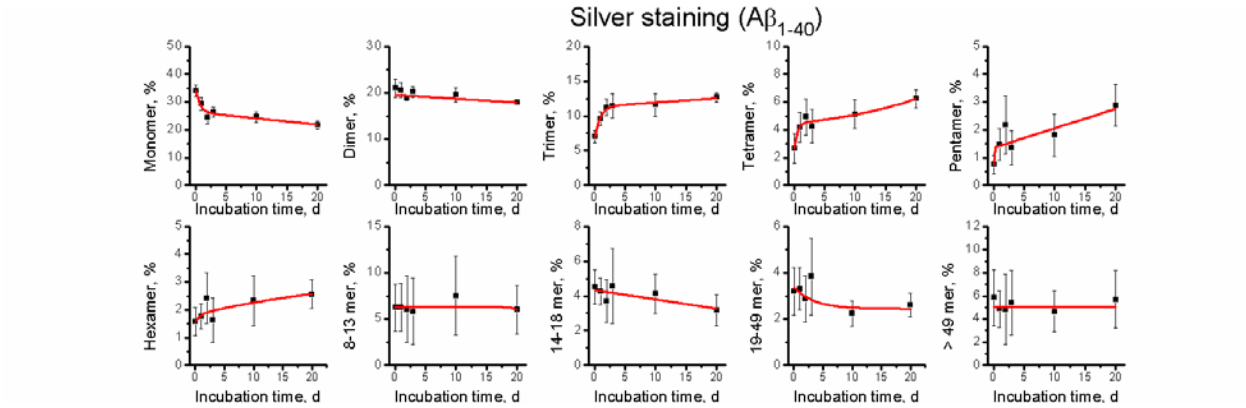

Figure A3-5. Relative abundance of various $A\beta_{1\text{-}40}$ aggregates of different size obtained after SDS-PAGE and silver staining. The intensity on the gel was corrected by subtraction with the blank (in the absence of protein). Each point represents the average of relative abundance of aggregates from six independent gels and samples; error bars represent the standard error of the mean.

A3-6. Pearson's correlation

Pearson's correlation, *r*, is a statistical measure of the correlation between two variables, giving a value between +1 and -1; a positive value implies a positive association and negative value implies the inverse relationship. The Pearson's correlation coefficient, *r*, is calculated by equation *(A3-1)*.

$$r = \frac{\sum_{i=1}^{n}(X_i-\bar{X})(Y_i-\bar{Y})}{\sqrt{\sum_{i=1}^{n}(X_i-\bar{X})^2(Y_i-\bar{Y})^2}} \qquad (A3\text{-}1)$$

where x_i represents aggregated Aβ species) and y_i represents probability of pore formation or cytotoxicity. We examined the Pearson's correlations between the relative abundance of each aggregated species obtained from the fit to the equation *(1)* and the probability of pore formation or cytotoxicity.

A3-7. Multiple Linear Regression

A multiple linear regression (MLR) model can be used to describe a given process for a complex interacting system. The purpose of Eq. (A3-2) is to clarify the nature of this complex interaction, in this case, a mixture of monomeric and aggregated Aβ species. The MLR model expresses a dependent variable as a linear function of a set of predicting variables with a constant as shown in Eq.(A3-2) under the following assumptions: 1) the relationship between the dependent variable and independent variables is linear, 2) the errors are independently and normally distributed, and 3) observations are independent of one another (*92*).

$$y = \beta_0 + \beta_1 x_1 + \beta_2 x_2 + \ldots + \beta_n x_n \qquad (A3\text{-}2)$$

where y = response or dependent variable,

x_i = predicting or independent variable

β_0 = regression constant,

β_i = coefficient on the i^{th} predicting variables,

n = number of predicting variables

The model is estimated by a least squares method, which minimizes the sum of squares of errors (ε_i^2) between predicted ($\hat{y}$) and observed data (y), as given by the following equation (*92*).

$$\sum_{i=1}^{n} \varepsilon_i^2 = \sum_{i=1}^{n} (y_i - \hat{y}_i)^2 \qquad \textit{(A3-3)}$$

For each model, we selected X_i values from different combinations of the relative abundance of aggregated Aβ species, while including the entire range of aggregated species in the model. Based on the control for both pore formation experiments and cytotoxicity assays, we determined the probability of pore formation (as well as the percentage of cell death) in the absence of Aβ (*i.e.*, when the relative abundance of all Aβ species was zero). We found that without Aβ, the probability of pore formation was 9.1 %, while the percentage of cell death was by definition 0. Given these two additional points, each data set for MLR analysis contained seven points, corresponding to the control experiment, and the experiments from Aβ samples with 0, 1, 2, 3, 10, and 20 d-incubation.

Determining the most appropriate MLR model

After performing the MLR analyses, we determined the quality of the fit by comparing the following parameters: 1) residual mean squares (RMS), which indicates the discrepancy between predicted and observed data; the small values are preferable, 2) *p*-values of all parameters, which indicate significance of the coefficient and the strength of the linear relationship between independent and dependent variables, and 3)

adjusted *R-squared* (R_a^2) values which measure a goodness of fit with a compensation of the degrees of freedom in the model as shown in equation *(A3-4)*,

$$R^2_a = 1 - \frac{n-1}{n-p-1}(1 - R^2), \qquad \textit{(A3-4)}$$

where *n* is the sample size, and *p* is the number of parameters (*92*).

Table A3-1. Deconvolution of CD spectra of Aβ in different preparation methods.

Preparation	% Content of secondary structure			
	Helix	β-sheet	β-turn	Unordered
$A\beta_{1\text{-}40}$-diH_2O $_{0\ d}$	3	25	14	59
$A\beta_{1\text{-}40}$-diH_2O $_{1\ d}$	3	32	17	48
$A\beta_{1\text{-}40}$-diH_2O $_{2\ d}$	4	34	19	43
$A\beta_{1\text{-}40}$-diH_2O $_{3\ d}$	6	35	19	41
$A\beta_{1\text{-}40}$-diH_2O $_{10\ d}$	4	34	20	42
$A\beta_{1\text{-}40}$-diH_2O $_{20\ d}$	9	43	23	24
$A\beta_{1\text{-}40}$-HFIP/diH_2O $_{2\ d}$	5	39	21	35
$A\beta_{1\text{-}42}$-diH_2O $_{0\ d}$	4	27	37	33
$A\beta_{1\text{-}42}$-diH_2O $_{1\ d}$	4	30	41	36
$A\beta_{1\text{-}42}$-diH_2O $_{2\ d}$	5	32	42	37
$A\beta_{1\text{-}42}$-diH_2O $_{3\ d}$	5	45	21	29
$A\beta_{1\text{-}42}$-diH_2O $_{10\ d}$	5	44	22	30
$A\beta_{1\text{-}42}$-diH_2O $_{20\ d}$	9	43	23	29
$A\beta_{1\text{-}42}$-HFIP/diH_2O $_{2\ d}$	5	41	21	33

References

1. Selkoe, D. J. (1991) The Molecular Pathology of Alzheimers-Disease, *Neuron 6*, 487-498.
2. Hardy, J. A., and Higgins, G. A. (1992) Alzheimers-Disease - the Amyloid Cascade Hypothesis, *Science 256*, 184-185.
3. LaFerla, F. M., Green, K. N., and Oddo, S. (2007) Intracellular amyloid-beta in Alzheimer's disease, *Nat. Rev. Neurosci. 8*, 499-509.
4. Glenner, G. G., and Wong, C. W. (1984) Alzheimers-Disease - Initial Report of the Purification and Characterization of a Novel Cerebrovascular Amyloid Protein, *Biochem. Biophys. Res. Commun. 120*, 885-890.
5. Wong, C. W., Quaranta, V., and Glenner, G. G. (1985) Neuritic Plaques and Cerebrovascular Amyloid in Alzheimer-Disease Are Antigenically Related, *Proc. Natl. Acad. Sci. U. S. A. 82*, 8729-8732.
6. Hardy, J., and Selkoe, D. J. (2002) The Amyloid Hypothesis of Alzheimer's Disease: Progress and Problems on the Road to Therapeutics, *Science 297*, 353-356.
7. Kang, J., Lemaire, H. G., Unterbeck, A., Salbaum, J. M., Masters, C. L., Grzeschik, K. H., Multhaup, G., Beyreuther, K., and Mullerhill, B. (1987) The Precursor of Alzheimers-Disease Amyloid-A4 Protein Resembles a Cell-Surface Receptor, *Nature 325*, 733-736.
8. Mattson, M. P. (2004) Pathways towards and away from Alzheimer's disease, *Nature 430*, 631-639.
9. Rangachari, V., Reed, D. K., Moore, B. D., and Rosenberry, T. L. (2006) Secondary structure and interfacial aggregation of amyloid-beta(1-40) on sodium dodecyl sulfate micelles, *Biochemistry (Mosc.) 45*, 8639-8648.
10. Parihar, M. S., and Hemnani, T. (2004) Alzheimer's disease pathogenesis and therapeutic interventions, *J. Clin. Neurosci. 11*, 456-467.
11. Broersen, K., Rousseau, F., and Schymkowitz, J. (2010) The culprit behind amyloid beta peptide related neurotoxicity in Alzheimer's disease: oligomer size or conformation?, *Alzheimers Res. Ther. 2*, 12.
12. Klyubin, I., Betts, V., Welzel, A. T., Blennow, K., Zetterberg, H., Wallin, A., Lemere, C. A., Cullen, W. K., Peng, Y., Wisniewski, T., Selkoe, D. J., Anwyl, R., Walsh, D. M., and Rowan, M. J. (2008) Amyloid beta protein dimer-containing human CSF disrupts synaptic plasticity: Prevention by systemic passive immunization, *J. Neurosci. 28*, 4231-4237.
13. Shankar, G. M., Leissring, M. A., Adame, A., Sun, X., Spooner, E., Masliah, E., Selkoe, D. J., Lemere, C. A., and Walsh, D. M. (2009) Biochemical and immunohistochemical analysis of an Alzheimer's disease mouse model reveals the presence of multiple cerebral A beta assembly forms throughout life, *Neurobiol. Dis. 36*, 293-302.
14. Shankar, G. M., Li, S. M., Mehta, T. H., Garcia-Munoz, A., Shepardson, N. E., Smith, I., Brett, F. M., Farrell, M. A., Rowan, M. J., Lemere, C. A., Regan, C. M., Walsh, D. M., Sabatini, B. L., and Selkoe, D. J. (2008) Amyloid-beta protein dimers isolated directly from Alzheimer's brains impair synaptic plasticity and memory, *Nat. Med. 14*, 837-842.
15. O'Nuallain, B., Freir, D. B., Nicoll, A. J., Risse, E., Ferguson, N., Herron, C. E., Collinge, J., and Walsh, D. M. (2010) Amyloid beta-Protein Dimers Rapidly Form Stable Synaptotoxic Protofibrils, *J. Neurosci. 30*, 14411-14419.
16. Podlisny, M. B., Ostaszewski, B. L., Squazzo, S. L., Koo, E. H., Rydell, R. E., Teplow, D. B., and Selkoe, D. J. (1995) Aggregation of Secreted Amyloid beta-Protein into Sodium Dodecyl Sulfate-Stable Oligomers in Cell Culture, *J. Biol. Chem. 270*, 9564-9570.
17. Townsend, M., Shankar, G. M., Mehta, T., Walsh, D. M., and Selkoe, D. J. (2006) Effects of secreted oligomers of amyloid beta-protein on hippocampal synaptic plasticity: a potent role for trimers, *J.Phys.-London 572*, 477-492.

18. Gong, Y. S., Chang, L., Viola, K. L., Lacor, P. N., Lambert, M. P., Finch, C. E., Krafft, G. A., and Klein, W. L. (2003) Alzheimer's disease-affected brain: Presence of oligomeric A beta ligands (ADDLs) suggests a molecular basis for reversible memory loss, *Proc. Natl. Acad. Sci. U. S. A. 100*, 10417-10422.
19. Viola, K. L., Velasco, P. T., and Klein, W. L. (2008) Why Alzheimer's is a disease of memory: The attack on synapses by A beta oligomers (ADDLs), *J. Nutr. Heath. Aging 12*, 51S-57S.
20. Lambert, M. P., Velasco, P. T., Chang, L., Viola, K. L., Fernandez, S., Lacor, P. N., Khuon, D., Gong, Y. S., Bigio, E. H., Shaw, P., De Felice, F. G., Krafft, G. A., and Klein, W. L. (2007) Monoclonal antibodies that target pathological assemblies of A beta, *J. Neurochem. 100*, 23-35.
21. Koh, J.-y., Yang, L. L., and Cotman, C. W. (1990) β-Amyloid protein increases the vulnerability of cultured cortical neurons to excitotoxic damage, *Brain Res. 533*, 315-320.
22. Lesne, S., Koh, M. T., Kotilinek, L., Kayed, R., Glabe, C. G., Yang, A., Gallagher, M., and Ashe, K. H. (2006) A specific amyloid-beta protein assembly in the brain impairs memory, *Nature 440*, 352-357.
23. Harper, J. D., Wong, S. S., Lieber, C. M., and Lansbury, P. T. (1997) Observation of metastable A beta amyloid protofibrils by atomic force microscopy, *Chemistry & Biology 4*, 119-125.
24. Walsh, D. M., Lomakin, A., Benedek, G. B., Condron, M. M., and Teplow, D. B. (1997) Amyloid beta-protein fibrillogenesis - Detection of a protofibrillar intermediate, *J. Biol. Chem. 272*, 22364-22372.
25. Kayed, R., Pensalfini, A., Margol, L., Sokolov, Y., Sarsoza, F., Head, E., Hall, J., and Glabe, C. (2009) Annular Protofibrils Are a Structurally and Functionally Distinct Type of Amyloid Oligomer, *J. Biol. Chem. 284*, 4230-4237.
26. Puzzo, D., and Arancio, O. (2006) Fibrillar beta-amyloid impairs the late phase of long term potentiation, *Curr. Alzheimer Res. 3*, 179-183.
27. Lorenzo, A., Yuan, M. L., Zhang, Z. H., Paganetti, P. A., Sturchler-Pierrat, C., Staufenbiel, M., Mautino, J., Sol Vigo, F., Sommer, B., and Yankner, B. A. (2000) Amyloid beta interacts with the amyloid precursor protein: a potential toxic mechanism in Alzheimer's disease, *Nat. Neurosci. 3*, 460-464.
28. Bucciantini, M., Giannoni, E., Chiti, F., Baroni, F., Formigli, L., Zurdo, J. S., Taddei, N., Ramponi, G., Dobson, C. M., and Stefani, M. (2002) Inherent toxicity of aggregates implies a common mechanism for protein misfolding diseases, *Nature 416*, 507-511.
29. Arispe, N., Pollard, H. B., and Rojas, E. (1993) Giant Multilevel Cation Channels Formed by Alzheimer-Disease Amyloid Beta-Protein [a-Beta-P-(1-40)] in Bilayer-Membranes, *Proc. Natl. Acad. Sci. U. S. A. 90*, 10573-10577.
30. Jang, H., Zheng, J., and Nussinov, R. (2007) Models of beta-amyloid ion channels in the membrane suggest that channel formation in the bilayer is a dynamic process, *Biophys. J. 93*, 1938-1949.
31. Kagan, B. L., Azimov, R., and Azimova, R. (2004) Amyloid peptide channels, *J. Membr. Biol. 202*, 1-10.
32. Yankner, A. L. a. B. A. (1994) b-Amyloid neurotoxicity requires fibril formation and is inhibited by Congo red, *Proc. Natl. Acad. Sci. USA 91*, 12243-12247.
33. Capone, R., Quiroz, F. G., Prangkio, P., Saluja, I., Sauer, A. M., Bautista, M. R., Turner, R. S., Yang, J., and Mayer, M. (2009) Amyloid-beta-Induced Ion Flux in Artificial Lipid Bilayers and Neuronal Cells: Resolving a Controversy, *Neurotox. Res. 16*, 1-13.
34. Lal, R., Lin, H., and Quist, A. P. (2007) Amyloid beta ion channel: 3D structure and relevance to amyloid channel paradigm, *BBA-BIOMEMBRANES 1768*, 1966-1975.
35. Arispe, N., Diaz, J. C., and Simakova, O. (2007) A beta ion channels. Prospects for treating Alzheimer's disease with A beta channel blockers, *BBA-BIOMEMBRANES 1768*, 1952-1965.

36. Kawahara, M. (2010) Neurotoxicity of beta-Amyloid Protein: Oligomerization, Channel Formation and Calcium Dyshomeostasis, *Curr. Pharm. Des. 16*, 2779-2789.
37. Jang, H., Arce, F. T., Capone, R., Ramachandran, S., Lal, R., and Nussinov, R. (2009) Misfolded Amyloid Ion Channels Present Mobile beta-Sheet Subunits in Contrast to Conventional Ion Channels, *Biophys. J. 97*, 3029-3037.
38. Quist, A., Doudevski, I., Lin, H., Azimova, R., Ng, D., Frangione, B., Kagan, B., Ghiso, J., and Lal, R. (2005) Amyloid ion channels: A common structural link for protein-misfolding disease, *Proc. Natl. Acad. Sci. U. S. A. 102*, 10427-10432.
39. Lin, H., Bhatia, R., and Lal, R. (2002) Amyloid beta protein forms ion channels: implications for Alzheimer's disease pathophysiology (vol 15, pg 2433, 2001), *FASEB J. 16*.
40. Strodel, B., Lee, J. W. L., Whittleston, C. S., and Wales, D. J. Transmembrane Structures for Alzheimer's A beta(1-42) Oligomers, *J. Am. Chem. Soc. 132*, 13300-13312.
41. Shafrir, Y., Durell, S. R., Anishkin, A., and Guy, H. R. (2010) Beta-barrel models of soluble amyloid beta oligomers and annular protofibrils, *Protein Struct. Funct. Bioinform. 78*, 3458-3472.
42. Schauerte, J. A., Wong, P. T., Wisser, K. C., Ding, H., Steel, D. G., and Gafni, A. (2010) Simultaneous Single-Molecule Fluorescence and Conductivity Studies Reveal Distinct Classes of A beta Species on Lipid Bilayers, *Biochemistry (Mosc.) 49*, 3031-3039.
43. Sokolov, Y., Kozak, J. A., Kayed, R., Chanturiya, A., Glabe, C., and Hall, J. E. (2006) Soluble Amyloid Oligomers Increase Bilayer Conductance by Altering Dielectric Structure, *J. Gen. Physiol. 128*, 637-647.
44. Sokolov, Y. V., Kayed, R., Kozak, A., Edmonds, B., McIntire, T. M., Milton, S., Cahalan, M., Glabe, C. G., and Hall, J. E. (2004) Soluble amyloid oligomers increase lipid bilayer conductance by increasing the dielectric constant of the hydrocarbon core, *Biophys. J. 86*, 382A-382A.
45. Micelli, S., Meleleo, D., Picciarelli, V., and Gallucci, E. (2004) Effect of sterols on beta-amyloid peptide (A beta P 1-40) channel formation and their properties in planar lipid membranes, *Biophys. J. 86*, 2231-2237.
46. Eliezer, D. (2006) Amyloid Ion Channels: A Porous Argument or a Thin Excuse?, *J. Gen. Physiol. 128*, 631-633.
47. Lin, H., Zhu, Y. W. J., and Lal, R. (1999) Amyloid beta protein (1-40) forms calcium-permeable, Zn^{2+}-sensitive channel in reconstituted lipid vesicles, *Biochemistry (Mosc.) 38*, 11189-11196.
48. Hirakura, Y., Lin, M. C., and Kagan, B. L. (1999) Alzheimer amyloid a beta 1-42 channels: Effects of solvent, pH, and Congo Red. (vol 57, pg 458, 1999), *J. Neurosci. Res. 58*, 726-726.
49. Rhee, S. K., Quist, A. P., and Lal, R. (1998) Amyloid beta protein-(1-42) forms calcium-permeable, Zn2+-sensitive channel, *J. Biol. Chem. 273*, 13379-13382.
50. Hortschansky, P., Schroeckh, V., Christopeit, T., Zandomeneghi, G., and Fandrich, M. (2005) The aggregation kinetics of Alzheimer's beta-amyloid peptide is controlled by stochastic nucleation, *Protein Sci. 14*, 1753-1759.
51. Hilbich, C., Kisterswoike, B., Reed, J., Masters, C. L., and Beyreuther, K. (1991) Aggregation and Secondary Structure of Synthetic Amyloid Beta-A4 Peptides of Alzheimers-Disease, *J. Mol. Biol. 218*, 149-163.
52. Kumar, S., Mohanty, S. K., and Udgaonkar, J. B. (2007) Mechanism of formation of amyloid protofibrils of barstar from soluble oligomers: Evidence for multiple steps and lateral association coupled to conformational conversion, *J. Mol. Biol. 367*, 1186-1204.
53. Snyder, S. W., Ladror, U. S., Wade, W. S., Wang, G. T., Barrett, L. W., Matayoshi, E. D., Huffaker, H. J., Krafft, G. A., and Holzman, T. F. (1994) Amyloid-Beta Aggregation - Selective-Inhibition of Aggregation in Mixtures of Amyloid with Different Chain Lengths, *Biophys. J. 67*, 1216-1228.

54. Zagorski, M. G., Yang, J., Shao, H. Y., Ma, K., Zeng, H., and Hong, A. (1999) Methodological and chemical factors affecting amyloid beta peptide amyloidogenicity, *Amyloid, Prions, and Other Protein Aggregates 309*, 189-204.
55. Barrow, C. J., Yasuda, A., Kenny, P. T. M., and Zagorski, M. G. (1992) Solution Conformations and Aggregational Properties of Synthetic Amyloid Beta-Peptides of Alzheimers-Disease - Analysis of Circular-Dichroism Spectra, *J. Mol. Biol. 225*, 1075-1093.
56. Burdick, D., Soreghan, B., Kwon, M., Kosmoski, J., Knauer, M., Henschen, A., Yates, J., Cotman, C., and Glabe, C. (1992) Assembly and Aggregation Properties of Synthetic Alzheimers A4/Beta Amyloid Peptide Analogs, *J. Biol. Chem. 267*, 546-554.
57. Fraser, P. E., Nguyen, J. T., Surewicz, W. K., and Kirschner, D. A. (1991) Ph-Dependent Structural Transitions of Alzheimer Amyloid Peptides, *Biophys. J. 60*, 1190-1201.
58. Harper, J. D., and Lansbury, P. T. (1997) Models of amyloid seeding in Alzheimier's disease and scrapie: Mechanistic truths and physiological consequences of the time-dependent solubility of amyloid proteins, *Annu. Rev. Biochem. 66*, 385-407.
59. Howlett, D. R., Jennings, K. H., Lee, D. C., Clark, M. S. G., Brown, F., Wetzel, R., Wood, S. J., Camilleri, P., and Roberts, G. W. (1995) Aggregation State and Neurotoxic Properties of Alzheimer Beta-Amyloid Peptide, *Neurodegeneration 4*, 23-32.
60. Kaneko, I. (1997) Conformations of beta-amyloid in solution - Reply, *J. Neurochem. 68*, 438-439.
61. Soto, C., Castano, E. M., Kumar, R. A., Beavis, R. C., and Frangione, B. (1995) Fibrillogenesis of synthetic amyloid-beta peptides is dependent on their initial secondary structure, *Neurosci. Lett. 200*, 105-108.
62. Brining, S. K. (1997) Predicting the in vitro toxicity of synthetic beta-amyloid (1-40), *Neurobiol. Aging 18*, 581-589.
63. May, P. C., Gitter, B. D., Waters, D. C., Simmons, L. K., Becker, G. W., Small, J. S., and Robison, P. M. (1992) Beta-Amyloid Peptide Invitro Toxicity - Lot-to-Lot Variability, *Neurobiol. Aging 13*, 605-607.
64. Sato, C., Castano, E. M., Kumar, R. A., Beavis, R. C., and Frangione, B. (1995) Fibrillogenesis of Synthetic Amyloid-Beta Peptides Is Dependent on Their Initial Secondary Structure, *Neurosci. Lett. 200*, 105-108.
65. Naiki, H., and Gejyo, F. (1999) Kinetic analysis of amyloid fibril formation, In *Amyloid, Prions, and Other Protein Aggregates*, pp 305-318.
66. Nichols, M. R., Moss, M. A., Reed, D. K., Hoh, J. H., and Rosenberry, T. L. (2005) Amyloid-beta aggregates formed at polar-nonpolar interfaces differ from amyloid-beta protofibrils produced in aqueous buffers, *Microsc. Res. Tech. 67*, 164-174.
67. Szabo, Z., Jost, K., Soos, K., Zarandi, M., Kiss, J. T., and Penke, B. (1999) Solvent effect on aggregational properties of beta-amyloid polypeptides studied by FT-IR spectroscopy, *Journal of Molecular Structure 481*, 481-487.
68. Jao, S. C., Ma, K., Talafous, J., Orlando, R., and Zagorski, M. G. (1997) Trifluoroacetic acid pretreatment reproducibly disaggregates the amyloid beta-peptide, *Amyloid-International Journal of Experimental and Clinical Investigation 4*, 240-252.
69. Jan, A., Hartley, D. M., and Lashuel, H. A. (2010) Preparation and characterization of toxic A beta aggregates for structural and functional studies in Alzheimer's disease research, *Nat. Protoc. 5*, 1186-1209.
70. Ennaceur, S. M., and Sanderson, J. M. (2005) Micellar aggregates formed following the addition of hexafluoroisopropanol to phospholipid membranes, *Langmuir 21*, 552-561.
71. Sanderson, K. L., Butler, L., and Ingram, V. M. (1997) Aggregates of a beta-amyloid peptide are required to induce calcium currents in neuron-like human teratocarcinoma cells: Relation to Alzheimer's disease, *Brain Res. 744*, 7-14.

72. Arispe, N., Rojas, E., and Pollard, H. B. (1993) Alzheimer-Disease Amyloid Beta-Protein Forms Calcium Channels in Bilayer-Membranes - Blockade by Tromethamine and Aluminum, *Proc. Natl. Acad. Sci. U. S. A. 90*, 567-571.
73. Bhatia, R., Lin, H., and Lal, R. (2000) Fresh and globular amyloid β protein (1-42) induces rapid cellular degeneration: evidence for AβP channel-mediated cellular toxicity, *FASEB J. 14*, 1233-1243.
74. Kagan, B. L., Hirakura, Y., Azimov, R., Azimova, R., and Lin, M. C. (2002) The channel hypothesis of Alzheimer's disease: current status, *Peptides 23*, 1311-1315.
75. Kourie, J., Culverson, A., Farrelly, P., Henry, C., and Laohachai, K. (2002) Heterogeneous amyloid-formed ion channels as a common cytotoxic mechanism, *Cell Biochem. Biophys. 36*, 191-207.
76. Kourie, J., Henry, C., and Farrelly, P. (2001) Diversity of Amyloid β Protein Fragment [1–40]-Formed Channels, *Cell. Mol. Neurobiol. 21*, 255-284.
77. Lin, M. C. A., and Kagan, B. L. (2002) Electrophysiologic properties of channels induced by A beta 25-35 in planar lipid bilayers, *Peptides 23*, 1215-1228.
78. Kurganov, B., Doh, M., and Arispe, N. (2004) Aggregation of liposomes induced by the toxic peptides Alzheimer's Aβs, human amylin and prion (106-126): facilitation by membrane-bound GM1 ganglioside, *Peptides 25*, 217-232.
79. Butterfield, S. M., and Lashuel, H. A. (2010) Amyloidogenic Protein Membrane Interactions: Mechanistic Insight from Model Systems, *Angew. Chem. Int. Ed. 49*, 5628-5654.
80. Majd, S., Yusko, E. C., Billeh, Y. N., Macrae, M. X., Yang, J., and Mayer, M. (2010) Applications of biological pores in nanomedicine, sensing, and nanoelectronics, *Curr. Opin. Biotechnol. 21*, 439-476.
81. Barnard, G. A. (1945) A New Test for 2x2 Tables, *Nature 156*, 177-177.
82. Barnard, G. A. (1947) 2x2 Tables - a Note on Pearson,E.S. Paper, *Biometrika 34*, 168-169.
83. Levine, H. (1995) Soluble Multimeric Alzheimer beta(1-40) pre-amyloid complexes in dilute-solution, *Neurobiol. Aging 16*, 755-764.
84. Vriens, G. N. (1954) Kinetics of Coupled Reversible Reactions, *Ind. Eng. Chem. 46*, 669-671.
85. Ryan, D. A., Narrow, W. C., Federoff, H. J., and Bowers, W. J. (2010) An improved method for generating consistent soluble amyloid-beta oligomer preparations for in vitro neurotoxicity studies, *J. Neurosci. Methods 190*, 171-179.
86. Freir, D. B., Nicoll, A. J., Klyubin, I., Panico, S., Mc Donald, J. M., Risse, E., Asante, E. A., Farrow, M. A., Sessions, R. B., Saibil, H. R., Clarke, A. R., Rowan, M. J., Walsh, D. M., and Collinge, J. (2011) Interaction between prion protein and toxic amyloid [beta] assemblies can be therapeutically targeted at multiple sites, *Nat. Commun. 2*, 336.
87. Barghorn, S., Nimmrich, V., Striebinger, A., Krantz, C., Keller, P., Janson, B., Bahr, M., Schmidt, M., Bitner, R. S., Harlan, J., Barlow, E., Ebert, U., and Hillen, H. (2005) Globular amyloid β-peptide$_{1-42}$ oligomer - a homogenous and stable neuropathological protein in Alzheimer's disease, *J. Neurochem. 95*, 834-847.
88. Bitan, G., Kirkitadze, M. D., Lomakin, A., Vollers, S. S., Benedek, G. B., and Teplow, D. B. (2003) Amyloid beta-protein (A beta) assembly: A beta 40 and A beta 42 oligomerize through distinct pathways, *Proc. Natl. Acad. Sci. U. S. A. 100*, 330-335.
89. Gellermann, G. P., Byrnes, H., Striebinger, A., Ullrich, K., Mueller, R., Hillen, H., and Barghorn, S. (2008) A beta-globulomers are formed independently of the fibril pathway, *Neurobiol. Dis. 30*, 212-220.
90. Hartley, D. M., Walsh, D. M., Ye, C. P. P., Diehl, T., Vasquez, S., Vassilev, P. M., Teplow, D. B., and Selkoe, D. J. (1999) Protofibrillar intermediates of amyloid beta-protein induce acute electrophysiological changes and progressive neurotoxicity in cortical neurons, *J. Neurosci. 19*, 8876-8884.

91. Ono, K., Condron, M. M., and Teplow, D. B. (2009) Structure-neurotoxicity relationships of amyloid beta-protein oligomers, *Proc. Natl. Acad. Sci. U. S. A. 106*, 14745-14750.
92. Chatterjee, S., and Hadi, A. S. (2006) *Regression Analysis by Example*, 4th ed., Wiley-Interscience, Hoboken, NJ.
93. Mueller, P., Wescott, W. C., Rudin, D. O., and Tien, H. T. (1963) Methods for Formation of Single Bimolecular Lipid Membranes in Aqueous Solution, *J. Phys. Chem. 67*, 534-&.
94. Capone, R., Blake, S., Restrepo, M. R., Yang, J., and Mayer, M. (2007) Designing nanosensors based on charged derivatives of gramicidin A, *J. Am. Chem. Soc. 129*, 9737-9745.
95. Kayed, R., Head, E., Thompson, J. L., McIntire, T. M., Milton, S. C., Cotman, C. W., and Glabe, C. G. (2003) Common structure of soluble amyloid oligomers implies common mechanism of pathogenesis, *Science 300*, 486-489.
96. Nilsson, M. R. (2004) Techniques to study amyloid fibril formation in vitro, *Methods 34*, 151-160.
97. Sreerama, N., and Woody, R. W. (2000) Estimation of protein secondary structure from circular dichroism spectra: Comparison of CONTIN, SELCON, and CDSSTR methods with an expanded reference set, *Anal. Biochem. 287*, 252-260.
98. Cardillo, G. (2009) MyBarnard: a very compact routine for Barnard's exact test on 2x2 matrix.

Chapter 4

Membrane Disruption in Unilamellar Liposomes Induced by Amyloid-beta (Aβ) Peptides at Different Aggregation States

Increasing evidence indicates that Aβ peptides, especially in their oligomeric states, play an important role in pathogenesis of AD. A possible pathogenic mechanism of Aβ oligomers is formation of pores through neuronal membranes, resulting in cell death. In this chapter, we examine the effect of Aβ on permeabilization of liposomes by using proton leakage and dye quenching assays. The studies confirm that Aβ is able to disrupt the membranes and cause the leakage of liposomal contents that range in size as small as protons to as large as dye molecules. With regards to aggregation states of Aβ, we demonstrate that the ability of Aβ to induce leakage in unilamellar liposomes decreased as the aggregation of Aβ progressed. A decrease in activity of membrane disruption in the liposomes could be because of a decrease in abundance of Aβ monomers, and small oligomers (dimers and trimers), which were decreasing over the incubation time, or a decrease in effective concentration of Aβ in the suspension (since small oligomers become larger assemblies). This observed trend does not correlate with results of pore formation in the planar lipid bilayers. We postulate that membrane permeabilization in these lipid models could be driven by different mechanisms due to

the fundamental differences in the experimental systems such as the membrane curvature, stability and sensitivity of lipid membranes.

4.1 Introduction

A disruption of membrane integrity or membrane permeabilization induced by peptide is considered as a primary indicator of toxicity (*1*). Biophysical and biochemical studies have demonstrated that the toxicity of Aβ along with other amyloid proteins is associated with their ability to disrupt membrane integrity (*1, 2*). However, the details regarding the membrane permeabilization induced by amyloid proteins still remain unclear at the molecular level (*3*).

The mechanism of membrane permeabilization depends on lipid composition, membrane integrity, and structure of peptides. Aggregation of Aβ peptides associates with stochastic process as the peptide samples exist in a heterogeneous mixture of assemblies and also depend on factors, such as ionic strength, pH, concentration of Aβ peptides, and chemical nature of impurities and residues in the Aβ samples (ions, solvents, etc.) (*4-6*). To date, several research groups considered that the oligomeric forms of Aβ are the most toxic species which can disrupt membrane structural integrity by inducing an unregulated passage of ions and small molecules through the membrane (*7*).

In chapter 2, we discuss two mechanisms of ion flux induced by Aβ, namely pore formation through membranes, and thinning of membranes. (*4*) We demonstrate by electrophysiological techniques that Aβ induce ion flux across membranes by inserting

through the membranes as opposed to the thinning of membranes, thus clarifying the controversy with regard to mechanism of Aβ-induced ion flux.

Biological membranes are complex mixtures of phospholipids, glycoproteins, and cholesterols, having several functions including transport, and maintaining the structural integrity of cells (*1, 8*). Given their spherical shape with water-filled interior, and ease of producing, lipid vesicles are commonly used lipid models in lipid-protein interaction studies.

Dye leakage assay is a common technique used for studying peptide-induced membrane permeabilization. The liposomes are loaded with self-quenching fluorescent dyes, such as carboxy-fluorescein, calcein, or sulforhodamine B, at high concentrations (*1, 9-11*). The peptide-induced permeabilization of membranes causes the dye molecules to leak from the inside of the liposomes to the outside, resulting in an increase in the fluorescence intensity upon the dilution of dyes in the external media. The other method to determine peptide-induced membrane permeabilization is by cation leakage assays using ion-sensitive dyes, such as Fura-2, a Ca^{2+} sensitive fluorescent dye (*12*).

In chapter 3, we examine the influence of Aβ at various aggregation conditions on pore formation in planar lipid bilayers. Our studies revealed that $A\beta_{1-40}$ and $A\beta_{1-42}$ yielded the highest probability of pore formation when the samples were pre-incubated in pure water for 2-3 days. These samples contained the highest relative abundance of Aβ oligomers (tetramer to 13-mer), as revealed by SDS-PAGE.

In this chapter, we investigate the effect of aggregation state of Aβ on permeabilization of unilamellar liposomes in order to compare the results with the planar

lipid bilayer (PLB) recordings in chapter 3. We employed liposome leakage assays to determine the leakage of protons or dye molecules upon the addition of Aβ using the same preparation methods used in PLB recordings. We assessed the membrane permeabilization in the unilamellar liposomes by detecting the change in fluorescent signal in response to leakage of protons or dye molecules whereas in the electrophysiological studies, we measured an electrical response (*i.e.*, current) due to conductivity of ions across the PLB.

The main advantage of the liposome-based leakage assay over the electrophysiological technique is that we could examine the overall membrane permeability from a large number of membranes in one experiment, while the PLB recording allows us to examine the permeability of one bilayer for each experiment. The properties and environment of lipid membranes in both lipid systems were; however, not strictly the same; thus various factors may influence membrane permeability differently in these membrane models.

4.2 Results and discussion

4.2.1 Characterization of Aβ

We examined the aggregation states of Aβ in water at each time point of aggregation using several techniques as described in chapter 3, including thioflavin T (ThT) binding assay, circular dichroism (CD), SDS-PAGE/Western blotting, and transmission electron microscopy (TEM). ThT binding assay revealed that a significant amount of Aβ fibrils were present in the samples after 2 d of incubation for $A\beta_{1-40}$

samples and within 1 d for $A\beta_{1-42}$ samples. The increase in fibril formation correlated with results from circular dichroism which also showed an increasing percentage of β-sheet structure over the incubation time.

Based on the Western blotting analysis, the relative abundance of monomers, dimers, and trimers decreased over the incubation time (see *Fig.* 3-4, Chapter 3). The intermediate aggregated species (*i.e.,* tetramers through 13-mers in the case of $A\beta_{1-40}$, and tetramers through hexamers for $A\beta_{1-42}$) increased and underwent the maximum after 2-d of incubation, while the larger aggregates (Aβ fibrils) increased over the incubation time. These findings were consistent with TEM images which confirmed that the large oligomers and fibrils increased with a longer period of incubation.

4.2.2 Calibration curves of relative fluorescence ratio (FS/SR) as a function of pH

The shape and conformational change in Aβ peptides during its aggregation may alter the properties of fluorophores. For instance, the ThT dye exhibits a distinct characteristic upon binding of Aβ fibrils, but not for small oligomers (*13*). Also, the fluorescence of dyes in indole family is quenched by prefibrillar Aβ, but not by the fibrillar states (*14*). In our studies, we found that the fluorescence intensity of the sodium-sensitive dye; sodium-binding benzofuran isophthalate (SBFI) was altered by the aggregation states of Aβ. We observed a significant increase in fluorescence intensity of SBFI in the presence of $A\beta_{1-40}$, when pre-incubated in diH_2O for longer than 1 d, with a loss of sensitivity of SBFI to sodium. This finding suggested that the aggregated species

of Aβ may bind to the SBFI dye molecules and alter its fluorescence properties. This observed effect varied for different samples, and was more pronounced in the case of $A\beta_{1\text{-}40}$ than $A\beta_{1\text{-}42}$ (see Appendix, *Fig.* A4-1). Therefore, we could not carry out the Na^+ leakage assay, using SBFI dye to study the membrane permeabilization by Aβ at various aggregation states.

Hence, it is critically important to examine the influence of aggregation states of Aβ peptides on the properties of fluorescent dyes being used in liposome leakage assays, and to ensure that the measurement of fluorescence intensity is due to the leakage, as opposed to an alteration of dye properties in the presence of peptides. We used the membrane-impermeable dyes in order to preclude the leakage of dyes through the membranes while monitoring the translocation of protons between two compartments. We chose a mixture of two fluorescent dyes, fluorescein-5-(and-6)-sulfonic acid (FS) and sulforhodamine B (SR) at 20:1 molar ratio as adapted from a previous study on the measurement of pH of *trans*-golgi in living cells (*15*). The fluorescence intensity of FS increased as a function of pH in the range of 5 to 9, while the fluorescence intensity of SR remained relatively constant throughout the same pH range.

We carried out the experiments to obtain a calibration curve of the ratio of fluorescence (FS/SR) in 20 mM HEPES buffer as a function of pH. We found that the Aβ samples which were pre-incubated for 0, 1, 2, or 3 d, quenched the fluorescence signal of both FS and SR dyes in buffer solutions in the range of pH 5 to 9 by ~ 10 %, and 25%, respectively; therefore the fluorescence ratio FS:SR increased by ~ 20% in the presence of Aβ. However, this quenching effect was independent from the aggregation

states of Aβ. Figure 4-1 shows a calibration curve of the fluorescence ratio of FS and SR in the solution as a function of pH, in the presence and absence of $A\beta_{1\text{-}40}$.

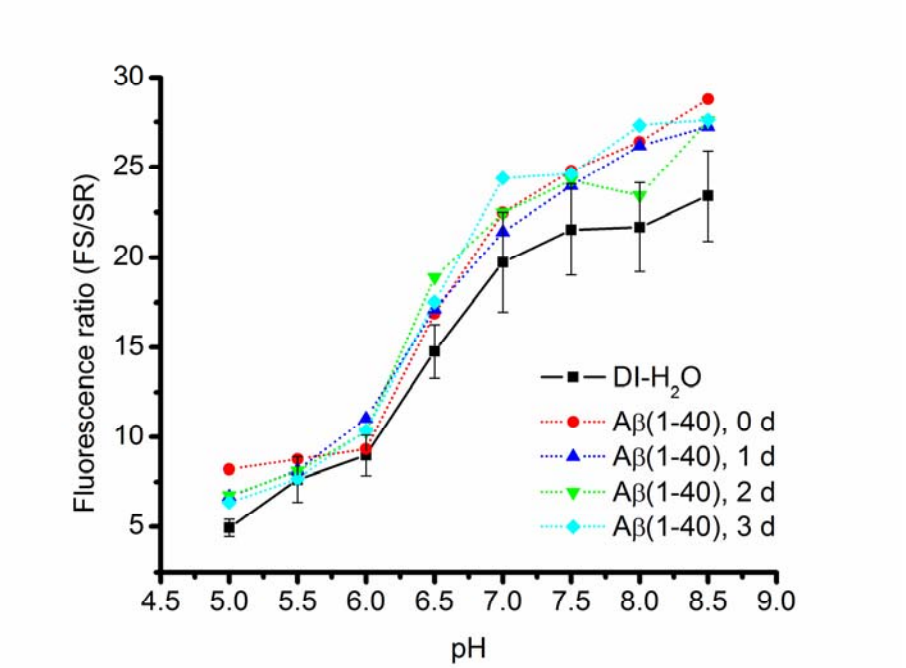

Figure 4-1. Calibration curves of fluorescence ratio of fluorescein sulfonate (FS) and sulforhodamine B (SR) in 20 mM HEPES as a function of pH. In the presence of $A\beta_{1\text{-}40}$ which were pre-incubated for 0, 1, 2, and 3 d, the fluorescence ratio increases by 20% due to quenching effect by Aβ. The influence of Aβ on fluorescence properties of dyes was not significantly different for all aggregation states.

We used a second approach for studying leakage of dye molecules through the membranes. Instead of using a pH-sensitive dye to monitor the Aβ-induced leakage of protons, we used the self-quenching dye, SR, and monitored the leakage of dye

molecules upon the addition of Aβ. We created a calibration curve of fluorescence intensity of SR as a function of dye concentration in the absence of Aβ (see *Fig.*4-2). The fluorescence intensity increased in a concentration-dependent manner at a low range of concentration, and reached its maximum at ~ 100 μM. The fluorescence intensity began to decline at the concentration of SR greater than 100 μM and was not detectable at 50 mM due to self-quenching of SR. For the dye leakage assay, we loaded 80 mM SR inside the liposomes, which led to self-quenching.

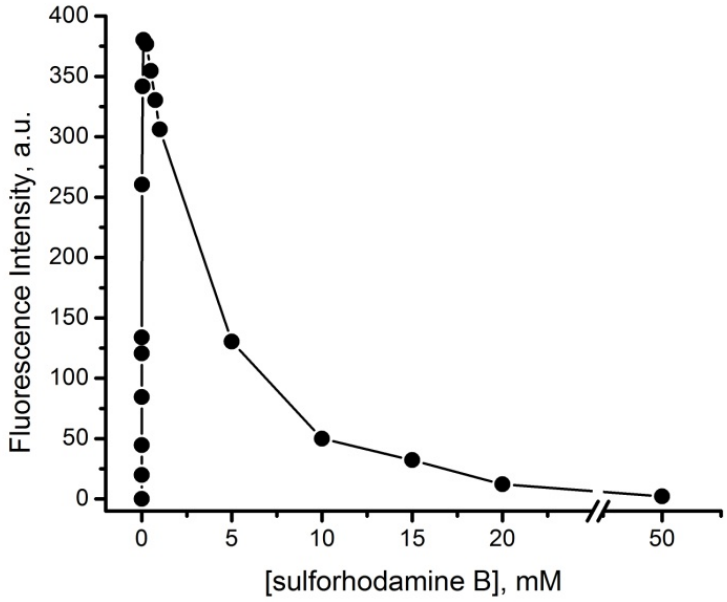

Figure 4-2. Calibration curve of fluorescence intensity of sulforhodamine B in 20 mM HEPES, pH 7.4 as a function of dye concentration

4.2.3 Leakage of protons induced by Aβ at various aggregation states

The purpose of this study is to investigate the influence of aggregation states of Aβ on the permeabilization of liposomes and to compare these results with the PLB systems in chapter 3. We prepared unilamellar liposomes of 100-nm diameter size, using a lipid composition, DOPS:POPE (1:1), as used previously for PLB formation in the electrophysiological studies.

To create a proton gradient across the liposome membranes, we prepared liposomes with a pH value of 5.5 inside and a pH value of 7.4 outside the liposomes by buffer exchange with a size exclusion column. We monitored the change in fluorescence ratio (FS:SR) due to the leakage of protons through the liposomes upon the addition of Aβ samples pre-incubated in diH_2O for 0, 1, 2, or 3 d at a monomeric concentration of 20 μM. Upon the leakage of protons induced by Aβ, deprotonation of the pH sensitive dye FS occurred, resulting in a change in fluorescence (F) ratio. We determined the percentage change in F ratio with respect to the maximum F ratio on addition of 0.2% triton x-100 that resulted in a complete membrane disruption. Figure 4-3 demonstrates that $Aβ_{1-40}$ and $Aβ_{1-42}$ samples with 0-d incubation yielded the highest percentage of proton leakage compared to Aβ samples with longer incubation time. In other words, the percentage of proton leakage decreased with an increasing incubation time for both $Aβ_{1-40}$ and $Aβ_{1-42}$ in the following order: 0 d > 1 d > 2 d > 3d. The effect of Aβ on the leakage of protons was greater than that of 20 nM gramicidin A, which is known as a well-defined cation-selective pore-forming peptide.

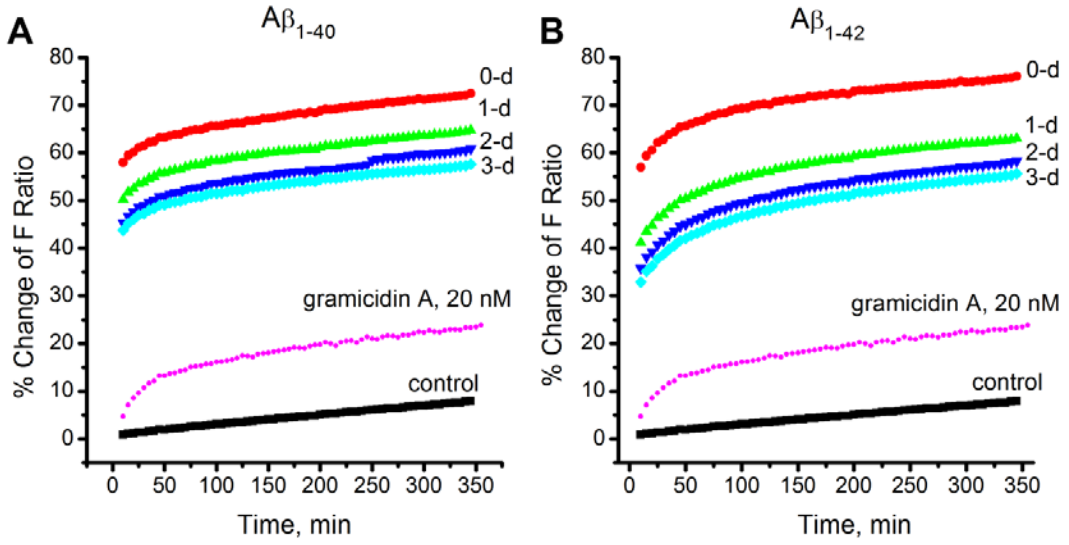

Figure 4-3. Percentage of change in fluorescence ratio inside the liposomes upon the addition of **A)** $A\beta_{1-40}$ and **B)** $A\beta_{1-42}$, which were prepared in diH_2O and incubated for different days, (●) 0 d, (▲) 1 d, (▼) 2 d and (◆) 3 d, compared to control (■) diH_2O, and (●) 20 nM gramicidin A. The liposomes were prepared from DOPS:POPE (1:1, w/w) in 20 mM HEPES at pH 5.5, and loaded with FS and SR dyes at 200 μM and 10 μM, respectively. The final concentration of monomeric Aβ in liposome suspension was 20 μM. The percentage of change in F ratio was an average of 5 independent experiments

In order to verify that the change in fluorescence was due to the leakage of protons from one side of liposomes to the other, we performed the leakage assay switching the orientation of proton gradient (*i.e.,* the pH inside the liposomes was at 7.4 instead of 5.5). We further examined the leakage in the absence of a proton gradient

(*i.e.,* both internal and external compartments of liposomes were at the same pH) to prove that a proton gradient was required for the leakage of protons through liposomes.

When the pH was higher in the internal than the external compartments of liposomes, the protons moved from the external compartment (pH 5.5) toward the inside of liposomes (pH 7.4) upon the addition of Aβ, which led to a protonation of the pH sensitive dye FS, and a decrease of F ratio decreased over time.

Similar to the liposomes with an internal pH of 5.5, the influence of aggregation time of Aβ on liposomes with an internal pH of 7.4 was followed the sequence: 0 d > 1 d > 2 d > 3 d, although the effect was not as pronounced as observed in the former case (see *Fig.* 4-4). In this experiment, we also examined the Aβ samples which had aggregated in diH_2O for 20 d (which contained relatively high amount of fibrils), and observed a minor leakage, suggesting that the Aβ fibrils (with the lowered effective concentration of Aβ in the suspension) did not effectively permeabilize the membranes.

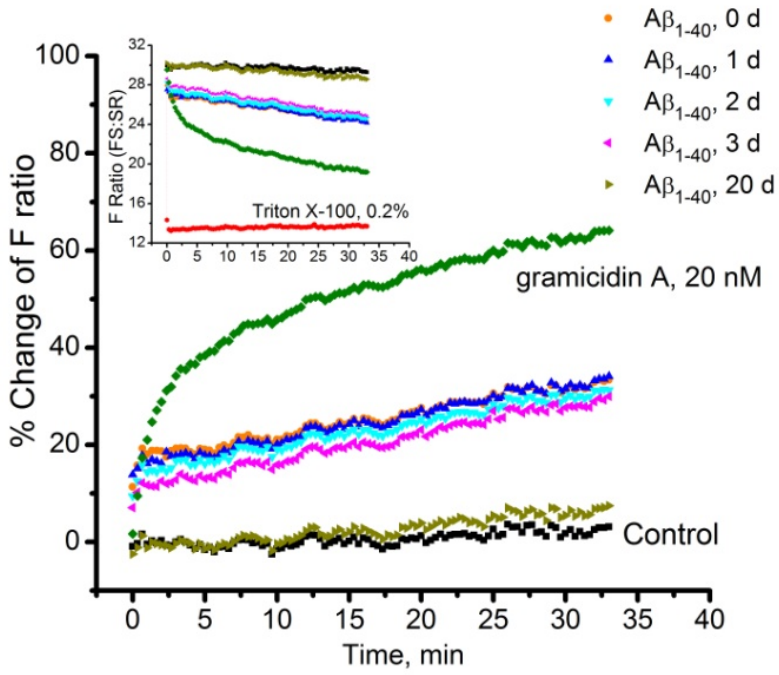

Figure 4-4. Percentage change in fluorescence ratio within liposomes prepared with an internal pH of 7.4 and an external pH of 5.5. The leakage of protons due to Aβ at various aggregation times was in the sequence of 0 d > 1 d > 2 d > 3 d >> 20 d. Inset shows the fluorescence ratio FS:SR decreased over time after the addition of Aβ or gramicidin A to the liposomes, due to the passage of protons from the outside to the inside of liposomes.

In the absence of a proton gradient (*i.e.*, the pH of both internal and external compartments were the same at 7.4), we observed no significant change in F ratio after addition of gA or Aβ. Figure 4-5A shows that the F ratio increased by approximately 1-2 units after addition of Aβ samples. The change in F ratio was due to the quenching of fluorescence dyes (both FS and SR) by Aβ peptides as described previously in section 4.2.1. This change was not significant compared to the change due to membrane

permeabilization in the presence of proton gradient, where the F ratio was typically 15 to 20 units greater than the control as shown in *Fig*. 4-5B. The proton leakage assays confirm that Aβ can induce the leakage of protons only when there is a difference in proton concentration between the interior and exterior of liposomes.

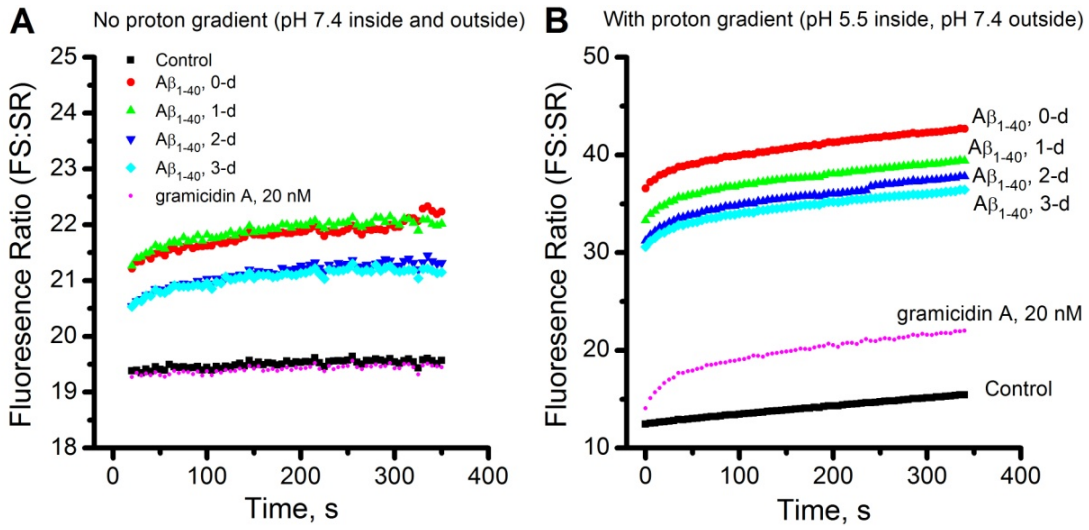

Figure 4-5. Comparison of F ratio (FS:SR) after addition of $A\beta_{1\text{-}40}$ at 0, 1, 2, and 3-d of incubation in water, **A)** in the absence and **B)** the presence of a proton gradient between the interior and exterior of liposomes. Aβ peptide itself quenched the fluorescence of both dyes, resulting in a small increase in F ratio, while the leakage of protons due to Aβ led to a significant change in F ratio. In the absence of a proton gradient, the change in F ratio with an addition of gramicidin A was not detectable, suggesting that no proton leakage occurs with the lack of proton gradient.

4.2.4 Influence of membrane curvature on membrane permeabilization

We found that the effect of Aβ at various aggregation states on the permeabilization of liposomes was not in agreement with the results from electrophysiological studies presented in chapter 3.

Since the curvatures of liposomal membranes are typically greater than the PLBs, we hypothesized that the curvatures may play a role in the membrane permeabilization by various aggregation states of Aβ. We attempted to investigate the proton leakage induced by the different aggregation states of Aβ, using the liposomes with lower curvature. We prepared liposomes with the same lipid composition, DOPS:POPE (1:1, w/w) having a size of larger than 100 nm in diameter by extruding the liposomes through an extrusion membrane filter with a size of 5 μm. The resulting liposomes; however, were obtained in the size range of 270 ± 130 nm diameter, as quantified by dynamic light scattering (see *Appendix* A4-2). The proton leakage assay using liposomes with lower membrane curvature revealed that the effectiveness of Aβ at different aggregation times was in same order (0 d > 1 d > 2 d > 3 d) as observed previously; thus the effect of membrane curvature on membrane permeabilization might not be significant. Further characterization may be required to understand the roles of membrane curvature on membrane permeabilization induced by various aggregation states of Aβ. The effect of Aβ at different aggregation states needs to be examined using various sizes of liposomes, ranging from small (< 50 nm diameter) to giant liposomes (> 1 μm diameter) (*1*). The membrane curvature could be another critical parameter that influences the membrane permeabilization of Aβ peptides in neuronal membranes, since the neurons typically possess high membrane curvature, which may

be prone to membrane defects and disruption induced by Aβ; however, the subject is beyond the scope of this study.

4.2.5 Influence of lipid composition on membrane permeabilization

The interaction of Aβ and lipid membrane is dependent on composition of the lipid headgroups. Previous studies have shown that Aβ prefers to interact with negatively charged lipid such as PG or PS lipids, rather than zwitterionic PC lipids (*16*), although the reports in literature are contradictory (*1*). We examined the influence of lipid composition on the membrane permeabilization induced by various aggregation states of Aβ.

The liposomes composed of DOPS:POPE(1:1) were not optimized for membrane stability in the liposome flux assays, as we observed the leakage of protons due to the membrane diffusion even without addition of Aβ. We performed the leakage assays using lipid compositions with an increased stability, DiphyPC : Cholesterol : DiphyPG : DPPE-PEG_{2000} (9:9:1:1, molar ratio) at a final concentration of 20 mg mL^{-1}. The presence of poly(ethylene glycol) (PEG) in the formulation of liposomes prevents nonspecific interactions with the membrane surface, while cholesterol reduces the fluidity of lipid membranes, thus enhancing its stability (*17, 18*). With the preparation of liposomes with improved stability, we found that the leakage of proton in the control liposomes became smaller than that observed in the DOPS:POPE lipid composition. Figure 4-6A shows that the leakage of protons induced by Aβ was generally weaker than

that observed previously, but the effect of incubation time followed the same trend in both lipid compositions (*i.e.*, 0 d > 1 d > 2 d > 3 d).

To explore the leakage in more pathologically relevant system, we prepared liposomes prepared from brain extract lipid, containing a mixture of phospholipids, PC: PE: PI: PS: PA in 9.6, 16.7, 1.6, 10.6, and 2.8%, respectively. The liposomes composed of this lipid composition were; however, not as stable as those from the other two lipid compositions. Despite the leakiness of the membranes, we observed the same pattern of effect of Aβ at various incubation times; yet not as pronounced as in the cases of the other two lipid compositions (see *Fig.* 4-6B).

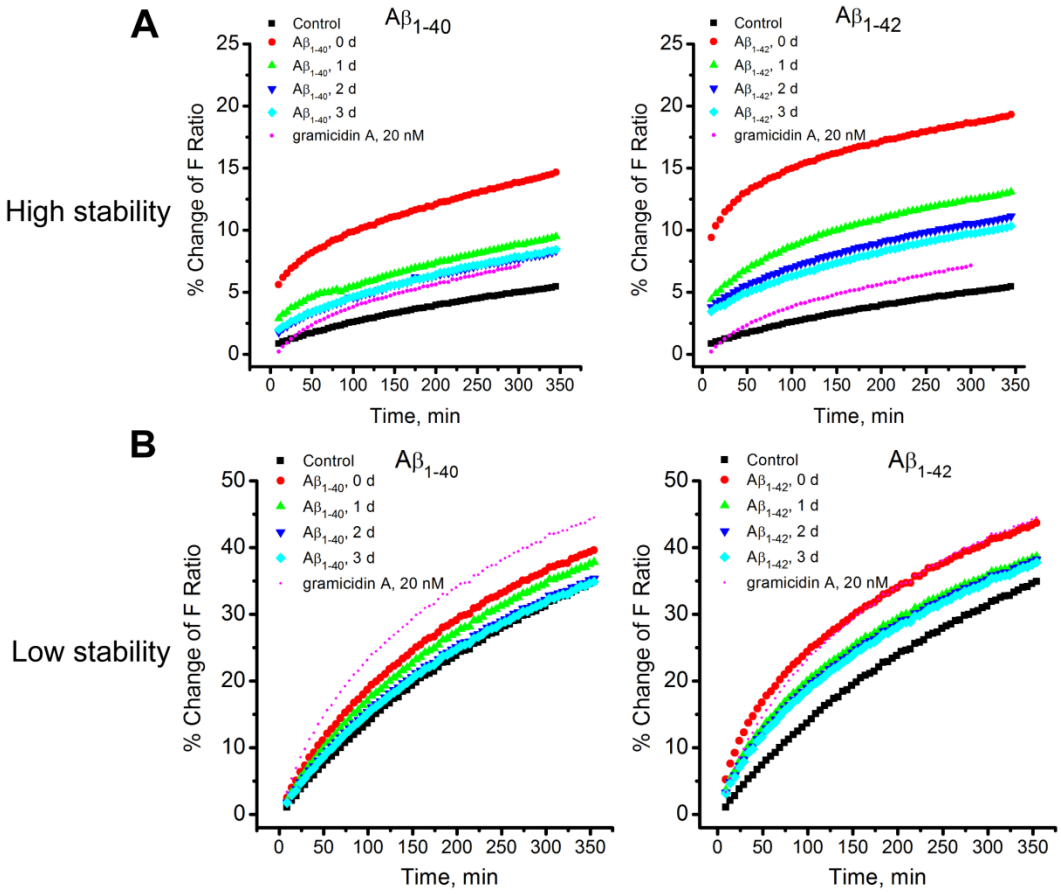

Figure 4-6. Leakage of protons induced by $A\beta_{1\text{-}40}$ and $A\beta_{1\text{-}42}$ which were pre-incubated in diH_2O for different times. Membrane permeabilization varied with the stability of liposomes, **A)** high stability lipid composition, DiphyPC : Cholesterol : DiphyPG : DPPE-PEG_{2000} (9:9:1:1), and **B)** low stability lipid composition, brain extract. In both lipid compositions, the leakage of protons decreased over the aggregation time of Aβ.

Based on the leakage of protons from liposomes prepared with three different lipid compositions, leakage was the strongest in the case of the liposomes composed of DOPS:POPE, possibly because of the preference of Aβ to interact with negatively charged lipids (PS) (*16*).

4.2.6 Dye quenching assay

We extended our studies from proton leakage assay to a dye-quenching assay in order to determine whether Aβ could disrupt the membranes and cause the leakage of dye molecules, which are significantly larger than protons. In this study, we loaded 80 mM of sulforhodamine B inside the liposomes composed of DOPS:POPE used previously in the proton leakage assay. In Figure 4-7, the addition of Aβ caused the liposomal membranes to disrupt, causing the dye molecules to leak.

We determined the percentage of dye leakage over time with respect to the maximum leakage obtained with the addition of 0.2% of Triton-x 100 to the liposomes. The leakage of dye molecules was not detectable in 30 minutes after addition of control sample (without Aβ). Consistent with results from proton leakage assays, we found that the leakage was the highest for Aβ with 0-d incubation, and decreased with increasing incubation time (see *Fig.* 4-7).

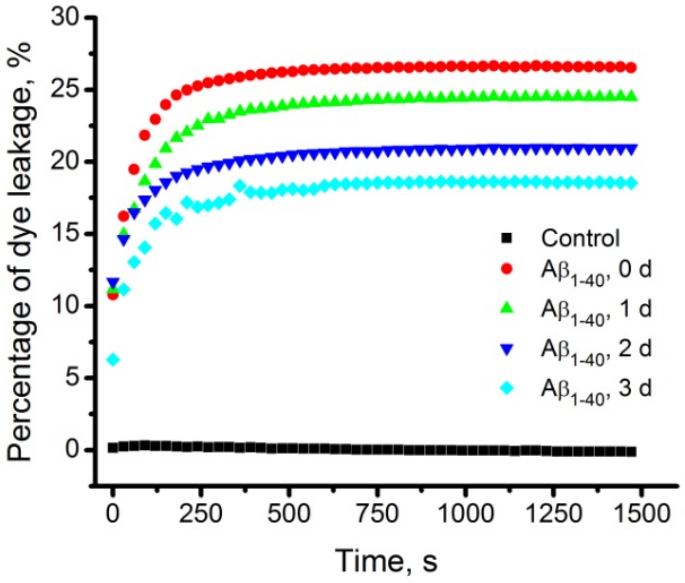

Figure 4-7. Percentage leakage of sulforhodamine B upon the addition of Aβ at different aggregation time with respect to the maximum leakage when 0.2 % Triton x-100 was added to the liposomes.

Taken together, our studies confirm that Aβ peptides induce leakage of the encapsulated molecules that range in size as small as protons to as large as dye molecules, and the activity of membrane permeabilization decreased as the Aβ samples were incubated for longer time. The leakage of dye was less than that of proton leakage, due to the faster rate of passage of protons. Nevertheless, the results from leakage assays do not provide the exact mechanism of membrane permeabilization. In the liposome-based assays, the observed leakage may not necessarily result from an insertion of peptides through the membranes, but could be due to the breakage of liposomes.

4.2.7 Membrane permeabilization of Aβ in planar lipid bilayers and liposomes are driven by different mechanisms

In chapter 3, electrophysiological studies revealed that the highest probability of pore formation in the PLBs was induced by Aβ samples which were pre-incubated 2 or 3 d when the relative abundance of Aβ oligomers was at the maximum as shown in *Fig.* 3-2. In liposome-based assays, we found that the effect of pre-incubation time of Aβ on the leakage was in the following sequence: 0 d > 1 d > 2 d > 3 d (>> 20 d), regardless of the size of contents that were released out of liposomes, and the stability of liposomes, suggesting that the effect of Aβ on membrane disruption decreased with the incubation time of Aβ. This finding was in agreement with previously published works that employed a calcein leakage assay in the study (*19*). The authors explained that the decreasing percentage of dye leakage over the pre-incubation time of Aβ was due to a decrease in amount of early state of Aβ oligomers. In our studies, SDS-PAGE/Western blotting analysis revealed that the relative abundance of Aβ monomers and small oligomers (*i.e.*, dimers and trimers) decreased over the incubation time, as they became larger assemblies (*i.e.*, large oligomers and fibrils) (see *Fig.* 3-3 and *Fig.*3-4, Chapter 3). The trend of relative abundance of these small aggregated species correlated with the reduction of activity of permeabilization of the liposomal membranes. The small aggregated Aβ species, which were mostly abundant in the samples, could be responsible for the membrane permeabilization as they may interact with the lipids via the hydrophobic interaction. The abundance of these aggregated species, on the other hand, showed a weak correlation with pore formation in the PLB experiments, suggesting that the mechanism of membrane permeabilization induced by various

aggregation states of Aβ could be different in PLBs and liposomes due to the differences in experimental conditions, based on the following observations.

First, the observed time for the Aβ-induced membrane permeabilization was much faster in liposomal membranes than the PLB recordings. In liposome-based leakage assays, we were able to detect the change in fluorescence signal due to the membrane disruption within seconds, while it took several minutes to observe the conductance due to membrane permeabilization in the PLBs after addition of Aβ, and the mixing upon the addition was necessary.

Second, the total surface area of lipid membranes in the liposome suspension was greater than the PLB. Given the same concentration of monomeric Aβ which were used in both systems, the likelihood of peptide-lipid interaction was much higher in the case of liposomes than in the PLB system.

Another aspect is that the structural properties of liposomes and PLBs are physically different. Besides the high membrane curvature which may induce the stress in membranes, the liposomes can move freely in the aqueous solution and are prone to fuse with one another, resulting in breakage. In contrast, the PLBs are immobilized on the aperture of the bilayer set-up, while the organic solvent used in the formation of PLBs by the "painted" method provides an additional support.

We hypothesized that the sharp increase in fluorescence intensity upon the addition of Aβ is caused by the breakage of membrane or bursting of liposomes rather than pore formation observed in the PLB recordings. Nonetheless, the breakage of lipid

membranes upon the addition of Aβ was unlikely to occur in the PLBs, since we could observe stepwise ion flux through the PLBs while the membrane was still intact.

In addition, one factor that could play an important role in the breakage of liposomes is the effective concentration of Aβ, which decreased over the aggregation time as the small oligomers became larger assemblies. In the liposome-based leakage assays in which the total surface area of lipid membranes was substantial, the effective concentration of Aβ, especially for Aβ with 0-d incubation time, was relatively high, leading to the high likelihood for peptides to interact with lipid membranes and induce rapid membrane disruption. On the other hand, the aged Aβ samples which contained lower effective concentrations of Aβ in suspension had less probability to interact with liposomes; thereby inducing the low amount of leakage. The observed leakage could simply reflect the number of bursting liposomes, which depended on the likelihood of peptide-lipid interactions. Figure 4-8 shows schematic models for membrane permeabilization by Aβ at different aggregation states in liposomes and PLB.

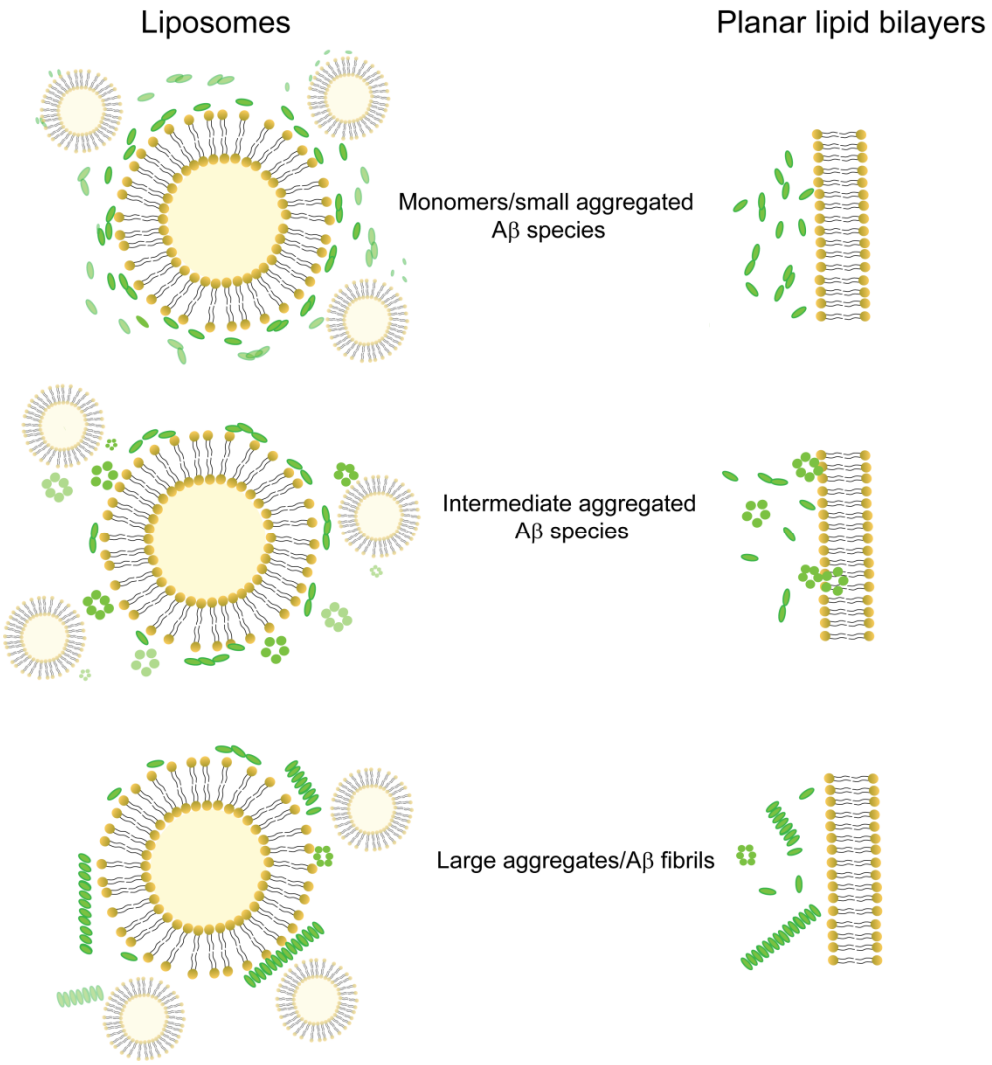

Figure 4-8. Schematic illustration of membrane permeabilization induced by Aβ at different aggregation states in two systems, the liposome-based leakage assay and the electrophysiological recordings (not drawn to scale). The total surface area of lipid membranes of liposomes is substantially higher than that of PLB. In liposomes (*left*), at early aggregation state of Aβ, the effective concentration of Aβ interacting with the membranes is high (*i.e.,* monomers and small aggregated species are the majority of the population); therefore the membrane disruption (*i.e*., bursting) could happen instantly. Over the aggregation time, the effective concentrations of Aβ in the solution decreased as the Aβ monomers and small oligomers become larger assemblies (*i.e.*, Aβ fibrils),

thereby reducing the chance of membrane disruption. In the electrophysiological recordings (*right*), the influence of effective concentration of Aβ on the membranes is less relevant than in the case of the liposome leakage assay. The surface area of PLB is small compared to the abundance of peptides in the solution. Aβ oligomers, rather than Aβ monomers and fibrils, could induce the ion flux across the membranes by pore formation.

A more detailed study is required for better understanding of the mechanism of Aβ-induced membrane disruption and the influence of aggregation states of Aβ. The advantage of this liposome flux assay is that it provides an opportunity to conduct experiments in high-throughput, making it possible to screen several potential drug candidates for their ability to inhibit or reduce the leakage of liposomes as presented in the *Appendix* A4-3.

4.3 Conclusions

We examined the influence of Aβ at various aggregation states on membrane permeabilization in liposomal membranes. The liposome-based leakage assays confirmed that Aβ was able to cause the leakage of liposomal contents (*i.e.*, both protons and dye molecules). The activity of leakage decreased as Aβ samples were incubated for longer period of time. This finding contradicted to the results from the electrophysiological studies. Due to fundamental differences between the two approaches, and the differences in physical properties of membranes, the mechanism of membrane permeabilization in both systems could be different (*i.e.*, bursting of

liposomes *versus* pore formation in PLB). SDS-PAGE/Western blotting quantification revealed a decreasing trend of relative abundance of monomers, dimers and trimers, as they become larger oligomers, resulting in a lower effective concentration of peptides. The reduction in leakage with an increase in pre-incubation time of Aβ was likely because of the lowered effective concentration of peptides in the solution as the likelihood of peptide-membrane interaction decreased. Another possibility is that the aggregated species smaller than tetramers could be sufficiently effective in bursting the liposomes upon their addition, whereas the intermediate oligomers (from tetramers to hexamers) could form pore through the PLB.

4.4 Materials and methods

4.4.1 Preparation of Aβ

We purchased the Aβ from GL Biochem (Shanghai) Ltd., and treated with HFIP, followed by 2-d lyophilization, according to the protocol described in material and method section in chapter 3.

4.4.2 Preparation of liposomes

We prepared liposomes from a total lipid concentration of 10 mM of desired composition. We obtained a lipid film by placing the lipid mixture dissolved in chloroform in a 10 mL round bottom flask, followed by rotary evaporation. We rehydrated the lipid film with 750 μL of 20 mM HEPES, pH 5.5,

containing a mixture of the pH-sensitive dye, fluorescein sulfonate (Molecular Probes, Eugene, OR) and a pH-insensitive dye, sulforhodamine B (Molecular Probes, Eugene, OR) at a concentration of 200 μM and 10 μM, respectively, and incubated the liposomes for 4 h at 37 °C. The resulting lipid vesicles were subjected to 15 freeze-thaw cycles and extruded through 100-nm membrane for 21 times. We used Sephadex-G25 M gel filtration columns (GE Healthcare, Buckinghamshire, UK) to separate liposomes with encapsulated fluorescent dyes from the fluorescent dyes in solution, and to change the solution outside the liposomes to 20 mM HEPES, pH 7.4.

Before each experiment, we determined the size distribution of liposomes by dynamic light scattering using 90 Plus particle analyzer (Brookhaven Instruments Corporation, Holtsville, NY) to confirm that the size of vesicles were in the range of 100 ± 30 nm unless indicated otherwise. We then transferred the resulting liposomes to 96-well plates (100 μL in each well) followed by addition of compounds of interest.

4.4.3 Fluorescence measurement

We transferred the liposomes with encapsulated dyes to 96-well plates (100 μL in each well), followed by addition of Aβ samples or gramicidin A. We monitored changes of fluorescence signal due to ion or dye leakage using Fluroskan Ascent FL (Thermo Fisher Scientific, Waltham, MA). The leakage of protons corresponded to a ratio of fluorescent signal at EX485/EM518 for Fluorescein sulfonate and EX560/EM590 for

sulforhodamine (non-pH sensitive dye). We determined the percentage of change in fluorescence ratio as calculated from

$$\% \text{ Change in F ratio} = (R\text{-}R_0)*100/(R_{max}\text{-}R_0),$$

when R is the fluorescence ratio at individual time point, R_0 is the initial fluorescence ratio before the addition of Aβ samples, and R_{max} is the maximum fluorescence ratio obtained by the addition of 0.2% Triton x-100 to freshly prepared liposomes.

For the self-quenching assay, we detected changes of fluorescence intensity upon the release of SR molecules into the medium. We observed an increasing fluorescent signal upon leakage of dye out of membranes over time and determined the percentage of leakage with respect to the maximum leakage.

$$\% \text{ Leakage} = (F\text{-}F_0)*100/(F_{max}\text{-}F_0),$$

when F is the fluorescence intensity of SR at individual time point, F_0 is the initial fluorescence intensity before the addition of Aβ samples, and F_{max} is the maximum fluorescence intensity obtained from the addition of 0.2% Triton x-100 to the liposomes.

Chapter 4 Appendix

A4-1. Influence of Aβ on fluorescence properties of sodium-sensitive dye; sodium-binding benzofuran isophthalate (SBFI)

We initially attempted to develop Na^+ leakage assay using sodium-sensitive dye, SBFI (Molecular Probes, Eugene, OR) to study Aβ-induced leakage. Figure A4-1.1 demonstrates a sensitivity of SBFI to concentration of sodium in the buffer solution. We, however, observed an interference of Aβ peptides with the fluorescence properties of SBFI as shown in *Fig.* A4-1.2. Therefore, we could not use this dye to study leakage of Na^+ in liposome leakage assays.

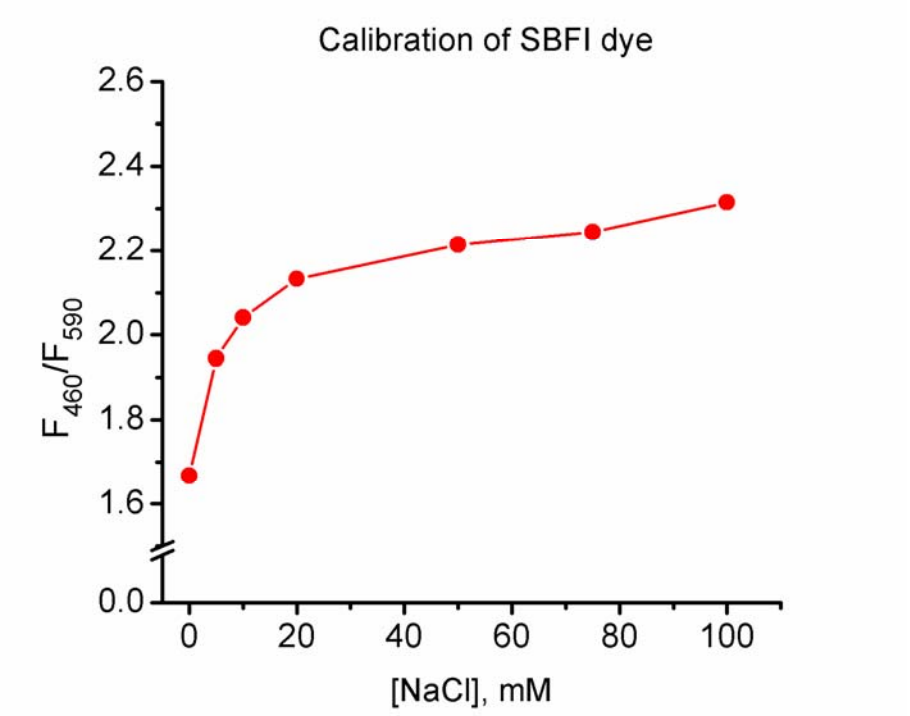

Figure A4-1.1. Calibration curve of SBFI dyes as a function of concentration of sodium chloride. The fluorescence intensity was measured at the emission wavelengths of 460

nm and 590, while the excitation wavelength was at 355 nm. The final concentration of SBFI was at 15 μM in 20 mM HEPES buffer at pH 7.4.

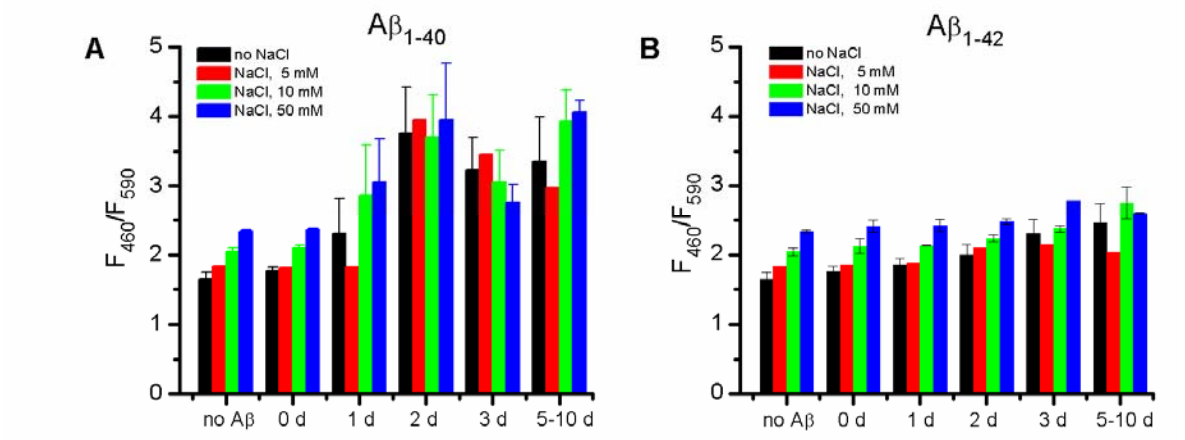

Figure A4-1.2. Effect of aggregated forms of Aβ on the sodium sensitivity of SBFI dyes. **A)** The intermediate $A\beta_{1\text{-}40}$ aggregated species in diH_2O (between in 1-3 d) induced a significant increase in fluorescence intensity and disturbed the sodium sensitivity of SBFI, whereas **B)** aggregated $A\beta_{1\text{-}42}$ did not have as strong influence on fluorescence properties of SBFI as in $A\beta_{1\text{-}40}$.

A4-2. Determination of size of liposomes by dynamic light scattering (DLS)

Dynamic light scattering (DLS) is a simple and rapid method for determining the size of liposomes, but this technique only provides an estimate of size distribution of the liposomes in bulk solution (*18*).

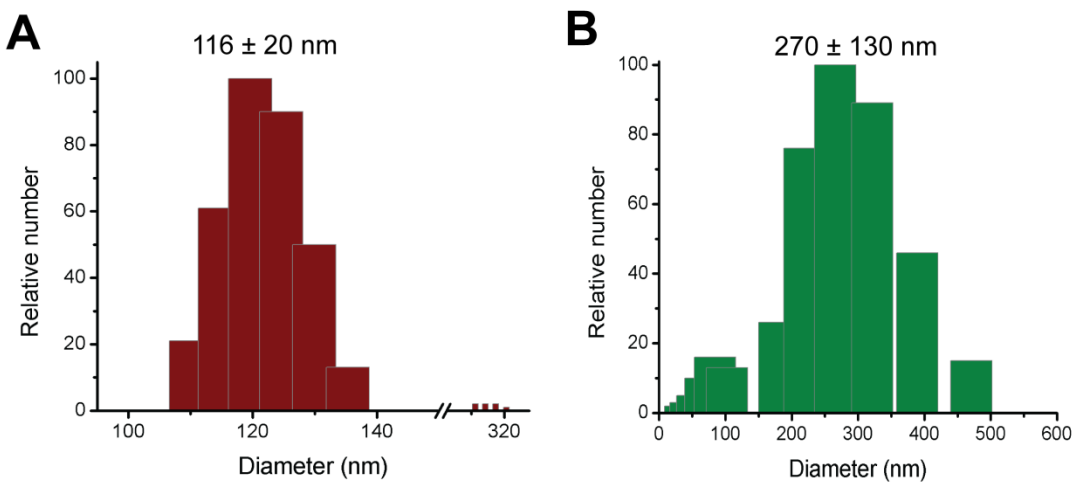

Figure A4-2. Distribution of the number of liposomes with various sizes as obtained by dynamic light scattering. The size of liposomes could be adjusted by using membrane filters of different sizes in the extrusion step, as shown for **A)** 100-nm sized and, **B)** 5-μm sized membrane filters. The liposomes were composed of DOPS:POPE (1:1, w/w) and contained 200 μM FS and 10 μM SR dyes.

A4-3. Using liposome-based assay for screening small molecules that can reduce the leakage on lipid membranes

We also employed the proton leakage assays for screening small molecules which could prevent the Aβ-induced membrane permeabilization. We selected the molecules that bind with high affinity to Aβ fibrils as examined by our collaborators and other research groups. We found that none of these molecules could significantly reduce the Aβ-induced proton leakage.

Among the testing molecules, we are particularly interested in two molecules, BTA-EG_4 and BTA-EG_6, as they showed promising results as potential therapeutic

molecules based on the molecular and behavioral studies (*23*). In our studies, we examined whether these molecules could reduce or inhibit the membrane permeabilization induced by Aβ in both PLB recording and leakage assays. We observed minor decrease in percentage of Aβ-induced proton leakage in the presence of these two molecules at low concentrations in a concentration-dependent manner for all of lipid compositions. The reduction in proton leakage was the most explicit in the case of liposomes composed of DiphyPC : Cholesterol : DiphyPG : DPPE-PEG_{2000} (9:9:1:1, molar ratio) as shown in *Fig.* A4-3.1. In electrophysiological studies, we tested the ion flux activity of $A\beta_{1-40}$ incubated for 2 d in diH_2O in the presence of BTA-EG_4 or BTA-EG_6 molecules at 10 :1 molar ratio in 10 experiments for each condition. In addition, we performed bilayer recording experiments to examine the inhibitory effect of Aβ-induced pore formation. Figure A4-3.2 demonstrates that the probability of pore formation induced by $A\beta_{1-40}$ at 2-d incubation had reduced from ~ 50% to 20% when either BTA-EG_4 or BTA-EG_6 was present.

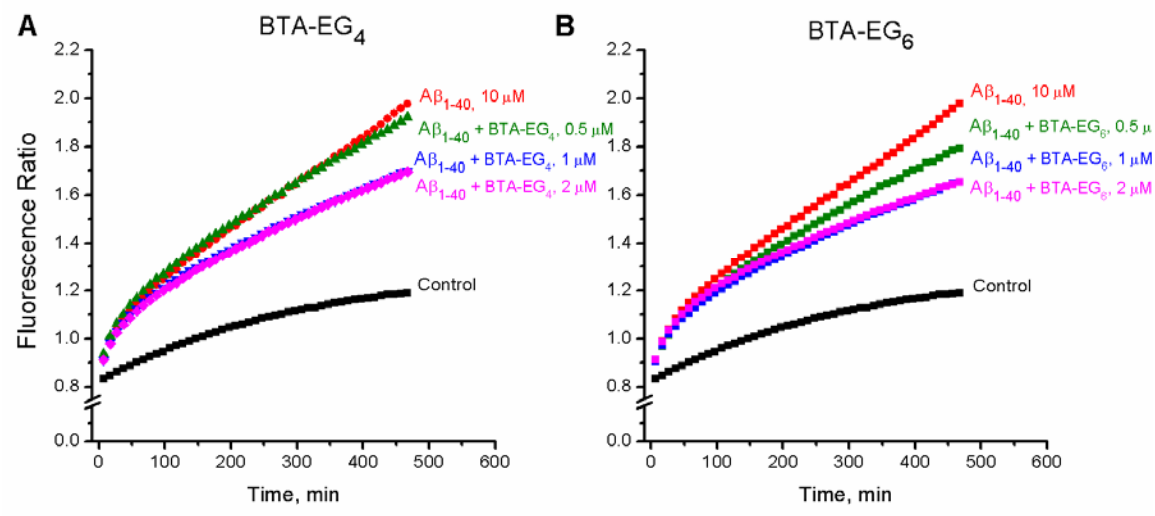

Figure A4-3.1. Reduction of change in F ratio, FS:SR, as a function of time upon the addition of $A\beta_{1\text{-}40}$ with **A)** BTA-EG_4 or **B)** BTA-EG_6. The leakage of protons induced by $A\beta_{1\text{-}40}$ was reduced in the presence of these two molecules at low concentrations. Liposomes was prepared from DiphyPC : Cholesterol : DiphyPG : DPPE-PEG_{2000} (9:9:1:1, molar ratio) at 20 mg mL^{-1}, and the final concentration of $A\beta_{1\text{-}40}$ was 10 μM.

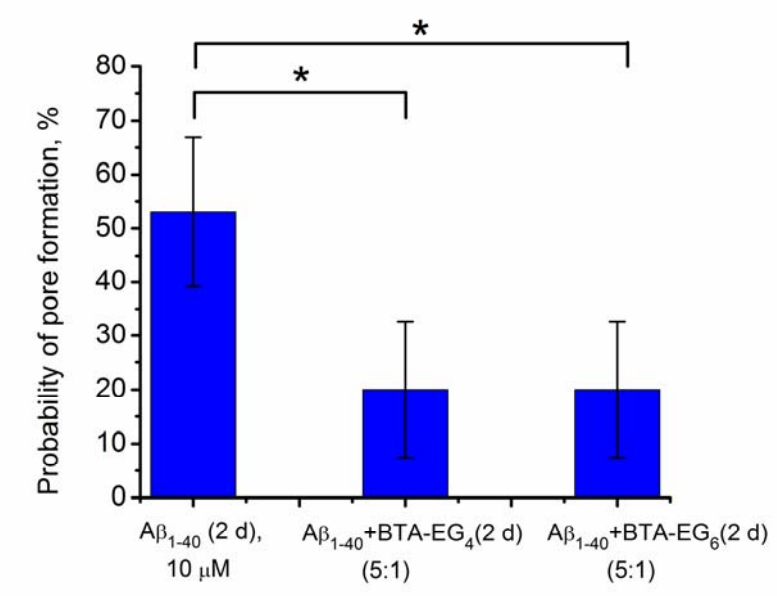

Figure A4-3.2. Probability (%) of Aβ-induced flux through planar lipid bilayers in electrophysiological studies. The probability of ion flux due to Aβ reduced when $A\beta_{1\text{-}40}$ was pre-incubated in di-H_2O with BTA-EG_4 or BTA-EG_6 at 10:1 molar ratio. Significance (*p*-value < 0.1) was indicated by an asterisk (*). The PLBs were composed of DOPS:POPE (1:1, w/w) and the final concentrations in the bilayer chamber were 10-15 μM for $A\beta_{1\text{-}40}$, and 2 μM for BTA-EG_4 and BTA-EG_6.

Despite the potential use of BTA-EG_4 and BTA-EG_6 as drug candidates for Alzheimer's disease, these molecules exhibited an undesired biological activity on the lipid membranes. The electrophysiological experiments revealed that BTA-EG_4 and BTA-EG_6 at the concentration above 10 μM could form channels through the membranes and induced toxicity in human cells. The details of BTA-EG_4 and BTA-EG_6 molecules with regards to their characteristics in pore formation and toxicity are discussed in chapter 5.

Acknowledgements

I would like to thank Divya Rao for her contribution in developing the proton leakage assay used in this study, and Dr. Jerry Yang for providing synthesized molecules to study.

References

1. Butterfield, S. M., and Lashuel, H. A. (2010) Amyloidogenic Protein Membrane Interactions: Mechanistic Insight from Model Systems, *Angew. Chem. Int. Ed. Engl. 49*, 5628-5654.
2. Relini, A., Cavalleri, O., Rolandi, R., and Gliozzi, A. (2009) The two-fold aspect of the interplay of amyloidogenic proteins with lipid membranes, *Chem. Phys. Lipids 158*, 1-9.
3. Querfurth, H. W., and LaFerla, F. M. (2010) Mechanisms of Disease: Alzheimer's Disease, *N. Engl. J. Med. 362*, 329-344.
4. Capone, R., Quiroz, F. G., Prangkio, P., Saluja, I., Sauer, A. M., Bautista, M. R., Turner, R. S., Yang, J., and Mayer, M. (2009) Amyloid-beta-Induced Ion Flux in Artificial Lipid Bilayers and Neuronal Cells: Resolving a Controversy, *Neurotox. Res. 16*, 1-13.
5. Zagorski, M. G., Yang, J., Shao, H. Y., Ma, K., Zeng, H., and Hong, A. (1999) Methodological and chemical factors affecting amyloid beta peptide amyloidogenicity, *Amyloid, Prions, and Other Protein Aggregates 309*, 189-204.
6. Hortschansky, P., Schroeckh, V., Christopeit, T., Zandomeneghi, G., and Fandrich, M. (2005) The aggregation kinetics of Alzheimer's beta-amyloid peptide is controlled by stochastic nucleation, *Protein Sci. 14*, 1753-1759.
7. Demuro, A., Parker, I., and Stutzmann, G. E. (2010) Calcium Signaling and Amyloid Toxicity in Alzheimer Disease, *J. Biol. Chem. 285*, 12463-12468.
8. Tien, H. T. O.-L., Angelica (2000) *Membrane biophysics as viewed from experimental bilayer lipid membranes*, 1st ed., Elsevier, Amsterdam, Netherland.
9. El Jastimi, R., and Lafleur, M. (1999) A dual-probe fluorescence method to examine selective perturbations of membrane permeability by melittin, *Biospectroscopy 5*, 133-140.
10. Pieri, L., Bucciantini, M., Guasti, P., Savistchenko, J., Melki, R., and Stefani, M. (2009) Synthetic Lipid Vesicles Recruit Native-Like Aggregates and Affect the Aggregation Process of the Prion Ure2p: Insights on Vesicle Permeabilization and Charge Selectivity, *Biophys. J. 96*, 3319-3330.
11. Qi, W., Zhang, A. M., Good, T. A., and Fernandez, E. J. (2009) Two Disaccharides and Trimethylamine N-Oxide Affect A beta Aggregation Differently, but All Attenuate Oligomer-Induced Membrane Permeability, *Biochemistry 48*, 8908-8919.
12. Volles, M. J., Lee, S. J., Rochet, J. C., Shtilerman, M. D., Ding, T. T., Kessler, J. C., and Lansbury, P. T. (2001) Vesicle permeabilization by protofibrillar alpha-synuclein: Implications for the pathogenesis and treatment of Parkinson's disease, *Biochemistry 40*, 7812-7819.

13. Levine, H. (1993) Thioflavine-T Interaction with Synthetic Alzheimers-Disease Beta-Amyloid Peptides - Detection of Amyloid Aggregation in Solution, *Protein Sci. 2*, 404-410.
14. Reinke, A. A., Seh, H. Y., and Gestwicki, J. E. (2009) A chemical screening approach reveals that indole fluorescence is quenched by pre-fibrillar but not fibrillar amyloid-beta, *Bioorg. Med. Chem. Lett. 19*, 4952-4957.
15. Seksek, O., Biwersi, J., and Verkman, A. S. (1995) Direct Measurement of Trans-Golgi Ph in Living Cells and Regulation by 2nd Messengers, *J. Biol. Chem. 270*, 4967-4970.
16. Matsuzaki, K. (2007) Physicochemical interactions of arnyloid-peptide with lipid bilayers, *Biochimica Et Biophysica Acta-Biomembranes 1768*, 1935-1942.
17. Stamou, D., Duschl, C., Delamarche, E., and Vogel, H. (2003) Self-assembled microarrays of attoliter molecular vessels, *Angew. Chem. Int. Ed. Engl. 42*, 5580-5583.
18. Torchilin, V. P. W., Volkmar (2003) *Liposomes: Practical Approach*, 2nd ed., Oxford University Press, New York.
19. Williams, T. L., Day, I. J., and Serpell, L. C. (2010) The Effect of Alzheimer's A beta Aggregation State on the Permeation of Biomimetic Lipid Vesicles, *Langmuir 26*, 17260-17268.
20. Inbar, P., Li, C. Q., Takayama, S. A., Bautista, M. R., and Yang, J. (2006) Oligo(ethylene glycol) derivatives of thioflavin T as inhibitors of protein-amyloid interactions, *Chembiochem 7*, 1563-1566.
21. Arispe, N., and Doh, M. (2003) Peptides that block Alzheimer's A beta P ion channels protect cells from A beta P toxicity, *Biophys. J. 84*, 53A-53A.
22. Permanne, B., Adessi, C., Saborio, G. P., Fraga, S., Frossard, M. J., Van Dorpe, J., Dewachter, I., Banks, W. A., Van Leuven, F., and Soto, C. (2002) Reduction of amyloid load and cerebral damage in a transgenic mouse model of Alzheimer's disease by treatment with a beta-sheet breaker peptide, *FASEB J. 16*, 860-+.
23. Habib, L. K., Lee, M. T. C., and Yang, J. (2010) Inhibitors of Catalase-Amyloid Interactions Protect Cells from beta-Amyloid-Induced Oxidative Stress and Toxicity, *J. Biol. Chem. 285*, 38933-38943.

Chapter 5

Self-assembled, cation-selective ion channels from an oligo(ethylene glycol) derivative of benzothiazole aniline[6]

This chapter describes the spontaneous formation of well-defined pores in planar lipid bilayers from the self-assembly of a small synthetic molecule that contains a benzothiazole aniline (BTA) group attached to a tetra-ethylene glycol) (EG_4) moiety. Macroscopic and single-channel current recordings suggest that these pores are formed by the assembly of four BTA-EG_4 monomers with an open pore diameter that appears similar to the one of gramicidin pores (~0.4 nm). The single-channel conductance of these pores is modulated by the pH of the electrolyte and has a minimum at pH ~3. Self-assembled pores from BTA-EG_4 are selective for monovalent cations and have long open channel lifetimes on the order of seconds. BTA-EG_4 monomers in these pores appear to be arranged symmetrically across both leaflets of the bilayer, and spectroscopy studies suggest that the fluorescent BTA group is localized inside the lipid bilayers. In terms of biological activity, BTA-EG_4 molecules inhibited growth of gram-positive *Bacillus subtilis* bacteria (IC_{50} ~50 μM) and human neuroblastoma SH-SY5Y cells

[6] Content of this chapter includes in submitted publication, **Prangkio P**., Rao D.K., Lance K.D., Rubinshtein M., Yang J.,Mayer M. (2011) "Self-assembled, cation-selective ion channels from an oligo(ethylene glycol) derivative of benzothiazole aniline"

(IC_{50} ~60 μM), while they were not toxic to gram-negative *Escherichia coli* bacteria at a concentration up to 500 μM. Based on these properties, this drug-like, synthetic, pore-forming molecule with a molecular weight below 500 g mol^{-1} might be appealing as a starting material for development of antibiotics or membrane-permeating moieties for drug delivery. From a biophysical point of view, long-lived, well-defined ion-selective pores from BTA-EG_4 molecules offer an example of a self-assembled synthetic supramolecule with biological function.

5.1 Introduction

Ion channel proteins mediate transport of ions across cell membranes and play a critical role in physiological processes such as signal transduction, regulation of membrane potentials, and cell proliferation (*1, 2*). Due to the importance of ion channels in applied fields, such as biosensing, and for the pathogenesis of certain diseases (*3-15*), semi-synthetic as well as synthetic versions of pore-forming molecules or artificial ion channels are attracting increasing attention (*16-24*). Additional applications of synthetic ion channels or engineered biological pores include their use as antimicrobial agents, drug delivery agents, fluidic diodes, and components of bio-inspired batteries (*13, 14, 25, 26*).

With regard to the synthesis of ion channel-forming molecules, two approaches have been applied: 1) covalent attachment of pore-forming residues to a molecular scaffold or template, which can have additional functionality as a

selectivity filter (*24, 27-31*), or 2) self-assembly of small molecules to pores, which can conduct ions across lipid membranes (*27, 30, 32-34*).

With regard to the templated approach, several research groups developed synthetic ion channels and pores by attaching amphiphilic moieties to cyclodextrin (*29, 35-37*), crown ethers (*38*), calixarenes (*39*), or cucurbituril templates (*40*). Some of these templated channels contained oligo(ethylene glycol) (OEG) groups or moieties with alternating oxygen and carbon molecules, which were typically attached to a cyclodextrin scaffold. Lehn *et al.* proposed in 1993 that OEG groups grafted on a cyclodextrin scaffold could form ion channels (*41*). Gin's group created ion channels composed of a β-cyclodextrin template with oligoether chains attached to the "primary face of cyclodextrin" through amine linkages (*29*). Liposome flux experiments revealed that this molecule was able to induce transport of Na^+ ions across lipid membranes. Recently, Badi *et al.* demonstrated by single-channel recordings through planar lipid bilayers that per-2,3-heptyl-β-cyclodextrin scaffolds modified with poly(ethylene oxide) (PEO) chains, could form ion channels in lipid membranes (*42*). These authors also showed that PEO moieties by themselves did not form pores at the equivalent concentrations, demonstrating the importance of the cyclodextrin scaffold.

With regard to self-assembly of synthetic ion channel-forming molecules, Neumann and colleagues have shown by fluorescence spectroscopy and ion channel recordings through planar lipid bilayers that molecules with an ester bond between a fatty acid and an OEG moiety can form ion channels (*43*). They also demonstrated by agar well diffusion assays that these molecules had

antibacterial activity against gram-positive bacteria (*44*). In addition, Yang *et al.*, Hirata *et al*., and Kim *et al.* have demonstrated by X-ray diffraction, TEM, molecular dynamics (MD) simulations, and liposome-based fluorescence assays that molecules with alternating oxygen and carbon atoms, including OEG, could interact with lipid membranes and form ion channels (*45-47*).

Here, we introduce a small synthetic molecule that self-assembles and forms ion-selective channels with surprisingly well-defined single-channel conductance in phospholipid membranes. This molecule has a molecular weight below 500 g mol^{-1} and is based on a tetra-ethylene glycol moiety that is attached to a relatively hydrophobic benzothiazole aniline (BTA) group (*Fig. 5-1A*). We chose this OEG derivative of BTA, which we call BTA-EG_4, based on our ongoing research in the context of Alzheimer's disease and HIV transmission, which revealed that BTA-EG_4 can readily cross cellular membranes and affect disease-related biological processes after uptake into mammalian cells (*48-50*). Based on the observed membrane permeability, we focused here on the effect of BTA-EG_4 on planar lipid bilayer membranes under well-defined experimental conditions. We show by single-channel recordings that BTA-EG_4 forms well-defined ion pores that are selective for monovalent cations. We characterize the open lifetime, the approximate number of monomers in each pore, the conformational stability of the pores, and the pH-dependence of the single-channel conductance. Finally, we show that this self-assembling, pore-forming molecule is toxic to the gram-positive bacterium *Bacillus subtilis* and to a human neuroblastoma cell line (SH-SY5Y), while it had no detectable toxic effect on the

gram-negative bacterium *Escherichia coli*. The cytotoxic concentration of BTA-EG_4 was similar to the concentrations necessary to observe ion channel activity, suggesting pore formation as the mechanism of toxicity.

5.2 Results and discussion

5.2.1 *BTA-EG_4 molecules self-assemble to well-defined pores with quantized conductance levels*

Figure 5-1 shows that BTA-EG_4 molecules were capable of forming ion channels with well-defined single-channel conductance steps at concentrations of 10 μM or above (*Fig. 5-1B*). In contrast, the reactants for the synthesis of BTA-EG_4, BTA or tetra-ethylene glycol (EG_4), did not form detectable ion channels at concentrations up to 100 μM in planar lipid bilayers. Remarkably, self-assembly of BTA-EG_4 appeared to form one predominant pore structure; only a few single channel events resulted in a single-channel conductance that was different from the predominant one (*Fig.* 5-1B and for an extended current *versus* time trace, see *Appendix, Fig.* A5-2). These sub-conductances typically had exactly half the current amplitude of the main conductance (see *Fig.*5-1B second channel opening event from the left). The probability for observing these sub-conductances was approximately one fifth of that for the main conductance and their lifetime was significantly shorter than that of the main conductance (*Fig.* A5-2). These sub-conductances may indicate a pair-wise organization of BTA-EG_4 pores, in which the activity of each pore is usually synchronized but not

always. Alternatively, BTA-EG_4 pores may have two conformations, of which the one with the larger pore is more stable than the sub-conductance state. Occasionally, we observed conductance values that were multiples of the amplitude of the main conductance value; we attribute these events to the simultaneous opening of two or more pores in the bilayer. From recordings at various applied potentials, we determined an average single-channel conductance of BTA-EG_4 of 37.8 ± 1.3 pS in an electrolyte solution containing 1.0 M CsCl with 10 mM HEPES, pH 7.4. Recordings of the single-channel conductance through BTA-EG_4 pores as a function of the concentration of CsCl revealed that the CsCl concentration required to reach half-maximal single-channel conductance (*51*) was 0.06 M (see *Appendix, Fig. A5-3*), and the maximum conductance was $\gamma_{max,Cs+}$ = 40.0 ± 1.7 pS.

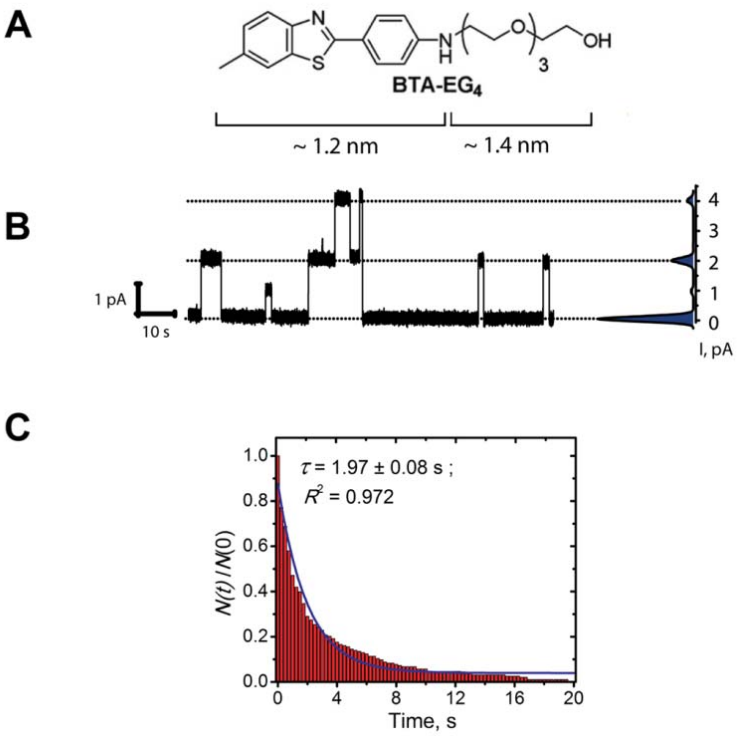

Figure 5-1. Benzothiazole aniline derivatives with four ethylene glycol units (BTA-EG_4) self-assemble to well-defined and long-lived ion channels in lipid bilayer membranes. **A)** Chemical structure of 2-(4-aminophenyl)benzothiazole tetra-ethylene glycol, BTA-EG_4. Molecular dimensions refer to the fully extended conformation as obtained by Macromodel software. **B)** Original current *versus* time trace from single ion channel recordings through self-assembled pores from BTA-EG_4 in a planar lipid bilayer composed of DiPhyPC lipids. The histogram of current amplitudes reflects their number of occurrence in the corresponding current trace. **C)** Normalized survival plot of the open channel lifetime determined from 174 single channel opening events under the same experimental conditions as in B). The lifetime, τ, of BTA-EG_4 pores was determined from a fit of the histogram to the equation, $N(t)/N(0) = \exp\{-t/\tau\}$, where $N(t)$ represents the number of channels with lifetimes longer than the time t, and $N(0)$ represents the total number of channels with observable single-channel conductance. BTA-EG_4 was added at a final concentration of 20 μM to

both bilayer compartments, the applied voltage was + 50 mV, and the electrolyte contained 1.0 M CsCl with 10 mM HEPES buffer, pH 7.4.

Table 5-1 Single-channel conductance of pores from BTA-EG_4 and gramicidin A in electrolytes of different ions at concentrations of 0.5 M and 1.0 M with 10 mM HEPES, pH 7.4

Electrolyte	Single-channel conductance, pS [a]		
	BTA-EG_4		Gramicidin A
	(0.5 M)	(1.0 M)	(1.0 M)
LiCl	1.6 ± 0.2	1.9 ± 0.1	2.2 ± 0.1
NaCl	7.9 ± 0.3	8.5 ± 0.5	12.8 ± 0.3
KCl	13.4 ± 1.0	16.8 ± 0.8	20.0 ± 0.1
CsCl	27.9 ± 0.4	37.8 ± 1.3	38.8 ± 0.9
HCl	n.d.	470 ± 90 [b]	860.2 ± 15.2
KF[c]	n.d.	14.8 ± 0.8	17.1 ± 0.7
KBr[c]	n.d.	19.6 ± 0.6	21.6 ± 0.5
KNO_3[c]	n.d.	18.2 ± 1.3	21.2 ± 0.6
$CaCl_2$	n.d.	<1.7 [d]	n.d

[a] Determined from the average slope of current-voltage (IV)-curves from multiple experiments (n ≥ 3) for each experimental condition, expressed in mean ± standard error of the mean.
[b] Since the conductances of BTA-EG_4 fluctuated strongly when recording in 1.0 M, we also provide the single-channel conductance in 0.01 M HCl (28.6 ± 2.0 pS).
[c] Contained 10 mM KCl to stabilize the potential of the Ag/AgCl electrodes.
[d] Unable to resolve a precise single-channel conductance.
n.d, not determined.

Table 5-1 compares single-channel conductance values of BTA-EG_4 pores to those of gramicidin A (gA) pores under the same experimental conditions. The single-channel conductance of BTA-EG_4 was only slightly smaller than that of gA, indicating that the inner diameter of pores from BTA-EG_4 was probably on a similar size scale as the diameter of gA pores (*i.e.,* ~ 0.4 nm) (*52*). This comparison assumes that the spatial arrangement of polar groups in the lumen of BTA-EG_4 pores was comparable to gA pores (see below) and that pores from BTA-EG_4 had approximately the same length as gA pores. Given the molecular dimensions of BTA-EG_4 (*Fig. 5-1A*), it is unlikely that pores from this molecule would be longer than the thickness of a lipid bilayer (*i.e.,* ~ 3.5 nm) and it is also unlikely that these transmembrane pores would be significantly shorter than gA pores (*i.e.,* ~ 2.6 nm) (*53*) since gA pores are already sufficiently short to induce a hydrophobic mismatch that leads to energetically unfavorable thinning of the lipid bilayer next to the opening of a gA pore (*54, 55*).

5.2.2 Self-assembled pores from BTA-EG_4 are selective for monovalent cations

Based on the small single-channel conductance of pores from BTA-EG_4, we investigated the ion selectivity of these pores. Table 5-1 shows that BTA-EG_4 pores were selective for monovalent cations, while divalent Ca^{2+} cations did not result in detectable single channel events. We were, however, able to observe macroscopic currents in an electrolyte containing 1.0 M $CaCl_2$, if the concentration of BTA-EG_4 exceeded 35 μM. When comparing various cations,

the slopes from current *versus* voltage curves revealed the following order of conductance through BTA-EG_4 pores: $H^+ >> Cs^+ > K^+ > Na^+ > Li^+ >> Ca^{2+}$. This order is exactly the same as in gA pores and it is close to the mobility sequence for these ions in water (*56*). Based on these findings and on the observation that the absolute values of the single conductances in electrolytes from these different cations are also similar to those of gA pores, we propose that BTA-EG_4 channels, like gA channels, behave essentially like water-filled pores (*56*).

In an electrolyte containing 1.0 M HCl (pH ~ 0), we observed large single-channel conductances through BTA-EG_4 pores that ranged from 200-800 pS, but the formation of open pores was less frequent than in less acidic electrolytes. For instance, in an electrolyte with 0.01 M HCl (pH ~2), pore formation by BTA-EG_4 was more frequent than at pH 0 and its single-channel conductance did not fluctuate more than in electrolytes with a pH value of 7.4. These experiments revealed that the single-channel conductance of BTA-EG_4 in 0.01 M HCl was comparable to its single-channel conductance in 1.0 M CsCl, indicating very high permeability of protons through these pores; a result that is consistent with a water-filled pore.

With regard to anions, monovalent potassium salts with large anions generated a slightly larger single-channel conductance through pores of BTA-EG_4 in this sequence: KBr > KNO_3 > KCl > KF; although the maximum difference of the single-channel conductance between electrolytes containing KBr and KF was only 24% and this difference was not statistically significant at a significance

level of 0.05. (For the bulk conductance of aqueous solutions with various potassium salts, see *Appendix, Table A5-1*).

Based on the observation that the single-channel conductance, and in particular, the ion selectivity of BTA-EG_4 pores, are very similar to that of gA pores, we propose that the mechanism of ion selectivity may also be similar. In gA pores, the selectivity filter is lined by the carbonyl oxygen atoms of the peptide backbone and cation selectivity results from interactions of this polar backbone with cations (*51, 57*). In BTA-EG_4 pores, the polar ethylene glycol oxygen atoms could serve as the selectivity filter by lining parts of the lumen of the pore. Another mechanism that may contribute to the cation selectivity of BTA-EG_4 pores is cation-π interaction of cations with the electron-rich π system of the BTA moiety. In this case, the interaction of the BTA group with small cations (e.g. Li^+) would be stronger than with large cations (e.g. Cs^+), leading to the observed reduction of single-channel conductance with decreasing size of monovalent cations (*26, 58, 59*). It is also possible that both mechanisms contribute to the strong cation selectivity of BTA-EG_4 pores.

5.2.3 Self-assembly of BTA-EG_4 forms long-lived, open pores in lipid bilayers

Figure 5-1C shows the lifetime of open channels from BTA-EG_4, which was approximately twice as long (τ = 1.97 ± 0.08 s) as that of gramicidin A pores (τ = 0.95 ± 0.02 s) under the same experimental conditions (see *Appendix, Fig. A5-4A*). The long lifetime of pores from BTA-EG_4 suggests either that the driving

forces for the assembly of BTA-EG_4 pores are stronger than the hydrogen bonding between the two hemi-channels in gA (*51, 60, 61*), or that the driving forces for the disassembly of BTA-EG_4 pores are smaller than the hydrophobic mismatch that drives disassembly of gA pores (*54, 55, 62*).

5.2.4 Each BTA-EG_4 pore contains approximately four monomers

In order to provide an estimate for the number of BTA-EG_4 molecules in each self-assembled pore, we performed time-averaged recordings of transmembrane current over discrete time intervals as a function of the concentration of BTA-EG_4 molecules (*63*). Figure 5-2 shows that increasing concentrations of BTA-EG_4 resulted in a strong increase in transmembrane current. For instance, at concentrations above 35 μM BTA-EG_4, multiple pores were opening at the same time, resulting in "macroscopic currents" across the membrane. By keeping the experimental conditions constant (e.g. constant applied voltage, ionic strength, type of electrolyte, bilayer thickness, etc.), we found that the time averaged currents and hence the macroscopic conductance, *G*, followed the relationship:

$$G \propto [\text{BTA-EG}_4]^n \qquad (5\text{-}1)$$

where *n* provides a rough estimate for the average number of monomers in the channels (*63-65*). To account for possible variations in membrane area during an experiment or between different experiments, we normalized all time averaged currents by the membrane capacitance, which is proportional to membrane area and directly measurable (*66*). This analysis suggests that pores from BTA-EG_4 consisted of 4.2 ±

0.9 BTA-EG_4 monomers (*Fig. 5-2*). For comparison, we performed a similar experiment with gA and obtained an estimate of 2.08 ± 0.08 monomers of gA in a single channel (see *Appendix, Fig. A5-4B*), which is in agreement with pore formation by dimerization of two gA monomers (*60*).

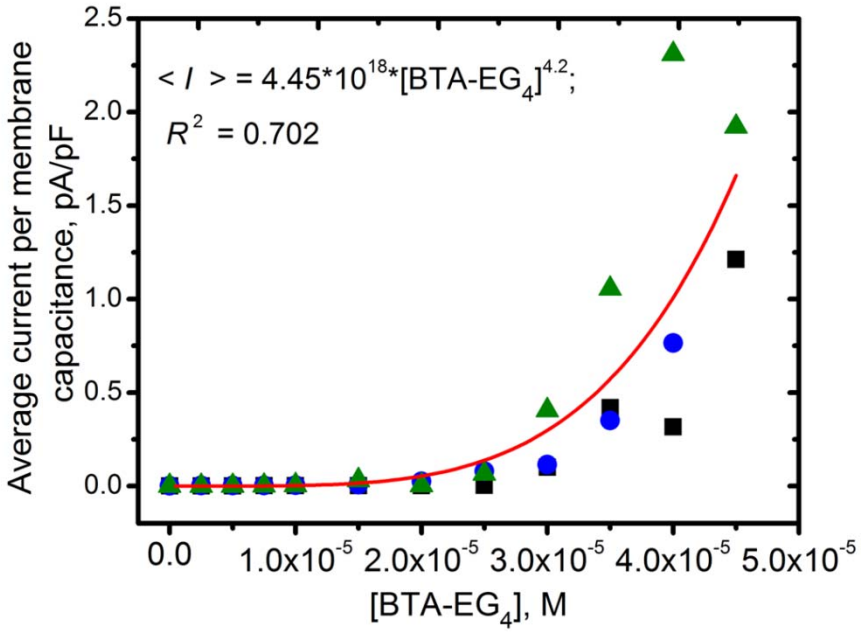

Figure 5-2. Macroscopic ion flux through planar lipid bilayers as a function of increasing concentrations of BTA-EG_4. The graph shows time averaged currents from 3 min recordings normalized to the membrane capacitance as a function of the concentrations of BTA-EG_4. Different symbols indicate three experiments performed independently under the same experimental conditions. The red curve is a global fit to the data from all experiments to equation 1 (considering that the time averaged current is directly proportional to the macroscopic conductance, *G*). The applied voltage was ± 50 mV, and the electrolyte contained 1.0 M CsCl with 10 mM HEPES buffer, pH 7.4.

Figure 5-2 shows that the self-assembly of BTA-EG_4 to pores in planar lipid bilayers required relatively large concentrations (≥ 10 μM), while gA is capable of forming pores at approximately one million-fold lower concentrations (see Figure A5-4B, *Appendix*). We attribute this difference mainly to the extremely low solubility of gA in aqueous solutions; at equilibrium gA partitions almost completely into the bilayer phase. BTA-EG_4, in contrast, is significantly more water soluble than gA and therefore it does not concentrate in the bilayer as much as gA. Moreover, self-assembly of tetrameric BTA-EG_4 pores may require a larger local concentration of BTA-EG_4 molecules in the bilayer than self-assembly of dimeric gA pores. In the context of a possible use of BTA-EG_4 as a starting molecule for the synthesis of pore-forming antibiotics, this requirement for micromolar concentrations is a disadvantage compared molecules such as gA. On the other hand, BTA-EG_4 meets the criteria of Lipinski's empirical rule of five (*67*) and small chemical modifications may increase its lipophilicity and potency while preserving its pore-forming activity.

5.2.5 The noise level of open BTA-EG_4 pores is larger than that of open gA pores

In order to assess the conformational stability of BTA-EG_4 pores, we compared the current noise through the main open state of BTA-EG_4 pores with the noise through single gA pores. For this analysis, we used original current traces that were hardware-filtered with a four-pole Bessel filter with a cutoff

frequency of 10 kHz and sampled at 50 kHz. Based on eight different open events of the main open state of BTA-EG_4 pores, we found an average rms current noise (*i.e.*, average standard deviation of the current from the mean current) of 0.650 ± 0.033 pA. For comparison, the average rms current noise from nine different opening events of individual gA pores was 0.277 ± 0.052 pA, when determined in the same way and under identical experimental conditions as for BTA-EG_4 channels. Note, these noise values represent the average rms current noise through the open channels after subtracting, in an rms fashion and with error propagation, the average rms current noise of the respective baseline current. These estimates of the channel noise assume that the current noise from the recording setup (*i.e.,* the baseline noise when no channel was open) and the current noise from fluctuations of ion flux through an open ion channel were both random and independent of each other. Since current histograms from the open events of BTA-EG_4 and gA channels could be fitted well with Gaussian distributions (*Fig.* 5-1B), the assumption of randomness appears justified. Finally this simplified approach also assumes that differences in frequency-dependence of these two noise sources can be neglected.

Based on these assumptions, two-sample T-tests revealed that the average rms current noise through open BTA-EG_4 pores was significantly larger than through open gA pores ($p < 0.01$). Given that a part of this rms current noise likely resulted from small conformational fluctuations of the channels (*68*), this difference suggests that these fluctuations were more prominent in open pores of BTA-EG_4 than of gA. This result may on the one hand be surprising since the lifetime of BTA-EG_4 pores is longer than that of gA pores, on the other hand,

BTA-EG_4 pores contain approximately four monomers that can each undergo small fluctuations in an open pore, while gA pores contain only two monomers.

5.2.6 The single-channel conductance through BTA-EG_4 pores has a minimum at pH ~ 3

In order to gain insight in the arrangement of BTA-EG_4 molecules to a pore, we characterized the pH dependence of the single-channel conductance through these pores. Since BTA-EG_4 contains an anilinium group with a pK_a of approximately 4.6 in pure water (*69, 70*), we hypothesized that protonation of this group in acidic electrolytes may reduce the permeation of cations through these pores by electrostatic repulsion. Figure 5-3 shows that the single-channel conductance of BTA-EG_4 pores had a minimum at a pH ~ 3. Since the high concentration of CsCl (3.0 M) in the electrolyte used for these recordings might have shifted the pK_a of the anilinium group towards a more acidic pK_a (*71*), we determined the pK_a of BTA-EG_4 in the presence of 3.0 M CsCl (and 12% DMSO to increase the solubility of BTA-EG_4 and to mimic the hydrophobic environment in the proximity of planar lipid membranes). Under these conditions, an acid-base titration experiment indicated a pK_a of ~ 3.5 for BTA-EG_4. This pK_a value is consistent with protonation of BTA-EG_4 molecules and with concomitant reduction of the single-channel conductance of cations through pores from BTA-EG_4 molecules at pH values below 4. Since the Debye screening length in this 3.0 M CsCl electrolyte was approximately 0.2 nm (*71*), the minimum conductance of BTA-EG_4 pores at a pH value of ~3 suggests that the aromatic ring with the protonated anilinium group was located either at the mouth of the pores or faced

the lumen of the pores. In contrast to the reduction of the single-channel conductance as the pH in the electrolyte was lowered from 7.4 to 2.8, the increase in conductance at pH values below 2.8 was likely due to the increased concentration of highly permeable protons in these increasingly acidic electrolytes (see *Table 5-1, and Appendix, Fig. A5-5*).

For comparison, Figure 5-3 shows data from gA pores, whose conductance increased steadily with increasing acidity in the same 3.0 M CsCl electrolyte, indicating that the observed minimum conductance of BTA-EG_4 pores at pH ~ 3 is characteristic for these pores and likely a consequence of protonation of the anilinium group of BTA-EG_4.

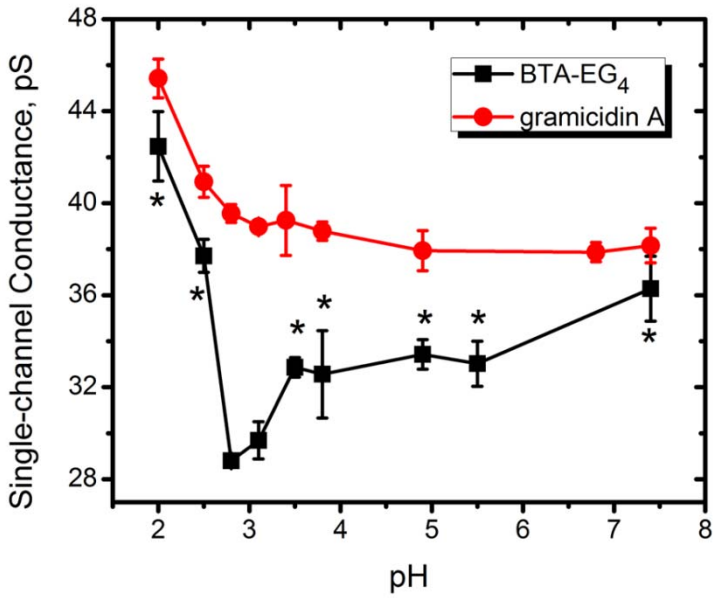

Figure 5-3. Single-channel conductance of BTA-EG_4 and gramicidin A as a function of the pH in the recording electrolyte. Ion channel recordings were performed with DiPhyPC bilayers in unbuffered electrolytes that contained 3.0 M

CsCl at various pH values that were adjusted by adding HCl. Statistical significance ($p<0.05$) of differences in single-channel conductance of BTA-EG_4 pores at different pH values was determined with respect to the minimum conductance at pH 2.8 and indicated by an asterisk (*). Error bars represent the standard error of the mean.

5.2.7 Fluorescence spectroscopy suggests localization of the BTA moiety inside lipid bilayers

To gain complementary insight in the assembly of BTA-EG_4 molecules to pores, we took advantage of the dependence of the fluorescence emission spectra of BTA derivatives on their chemical environment. Excitation at 350 nm revealed a shift to shorter emission wavelengths when BTA-EG_4 molecules were dissolved in octanol compared to water. The wavelengths of maximum emission of BTA-EG_4 in an aqueous suspension of liposomes was between the wavelength of maximum emission in water and octanol, suggesting that at least a part of the fluorescent BTA moiety was located inside the bilayer membrane (*Fig. 5-4*).

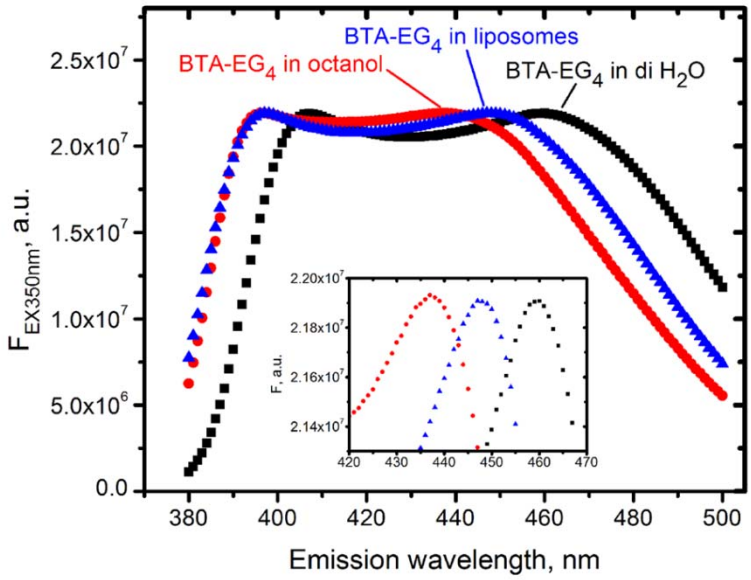

Figure 5-4. Comparison of fluorescence emission spectra of 50 μM BTA-EG_4 in pure H_2O (■), pure octanol (●), and in an aqueous liposome suspension (▲) using an excitation wavelength of 350 nm. Liposomes were made of DiPhyPC with a total lipid concentration of 10 mM in water.

5.2.8 Asymmetric addition of BTA-EG_4 to one side of the bilayer leads to symmetric current-voltage relationships

In order to test whether membrane incorporation of BTA-EG_4 molecules from only one side of the bilayer would lead to pores with transverse asymmetry across the bilayer (72), we obtained a current *versus* voltage curve after addition of BTA-EG_4 only to the cis-compartment. Since the resulting current *versus* voltage curve was linear with the same slope at both polarities, we did not

observe a measurable indication of transverse asymmetry of BTA-EG_4 pores in DiPhyPC bilayers (see *Appendix, Fig. A5-1*).

5.2.9 High concentrations of BTA-EG_4 molecules destabilize lipid bilayers

At concentrations above 35 μM, BTA-EG_4 occasionally destabilized planar bilayers sufficiently to break the membranes irreversibly. We observed this effect in approximately 20% of experiments. In addition, liposomal leakage assays revealed that BTA-EG_4 induced leakage of protons through liposome membranes (see *Appendix, Fig. A5-6*). The same liposome-based assay revealed that EG_4 by itself did not cause detectable leakage, while BTA by itself was capable of inducing approximately half the rate of proton leakage than BTA-EG_4. We could not, however, detect any ion channel activity from BTA by itself (or from EG_4 by itself) in planar lipid bilayer recordings.

5.2.10 BTA-EG_4 has antibacterial activity

Gramicidin A and its analogs have antibiotic activity by forming cation-selective pores in biological membranes (*57, 61, 73*). This activity is directed against gram-positive bacteria, not gram-negative bacteria, due to differences in structure of the bacterial cell walls (*74, 75*). Since we observed similarities in the characteristics of pores from BTA-EG_4 and gA, we tested the antibacterial activity of BTA-EG_4 molecules on a gram-positive and a gram-negative bacterium.

Figure 5-5 shows that BTA-EG_4 inhibited the growth of the gram-positive bacterium *Bacillus subtilis*: a concentration of 100 μM BTA-EG_4 completely suppressed the growth of these bacteria after overnight exposure. The extent of this inhibitory effect was similar to that of 10 μM kanamycin or 5 μM gA, as shown in Figure A5-7 of the Appendix. Consequently, we estimate a MIC value (*i.e.,* the minimal concentration that inhibited visible growth over night) of ~100 μM BTA-EG_4, while its IC_{50} value was ~50 μM. For comparison, we found the following values for five other pore-forming, antimicrobial peptides against gram-positive bacteria: i) alamethicin, IC_{50} = 1-3 μM (*76*); ii) gramicidin D, MIC = 0.5 μM; iii) melittin, MIC = 8.5 μM; iv) magainin II, MIC = 18 μM; and v) human defensing HNP-1, MIC >60 μM (*77*). In contrast, BTA-EG_4 concentrations up to 500 μM did not show significant toxicity on gram-negative *E. coli* bacteria (see *Appendix, Fig. A5-8*).

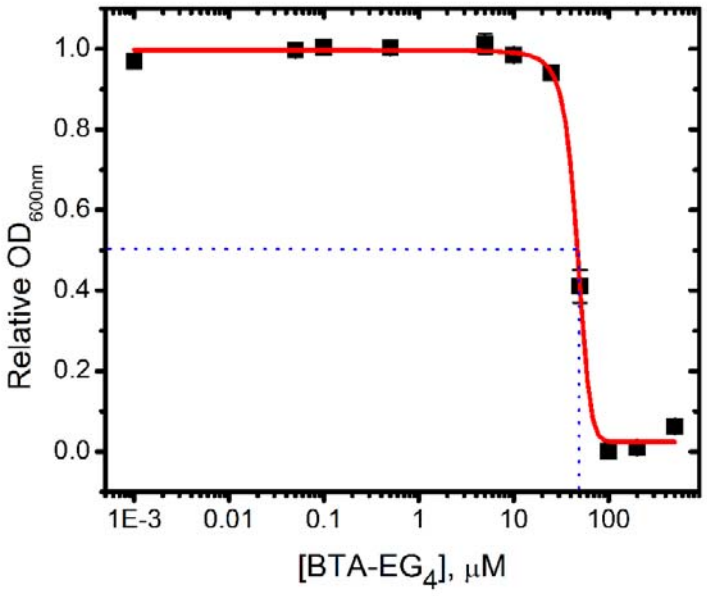

Figure 5-5. Inhibitory effect of BTA-EG_4 on the growth of *Bacillus subtilis* bacteria 22 h after incubation in LB media containing various concentrations of BTA-EG_4. Growth was quantified by the optical density at a wavelength of 600 nm relative to untreated control cells. The concentration of BTA-EG_4 molecules that inhibited growth by 50% (IC_{50} value) was ~ 50 μM. Each point represents the mean of two experiments with three replicates in each experiment; error bars represent the standard error of the mean.

5.2.11 BTA-EG_4 is toxic to human neuroblastoma cells

Since BTA-EG_4 was capable of forming ion channels in artificial lipid bilayers and exhibited antibacterial activity against gram-positive bacteria, we investigated the effect of BTA-EG_4 on the viability of a human neuroblastoma cell line. After treating SH-SY5Y cells for 24 h in serum-free media containing

various doses of BTA-EG_4, we determined their viability by an MTT assay (*78*). Figure 5-6 shows that BTA-EG_4 was toxic to these mammalian cells in a dose-dependent manner with an IC_{50} value of ~ 60 μM. For comparison, the IC_{50} value of gA in human embryonic kidney (HEK) cells was ~0.12 μM.

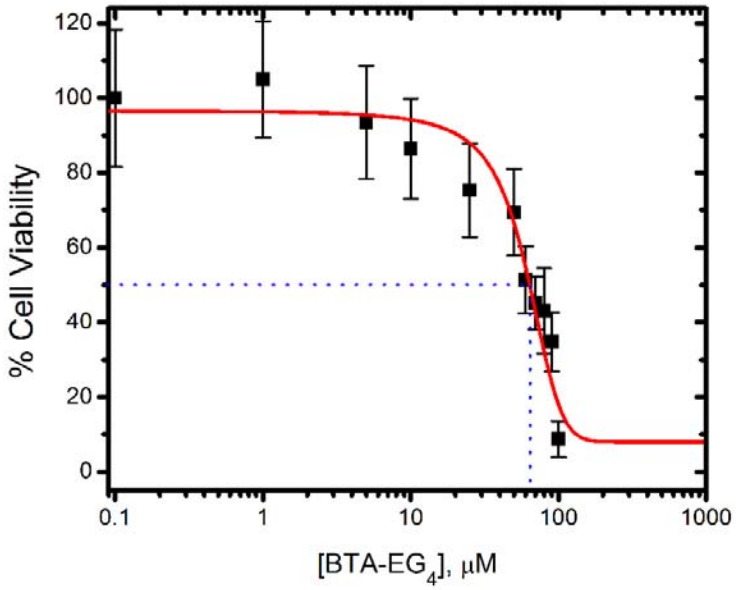

Figure 5-6. Cytotoxicity of BTA-EG_4 on human neuroblastoma cells (SH-SY5Y) 24 h after exposure. Each point represents the mean of two or three experiments with six replicates in each experiment. Error bars reflect the standard error of the mean. The red curve is a fit of the equation, $y = A_2 + \frac{(A_1 - A_2)}{1+10^{(IC50-x)*Hillslope}}$ to the data on a linear x-scale, where A_1, A_2, and *Hillslope* are constants. The IC_{50} value was ~ 60 μM.

Since BTA-EG_4 concentrations above 35 μM occasionally broke planar lipid bilayers irreversibly and since the IC_{50} values for killing gram-positive bacteria and neuroblastoma cells were above this concentration, we tested whether BTA-EG_4 exerted its cytotoxic activity by cell lysis or by pore formation. To this end, we performed a hemolysis assay by exposing red blood cells to increasing concentrations of BTA-EG_4. This assay revealed that BTA-EG_4 does indeed have hemolytic activity, which, at BTA-EG_4 concentrations above 200 μM, can reach 80% of the maximum hemolytic activity (*Fig.* A5-9). The concentration to reach half-maximal hemolytic activity (~140 μM), however, was significantly higher than the IC_{50} values of ~ 50 and ~ 60 μM for killing bacteria or neuroblastoma cells. In fact, below a concentration of 80 μM, BTA-EG_4 had no detectable hemolytic activity. Together, these findings suggest pore formation with concomitant disruption of ionic gradients as a possible mechanism of toxicity of BTA-EG_4 molecules. Similar to gA molecules, the large conductance to protons may cause BTA-EG_4 molecules to act as an uncoupler of oxidative phosphorylation (*79, 80*).

5.3 Conclusion

Self-assembly of a tetra-ethylene glycol derivative of benzothiazole aniline in planar lipid bilayers led to well-defined and long-lived transmembrane ion pores that are strongly selective for monovalent cations. In contrast to pores formed by gramicidin A, pores from BTA-EG_4 have a minimum single-channel conductance at pH ~ 3, which suggests that the protonatable anilinium group is located less than 2 Å away from the lumen of the pores. Likely due to its pore-forming ability, this molecule exhibits antibiotic activity against gram-positive bacteria with an IC_{50} value of ~ 50 μM, but not against gram-negative bacteria. As expected for a pore former, BTA-EG_4 was also toxic to human neuroblastoma cells with an IC_{50} value of approximately ~ 60 μM. Given the recent development of molecules with similar general structure (*i.e.*, a short hydrophobic/aromatic component attached to a short OEG group) as in vivo diagnostic agents for Alzheimer's disease (*48, 50*), our findings highlight the risk of pore formation as a mechanism for possible cytotoxic side effects. On the other hand, this small synthetic pore-forming molecule might be appealing as a starting material for development of synthetic ion channels, antibiotics, membrane-permeating agents for drug delivery, or as uncouplers of oxidative phosphorylation since it is able to cross cellular membranes (*50*) and since oligo(ethylene glycol) moieties are biocompatible and suitable for polymeric drug delivery (*81*).

5.4 Materials and methods

5.4.1 Materials

We purchased cesium chloride (CsCl) from International Biotechnologies Inc.; sodium chloride (NaCl), and potassium bromide (KBr) from Fluka; and potassium chloride (KCl), HEPES, and hexane from Fisher Scientific. All other chemicals and reagents were obtained from Sigma-Aldrich (St. Louis, MO).

5.4.2 Formation of planar lipid bilayers

We used 1,2-diphytanoyl-*sn*-glycero-3-phosphatidylcholine (DiPhyPC) from Avanti Polar Lipids (Alabaster, Alabama) for the formation of all bilayers in this work. We prepared planar lipid bilayers by the "painting method" by applying a solution of 20 mg mL^{-1} DiPhyPC in *n*-heptane or *n*-decane over an aperture with a diameter of ~ 250 μm in a Delrin cup (Warner Instruments) (*11, 82*). Before bilayer formation, we pretreated these apertures with a droplet of a solution of 20 mg mL^{-1} DiPhyPC in n-hexane. Both compartments of the chamber (cis and trans) were filled symmetrically with electrolytes containing 1.0 M concentrations of various salts with 10 mM HEPES buffer adjusted to pH 7.4 with HCl unless indicated otherwise. For each experiment, we confirmed the stability of the lipid membrane by applying a voltage of ± 100 mV for 10 min before addition of reagents to both compartments with stirring for 5 min using a stir plate for planar bilayer recordings (SPIN-2, Warner Instruments).

5.4.3 Current recordings across planar lipid bilayers

For current recordings, we used amplifiers in voltage clamp mode (either Geneclamp-500 amplifier from Axon Instruments, or a BC-535 amplifier from Warner Instruments). The compartment of the bilayer chamber that was connected to the amplifier head stage by a Ag/AgCl electrode is referred to as cis compartment, the other one as trans compartment. We monitored the ionic current across the planar bilayers with a filter cutoff frequency of 10 kHz of the 4-Pole Bessel filters of the amplifiers and recorded currents using LabVIEW 7.1 and an A/D converter card from National Instruments (PCI-6221) with a sampling frequency of 50 kHz. For analysis, data were filtered with a Gaussian filter at 100 Hz and analyzed by using the software Clampfit 9.2 (Axon Instruments). We determined all single-channel conductance values from the slope of current *versus* voltage (IV) curves, which were linear up to voltages of ±100 mV (see *Appendix, Fig. A5-1*). Ion channel recording was repeated at least 3 times for each experimental condition. We monitored the capacitance of the bilayers throughout the recordings using the built-in capacitance compensation of the amplifiers. For the determination of the estimate of the number of BTA-EG_4 molecules in each self-assembled pore, we used time-averaged currents over discrete time intervals (3 min) as a function of increasing concentrations of BTA-EG_4. We averaged transmembrane currents at positive and negative voltages at ± 50 mV by integrating areas under current *versus* time traces and dividing the resulting area by the total recording time followed by normalizing the averaged currents by the membrane capacitance. All experiments were performed in 1.0 M or 3.0 M CsCl with 10 mM HEPES, pH 7.4 unless otherwise noted.

5.4.4 Statistical analysis of differences in single-channel conductance

To determine statistical significance of differences in single-channel conductance of BTA-EG_4 or gA at different pH values, we compared all single-channel conductances obtained from different applied voltages. We determined *P*-values using a two-sample Student's *t*-test included in the Origin 8.0 software package (Northampton, MA).

5.4.5 Liposome leakage assay

We prepared liposomes from a total lipid concentration of 10 mM of the following lipids, DiPhyPC:cholesterol:DiPhyPG:DPPE-PEG_{2000} in a 9:9:1:1 molar ratio. See section 4.4.3 in Chapter 4 for experimental method.

5.4.6 Cell viability assay

See section 3.3.5 in Chapter 3 for cell culture maintenance. We determined the cell viability using an MTT cell proliferation assay, according to the instructions from the supplier (*78*).

5.4.7 Microbial toxicity

E. coli and *B. subtilis* were grown in LB media overnight at 37 ^{o}C and 31 ^{o}C, respectively. The cells were harvested, washed, and subsequently resuspended in fresh LB medium containing compounds of interest at various concentrations. We added 200 μL of cells to each well of 96-well plates with three replicates for each condition and allowed the cells to grow for 30 h while shaking. We monitored the growth of bacteria by measuring optical density at 600 nm relative to control cells every 15 min, using a VersaMax microplate reader (Molecular Devices Inc., East Falmouth, MA).

5.4.8 Hemolysis assay

We purchased bovine red blood cells (bRBC) from Lampire Biological Laboratories (Pipersville, PA). After washing bRBC in phosphate buffered saline (PBS) buffer (Dulbecco's PBS, Gibco) at pH 7.4, we prepared the stock bRBC suspension by diluting the originally purchased suspension 10-fold in PBS buffer (after several wash steps in PBS). We pipetted 200 μL of the resulting bRBC stock solution into reaction vials and added various final concentrations of BTA-EG_4 in PBS such that the final volume of all vials was 1 mL. These suspensions were mixed and incubated at 37 °C for 1 h followed by centrifugation at 10,000 x g for 5 min at a temperature of 21 °C. To assess hemolysis, we collected the supernatant from each tube and determined the absorbance at 541 nm. We added 800 μL PBS as the negative control, which yielded 0% hemolysis

and 800 μL diH_2O as the positive control, which yielded 100% hemolysis. We performed the experiment in triplicates for each condition.

5.4.9 Measurement of fluorescence emission spectra

We diluted BTA-EG_4 molecules to a final concentration of 50 μM in deionized H_2O, pure octanol, and a liposome suspension. The liposomes were prepared from a total lipid concentration of 10 mM of DiPhyPC in water by the gentle dehydration rehydration method, followed by tip sonication. We transferred 800 μL of each BTA-EG_4 sample to a disposable cuvette (Precision Cells, Inc., Farmingdale, NY), and measured fluorescence emission spectra at an excitation wavelength of 350 nm, using a Fluorolog-3 spectrofluorometer (Horiba-Jobin Yvon, Edison, NJ).

Chapter 5 Appendix

***A5-1* Current-voltage (IV) curves of BTA-EG$_4$ ion channels**

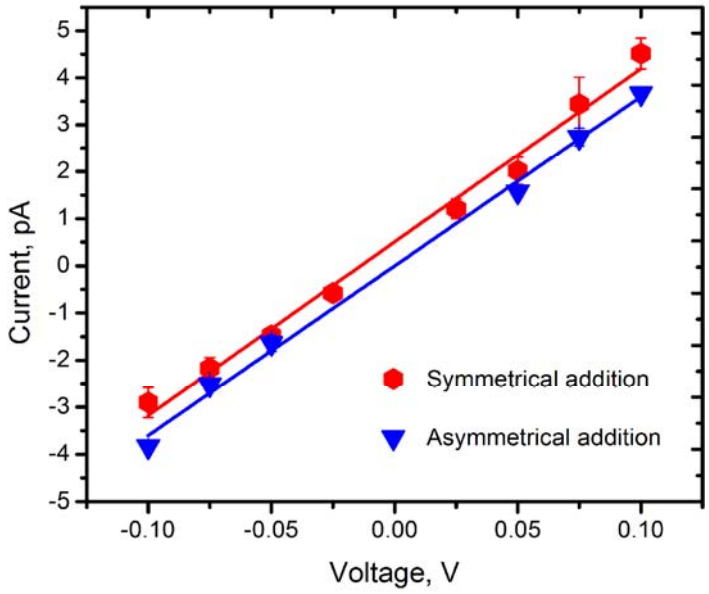

Figure A5-1. Single-channel current-voltage relationship of pores formed by BTA-EG$_4$. The solid lines represent linear fits to the data. The results indicate a single-channel conductance of 36.8 ± 1.4 pS (R^2 = 0.99) for symmetrical addition of BTA-EG$_4$ (red) and 36.0 ± 1.1 pS (R^2 = 0.99) when adding BTA-EG$_4$ to the cis compartment only (blue). Both conductance values were the same within error. The planar lipid bilayer consisted of DiPhyPC lipids and the electrolyte contained 1.0 M CsCl with 10 mM HEPES, pH 7.4 in both compartments. The offset in the y-intercept between the two lines was due to a small voltage offset.

A5-2. Single-channel recordings at different applied voltages

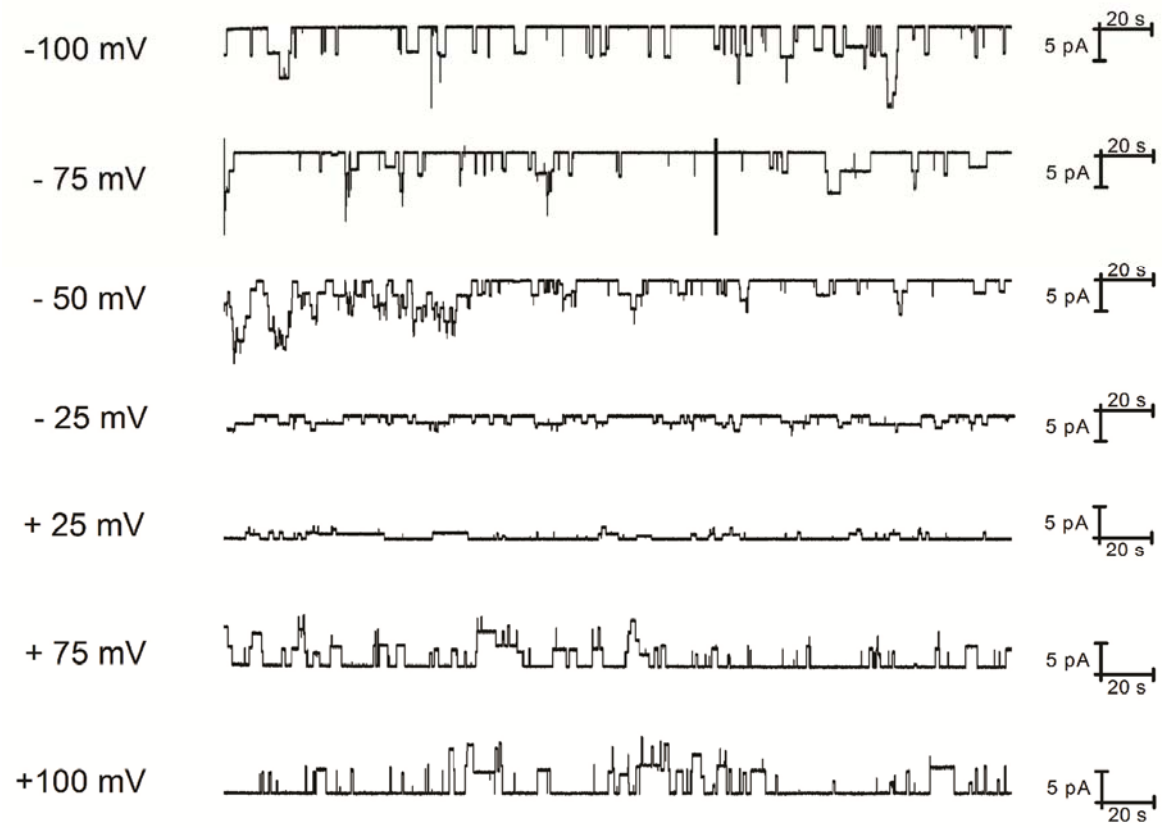

Figure A5-2. Single-channel recordings of pores from BTA-EG_4 (20 μM) through lipid bilayers composed of DiPhyPC in 1.0 M CsCl with 10 mM HEPES buffer, pH 7.4 at various applied voltages. Each current-time trace was recorded for 5 min.

A5-3. Single-channel conductance as a function of the concentration of CsCl in the recording electrolyte

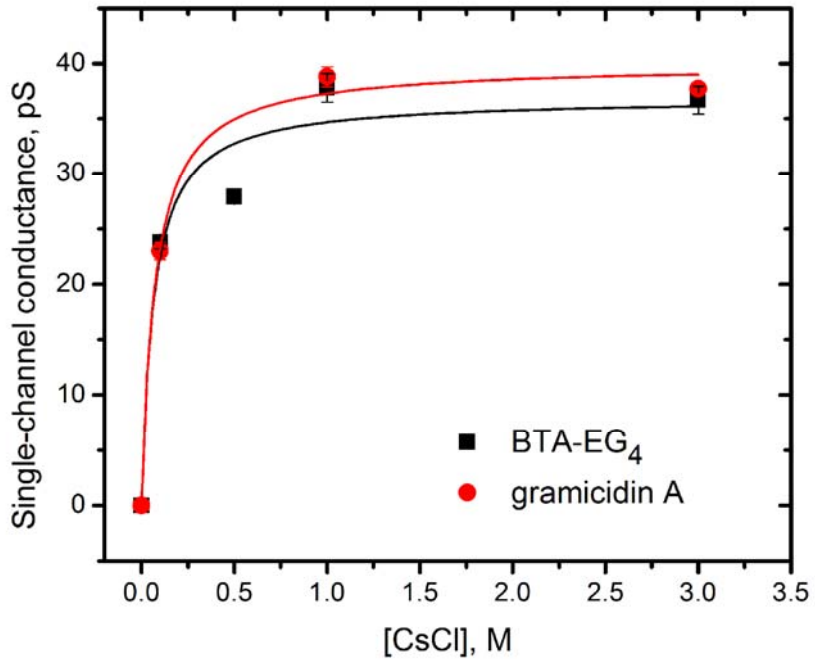

Figure A5-3. Single-channel conductance as a function of the concentration of CsCl in the recording electrolyte. As the concentration of CsCl increases, the single-channel conductances of both BTA-EG_4 and gA pores increase and reach saturation. The curves are best fits of the data to the following equation: $\gamma_{Cs} = \gamma_{max,\,Cs}/(1+ K_{Cs}/[Cs])$, where $\gamma_{max,\,Cs}$ represents the maximal single-channel conductance that can be reached with Cs^+ ions and the concentration for half-maximal single-channel conductance, $\gamma_{0.5\,max,\,Cs}$, is K_{Cs}. The curves yield $\gamma_{max,\,Cs}$ values of 36.9 ± 3.2 pS and K_{Cs} values of ~ 0.06 M for BTA-EG_4 as well as $\gamma_{max,\,Cs}$ values of 40.0 ± 1.7 pS and K_{Cs} values of ~ 0.07 M for gA pores. The planar bilayer consisted of DiPhyPC lipids.

Table A5-1: Bulk conductivity of aqueous electrolyte solutions containing different anions at 22 °C

Electrolyte	MW, g mol^{-1}	Conductivity, mS/cm		
		0.01 M	0.1 M	1.0 M
KF	58.09	1.27	12.23	95.8
KCl	74.55	1.49	15.19	130.6
KNO_3	101.10	1.48	13.93	104.5
KBr	119.00	1.56	15.21	133.4

A5-4. Characterization of ion channel formation by gramicidin A

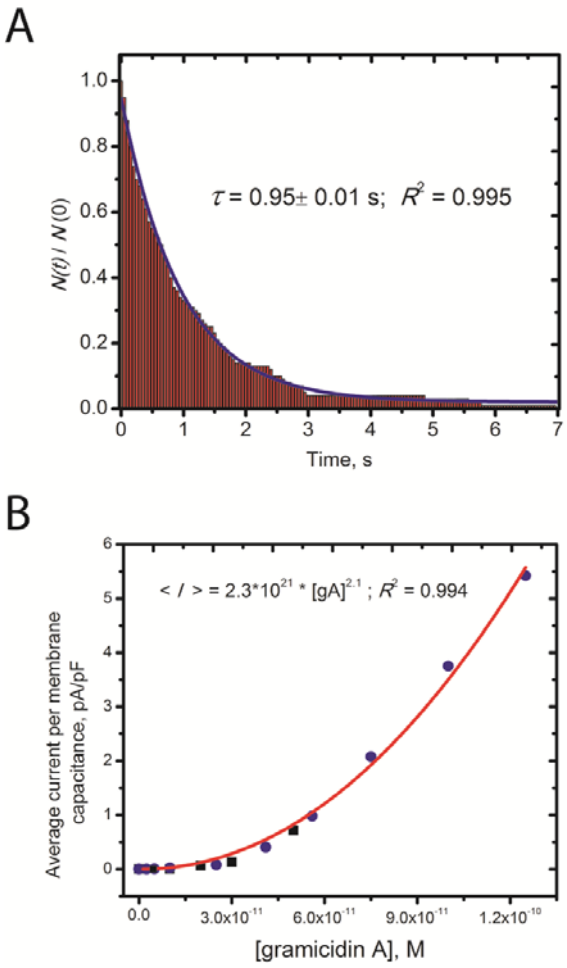

Figure A5-4. Characterization of ion channel formation by gramicidin A. **A)** Lifetime, τ, of gramicidin A pores as determined from a best-curve fit of a normalized survival plot of the open channel lifetime to an exponential decay function. **B)** Time-averaged current across the lipid bilayer normalized to the membrane capacitance as a function of the concentration of gA in the electrolyte solution. The data was fit well with a power law (equation 1; main text) with an exponent of 2.08 ± 0.08, suggesting that two molecules of gA assemble to form a single pore through lipid membranes. Two independent

experiments are indicated in different symbols. The applied potential was ± 50 mV and the electrolyte contained 1.0 M CsCl with 10 mM HEPES, pH 7.4.

***A5-5*. Dependence of the single-channel conductance of BTA-EG$_4$ pores on the proton concentration in an electrolyte**

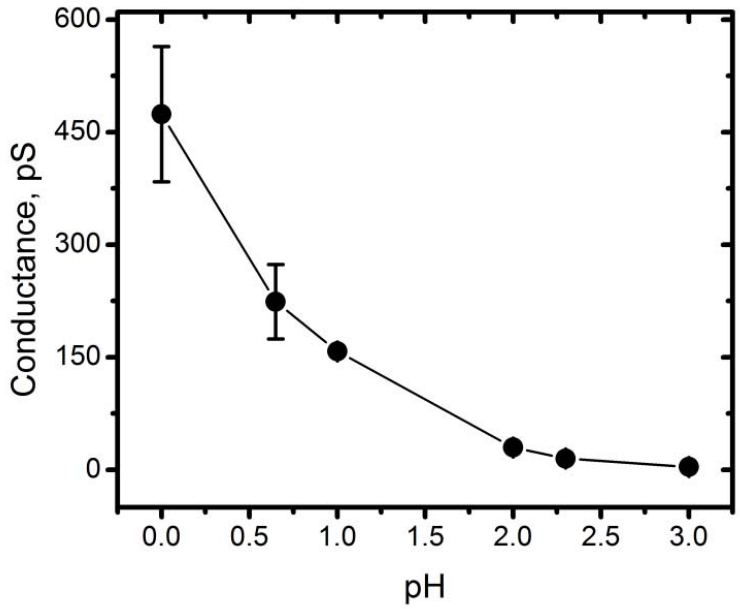

Figure A5-5. Dependence of the single-channel conductance of BTA-EG$_4$ pores in DiPhyPC bilayers on the proton concentration in an electrolyte that did not contain other ions than HCl. The single-channel conductance of protons was not detectable at HCl concentrations below 1.0 mM (pH 3). In the absence of other ions, the effect of increasing proton concentration was stronger than the electrostatic repulsion of protons as a result of protonation of the BTA moiety. Therefore, in the absence of 3.0 M CsCl, the single-channel conductance of BTA-EG$_4$ did not have a detectable minimum between pH 2 and 3.

A5-6. Leakage of protons through liposomes as detected by change of fluorescence ratio

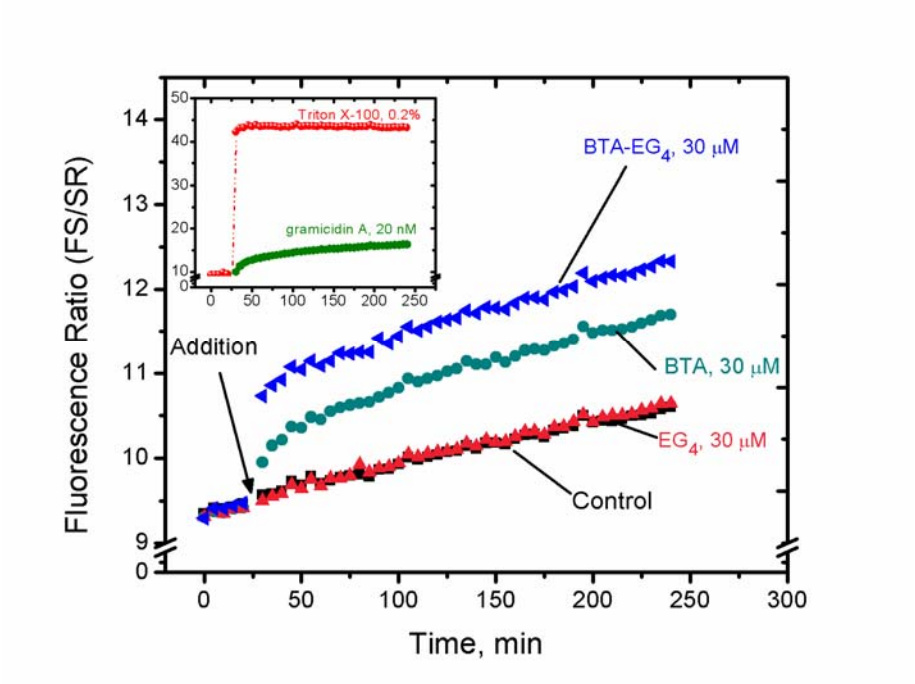

Figure A5-6. Leakage of protons through liposomes after addition of BTA-EG_4 expressed as fluorescence ratio of the pH-sensitive fluorophore, fluorescein sulfonate (FS) and the pH-insensitive fluorophore, sulforhodamine B (SR). Control: liposomes only, without addition of compounds. Inset: 0.2% of Triton X-100, and 20 nM gramicidin A were used as positive controls for leakage of protons. The lipid composition of the liposomes was DiPhyPC:cholesterol: DiPhyPG:DPPE-PEG_{2000} (9:9:1:1). The excitation/emission wavelengths were 485 nm/518 nm for FS and 560 nm/590 nm for SR.

A5-7. Inhibitory effect of BTA-EG$_4$ on the growth of Bacillus subtilis

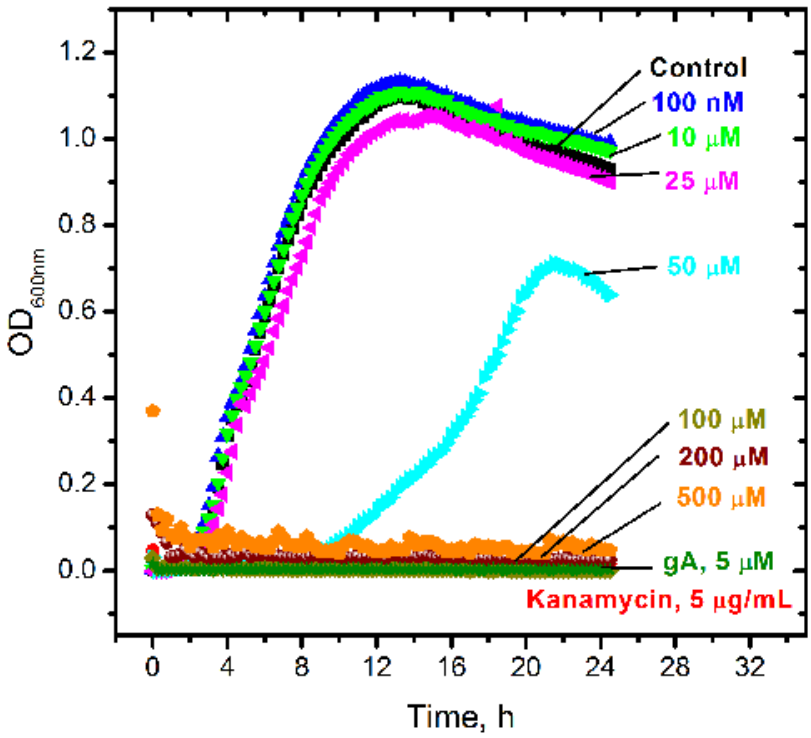

Figure A5-7. Inhibitory effect of BTA-EG$_4$ on the growth of *Bacillus subtilis* at various concentrations determined by the optical density at a wavelength of 600 nm. Growth of bacteria was compared to control cells that were not treated with compounds. Kanamycin (10 μM) and gA (5 μM) were used as positive controls for antibiotic compounds.

A5-8. BTA-EG$_4$ shows no inhibitory effect of on the growth of E.coli

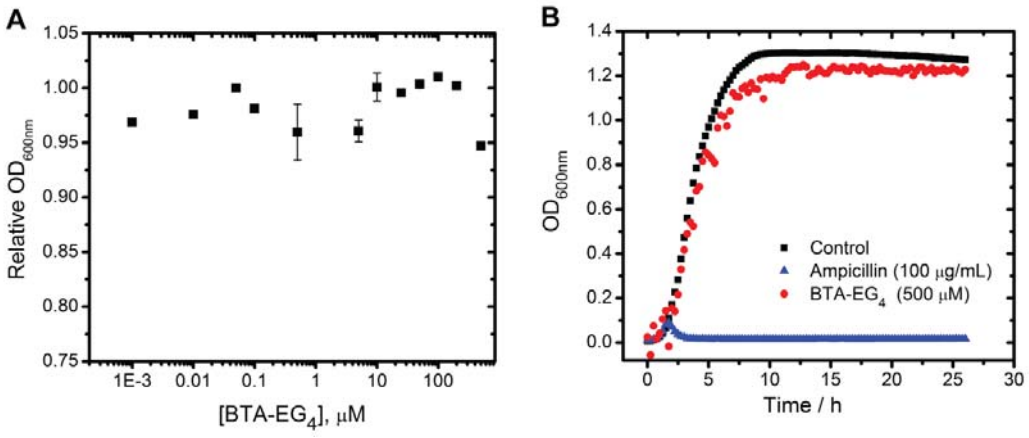

Figure A5-8. Effect of BTA-EG$_4$ on the growth of *E. coli* bacteria. **A)** Comparison of the bacterial growth 22 h after exposure to LB media containing BTA-EG$_4$ at various concentrations relative to control cells (no treatment). BTA-EG$_4$ did not show significant toxicity at concentrations up to 500 μM. Each point resulted from an average of one or two experiments with three replicates for each experiment; error bars represent standard error of the mean. **B)** Growth of *E. coli* with or without treatment of BTA-EG$_4$ at 500 μM as determined by optical density at a wavelength of 600 nm.

A5-9. Hemolytic activity of BTA-EG$_4$ as a function of its concentration

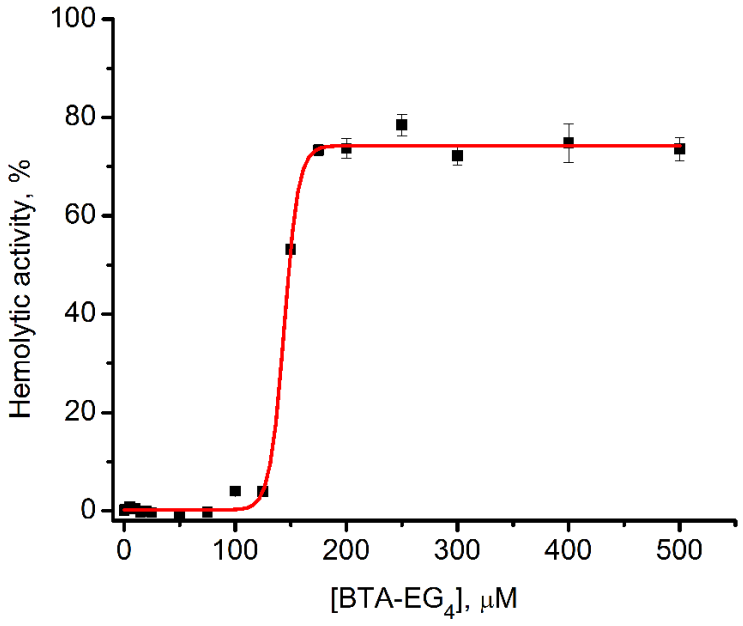

Figure A5-9. Hemolytic activity of BTA-EG$_4$ as a function of its concentration. Each point presents the mean and the standard error of the mean of three independent experiments done in triplicate. The red curve is a fit to an equation, $y = A_2 + \frac{(A_1 - A_2)}{1+10^{(IC50-x)*Hillslope}}$, where A_1, A_2, and *Hillslope* are constants. The obtained IC_{50} of BTA-EG$_4$ dose response curve was ~ 140 μM.

A5-10. Additional results on BTA-EG$_6$ molecule

In our studies, we also conducted the same experiments on another molecule in the same family as BTA-EG$_4$. This molecule is a derivative of BTA, attached to hexa(ethylene glycol), which we refer to BTA-EG$_6$. BTA-EG$_6$ molecule is also capable of forming well-defined ion channels through PLB, with similar conductances as BTA-EG$_4$. In addition, this molecule exhibits the same sequence of cation selectivity, and minimum conductance at pH ~ 3 as observed in BTA-EG$_4$. Some distinct characteristics are summarized below.

lifetime, τ:	3.58 ± 0.06 s
estimated number of molecules assembled in a channel :	5.9 ± 0.9
antibacterial activity against *Bacillus subtillis*:	IC_{50} ~ 100 μM
cytotoxicity in neuroblastoma cells :	IC_{50} ~ 60 μM

A5-11. Synthesis of BTA-EG$_4$ and BTA-EG$_6$ molecule

2-(2-(2-(2-hydroxyethoxy)ethoxy)ethoxy)ethyl toluenesulfonate

In a clean, dry 1 L round bottom flask equipped with a stir bar, we dissolved tetra-ethylene glycol (10.0 g, 51.5 mmol) in 500 mL dry dichloromethane (DCM) and stirred at room temperature. After 5 min, potassium iodide (1.71 g, 10.3 mmol), Ag_2O (17.9 g, 77.2 mmol), and *p*-toluenesulfonyl chloride (10.8 g, 56.6 mmol) were successively added

to the reaction flask. The reaction mixture was stirred vigorously for 2 h, filtered through celite to remove the solids and concentrated in vacuo. The residue was purified via silica column chromatography (100% DCM to 95:5 DCM:CH_3OH) giving 2-(2-(2-(2-hydroxyethoxy)ethoxy)ethoxy)ethyl toluenesulfonate as a colorless oil (13.2 g, 74%). ^{1}H-NMR (400 MHz, $CDCl_3$): δ = 7.74 (d, 8.0 Hz, 2H), 7.30 (d, 8.0 Hz, 2H), 4.11 (t, 4.8 Hz, 2H), 3.66-3.53 (m, 12H), 2.79 (s, 1H), 2.39 (s, 3H). ^{13}C-NMR (100 MHz, $CDCl_3$); δ = 145.04, 133.17, 130.10 (2C), 128.19 (2C), 70.95, 70.79, 70.70, 69.49, 68.88, 21.87. ESI-MS (*m/z*) calculated for $C_{15}H_{24}O_7S$ $[M]^+$ 348.1243; found $[M+H]^+$ 348.96, $[M+NH_4]^+$ 365.94 and $[M+Na]^+$ 371.08.

2-(2-(2-(2-iodoethoxy)ethoxy)ethoxy)ethanol

We combined 2-(2-(2-(2-hydroxyethoxy)ethoxy)ethyoxy)ethyl toluenesulfonate (12.01 g, 34.5 mmol), sodium iodide (20.7 g, 137.9 mmol) and 200 mL dry acetone in a clean, dry round bottom flask and heated to reflux with vigorous stirring. After 12 h the reaction was cooled to room temperature and diluted with 100 mL ethyl acetate. The organic phase was washed with 10% $Na_2S_2O_3$, (2 x 10 mL), deionized H_2O (1 x 20 mL), saturated NaCl (1 x 20 mL), dried over anhydrous Na_2SO_4, filtered, and concentrated in vacuo giving 2-(2-(2-(2-iodoethoxy)ethoxy)ethoxy)ethanol as a pale yellow oil (5.61 g, 54%). ^{1}H-NMR (400 MHz, $CDCl_3$): δ = 3.73-3.58 (m, 14H), 3.24 (t, 2H), 2.59 (s, 1H). ^{13}C-NMR (100 MHz, $CDCl_3$); δ = 72.70, 72.19, 70.90, 70.76, 70.58, 70.39, 61.94, 3.07.

BTA-EG$_4$

A microwave reaction tube was charged with 2-(2-(2-(2-iodoethoxy)ethoxy)ethoxy)ethanol(1.47 g, 4.83 mmol), benzothiazole aniline (3.49 g,

14.5 mmol), potassium carbonate (3.34 g, 24.2 mmol) and 20 mL dry THF. The tube was then equipped with a small stir bar, sealed and placed in a microwave reactor. The reaction was heated at 125 ^{o}C for 2 h. The reaction was cooled to room temperature and filtered to remove the solids. The solids washed several times with DCM until the filtrate was colorless. The combined organic layers were concentrated in vacuo and purified by column chromatography to give the desired BTA-EG_4 compound as a yellow solid (1.13g, 56%). ^{1}H-NMR (400 MHz, $CDCl_3$): δ = 7.87 (d, 8.8 Hz, 2H), 7.83 (d, 8.4 Hz, 1H) 7.63 (s, 1H) 7.23 (d, 8.4 Hz, 1H), 6.68 (d, 8.8 Hz, 2H), 3.76-3.64 (m, 14H), 3.37 (t, 5.2 Hz, 2H), 2.47 (s, 3H). ^{13}C-NMR (100 MHz, $CDCl_3$); δ = 168.03, 152.64, 150.92, 134.87, 134.47, 129.13 (2C), 127.70, 122.88, 122.03, 121.41, 112.82 (2C), 72.86, 70.88, 70.69, 70.43 (2C), 69.64, 61.91, 43.32, 21.70. HR-ESI-MS (*m/z*) calculated for $C_{22}H_{28}N_2O_4SNa$ [M+Na] 439.1662; found $[M+Na]^+$ 439.1660.

BTA-EG$_6$

17-Iodo-3,6,9,12,15-pentaoxaheptadecan-1-ol was prepared according to literature. 17-Iodo-3,6,9,12,15-pentaoxaheptadecan-1-ol (0.18 g, 0.45 mmol) was coupled to 2-(p-aminophenyl)-6-methyl-benzothiazole (0.09 g, 0.38 mmol) with potassium carbonate (0.39 g, 2.8 mmol) in dry acetone (4 mL) under reflux conditions. The acetone was removed and the residue was taken up into dichloromethane, and separated from an insoluble precipitate (presumably excess potassium carbonate and potassium iodide). After the precipitate was removed by filtration, the solution was washed with brine, dried over sodium sulfate, and the solvent was removed under reduced pressure. The residue was purified via flash chromatography using 4% methanol in ethyl acetate as the eluent to yield a yellow oil (isolated yield was 28%). ^{1}H-NMR (400 MHz, $CDCl_3$): δ = 7.83-7.79

(m, 3H), 7.54 (s, 1H), 7.17 (dd, 8.8 Hz, 1.0 Hz, 1H), 6.61 (d, 8.8 Hz, 2H), 3.67-3.51 (m, 24H), 3.28 (t, 5.2 Hz, 2H), 2.39 (s, 3H). ^{13}C-NMR (100 MHz, $CDCl_3$); δ = 168.04, 151.82, 151.03, 134.50, 134.29, 129.14 (2C), 127.80, 121.93, 121.65, 121.39, 112.68 (2C), 72.73, 70.64 (6C), 70.40 (2C), 69.35, 61.61, 43.16, 21.63. ESI-MS (*m/z*) calculated for $C_{26}H_{36}N_2O_6S$ $[M]^+$ 504.2294; found $[M+H]^+$ 505.25 and $[M+Na]^+$ 507.20.

Acknowledgements

We thank the Xiaoxia Nina Lin lab (University of Michigan) for providing *E. coli* cells and facilities for microbial toxicity studies, the Lyle Simmons lab (University of Michigan) for providing *B. subtilis* cells. This work was supported by the Wallace H. Coulter Foundation (M.M.). M.R. and J.Y. acknowledge support from the Alzheimer's Association (NIRG-08-01651), a California HIV/AIDS IDEA Award (ID10-SD-034), and an NSF CAREER Award to J.Y. (CHE-0847530). P.P. is supported by the government of Thailand.

References

1. Ashcroft, F. M. (2000) *Ion Channels and Disease*, Academic Press, San Diego.
2. Estes, D. J., Memarsadeghi, S., Lundy, S. K., Marti, F., Mikol, D. D., Fox, D. A., and Mayer, M. (2008) High-throughput profiling of ion channel activity in primary human lymphocytes, *Anal. Chem. 80*, 3728-3735.
3. Berkane, E., Orlik, F., Charbit, A., Danelon, C., Fournier, D., Benz, R., and Winterhalter, M. (2005) Nanopores: maltoporin channel as a sensor for maltodextrin and lambda-phage, *Journal of Nanobiotechnology 3*, 3.
4. Gu, L. Q., Braha, O., Conlan, S., Cheley, S., and Bayley, H. (1999) Stochastic sensing of organic analytes by a pore-forming protein containing a molecular adapter, *Nature 398*, 686-690.
5. Tien, H. T., Salamon, Z., and Ottova, A. (1991) Lipid Bilayer-Based Sensors and Biomolecular Electronics, *Crit. Rev. Biomed. Eng. 18*, 323-340.
6. Bezrukov, S. M., Vodyanoy, I., and Parsegian, V. A. (1994) Counting Polymers Moving through a Single-Ion Channel, *Nature 370*, 279-281.

7. Cornell, B. A., BraachMaksvytis, V. L. B., King, L. G., Osman, P. D. J., Raguse, B., Wieczorek, L., and Pace, R. J. (1997) A biosensor that uses ion-channel switches, *Nature 387*, 580-583.
8. Schmidt, C., Mayer, M., and Vogel, H. (2000) A Chip-Based Biosensor for the Functional Analysis of Single Ion Channels, *Angew. Chem. Int. Ed. Engl. 39*, 3137 - 3140.
9. Terrettaz, S., Mayer, M., and Vogel, H. (2003) Highly electrically insulating tethered lipid bilayers for probing the function of ion channel proteins, *Langmuir 19*, 5567-5569.
10. Sondermann, M., George, M., Fertig, N., and Behrends, J. C. (2006) High-resolution electrophysiology on a chip: Transient dynamics of alamethicin channel formation, *Biochim. Biophys. Acta.-Biomembranes 1758*, 545-551.
11. Capone, R., Blake, S., Restrepo, M. R., Yang, J., and Mayer, M. (2007) Designing nanosensors based on charged derivatives of gramicidin A, *J. Am. Chem. Soc. 129*, 9737-9745.
12. Blake, S., Mayer, T., Mayer, M., and Yang, J. (2006) Monitoring chemical reactions by using ion-channel-forming peptides, *Chembiochem 7*, 433-435.
13. Majd, S., Yusko, E. C., Billeh, Y. N., Macrae, M. X., Yang, J., and Mayer, M. (2010) Applications of biological pores in nanomedicine, sensing, and nanoelectronics, *Curr. Opin. Biotechnol. 21*, 439-476.
14. Majd, S., Yusko, E. C., MacBriar, A. D., Yang, J., and Mayer, M. (2009) Gramicidin Pores Report the Activity of Membrane-Active Enzymes, *J. Am. Chem. Soc. 131*, 16119-16126.
15. Yusko, E. C., Johnson, J. M., Majd, S., Prangkio, P., Rollings, R. C., Li, J. L., Yang, J., and Mayer, M. (2011) Controlling protein translocation through nanopores with bio-inspired fluid walls, *Nature Nanotechnology 6*, 253-260.
16. Mutter, M., Altmann, K. H., Tuchscherer, G., and Vuilleumier, S. (1988) Strategies for the de novo Design of Proteins, *Tetrahedron 44*, 771-785.
17. Oiki, S., Danho, W., and Montal, M. (1988) Channel Protein Engineering - Synthetic 22-Mer Peptide from the Primary Structure of the Voltage-Sensitive Sodium-Channel Forms Ionic Channels in Lipid Bilayers, *Proc. Natl. Acad. Sci. U. S. A. 85*, 2393-2397.
18. Degrado, W. F., Wasserman, Z. R., and Lear, J. D. (1989) Protein Design, a Minimalist Approach, *Science 243*, 622-628.
19. Futaki, S., Fukuda, M., Omote, M., Yamauchi, K., Yagami, T., Niwa, M., and Sugiura, Y. (2001) Alamethicin-leucine zipper hybrid peptide: A prototype for the design of artificial receptors and ion channels, *J. Am. Chem. Soc. 123*, 12127-12134.
20. Movileanu, L., Howorka, S., Braha, O., and Bayley, H. (2000) Detecting protein analytes that modulate transmembrane movement of a polymer chain within a single protein pore, *Nat. Biotechnol. 18*, 1091-1095.
21. Sisson, A. L., Shah, M. R., Bhosale, S., and Matile, S. (2006) Synthetic ion channels and pores (2004-2005), *Chem. Soc. Rev. 35*, 1269-1286.
22. Koert, U., Al-Momani, L., and Pfeifer, J. R. (2004) Synthetic ion channels, *Synthesis-Stuttgart*, 1129-1146.
23. Matile, S., Som, A., and Sorde, N. (2004) Recent synthetic ion channels and pores, *Tetrahedron 60*, 6405-6435.
24. Sakai, N., Mareda, J., and Matile, S. (2007) Ion channels and pores, made from scratch, *Mol. Biosyst. 3*, 658-666.
25. Macrae, M. X., Blake, S., Jiang, X., Capone, R., Estes, D. J., Mayer, M., and Yang, J. (2009) A semi-synthetic ion channel platform for detection of phosphatase and protease activity, *ACS Nano 3*, 3567-3580.
26. Takeuchi, T., Sakai, N., and Matile, S. (2009) Counterion-activated polyions as soft sensing systems in lipid bilayer membranes: from cell-penetrating peptides to DNA, *Faraday Discuss. 143*, 187-203; discussion 265-175.
27. Sansom, M. S. P. (1991) The Biophysics of Peptide Models of Ion Channels, *Prog. Biophys. Mol. Biol. 55*, 139-235.

28. Tabushi, I., Kuroda, Y., and Yokota, K. (1982) A,B,D,F-Tetrasubstituted Beta-Cyclodextrin as Artificial Channel Compound, *Tetrahedron Lett. 23*, 4601-4604.
29. Madhavan, N., Robert, E. C., and Gin, M. S. (2005) A highly active anion-selective aminocyclodextrin ion channel, *Angew. Chem. Int. Ed. Engl. 44*, 7584-7587.
30. Gokel, G. W., and Mukhopadhyay, A. (2001) Synthetic models of cation-conducting channels, *Chem. Soc. Rev. 30*, 274-286.
31. Pawlak, M., Meseth, U., Dhanapal, B., Mutter, M., and Vogel, H. (1994) Template-Assembled Melittin - Structural and Functional-Characterization of a Designed, Synthetic Channel-Forming Protein, *Protein Sci. 3*, 1788-1805.
32. Montal, M., Montal, M. S., and Tomich, J. M. (1990) Synporins - Synthetic Proteins That Emulate the Pore Structure of Biological Ionic Channels, *Proc. Natl. Acad. Sci. U. S. A. 87*, 6929-6933.
33. Ghadiri, M. R., Granja, J. R., and Buehler, L. K. (1994) Artificial Transmembrane Ion Channels from Self-Assembling Peptide Nanotubes, *Nature 369*, 301-304.
34. Woolley, G. A., Epand, R. M., Kerr, I. D., Sansom, M. S. P., and Wallace, B. A. (1994) Alamethicin Pyromellitate - an Ion-Activated Channel-Forming Peptide, *Biochemistry (Mosc.) 33*, 6850-6858.
35. Roux, M., Perly, B., and Djedaini-Pilard, F. (2007) Self-assemblies of amphiphilic cyclodextrins, *European Biophysics Journal with Biophysics Letters 36*, 861-867.
36. Topchieva, I. N., Mischnick, P., Kuhn, G., Polyakov, V. A., Elezkaya, S. V., Bystryzky, G. I., and Karezin, K. I. (1998) Novel derivatives of cyclodextrins, modified with poly(ethylene oxide) and their complexation properties, *Bioconjug. Chem. 9*, 676-682.
37. Harada, A., Li, J., and Kamachi, M. (1993) Preparation and properties of inclusion complexes of poly(ethylene glycol) with alpha-cyclodextrin, *Macromolecules 26*, 5698-5703.
38. Gokel, G. W., Ferdani, R., Liu, J., Pajewski, R., Shabany, H., and Uetrecht, P. (2001) Hydraphile channels: Models for transmembrane, cation-conducting transporters, *Chemistry-a European Journal 7*, 33-39.
39. Husaru, L., Gruner, M., Wolff, T., Habicher, W. D., and Salzer, R. (2005) Photoresponsive upper-rim azobenzene substituted calix[4]resorcinarenes, *Tetrahedron Lett. 46*, 3377-3379.
40. Jeon, Y. J., Kim, H., Jon, S., Selvapalam, N., Oh, D. H., Seo, I., Park, C. S., Jung, S. R., Koh, D. S., and Kim, K. (2004) Artificial ion channel formed by cucurbit[n]uril derivatives with a carbonyl group fringed portal reminiscent of the selectivity filter of K+ channels, *J. Am. Chem. Soc. 126*, 15944-15945.
41. Jullien, L., Lazrak, T., Canceill, J., Lacombe, L., and Lehn, J.-M. (1993) An approach to channel-type molecular structures. Part 3. Incorporation studies of the bouquet-shaped BM and BCD in phosphatidylcholine vesicles, *J. Chem.Soc., Perk. T2*, 1011-1020.
42. Badi, N., Auvray, L., and Guegan, P. (2009) Synthesis of Half-Channels by the Anionic Polymerization of Ethylene Oxide Initiated by Modified Cyclodextrin, *Adv. Mater. 21*, 4054-4057.
43. Renkes, T., Schafer, H. J., Siemens, P. M., and Neumann, E. (2000) Fatty acid-oligo(ethylene glycol) ester forms ion channels in lipid membranes, *Angew. Chem. Int. Ed. Engl. 39*, 2512-2516.
44. Renkes, T., Schafer, H. J., Siemens, P. M., and Neumann, E. (2002) Antibacterial properties of ion channel forming fatty acid oligo (ethylene glycol) esters, *Materials Science & Engineering C-Biomimetic and Supramolecular Systems 22*, 275-278.
45. Yang, W. Y., Ahn, J. H., Yoo, Y. S., Oh, N. K., and Lee, M. (2005) Supramolecular barrels from amphiphilic rigid-flexible macrocycles, *Nat. Mater. 4*, 399-402.
46. Hirata, T., Fujimura, F., and Kimura, S. (2007) A novel polypseudorotaxane composed of cyclic beta-peptide as bead component, *Chem. Commun.*, 1023-1025.

47. Kim, H. J., Jeong, Y. H., Lee, E., and Lee, M. (2009) Channel Structures from Self-Assembled Hexameric Macrocycles in Laterally Grafted Bent Rod Molecules, *J. Am. Chem. Soc. 131*, 17371-17375.
48. Inbar, P., Li, C. Q., Takayama, S. A., Bautista, M. R., and Yang, J. (2006) Oligo(ethylene glycol) derivatives of thioflavin T as inhibitors of protein-amyloid interactions, *Chembiochem 7*, 1563-1566.
49. Olsen, J. S., Brown, C., Capule, C. C., Rubinshtein, M., Doran, T. M., Srivastava, R. K., Feng, C. Y., Nilsson, B. L., Yang, J., and Dewhurst, S. (2010) Amyloid-binding Small Molecules Efficiently Block SEVI (Semen-derived Enhancer of Virus Infection)- and Semen-mediated Enhancement of HIV-1 Infection, *J. Biol. Chem. 285*, 35488-35496.
50. Habib, L. K., Lee, M. T. C., and Yang, J. (2010) Inhibitors of Catalase-Amyloid Interactions Protect Cells from beta-Amyloid-Induced Oxidative Stress and Toxicity, *J. Biol. Chem. 285*, 38933-38943.
51. Hille, B. (2001) *Ion Channels of Excitable Membranes*, 3rd ed., Sinauer Associates, Inc., Sunderland.
52. Wallace, B. A. (1990) Gramicidin channels and pores, *Annu. Rev. Biophys. Biophys. Chem. 19*, 127-157.
53. Macrae, M. X., Blake, S., Mayer, M., and Yang, J. (2010) Nanoscale Ionic Diodes with Tunable and Switchable Rectifying Behavior, *J. Am. Chem. Soc. 132*, 1766-1767.
54. Mobashery, N., Nielsen, C., and Andersen, O. S. (1997) The conformational preference of gramicidin channels is a function of lipid bilayer thickness, *FEBS Lett. 412*, 15-20.
55. Watnick, P. I., Chan, S. I., and Dea, P. (1990) Hydrophobic mismatch in gramicidin-A' lecithin systems, *Biochemistry (Mosc.) 29*, 6215-6221.
56. Gennis, R. B. (1989) Springer Advanced Texts in Chemistry Biomembranes Molecular Structure and Function, In *Gennis, R. B. Springer Advanced Texts in Chemistry: Biomembranes: Molecular Structure and Function. Xvii+533p. Springer-Verlag New York Inc.: Secaucus, New Jersey, USA; Berlin, West Germany. Illus*.
57. Kelkar, D. A., and Chattopadhyay, A. (2007) The gramicidin ion channel: A model membrane protein, *Biochim. Biophys. Acta.-Biomembranes 1768*, 2011-2025.
58. Tedesco, M. M., Ghebremariam, B., Sakai, N., and Matile, S. (1999) Modeling the selectivity of potassium channels with synthetic, ligand-assembled pi slides, *Angewandte Chemie-International Edition 38*, 540-543.
59. Amicangelo, J. C., and Armentrout, P. B. (2000) Absolute binding energies of alkali-metal cation complexes with benzene determined by threshold collision-induced dissociation experiments and ab initio theory, *Journal of Physical Chemistry A 104*, 11420-11432.
60. Urry, D. W. (1971) Gramicidin-a Transmembrane Channel - Proposed Pi(L,D) Helix, *Proc. Natl. Acad. Sci. U. S. A. 68*, 672-&.
61. Koeppe, R. E., and Andersen, O. S. (1996) Engineering the gramicidin channel, *Annu. Rev. Biophys. Biomol. Struct. 25*, 231-258.
62. Andersen, O. S., Koeppe, R. E., and Roux, B. (2005) Gramicidin channels, *IEEE Trans. Nanobioscience 4*, 10-20.
63. Mayer, M., Semetey, V., Gitlin, I., Yang, J., and Whitesides, G. M. (2008) Using ion channel-forming peptides to quantify protein-ligand interactions, *J. Am. Chem. Soc. 130*, 1453-1465.
64. Hall, J. E., Vodyanoy, I., Balasubramanian, T. M., and Marshall, G. R. (1984) Alamethicin - a Rich Model for Channel Behavior, *Biophys. J. 45*, 233-247.
65. Bhosale, S., and Matile, S. (2006) A simple method to identify supramolecules in action: Hill coefficients for exergonic self-assembly, *Chirality 18*, 849-856.
66. Mayer, M., Kriebel, J. K., Tosteson, M. T., and Whitesides, G. M. (2003) Microfabricated teflon membranes for low-noise recordings of ion channels in planar lipid bilayers, *Biophys. J. 85*, 2684-2695.

67. Lipinski, C. A., Lombardo, F., Dominy, B. W., and Feeney, P. J. (1997) Experimental and computational approaches to estimate solubility and permeability in drug discovery and development settings, *Advanced Drug Delivery Reviews 23*, 3-25.
68. Sigworth, F. J. (1985) Open Channel Noise .1. Noise in Acetylcholine-Receptor Currents Suggests Conformational Fluctuations, *Biophys. J. 47*, 709-720.
69. Jensen, J. L., and Gardner, M. P. (1973) Solvent Isotope-Effects on Pka of Anilinium Ions in Aqueous Sulfuric-Acid, *J. Phys. Chem. 77*, 1557-1562.
70. Garrido, G., Roses, M., Rafols, C., and Bosch, E. (2008) Acidity of several anilinium derivatives in pure tetrahydrofuran, *Journal of Solution Chemistry 37*, 689-700.
71. Chang, R. (2005) *Physical Chemistry for the Life Sciences*, University Science Books, Sausalito, CA.
72. Vodyanoy, I., Hall, J. E., and Balasubramanian, T. M. (1983) Alamethicin-induced current-voltage curve asymmetry in lipid bilayers, *Biophys. J. 42*, 71-82.
73. Harold, F. M., and Baarda, J. R. (1967) Gramicidin Valinomycin and Cation Permeability of Streptococcus faecalis, *J. Bacteriol. 94*, 53-60.
74. Akira, S., Uematsu, S., and Takeuchi, O. (2006) Pathogen recognition and innate immunity, *Cell 124*, 783-801.
75. Ando, S., Aoyagi, H., Shinagawa, S., Nishino, N., Waki, M., Kato, T., and Izumiya, N. (1983) 4,4'-D-diaminopropionic-acid gramicidin-S- a synthetic gramicidin-S analog with anti-microbial activity against gram-negative bacteria, *FEBS Lett. 161*, 89-92.
76. Thippeswamy, H. S., Sood, S. K., Venkateswarlu, R., and Raj, I. (2009) Membranes of five-fold alamethicin-resistant Staphylococcus aureus, Enterococcus faecalis and Bacillus cereus show decreased interactions with alamethicin due to changes in membrane fluidity and surface charge, *Ann. Microbiol. 59*, 593-601.
77. Peschel, A., Jack, R. W., Otto, M., Collins, L. V., Staubitz, P., Nicholson, G., Kalbacher, H., Nieuwenhuizen, W. F., Jung, G., Tarkowski, A., van Kessel, K. P. M., and van Strijp, J. A. G. (2001) Staphylococcus aureus resistance to human defensins and evasion of neutrophil killing via the novel virulence factor MprF is based on modification of membrane lipids with L-lysine, *J. Exp. Med. 193*, 1067-1076.
78. ATCC. (2001) MTT Cell Proliferation Assay Instructions.
79. Rottenberg, H., and Koeppe, R. E. (1989) Mechanism of uncoupling of oxidative-phosphorylation by gramicidin, *Biochemistry (Mosc.) 28*, 4355-4360.
80. Matsunoyagi, A., and Hatefi, Y. (1989) Uncoupling of oxidative-phosphorylation-different effects of lipophilic weak acids and electrogenic ionophores on the kinetics of ATP synthesis, *Biochemistry (Mosc.) 28*, 4367-4374.
81. Knop, K., Hoogenboom, R., Fischer, D., and Schubert, U. S. (2010) Poly(ethylene glycol) in Drug Delivery: Pros and Cons as Well as Potential Alternatives, *Angew. Chem. Int. Ed. Engl. 49*, 6288-6308.
82. Mueller, P., Wescott, W. C., Rudin, D. O., and Tien, H. T. (1963) Methods for Formation of Single Bimolecular Lipid Membranes in Aqueous Solution, *J. Phys. Chem. 67*, 534-&.

Chapter 6

Conclusions and Future Works

Inconsistent evidence with regards to pore formation and cytotoxicity has been observed across the literature in this research field as well as the same research groups over time (*1*). This variability is mostly due to various aggregation states of Aβ from different preparation methods (*2*). A number of studies have provided evidence that the intermediate aggregated Aβ species can permeabilize cellular membranes and induce the unregulated passage of ions, in particular Ca^{2+}, resulting in cell death (*3*). The controversies regarding membrane permeabilization mechanisms by Aβ (*i.e.*, pore formation *versus* membrane thinning mechanisms) had been going on for a decade, thereby slowing the progress of understanding the underlying mechanism of Aβ neurotoxicity (*4, 5*).

In this thesis, we combined electrophysiological techniques with the cytotoxicity assays, along with various biochemical and biophysical techniques to investigate the effect of aggregation conditions of Aβ on pore formation in lipid bilayers and cytotoxicity. We summarize the conclusions of this work and suggestions for future works in the following sections.

6.1 Concluding remarks

6.1.1 Resolving the controversy of mechanism of Aβ-induced ion flux across membranes

In Capone et al., 2009 (*6*), we provided evidence that Aβ can induce ion channel-like ion flux through the membranes of artificial lipid and neuronal cell. This effect could contribute to the disruption of Ca^{2+} homeostasis. We also showed that the previously reported "thinning membrane" mechanism, on the other hand, was due to an artifact from the residual amount of the solvent HFIP, which was used in the preparation procedure to break up fibrils and large aggregates of Aβ. These findings resolved the controversy with regard to membrane permeabilization of Aβ, and also provided a caution for using HFIP in lipid bilayer experiments or cellular studies, since this solvent, which is commonly used for dissolving various types of proteins or polymers effectively (*7*), could disrupt the lipid membranes or cause cytotoxic effect, if not removed properly.

6.1.2 Development of HFIP-treatment procedure for Aβ preparation

In order to obtain reliable results in all experiments, it is important to prepare the Aβ samples with well-defined starting aggregation states for each experiment. We developed a protocol for Aβ preparation. The protocol uses the solvent HFIP to disaggregate the peptides, followed by lyophilization for 2 d to remove the HFIP solvent. This preparation protocol improved the solubility of Aβ in water and reduced the amount

of large aggregates, which are considered the major cause of irreproducibility in functional experiments such as ion channel recordings on planar lipid bilayers, and neurotoxicity assays (*2, 3*). Throughout these studies, we carried out experiments using this developed HFIP-treatment procedure.

6.1.3 Determination of the aggregated Aβ species which correlate with pore formation and cytotoxicity by using multiple linear regression models

We investigated the aggregation conditions of Aβ that yield the maximal probability of pore formation in lipid bilayers and cytotoxicity in neuroblastoma cells. We found that the probability of pore formation was highest when Aβ samples were incubated in water for 2-3 days in the case of $A\beta_{1-40}$ or for 2 days in the case of $A\beta_{1-42}$. The cytotoxicity studies revealed that the Aβ was the most toxic to neuroblastoma cells were when Aβ samples had aggregated for 10 d in the case of $A\beta_{1-40}$, and 3 d in the case of $A\beta_{1-42}$.

With regard to the question of which aggregation state of Aβ is important for pore formation and neurotoxicity mechanisms, multiple linear regression models revealed that the most strongly correlated aggregated species of $A\beta_{1-40}$ were tetramers to hexamers for pore formation and tetramers to 18 mers for cytotoxicity. Whereas in the case of $A\beta_{1-42}$, tetramers to hexamers were most strongly correlated with pore formation, while hexamer was the important aggregated species found for cytotoxicity. These findings

were in a good agreement with literatures where different techniques have been employed.

6.1.4 Membrane permeabilization of Aβ in different lipid systems are driven by different mechanisms

We further investigated the effect of Aβ at various aggregation states on membrane permeabilization in another lipid system, liposomes, by monitoring the leakage of fluorescent dyes or protons induced by Aβ. We found that Aβ peptides disrupted the membrane of liposomes, resulting in leakage of liposomal contents. Unlike the observation in PLB recordings, the activity of membrane disruption was highest for Aβ with 0-d incubation and decreased as Aβ samples were incubated for longer period of time. The decreasing trend of leakage over the incubation time of Aβ suggested that membrane disruption on liposomes was likely due to Aβ monomers and small oligomers (dimers and trimers), which were mostly abundant in the early aggregation time, whereas the aggregated species which were highly correlated with pore formation in PLB were oligomeric species (tetramers through 13 mers). We concluded that the leakage observed in these liposome-based assays resulted from bursting of liposomes as opposed to the pore formation in the planar lipid bilayers. One of the possibilities accounting for the different mechanisms included the physical properties of both lipid models such as the membrane curvature, stability, and mobility of lipid membranes.

6.1.5 Discovery of novel drug-like pore-forming synthetic molecules

In a search for a specific blocker of Aβ-induced pores in membranes, we examined several compounds that were designed by our collaborators' research lab based on the interaction of aggregated Aβ peptides and cellular proteins. We examined two promising molecules, which are derivatives of benzothiazole (BTA) attached to oligo(ethylene glycol), so-called BTA-EG_4 and BTA-EG_6. We demonstrated that each of these molecules could reduce the probability of pore formation from 50% to 20% when it was incubated with $A\beta_{1\text{-}40}$ in diH_2O for 2 d at 1:5 molar ratio (BTA-EG_x : monomeric Aβ). In addition, the works from our collaborators have shown that these molecules were able to reduce Aβ-induced oxidative stress (*8*) and improve the memory of transgenic mice in the behavioral studies. These molecules could be potential drug candidates for AD treatment, as they could mediate the aggregation process of Aβ and reduce the ability of Aβ to form pores through cellular membranes; however a large number of PLB recordings need to be carried out to confirm this statistical significance.

Aside from the effect on Aβ-induced ion flux, we found that both BTA-EG_4 and BTA-EG_6 molecules self-assemble and form well-defined channels in PLB. *The characteristics of these channels from BTA-EG_x mostly resemble those of gramicidin A (gA), such as cation selectivity, and conductance values.* We also found that these molecules exhibited anti bacterial activity against gram-positive bacterium, *Bacillus subtilis*, but not gram-negative bacterium, *Escherichia coli. Unlike gA, the* single-channel conductance of these pores could be modulated by the pH of the electrolyte with a minimum conductance observed at pH ~3.

6.2 Future Works

6.2.1 Investigation of Aβ-induced ion flux in high-throughput PLB recordings

A traditional electrophysiological technique typically allows one PLB recording at a time. The Aβ-induced ion flux in PLB experiments occurred with only a certain probability. In our studies, we compared the pore formation by Aβ with various aggregation conditions. It was necessary to perform the several experiments to obtain the meaningful statistical significance. An individual PLB recording experiment for measuring activity of Aβ generally requires at least one hour (sometimes several hours)starting from the formation of a stable lipid bilayer, waiting for the peptide to incorporate into the PLB, monitoring the current activity, and finally the cleaning steps. Therefore, this low-throughput and laborious technique may result in a slow progress of studies and lack of reports with regards to pore formation by Aβ.

Recently, an electrophysiological technique for measuring ion channels in a high-throughput lipid membrane platform has become available in another research group (*9*). This high throughput system allows measurements of ion channel activity in over 2200 lipid membranes simultaneously in 3 h with automated liquid-handling equipment, enabling the measurement of a large number of different samples with multiple repetitions. We could potentially apply this approach to study ion flux induced by Aβ from various conditions in multiple experiments in order to obtain powerful statistical analyses for all different aggregation conditions. For extensive studies, the investigation of pore formation could also be carried out with more aggregation time points of Aβ, especially within the time window that the intermediate Aβ species are mostly present.

After we establish optimal conditions for Aβ to form pores in the PLB along with the careful characterization of Aβ, we could employ the similar high-throughput approach for screening small molecules which provide an inhibitory effect of Aβ-induced ion flux, including the potential drug candidates, BTA-EG_4 and BTA-EG_6. Ultimately, this approach may direct us to discover new lead compounds for AD treatment.

6.2.2 Investigation of Aβ-induced ion flux in cellular membranes using high-throughput technology

In chapter 2 of the thesis, we demonstrated by a semi-automated patch-clamp technique that Aβ is capable of forming pores and inducing ion flux across cellular membranes. To gain more powerful statistical analysis, we could also adopt the high-throughput approach for electrophysiological recordings in live cells. The available high-throughput technology, IonWorks HT device (Essen Instruments, Ann Arbor) enables measurements of ion channel activity in a large number of cells in parallel within one hour (*10*). One disadvantage of this technology is that it is not optimized for ion channel recording over 30 min, whereas these experiments typically take several minutes for the ion flux to occur after the addition of Aβ, and the addition of Aβ onto the cells could cause a reduction of seal resistance, thereby reducing the efficiency of the assay.

6.2.3 Investigation of the influence of membrane curvature on the membrane disruption induced by Aβ at various aggregation states

Based on the findings in chapters 3 and 4, one of the possibilities that we obtained different results regarding the effects of Aβ at various aggregation states on membrane permeabilization in the two lipid systems (planar lipid bilayer and liposomes) could be the membrane curvatures. To test this hypothesis, we could perform leakage assays on various sizes of liposomes, ranging from small (< 50 nm diameter) to giant liposomes (> 1 μm diameter), and compare the effects of aggregation states of Aβ on the leakage. The size of liposomes could be determined by dynamic light scattering technique. In the case of giant liposomes, one could monitor the leakage of fluorescent dyes through liposomal membrane upon addition of Aβ, by using confocal fluorescence microscopy. This approach will allow us to visualize the membrane disruption due to Aβ on each liposome and compare the effect among Aβ with various aggregation states.

6.2.4 Modification of BTA-EG_4 and BTA-EG_6 structures to improve biocompatibility

Both BTA-EG_4 and BTA-EG_6 molecules have shown promise as potential drugs for AD in molecular and behavioral studies. Moreover, these molecules exhibit antibacterial activity against gram-positive bacterium *Bacillus subtilis*. These small synthetic molecules might also be appealing as starting materials for development of antibiotics. Nevertheless, these molecules form ion channels in lipid membranes and induce cytotoxicity in human neuroblastoma cells at micromolar concentrations, resulting in a biocompatibility issue in drug development.

To minimize the cytotoxicity of these BTA-EG_x molecules, we could potentially modify the molecular structures of these molecules in an attempt to improve biocompatibility. It is worthwhile to increase understanding of how these molecules assemble into channels. Based on our current findings, we proposed that the annilinium group of the BTA moieties could play a major role in ion channel assembly and conductivity. If this group had been replaced by a non-charged substituent (e.g. methyl group or hydrogen), the pore-formation activity, and potentially cytotoxic effect could be diminished. If new design of these compounds can no longer form channels in the membranes and also provide a minimal cytotoxic effect, while retaining the protective effects of reducing pore formation induced by Aβ and reducing production of reactive oxygen species (ROS) induced by Aβ, these molecules could be promising drug candidates for AD treatment.

References:

1. Demuro, A., Parker, I., and Stutzmann, G. E. (2010) Calcium Signaling and Amyloid Toxicity in Alzheimer Disease, *J. Biol.Chem. 285*, 12463-12468.
2. Zagorski, M. G., Yang, J., Shao, H. Y., Ma, K., Zeng, H., and Hong, A. (1999) Methodological and chemical factors affecting amyloid beta peptide amyloidogenicity, *Amyloid, Prions, and Other Protein Aggregates 309*, 189-204.
3. Kagan, B. L., and Thundimadathil, J. (2010) Amyloid Peptide Pores and the Beta Sheet Conformation, In *Proteins: Membrane Binding and Pore Formation* (Anderluh, G. L. J., Ed.), pp 150-167.
4. Marx, J. (2007) Alzheimer's disease - Fresh evidence points to an old suspect: Calcium, Science 318, 384-385
5. Eliezer, D. (2006) Amyloid Ion Channels: A Porous Argument or a Thin Excuse?, *J. Gen. Physiol.* 128, 631-633.
6. Capone, R., Quiroz, F. G., Prangkio, P., Saluja, I., Sauer, A. M., Bautista, M. R., Turner, R. S., Yang, J., and Mayer, M. (2009) Amyloid-beta-Induced Ion Flux in Artificial Lipid Bilayers and Neuronal Cells: Resolving a Controversy, *Neurotox. Res. 16*, 1-13.
7. Shuklov, I. A., Dubrovina, N. V., and Boerner, A. (2007) Fluorinated alcohols as solvents, cosolvents and additives in homogeneous catalysis, *Synthesis-Stuttgart*, 2925-2943.

8. Habib, L. K., Lee, M. T. C., and Yang, J. (2010) Inhibitors of Catalase-Amyloid Interactions Protect Cells from beta-Amyloid-Induced Oxidative Stress and Toxicity, *J. Biol. Chem. 285*, 38933-38943.
9. Poulos, J. L., Jeon, T.-J., Damoiseaux, R., Gillespie, E. J., Bradley, K. A., and Schmidt, J. J. (2009) Ion channel and toxin measurement using a high throughput lipid membrane platform, *Biosensors & Bioelectronics 24*, 1806-1810.
10. Estes, D. J., Memarsadeghi, S., Lundy, S. K., Marti, F., Mikol, D. D., Fox, D. A., and Mayer, M. (2008) High-throughput profiling of ion channel activity in primary human lymphocytes, *Anal. Chem. 80*, 3728-3735.